CHAPTER 17
HEAT EXCHANGERS

R. K. Shah* and D. P. Sekulić
University of Kentucky

INTRODUCTION

A *heat exchanger* is a device that is used for transfer of thermal energy (enthalpy) between two or more fluids, between a solid surface and a fluid, or between solid particulates and a fluid, at differing temperatures and in thermal contact, usually without external heat and work interactions. The fluids may be single compounds or mixtures. Typical applications involve heating or cooling of a fluid stream of concern, evaporation or condensation of a single or multicomponent fluid stream, and heat recovery or heat rejection from a system. In other applications, the objective may be to sterilize, pasteurize, fractionate, distill, concentrate, crystallize, or control process fluid. In some heat exchangers, the fluids exchanging heat are in direct contact. In other heat exchangers, heat transfer between fluids takes place through a separating wall or into and out of a wall in a transient manner. In most heat exchangers, the fluids are separated by a heat transfer surface, and ideally they do not mix. Such exchangers are referred to as the *direct transfer type,* or simply *recuperators.* In contrast, exchangers in which there is an intermittent heat exchange between the hot and cold fluids—via thermal energy storage and rejection through the exchanger surface or matrix—are referred to as the *indirect transfer type* or *storage type,* or simply *regenerators.* Such exchangers usually have leakage and fluid carryover from one stream to the other.

A heat exchanger consists of heat exchanging elements such as a core or a matrix containing the heat transfer surface, and fluid distribution elements such as headers, manifolds, tanks, inlet and outlet nozzles or pipes, or seals. Usually there are no moving parts in a heat exchanger; however, there are exceptions such as a rotary regenerator (in which the matrix is mechanically driven to rotate at some design speed), a scraped surface heat exchanger, agitated vessels, and stirred tank reactors.

The heat transfer surface is a surface of the exchanger core that is in direct contact with fluids and through which heat is transferred by conduction. The portion of the surface that also separates the fluids is referred to as the *primary* or *direct surface.* To increase heat transfer area, appendages known as fins may be intimately connected to the primary surface to provide *extended, secondary,* or *indirect surface.* Thus, the addition of fins reduces the thermal resistance on that side and thereby increases the net heat transfer from/to the surface for the same temperature difference. The heat transfer coefficient can also be higher for fins.

A gas-to-fluid heat exchanger is referred to as a *compact heat exchanger* if it incorporates a heat transfer surface having a surface area density above about 700 m²/m³ (213 ft²/ft³) on at

---

* Current address: Delphi Harrison Thermal Systems, Lockport, New York.

least one of the fluid sides, which usually has gas flow. It is referred to as a *laminar flow heat exchanger* if the surface area density is above about 3000 m^2/m^3 (914 ft^2/ft^3), and as a *micro-heat exchanger* if the surface area density is above about 10,000 m^2/m^3 (3050 ft^2/ft^3). A liquid/two-phase fluid heat exchanger is referred to as a *compact heat exchanger* if the surface area density on any one fluid side is above about 400 m^2/m^3 (122 ft^2/ft^3). A typical process industry shell-and-tube exchanger has a surface area density of less than 100 m^2/m^3 on one fluid side with plain tubes and 2–3 times that with the high-fin-density, low-finned tubing. Plate-fin, tube-fin, and rotary regenerators are examples of compact heat exchangers for gas flows on one or both fluid sides, and gasketed and welded plate heat exchangers are examples of compact heat exchangers for liquid flows.

CLASSIFICATION OF HEAT EXCHANGERS

Heat exchangers may be classified according to transfer process, construction, flow arrangement, surface compactness, number of fluids and heat transfer mechanisms as shown in Fig. 17.1 modified from Shah [1] or according to process functions as shown in Fig. 17.2 [2]. A brief description of some of these exchangers classified according to construction is provided next along with their selection criteria. For further general description, see Refs. 1–4.

Shell-and-Tube Exchangers

The tubular exchangers are widely used in industry for the following reasons. They are custom designed for virtually any capacity and operating conditions, such as from high vacuums to ultra-high pressures (over 100 MPa or 15,000 psig), from cryogenics to high temperatures (about 1100°C, 2000°F), and any temperature and pressure differences between the fluids, limited only by the materials of construction. They can be designed for special operating conditions: vibration, heavy fouling, highly viscous fluids, erosion, corrosion, toxicity, radioactivity, multicomponent mixtures, and so on. They are the most versatile exchangers made from a variety of metal and nonmetal materials (graphite, glass, and Teflon) and in sizes from small (0.1 m^2, 1 ft^2) to super-giant (over 100,000 m^2, 10^6 ft^2). They are extensively used as process heat exchangers in the petroleum-refining and chemical industries; as steam generators, condensers, boiler feed water heaters, and oil coolers in power plants; as condensers and evaporators in some air-conditioning and refrigeration applications; in waste heat recovery applications with heat recovery from liquids and condensing fluids; and in environmental control.

Shell-and-tube exchangers are basically noncompact exchangers. Heat transfer surface area per unit volume ranges from about 50 to 100 m^2/m^3 (15 to 30 ft^2/ft^3). Thus, they require a considerable amount of space, support structure, and capital and installation costs. As a result, overall they may be quite expensive compared to compact heat exchangers. The latter exchangers have replaced shell-and-tube exchangers in those applications today where the operating conditions permit such use. For the equivalent cost of the exchanger, compact heat exchangers will result in high effectiveness and be more efficient in energy (heat) transfer.

Shell-and-tube heat exchangers are classified and constructed in accordance with the widely used Tubular Exchanger Manufacturers Association (TEMA) standards [5], DIN and other standards in Europe and elsewhere, and ASME Boiler and Pressure Vessel Codes. TEMA has developed a notation system to designate the main types of shell-and-tube exchangers. In this system, each exchanger is designated by a three-letter combination, the first letter indicating the front-end head type, the second the shell type, and the third the rear-end head type. These are identified in Fig. 17.3. Some of the common shell-and-tube exchangers are BEM, BEU, BES, AES, AEP, CFU, AKT, and AJW. Other special types of commercially available shell-and-tube exchangers have front-end and rear-end heads different from those in Fig. 17.3; these exchangers may not be identifiable by the TEMA letter designation.
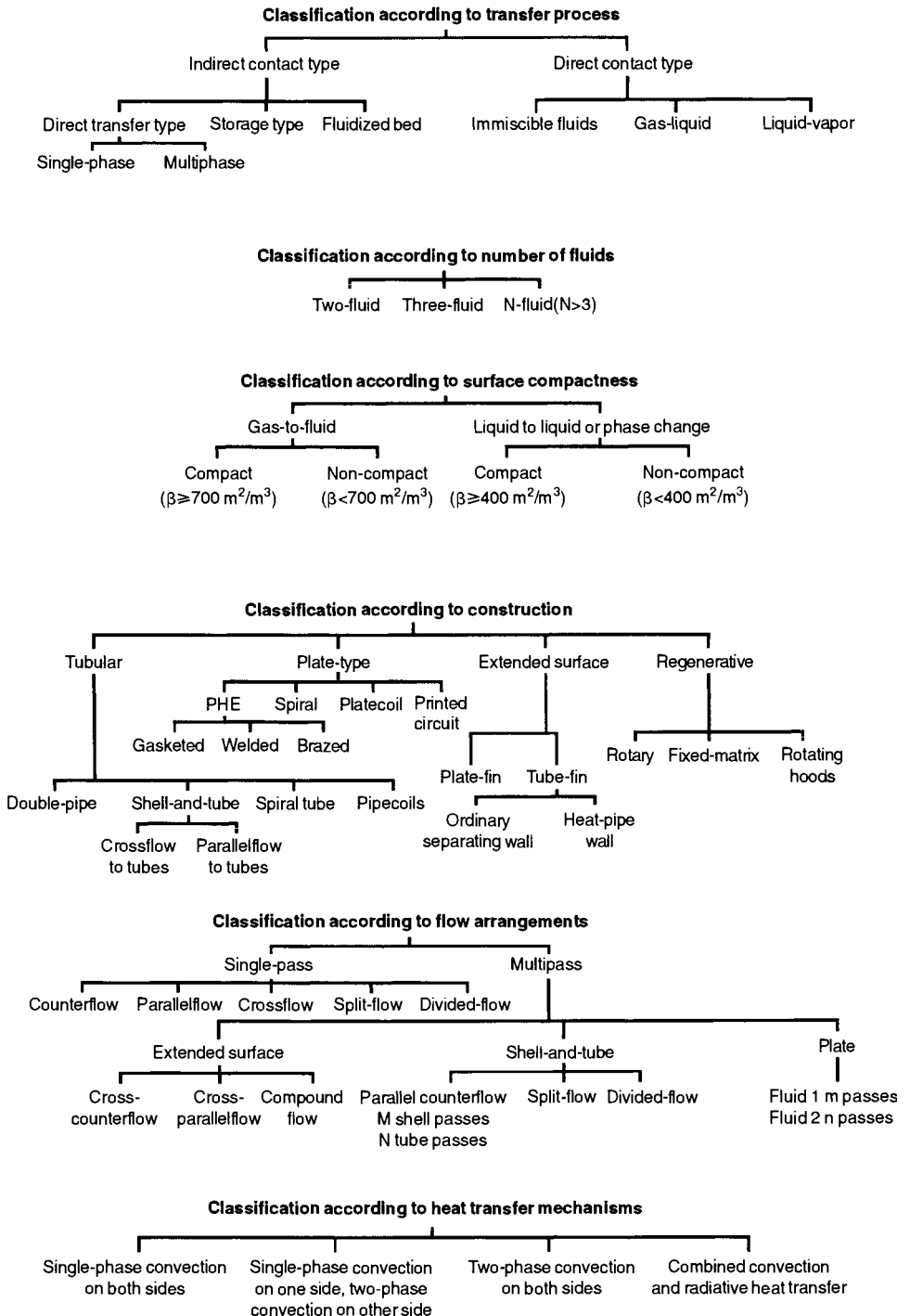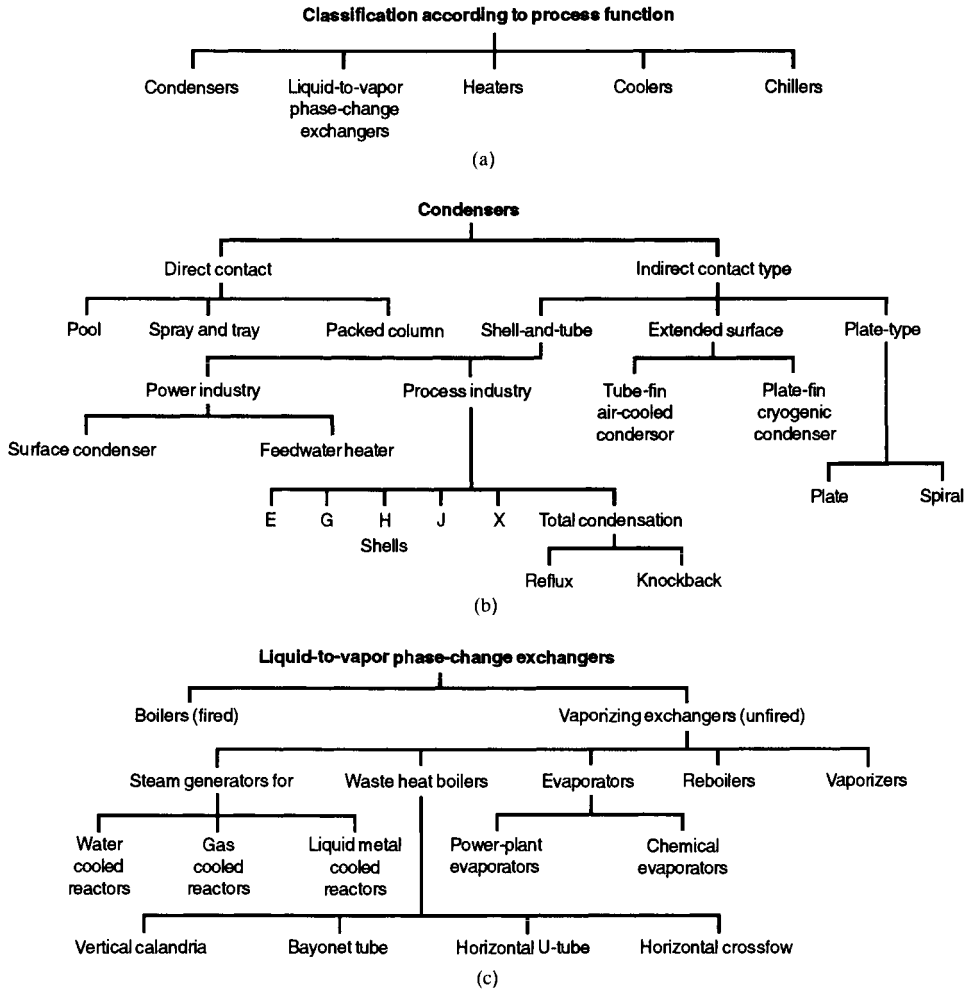
Classification according to transfer process

Indirect contact type

Direct contact type

Direct transfer type — Storage type — Fluidized bed

Immiscible fluids — Gas-liquid — Liquid-vapor

Single-phase — Multiphase

Classification according to number of fluids

Two-fluid — Three-fluid — N-fluid(N>3)

Classification according to surface compactness

Gas-to-fluid

Liquid to liquid or phase change

Compact
$(\beta \geqslant 700 \text{ m}^2/\text{m}^3)$

Non-compact
$(\beta < 700 \text{ m}^2/\text{m}^3)$

Compact
$(\beta \geqslant 400 \text{ m}^2/\text{m}^3)$

Non-compact
$(\beta < 400 \text{ m}^2/\text{m}^3)$

Classification according to construction

Tubular — Plate-type — Extended surface — Regenerative

PHE — Spiral — Platecoil — Printed circuit

Gasketed — Welded — Brazed

Rotary — Fixed-matrix — Rotating hoods

Plate-fin — Tube-fin

Double-pipe — Shell-and-tube — Spiral tube — Pipecoils

Ordinary separating wall — Heat-pipe wall

Crossflow to tubes — Parallelflow to tubes

Classification according to flow arrangements

Single-pass

Multipass

Counterflow — Parallelflow — Crossflow — Split-flow — Divided-flow

Extended surface

Shell-and-tube

Plate

Cross-counterflow — Cross-parallelflow — Compound flow

Parallel counterflow M shell passes N tube passes — Split-flow — Divided-flow

Fluid 1 m passes
Fluid 2 n passes

Classification according to heat transfer mechanisms

Single-phase convection on both sides

Single-phase convection on one side, two-phase convection on other side

Two-phase convection on both sides

Combined convection and radiative heat transfer

FIGURE 17.1 Classification of heat exchangers.

Classification according to process function

| Condensers | Liquid-to-vapor phase-change exchangers | Heaters | Coolers | Chillers |

(a)

Condensers

Direct contact — Indirect contact type

Direct contact: Pool | Spray and tray | Packed column

Indirect contact type: Shell-and-tube | Extended surface | Plate-type

Shell-and-tube: Power industry | Process industry

Power industry: Surface condenser | Feedwater heater

Extended surface: Tube-fin air-cooled condersor | Plate-fin cryogenic condenser

Plate-type: Plate | Spiral

Process industry Shells: E G H J X | Total condensation

Total condensation: Reflux | Knockback

(b)

Liquid-to-vapor phase-change exchangers

Boilers (fired) — Vaporizing exchangers (unfired)

Boilers (fired): Steam generators for | Waste heat boilers

Vaporizing exchangers (unfired): Evaporators | Reboilers | Vaporizers

Steam generators for: Water cooled reactors | Gas cooled reactors | Liquid metal cooled reactors

Evaporators: Power-plant evaporators | Chemical evaporators

Vertical calandria | Bayonet tube | Horizontal U-tube | Horizontal crossfow

(c)

FIGURE 17.2 (*a*) Classification according to process function. (*b*) Classification of condensers. (*c*) Classification of liquid-to-vapor phase-change exchangers.

The three most common types of shell-and-tube exchangers are fixed tubesheet design, U-tube design, and the floating head type. In all types, the front-end head is stationary, while the rear-end head could be either stationary or floating depending upon the thermal stresses in the shell, tube, or tubesheet due to temperature differences as a result of heat transfer.

The exchangers are built in accordance with three mechanical standards that specify design, fabrication, and materials of unfired shell-and-tube heat exchangers. Class R is for generally severe requirements of petroleum and related processing applications. Class C is for generally moderate requirements for commercial and general process applications. Class B is for chemical process service. The exchangers are built to comply with the applicable ASME (American Society of Mechanical Engineers) Boiler and Pressure Vessel Code Section VIII, or other pertinent codes and/or standards. The TEMA standards supplement and define the ASME code for heat exchanger applications. In addition, the state and local codes applicable to the plant location must also be met. In this chapter, we use the TEMA standards, but there are other standards such as DIN 28 008.
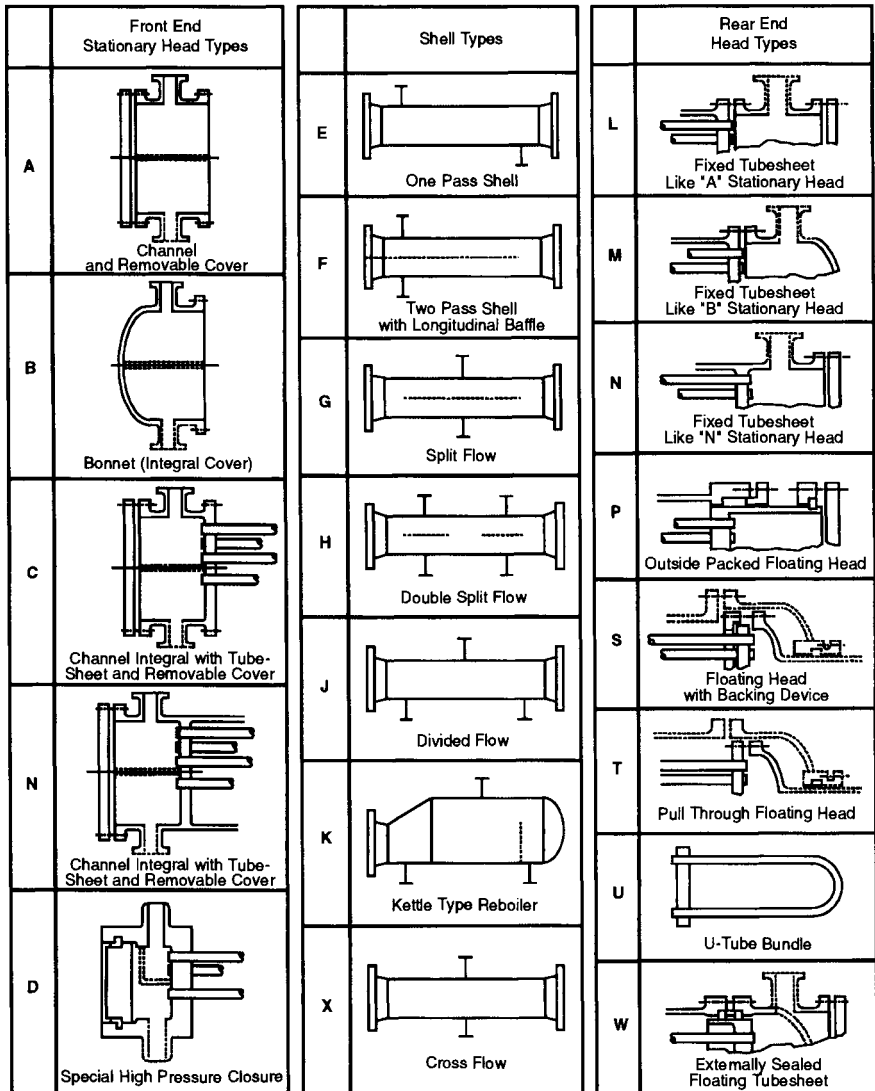
Front End Stationary Head Types		Shell Types		Rear End Head Types	
A	Channel and Removable Cover	E	One Pass Shell	L	Fixed Tubesheet Like 'A' Stationary Head
B	Bonnet (Integral Cover)	F	Two Pass Shell with Longitudinal Baffle	M	Fixed Tubesheet Like 'B' Stationary Head
C	Channel Integral with Tube-Sheet and Removable Cover	G	Split Flow	N	Fixed Tubesheet Like 'N' Stationary Head
		H	Double Split Flow	P	Outside Packed Floating Head
N	Channel Integral with Tube-Sheet and Removable Cover	J	Divided Flow	S	Floating Head with Backing Device
		K	Kettle Type Reboiler	T	Pull Through Floating Head
				U	U-Tube Bundle
D	Special High Pressure Closure	X	Cross Flow	W	Externally Sealed Floating Tubesheet

FIGURE 17.3 Standard front-end head, shell-type, and rear-end head types, from TEMA [5].

The TEMA standards specify the manufacturing tolerances for various mechanical classes, the range of tube sizes and pitches, baffling and support plates, pressure classification, tubesheet thickness formulas, and so on, and must be consulted for all these details.

Criteria for Mechanical Selection

Shells. Shells are generally made from standard pipes for shell diameters less than 610 mm (2 ft) and by rolling and welding plates to the desired diameters for larger sizes. The shell diameters range from less than 50 mm (2 in) to 6.10 m (20 ft) for special applications. The E shell (see Fig. 17.3) is a single-pass shell that is economical and usually has the most efficient thermal arrangement (i.e., it has the highest mean temperature difference correction factor

F). However, if the F factor is low enough to require two E shells in series for multipass tube-side exchangers, the F shell (a two-pass shell; a counterflow unit) can be used as an equivalent but more economical unit. However, the F shell baffle is subject to fluid and thermal leakage across the longitudinal baffle, so it must be carefully designed and constructed. It also provides more problems in removing or replacing the tube bundle. The F shell is used for single-phase applications. If the pressure drop in an F shell is limiting, a split-flow G or H shell can be used with some sacrifice in the F factor. The G shell is used in many applications, with the shellside thermosiphon and forced convective boiling as one of the common applications. If shellside pressure drop becomes limiting, the divided-flow J shell is used; however, there is some loss in the thermal efficiency (a lower F factor). The J shell is commonly used in vacuum condensing applications. The X shell is used for large shell flows or for the lowest shellside Δp for a given flow rate. In the X shells, full-size support plates are used to prevent tube vibration. For high flow rates (inlet velocity), alternately H or J shells with two inlet nozzles are used. The G and H shells are seldom used for shellside single-phase applications, since there is no advantage over E or X shells. They are used for thermosiphon reboilers, condensers, and other phase-change applications. The K shell is exclusively used for vaporization of liquid on the shell side.

The type of shell shown in Fig. 17.3 has either one or two shell passes per shell. Because of the high cost of the shell compared to tubes, three or four shell passes in a shell could be made by the use of longitudinal baffles with positive sealing. However, such multipassing will reduce the flow area compared to a single-pass unit with possibly higher Δp. Alternatively, multiple shells in series are used in some applications (such as up to six shells in series in heat recovery trains) for increased effectiveness, part-load operation, spare bundle requirement, and shipping and handling requirements.

Stationary Heads.   These are used to get the tubeside fluid into the tubes. There are two basic types of stationary (front-end) heads: the bonnet and the channel. The bonnet (B) has either a side-entering or end-entering nozzle and is used for generally clean tubeside fluids; it has fewer joints (and hence is less expensive than the A head) but does require breaking the piping joints in order to clean or inspect the tubes. The channel head can be removable (A) or integral with the tubesheet (C and N). It has side-entering nozzles and a removable cover plate allowing easy access to the tubes without disturbing the piping. While the shell is flanged in the C head, it is welded in the N head to eliminate any potential leak between the shell and tubes. The D head has a special high pressure enclosure and is used in feedwater heaters having tubeside pressures 10–40 MPa (1500–6000 psig) range.

Rear-End Heads.   Shells and tubes are exposed to different temperatures in operation, resulting in thermal stresses that can cause bending, buckling, or fracture of the tubes or shell or failure of tube-to-tubesheet joints. This thermal stress problem can be further compounded if the shell and tube materials are different, or residual stresses remain after the exchanger fabrication. Proper rear head design can minimize/eliminate these thermal stresses, and the specific design depends upon the thermal stresses in the operation.

The fixed tubesheet (L, M, or N) is a rigid design and permits differential thermal expansion to moderate inlet temperature differences ($< 56°C$ or $100°F$) between the tubes and shell. Use of a shell expansion joint can raise this temperature difference limit to $83°C$ ($150°F$). Any number of tube passes can be used. However, the shell side can only be chemically cleaned. Individual tubes can be replaced. These heads allow the least clearance between the shell and the tube bundle (10–12 mm, 0.4–0.5 in), thus minimizing the bundle-to-shell bypass flow. Fixed tubesheet exchangers are used for low temperatures ($315°C$ or $600°F$ max) coupled with low pressures (2100 kPa gauge or 300 psig max). This is a low-cost exchanger but slightly higher in cost than the U-tube exchanger.

The U-tube head (U) is a very simple design requiring a bundle of U tubes, only one tubesheet, no expansion joints, and no rear-end head at all, allowing easy removal of the bundle. The thermal stress problem is eliminated because each tube is free to expand/contract independently. In this design, individual tube replacement is not possible except in the outer rows, and an even number of tube passes is required. Some tubes are lost in the center due to

tube bend limit, and tubeside mechanical cleaning of the bends is difficult. Flow-induced vibration could be a problem for tubes in the outermost row. It is the lowest-cost design because there is no need for the second tubesheet.

The outside packed floating head (P) provides for expansion and can be designed for any number of passes. Shell and tube fluids cannot mix if gaskets or packing develop leaks, since the leak is to the atmosphere; however, very toxic fluids are not used. This P head requires a larger bundle-to-shell clearance, and sealing strips are used in some designs to block the bundle-to-shell bypass flow partially. This design allows only an even number of tube passes. For a given amount of surface area, it requires a larger shell diameter compared to the L, M, or N head design. This is a high-cost design.

The split-ring floating head (S) has the tubesheet sandwiched between a removable split ring and the cover, which has a larger diameter than the shell. This permits a smaller clearance between the shell and bundle, and the sealing strip is required for only selected applications. On account of the floating head location, the minimum outlet baffle spacing is the largest of any design. Gasket failure is not visible and allows mixing of tube and shell fluids. To remove the bundle or clean the tubes, both ends of the exchanger must be disassembled. Cleaning costs somewhat more than for the pull-through type (T), and the exchanger cost is relatively high.

The pull-through floating head (T) can be removed from the shell by disassembling the stationary head. Because of the floating-head flange bolting, this design has the largest bundle-to-shell clearance, and thus sealing strips are necessary. Even-numbered multipassing is imposed. Again, gasket leakage allows mixing of shell and tube fluids and is not externally visible. Cost is relatively high.

The packed floating head with lantern ring (W) has the lantern ring packing compressed by the rear head bolts. Bundle-to-shell clearance is relatively small. A single- or two-pass arrangement is possible. Potential leakage of either shell or tube fluid is to the atmosphere; however, mixing of these two fluids is possible in the leakage area. Hence, this design is used for benign fluids and low to very moderate pressures and temperatures. The bundle is easily removed, but this design is not recommended on account of severe thermal fluctuations, which can loosen the packing. This floating head design is the lowest in cost. The design features of shell-and-tube exchangers with various rear heads are summarized in Table 17.1.

Baffles.   Longitudinal baffles are used in the shell to control the overall flow direction of the shell fluid as in F, G, and H shells. The transverse baffles may be classified as plate baffles and axial-flow baffles (rod, NEST, etc.). The plate baffles (see Fig. 17.4) are used to support the tubes, to direct the fluid in the tube bundle at about 90° to the tubes, and to increase the turbulence of the shell fluid. The rod (and other axial-flow) baffles (see Fig. 17.5) are used to support the tubes, to have the fluid flowing axially over the tubes, and to increase the turbulence of the shell fluid. Flow-induced vibration is virtually eliminated in rod and other axial-flow baffles having axial shellside flows.

Plate baffles can be segmental with or without tubes in the window, multisegmental, or disk-and-doughnut (see Fig. 17.4). The single-segmental baffle is most common and is formed by cutting a segment from a disk. As shown in Fig. 17.4, the cuts are alternately 180° apart and cause the shell fluid to flow back and forth across the tubes more or less perpendicularly. Baffle cut and baffle spacing are selected from the shellside fouling and Δp considerations. In fouling situations, the baffle cut should be below 25 percent. Baffle spacing is chosen to avoid tube vibrations and optimize heat transfer/pressure drop by keeping about the same flow area in the crossflow and window zone. The direction of the baffle cut is preferred horizontal for very viscous liquids for better mixing (as shown for segmental baffles in Fig. 17.4). The direction of baffle cut is selected vertical for shellside consideration (for better drainage), evaporation/boiling (to promote more uniform flow), solids entrained in liquid, and multipassing on the shellside. One disadvantage of the segmental types is the flow bypassing that occurs in the annular spaces (clearances) between the tube bundle and shell. If the pressure drop is too high or more tube supports are needed to prevent vibration, the segmental baffle is further subdivided into a double-segmental or triple-segmental arrangement. An alternate method of

TABLE 17.1   Design Features of Shell-and-Tube Heat Exchangers [1]

Design features	Fixed tubesheet	Return bend (U-tube)	Outside-packed stuffing box	Outside-packed latern ring	Pull-through bundle	Inside split backing ring
TEMA rear-head type	L, M, N	U	P	W	T	S
Tube bundle removable	No	Yes	Yes	Yes	Yes	Yes
Spare bundles used	No	Yes	Yes	Yes	Yes	Yes
Provides for differential movement between shell and tubes	Yes, with bellows in shell	Yes	Yes	Yes	Yes	Yes
Individual tubes can be replaced	Yes	Yes[a]	Yes	Yes	Yes	Yes
Tubes can be chemically cleaned, both inside and outside	Yes	Yes	Yes	Yes	Yes	Yes
Tubes can be mechanically cleaned on inside	Yes	With special tools	Yes	Yes	Yes	Yes
Tubes can be mechanically cleaned on outside	Yes	Yes[b]	Yes[b]	Yes[b]	Yes[b]	Yes[b]
Internal gaskets and bolting are required	No	No	No	No	Yes	Yes
Double tubesheets are practical	Yes	Yes	Yes	No	No	No
Number of tubesheet passes available	Any	Any even number	Any[c]	One or two[d]	Any[e]	Any[e]
Approximate diametral clearance (mm) (Shell ID–D_{otl})	11–18	11–18	25–50	15–35	95–160	35–50
Relative costs in ascending order, least expensive = 1	2	1	4	3	5	6

[a] Only those in outside rows can be replaced without special designs.
[b] Outside mechanical cleaning possible with square or rotated square pitch, or wide triangular pitch.
[c] Axial nozzle required at rear end for odd number of passes.
[d] Tube-side nozzles must be at stationary end for two passes.
[e] Odd number of passes requires packed gland or bellows at floating head.

improving tube support for vibration prevention is to eliminate tubes in the window zone, in which case intermediate support baffles can be used. This design requires a larger shell to contain the same number of tubes in a segmental baffle exchanger, but a lower pressure drop and improved heat transfer (due to improved flow distribution and less fouling) can help to reduce this diameter increase.

   Tube Pitch and Layout.   The selection of tube pitch (see Fig. 17.6 for the definition) is a compromise between a close pitch for increased shellside heat transfer and surface compactness, and an open pitch for decreased shellside plugging and ease in shellside cleaning. In most shell-and-tube exchangers, the ratio between tube pitch and outside diameter ratio varies from 1.25 to 2.00. The recommended ligament width depends upon the tube diameter and pitch; the values are provided by TEMA [5]; the minimum value is 3.18 mm (1/8 in) for clean services and 6.35 mm (1/4 in) where mechanical cleaning is required.

(a) Single-segmental baffle

(b) Double-segmental baffle

(c) Triple-segmental baffle

(d) No-tubes-in-window segmental baffle

(e) Disk-and-doughnut baffle
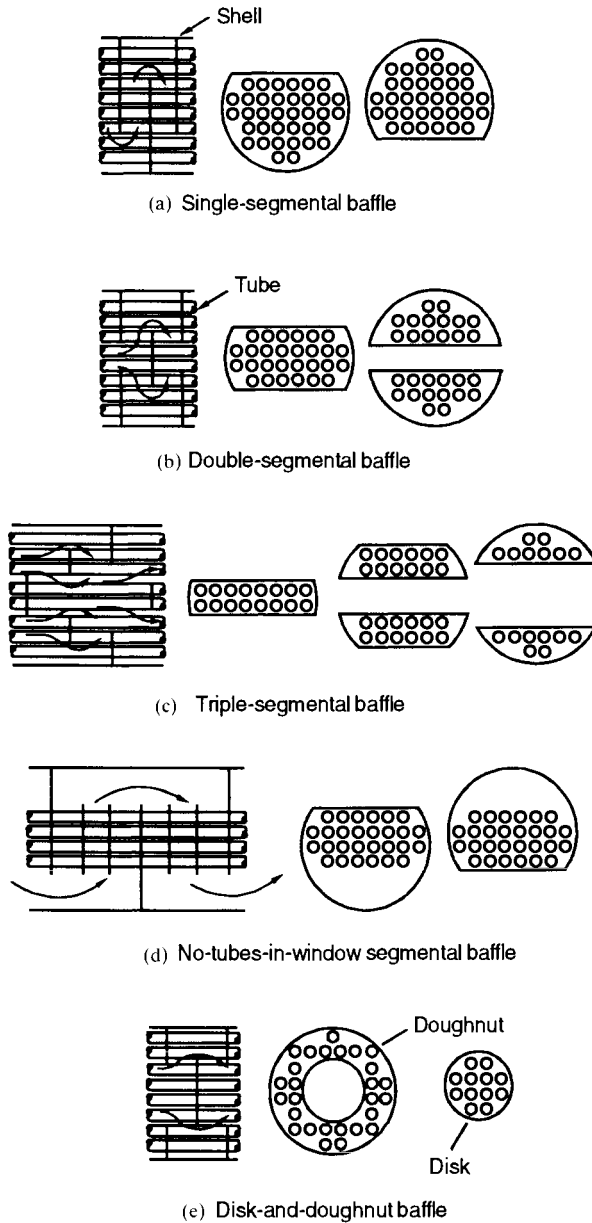
FIGURE 17.4 Plate baffle types: (a) single-segmental baffle, (b) double-segmental baffle, (c) triple-segmental baffle, (d) no-tubes-in-window segmental baffle, and (e) disc-and-doughnut baffle.
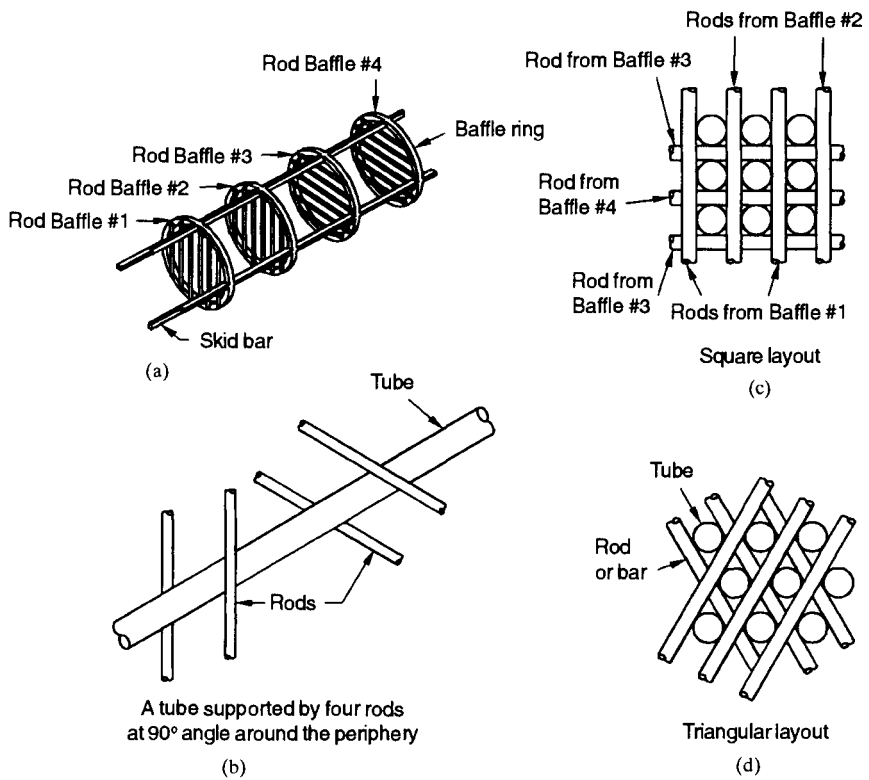
FIGURE 17.5 Rod baffle supports: (a) four rod baffles supported by skid bars (no tubes shown), (b) a tube supported by four rods at 90° angle around the periphery, (c) a square layout of tubes with rods, (d) a triangular layout of tubes with rods.

	30° Triangular Staggered Array	60° Rotated Triangular Staggered Array	90° Square Inline Array	45° Rotated Square Staggered Array
Transverse tube pitch X_t	p_t	$\sqrt{3}\,p_t$	p_t	$\sqrt{2}\,p_t$
Longitudinal tube pitch X_ℓ	$\left(\sqrt{3}/2\right)p_t$	$p_t/2$	p_t	$p_t/\sqrt{2}$
Ratio of minimum free flow area to frontal area, $A_o/A_{fr} = \sigma$	$\dfrac{p_t - d_o}{p_t}$	$\dfrac{\sqrt{3}\,p_t - d_o}{\sqrt{3}\,p_t}$ for $\dfrac{p_t}{d_o} \geq 3.732$ $\dfrac{\sqrt{2}\,p_t - d_o}{\sqrt{3}\,p_t}$ for $\dfrac{p_t}{d_o} \leq 3.732$	$\dfrac{p_t - d_o}{p_t}$	$\dfrac{\sqrt{2}\,p_t - d_o}{\sqrt{2}\,p_t}$ for $\dfrac{p_t}{d_o} \geq 1.707$ $\dfrac{\sqrt{2}\,p_t - d_o}{\sqrt{2}\,p_t}$ for $\dfrac{p_t}{d_o} \leq 1.707$
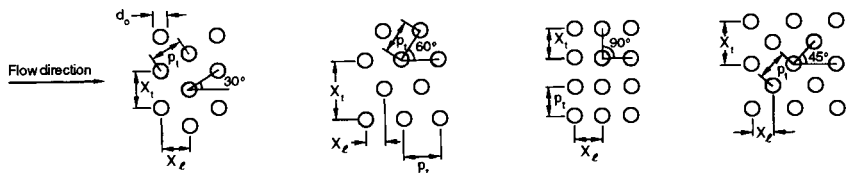
FIGURE 17.6 Nomenclature and geometrical properties of tube banks common in shell-and-tube exchangers.

Two standard types of tube layouts are the square and the equilateral triangle, as shown in Fig. 17.6. The equilateral tube layout can be oriented at a 30° or 60° angle to the flow direction. For the square tube layout, it is 45° and 90°. Note that the 30° and 45° arrangements are staggered, and the 60° and 90° are inline.

For identical tube pitch and flow rates, the tube layouts in decreasing order of shellside heat transfer coefficient and pressure drop are: 30°, 45°, 60°, and 90°, with the 90° layout having the lowest heat transfer coefficient and pressure drop.

The square tube layout (90° or 45°) is used when jet or mechanical cleaning is necessary on the shell side. The triangular tube layout is generally used in the fixed tubesheet design because there is no need for cleaning. It provides a more compact arrangement, usually resulting in a smaller shell, and the strongest header sheet for a specified shellside flow area. Hence, it is preferred when the operating pressure difference between two fluids is large. When mechanical cleaning is required, the 45° layout is preferred for laminar or turbulent flow of a single-phase fluid and for condensing fluid on the shell side. If the pressure drop is constrained on the shell side, the 90° layout is used for turbulent flow. For boiling applications, the 90° layout, which provides vapor escape lanes, is preferred. However, if mechanical cleaning is not required, the 30° layout is preferred for single-phase laminar or turbulent flow and condensing applications involving high ΔT range (a mixture of condensibles). The 60° layout is preferred for condensing applications involving high ΔT range (generally pure vapor condensation) and for boiling applications. Horizontal tube bundles are used for shellside condensation or vaporization.

Tubes.   The tubes are either plain or finned with low fins (0.79–1.59 mm or 0.031–0.063 in) or high fins (generally 15.88 to 19.05 mm or 0.63 to 0.75 in) with 630–1260 fins/m (16–32 fins/in). Consult manufacturers' catalogs for dimensions. The plain tubes range 6.35–50.8 mm (0.25–2 in) in outside diameter. For small exchangers of less than 203 mm (8 in) shell diameter, smaller tubes and pitches are used, but these exchangers fall outside the range of TEMA standards. For mechanical cleaning, the smallest practical tube diameter is 19.05 mm (3/4 in). The tube diameter and length are based on the type of cleaning to be used. If a drilling operation is required, the minimum tube diameter considered is 19.05 or 25.4 mm (3/4 or 1 in), and the maximum tube length is 4.9 m (16 ft). Longer exchangers made with plain tubes are up to 30 m (100 ft), the length limited by the ability to handle such long exchangers in the shop and field.

Tubes are fastened to tubesheets by welding, mechanical rolling, or both. However, these joints are susceptible to thermal and pressure stresses and may develop leaks. In those instances where mixing of the shell and tube fluids would result in corrosive or other hazardous conditions, special designs such as double tubesheets are used, with the space between the tubesheets vented. A double tubesheet can be used only in the following rear head designs: fixed tubesheets (L, M, or N) and the outside packed head (P). Bimetal tubes are used when corrosive conditions of shell and tube fluids require the use of different metals.

Pass Arrangements.   The number of tube passes per exchanger can range from 1 to 16. If more than one pass is used, some loss in thermal efficiency results because of the effect of flow pattern on the mean temperature difference. A design for large numbers of passes results from the need to compensate for low flow rates or the need to maintain high velocities to reduce fouling and get good heat transfer. However, large temperature changes in the tube fluid can, by thermal expansion, cause the floating tubesheets to cock and bind. The passes should be so arranged as to minimize the number of lanes between the passes that are in the same direction as the shell fluid flow. Also, the passes should be arranged so that the tube side can be drained and vented.

Shell Nozzles and Impingement Methods.   Whenever a high-velocity two-phase flow enters the shell, some type of impingement protection is required to avoid tube erosion and vibration; some examples are shown in Fig. 17.7: annular distributors (*d*), impingement plates (*a*, *c*), and impingement rods (*b*). The nozzles must also be sized with the understanding that the tube bundle will partially block the opening. In order to provide escape area with impingement plates, some tubes may have to be removed. The annular distributor is an excellent design that allows any orientation of the nozzles, provides impingement protection, and
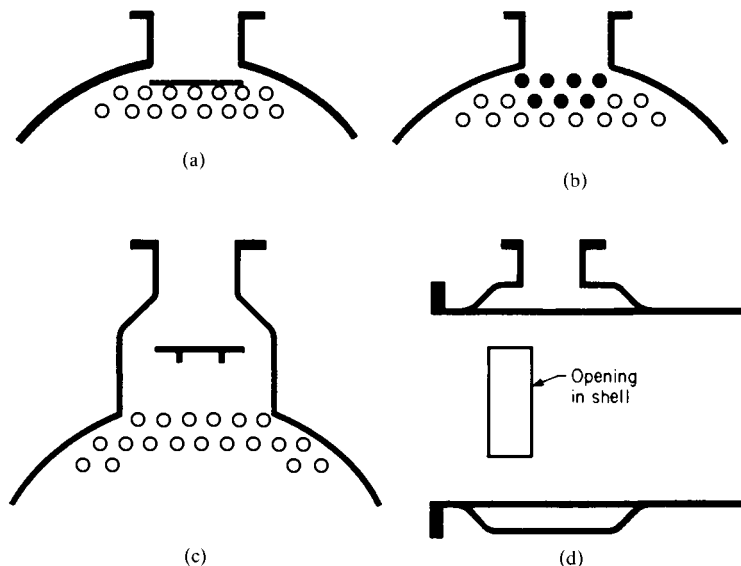
FIGURE 17.7 Impingement protection designs: (*a*) impingement plate, (*b*) impingement rods, (*c*) nozzle impingement baffle, (*d*) vapor belt.

allows baffling closer to the tubesheets and thus higher velocities; however, it is a very expensive design. Dummy rods or extra-heavy walled tubes near the nozzles are also good impingement devices.

Drains and Vents. All exchangers need to be drained and vented; therefore, care should be taken to locate and size drains and vents properly. The proper location depends upon the exchanger design and orientation. Additional openings may be required for instruments such as pressure and temperature sensors.

Selection Procedure. The selection procedure for a specific design of exchanger involves the consideration of many and often conflicting requirements of process conditions, operation, and maintenance. Depending upon the relative importance of these factors as determined by the designer, one or several designs may be selected for evaluation.

Selecting Tubeside Fluid. The choice of the fluid to be on the tube side will influence the selection of the type of exchanger and require evaluation of the following factors to arrive at a satisfactory compromise.

Cleanability. The shell is difficult to clean and requires the cleaner fluid.

Corrosion. Corrosion or process cleanliness may dictate the use of expensive alloys; therefore, the more corrosive fluids are placed inside the tubes in order to save the cost of an alloy shell.

Pressure. High-pressure shells, because of their diameters, are thick-walled and expensive; therefore, high-pressure fluids are placed in the tubes.

Temperatures. The high-temperature fluid should be inside the tubes. High temperatures reduce the allowable stresses in materials, and the effect is similar to high pressure in determining shell thickness. Furthermore, safety of personnel may require the additional cost of insulation if the high-temperature fluid is in the shell.

Hazardous or expensive fluids. The more hazardous or expensive fluid should be placed on the tighter side of the exchanger, which is the tube side of some types of exchangers.

Quantity. A better overall design may be obtained when the smaller quantity of fluid (i.e., the fluid with lower mass flow rate) is placed in the shell. This choice may be to avoid multipass construction with consequent loss of exchanger effectiveness (or the F factor) or to obtain turbulent flow in the shell at low Reynolds numbers.

Viscosity. The critical Reynolds number for turbulent flow on the shell side is about 200; hence, when the fluid flow in the tubes is laminar, it may be turbulent if that same fluid is placed in the shell. However, if the flow is still laminar when in the shell, then it is best to place the fluid back inside the tubes, as it will be somewhat easier to predict both heat transfer and flow distribution.

Pressure drop. If the pressure drop of one fluid is critical and must be accurately predicted, then place that fluid inside the tubes. Pressure drop inside tubes can be calculated with less error, as the pressure drop in the shell will deviate widely from theoretical values depending upon the shell leakage clearances in the particular exchanger.

Selecting Shell and Head. The E shell is the best arrangement; however, if shellside pressure drop is too high, a divided-flow J or G shell may be used. The F shell is a possible alternative when a temperature cross occurs and more than one shell pass is required. Accessibility to the tubes governs the selection of the stationary head, while thermal stress, need for cleaning, possible gasket problems, leakage, plant maintenance experience, and cost are factors influencing the rear head selection. See the earlier section on criteria for mechanical selection for comments on specific heads.

Selecting Tube Size and Layout. The best ratio of heat transfer to pressure drop is obtained with the smallest-diameter tubes; however, the minimum size is determined by the ability to clean the tubes. Pressure drop, tube vibration, tubesheet joints, and cost are several factors limiting the minimum size. Also, a reasonable balance between the tubeside and shellside heat transfer coefficients is desired. The ligament between tubes is governed by the pitch ratio and tube size selected; however, for tubesheet strength, drilling tolerances, and the ability to roll a tight tube joint, a minimum ligament of 3.2 mm (1/8 in) to 6.4 mm (1/4 in) is recommended; the more conservative design uses larger ligaments. The pitch ratio and ligament thickness also affect the shellside fluid velocity and hence the heat transfer and pressure drop.

Tube layouts are either triangular or square; the choice usually depends on the need for shellside cleaning. The square pitch is particularly suitable for cleaning; however, a larger triangular pitch can also be used. For example, a 25.4-mm (1-in) tube on a 34.9-mm (1-3/8-in) triangular pitch will have essentially the same tube count, shell velocities, and heat transfer coefficients; it will also have almost the same clearances for cleaning as a 25.4-mm (1-in) tube on a 31.8-mm (1-1/4-in) square pitch, but the 9.5-mm (3/8-in) ligament will be 50 percent stronger. Other factors including number of tubes and heat transfer for different flow angles (30°, 45°, etc.) are discussed above.

Selecting Baffles. The segmental baffle is commonly used unless problems of pressure drop, tube vibration, or tube support dictate the use of double, triple, or rod baffling or a no-tube-in-window configuration. Note that these alternate choices also seriously affect the reliability of the correlations for heat transfer and pressure drop. The segmental baffles are spaced at a minimum distance of 50.8 mm (2 in) or $0.2D_s$, whichever is larger, and a maximum spacing of D_s. The baffle cut also depends linearly on the baffle spacing and should be 20 percent of D_s at $0.2D_s$ spacing and 33 percent at D_s. The maximum spacing is also determined by the need for tube support. The TEMA maximum unsupported length depends on tube size and material but ranges from 50 to 80 tube diameters (see TEMA standards for specific values). This maximum length usually occurs at the ends of the exchanger in the window area of the first or last baffle, since the end baffle spacing generally is greater (due to nozzle location) than the central baffle. Baffle spacing is selected to obtain a high velocity within a pressure drop limit.

Selecting Nozzles. Nozzle sizes and impingement devices are related by the TEMA rule-of-thumb value of ρV^2 where ρ is the shell fluid density and V is the shell fluid velocity at the

nozzle exit and entrance to the shell side. If $\rho V^2 > 2250$ kg/(m·s²) or 1500 lbm/(ft·s²) for non-corrosive or nonabrasive single-phase fluids, or 750 kg/(m·s²) [500 lbm/(ft·s²)] for other liquids, any vapor-liquid mixture or saturated vapor, then an impingement device is needed. There are several possible configurations indicated in Fig. 17.7. Also the entrance into the tube bundle should have a ρV^2 less than 6000 kg/(m·s²) or 4000 lbm/(ft·s²). The entrance area is the total free area between a nozzle and the projected area on the tube bundle. Meeting these requirements may require removal of some tubes. Usually such dimensions and area are not available until the mechanical drawings have been made. In the design stage, an estimate of these effects is made or a final check calculation is made based on final drawings if the shell pressure drops are marginal. Nozzle locations with respect to the shell flange are governed by pressure vessel codes.

Selecting Tube Passes.   The number of tube passes is kept as low as possible in order to get simple head and tubesheet designs. For even numbers of multiple pass designs, no off-center nozzle on the floating head is required. The flow quantity and the desired minimum tubeside velocity determine the number of tubes per pass; and the total area and tube length then fix the number of passes for the desired performance. However, the number of tube passes must be an even integer; hence, the tube length is variable.

Newer Designs of Shell-and-Tube Exchangers

In a conventional shell-and-tube exchanger, transverse plate baffles are used to support the tubes and direct the shellside stream to flow across the tubes. However, it results in the shell-side flow that wastes pressure drop in turning back and forth without yielding the corresponding heat transfer. The high turnaround pressure drop also results in more leakage flow (shell-to-baffle and baffle-to-tube), lower crossflow, and subsequent lower heat transfer coefficients. The transverse baffles create dead spots or recirculation zones that could promote fouling. Various leakage and bypass flows on the shell side reduce the mean temperature difference in the exchanger and the performance of the exchanger; a very high exchanger effectiveness may not be achievable in this type of exchanger regardless of a large increase in the surface area.

Some of these problems can be eliminated by modifying the shellside design to achieve axial or longitudinal flows; one construction with rod baffles is shown in Fig. 17.5. Such designs require different ways to support the tubes and may virtually eliminate the flow-induced tube vibration problem. Usually heat transfer rate per unit pressure drop is high in such designs; but on the absolute scale, both heat transfer rate and pressure drops are low. As a result, the exchanger usually ends up with a relatively large shell length-to-diameter ratio. In addition to rod and NEST baffle types, several new designs have been developed to induce axial flows, as shown in Fig. 17.8. Figure 17.8a shows a design with a full circle baffle with
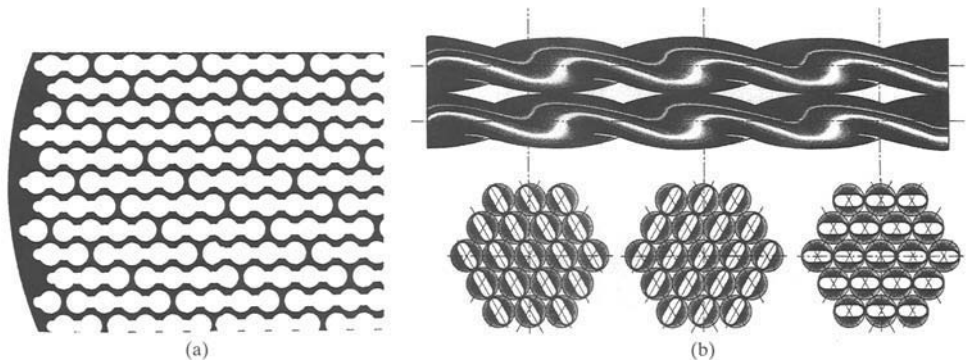

FIGURE 17.8   (*a*) Axial flow baffle, courtesy of Brown Fintube Company, Houston, Texas, (*b*) a twisted tube exchanger, courtesy of ABB Lummus Heat Transfer, Bloomfield, New Jersey.
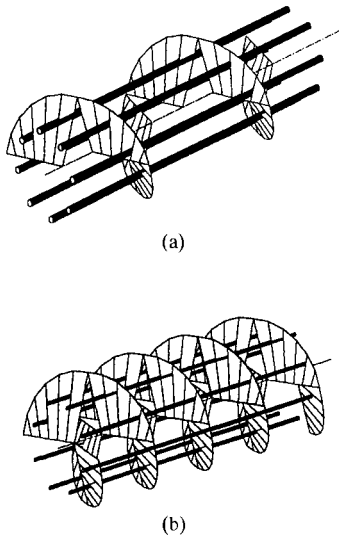
(a)

(b)

FIGURE 17.9 A helical baffle shell-and-tube exchanger: (a) single helix, (b) double helix, courtesy of ABB Lummus Heat Transfer, Bloomfield, New Jersey.

extra space for shellside fluid flow. Figure 17.8b delineates a design with twisted flattened tubes that would yield about 40 percent higher heat transfer coefficient than the conventional shell-and-tube exchanger for the same pressure drop. Plain tubes may be interspersed between twisted tubes for greater design flexibility.

An alternative to conventional and axial flow shell-and-tube exchangers is an exchanger with helical shellside flow. It can be either a single-helix baffle, as shown in Fig. 17.9a, or a double-helix baffle as shown in Fig. 17.9b. There are several variations of angled baffle exchangers available commercially. The helical flow reduces the shellside flow turning losses and fouling tendency compared to a conventional shell-and-tube exchanger, but introduces radial variations in shellside mass flow rate and temperature variations that can be overcome by a radial variation in the tube pitch design.

Compact Heat Exchangers

As defined earlier, compact heat exchangers are characterized by a large heat transfer surface area per unit volume of the exchanger, resulting in reduced space, weight, support structure, and footprint; reduced energy requirement and cost; improved process design, plant layout, and processing conditions; and low fluid inventory compared to conventional designs such as shell-and-tube exchangers. Extremely high heat transfer coefficients h are achievable with small-hydraulic-diameter flow passages with gases, liquids, and two-phase flows. A typical plate heat exchanger has about two times the heat transfer coefficient (h) or overall heat transfer coefficient (U) of a shell-and-tube exchanger for water/water applications. Basic constructions of gas-to-gas compact heat exchangers are plate-fin, tube-fin, and all prime surface recuperators (includes polymer film and laminar flow exchangers) and compact regenerators; basic flow arrangements of two fluids are single-pass crossflow, counterflow, and multipass cross-counterflow. The last two flow arrangements can yield very high exchanger effectiveness or very small temperature differences between fluid streams and very small pressure drops compared to shell-and-tube exchangers. Basic constructions for liquid-to-liquid and liquid-to-phase-change-fluid compact exchangers are: gasketed and welded plate-and-frame, welded stacked plate (without frames), spiral plate, printed circuit, and dimple plate heat exchangers.

Gas-to-Fluid Exchangers. The unique characteristics of compact extended (plate-fin and tube-fin) surface exchangers, as compared with the conventional shell-and-tube exchangers, are: (1) there are many surfaces available with different orders of magnitude of surface area density; (2) there is flexibility in distributing surface area on the hot and cold sides as warranted by design considerations; and (3) there is generally substantial cost, weight, or volume savings.

The important design and operating considerations for compact *extended* surface exchangers are: (1) usually at least one of the fluids is a gas or specific liquid that has low h; (2) fluids must be clean and relatively noncorrosive because of small-hydraulic-diameter (D_h) flow passages and no easy techniques for mechanically cleaning them; (3) the fluid pumping power (i.e., pressure drop) design constraint is often as equally important as the heat transfer rate; (4) operating pressures and temperatures are somewhat limited compared to shell-and-tube exchangers due to joining of the fins to plates or tubes such as brazing and mechanical expansion; (5) with the use of highly compact surfaces, the resultant shape of a gas-to-fluid exchanger is one having a large frontal area and a short flow length; the header design of a compact heat exchanger is thus important for a uniform flow distribution among the very

large number of small flow passages; and (6) the market potential must be large enough to warrant the sizable manufacturing research and tooling costs for new forms to be developed.

Some of the advantages of plate-fin exchangers over conventional shell-and-tube exchangers are as follows. Compact heat exchangers, generally fabricated from thin metallic plates, yield large heat transfer surface area per unit volume (β), typically up to ten times greater than the 50 to 100 m^2/m^3 provided by a shell-and-tube exchanger for general process application and from 1000 to 6000 m^2/m^3 for highly compact gas-side surfaces. Compact liquid or two-phase fluid side surfaces have a ratio ranging from 400 to 600 m^2/m^3. A compact exchanger provides a tighter temperature control and thus is useful for heat sensitive materials. It improves the product (e.g., refining fats from edible oil) and quality (such as a catalyst bed). Also, a compact exchanger provides rapid heating or cooling of a process stream, thus further improving the product quality. The plate-fin exchangers can accommodate multiple (up to 12 or more) fluid streams in one exchanger unit with proper manifolding, thus allowing process integration and cost-effective compact solutions.

The major limitations of plate-fin and other compact heat exchangers are as follows. Plate-fin and other compact heat exchangers have been and can be designed for high-temperature applications (up to about 850°C or 1550°F), high-pressure applications (over 20 MPa or 3000 psig), and moderate fouling applications. However, applications usually do not involve both high temperature and high pressure simultaneously. Highly viscous liquids can be accommodated in the plate-fin exchangers with a proper fin height; fibrous or heavy fouling fluids are not used in the plate-fin exchangers because mechanical cleaning in general is not possible. However, these liquids can be readily accommodated in plate heat exchangers. Most of the plate-fin heat exchangers are brazed. At the current state-of-the-art, the largest size exchanger that can be brazed is about $1.2 \times 1.2 \times 6$ m ($4 \times 4 \times 20$ ft). While plate-fin exchangers are brazed in a variety of metals including aluminum, copper, stainless steels, nickel, and cobalt-based superalloys, the brazing process is generally of proprietary nature and is quite expensive to set up and develop. The plate-fin exchanger is readily repairable if leaks occur at the external border seams.

Fouling is one of the major potential problems in compact heat exchangers (except for plate-and-frame heat exchangers), particularly having a variety of fin geometries or very fine circular or noncircular flow passages that cannot be cleaned mechanically. Chemical cleaning may be possible; thermal baking and subsequent rinsing is possible for small-size units. Hence, extended surface compact heat exchangers may not be used in heavy fouling applications. Nonfouling fluids are used where permissible, such as for clean air or gases, light hydrocarbons, and refrigerants.

Other important limitations of compact heat exchangers are as follows. With a high-effectiveness heat exchanger and/or large frontal area, flow maldistribution could be another serious problem. More accurate thermal design is required, and a heat exchanger must be considered a part of a system. Due to short transient times, a careful design of controls is required for startup of some compact heat exchangers compared to shell-and-tube exchangers. Flow oscillation could be a problem for some compact heat exchangers. No industry standards or recognized practice for compact heat exchangers are yet available, particularly for the power and process industry (note that this is not a problem for aircraft, vehicular, and marine transportation industries). Structural integrity is required to be examined on a case-by-case basis utilizing standard pressure vessel codes.

Liquid-to-Liquid Exchangers. Liquid-to-liquid and phase-change exchangers are plate-and-frame and welded PHE, spiral plate, and printed circuit exchangers. Some of these are described in some detail later in this section. Some compact heat exchangers and their applications are now summarized.

Plate-Fin Exchangers. This type of exchanger has corrugated fins (having triangular and rectangular cross sectional shapes most common) sandwiched between parallel plates (referred to as *plates* or *parting sheets*), as shown in Fig. 17.10. Sometimes fins are incorpo-
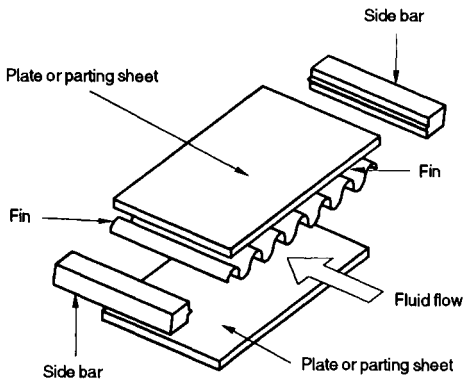
FIGURE 17.10   A plate-fin assembly.

rated in a flat tube with rounded corners (referred to as a *formed tube*), thus eliminating a need for the side bars. If liquid or phase-change fluid flows on the other side, the parting sheet is usually replaced by a flat tube with or without inserts/webs (Fig. 17.11). Other plate-fin constructions include drawn-cup (see Fig. 17.12) or tube-and-center configurations. Fins are die- or roll-formed and are attached to the plates by brazing, soldering, adhesive bonding, welding, or extrusion. Fins may be used on both sides in gas-to-gas heat exchangers. In gas-to-liquid applications, fins are usually used only on the gas side; if employed on the liquid side, they are used primarily for structural strength and flow mixing purposes. Fins are also sometimes used for pressure containment and rigidity.

Plate fins are categorized as (1) plain (i.e., uncut) and straight fins such as plain triangular and rectangular fins, (2) plain but wavy fins (wavy in the main fluid flow direction), and (3) interrupted fins such as offset strip, louver, and perforated. Examples of commonly used fins are shown in Fig. 17.13.

Plate-fin exchangers have been built with a surface area density of up to 5900 m^2/m^3 (1800 ft^2/ft^3). There is a total freedom of selecting fin surface area on each fluid side, as required by the design, by varying fin height and fin density. Although typical fin densities are 120 to 700 fins/m (3 to 18 fins/in), applications exist for as many as 2100 fins/m (53 fins/in). Common fin thicknesses range from 0.05 to 0.25 mm (0.002–0.01 in). Fin heights range from 2 to 25 mm (0.08–1.0 in). A plate-fin exchanger with 600 fins/m (15.2 fins/in) provides about
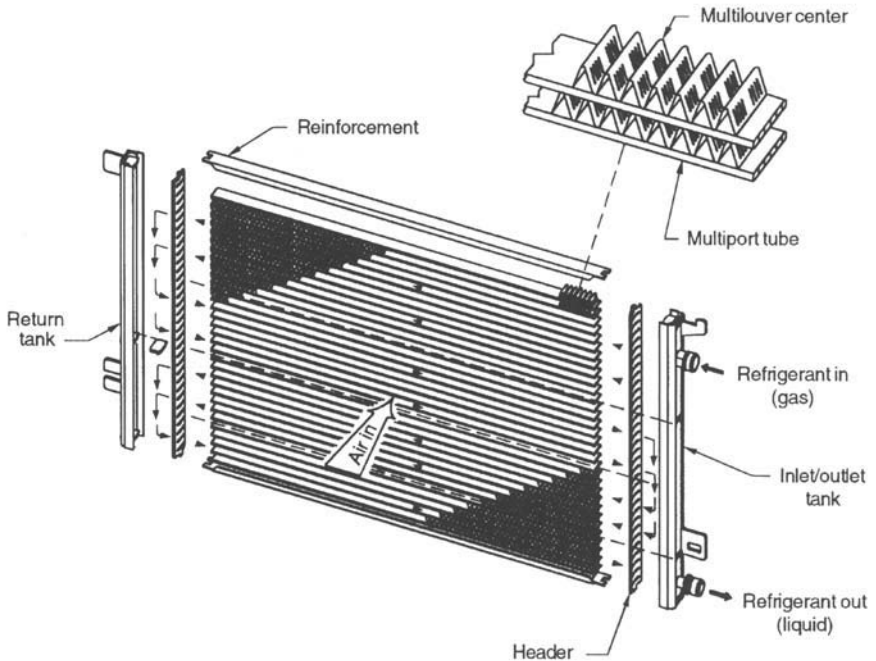
FIGURE 17.11   Flat webbed tube and multilouver fin automotive condenser, courtesy of Delphi Harrison Thermal Systems, Lockport, New York.
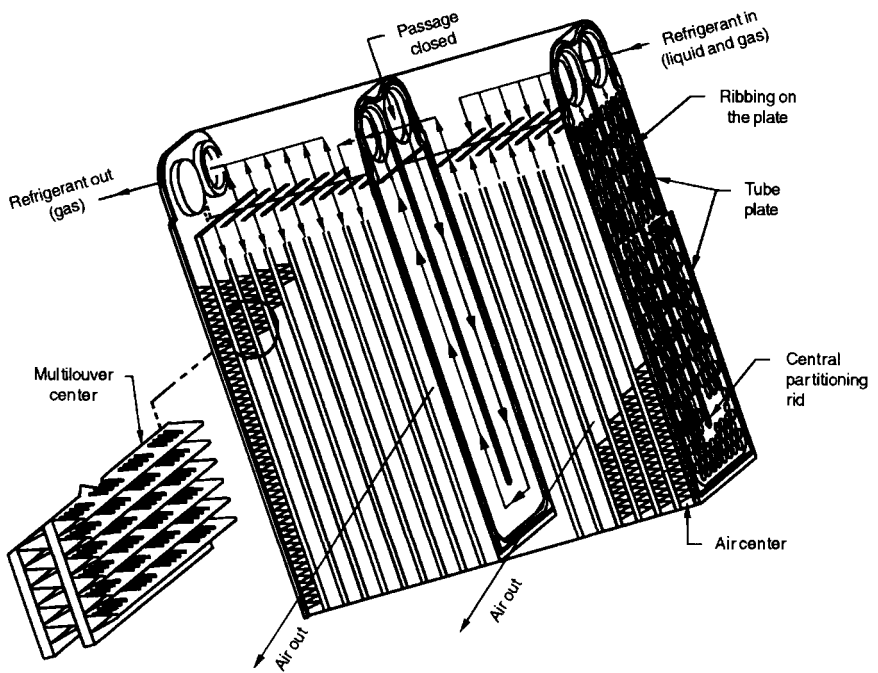
FIGURE 17.12 U-channel ribbed plates and multilouver fin automotive evaporator, courtesy of Delphi Harrison Thermal Systems, Lockport, New York.
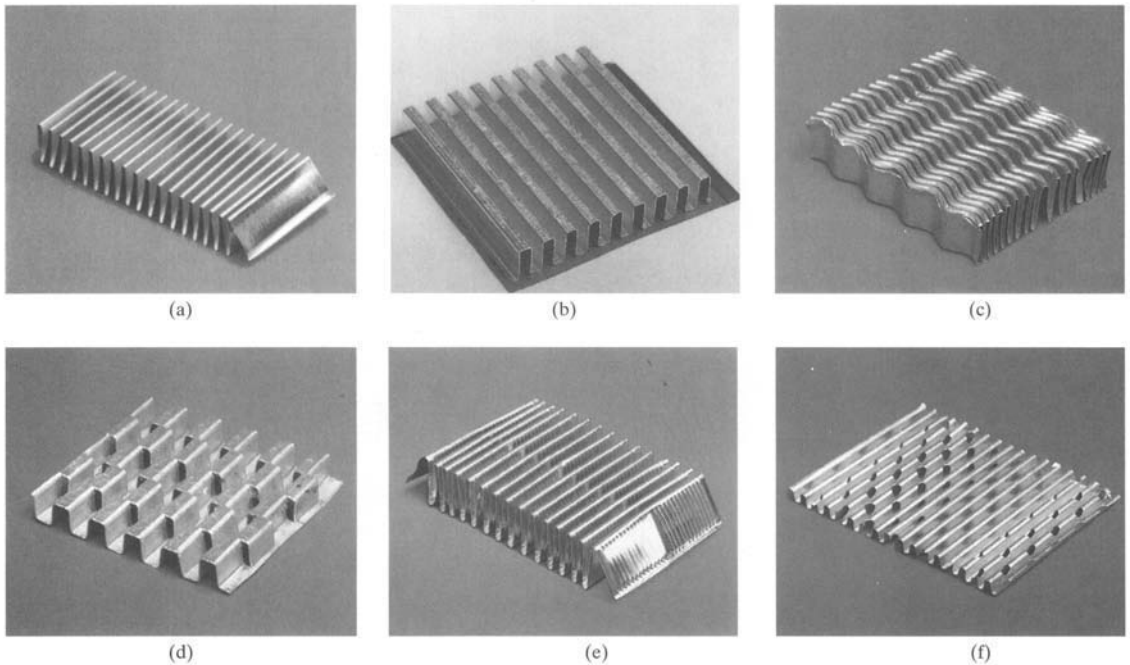
FIGURE 17.13 Fin geometries for plate-fin heat exchangers: (a) plain triangular fin, (b) plain rectangular fin, (c) wavy fin, (d) offset strip fin, (e) multilouver fin, and (f) perforated fin.

1300 m^2 (400 ft^2/ft^3) of heat transfer surface area per cubic meter volume occupied by the fins. Plate-fin exchangers are manufactured in virtually all shapes and sizes and are made from a variety of materials.

Plate-fin exchangers are widely used in electric power plants (gas turbine, steam, nuclear, fuel cell), propulsive power plants (automobile, truck, airplane), thermodynamic cycles (heat pump, refrigeration), and in electronics, cryogenics, gas-liquefaction, air-conditioning, and waste heat recovery systems.

Tube-Fin Exchangers.   In this type of exchanger, round and rectangular tubes are the most common, although elliptical tubes are also used. Fins are generally used on the outside, but they may be used on the inside of the tubes in some applications. They are attached to the tubes by a tight mechanical (press) fit, tension winding, adhesive bonding, soldering, brazing, welding, or extrusion. Depending upon the fin type, the tube-fin exchangers are categorized as follows: (1) an individually finned tube exchanger or simply a *finned tube exchanger,* as shown in Figs. 17.14a and 17.15, having normal fins on individual tubes; (2) a tube-fin exchanger having flat (continuous) fins, as shown in Figs. 17.14b and 17.16; the fins can be plain, wavy, or interrupted, and the array of tubes can have tubes of circular, oval, rectangular, or other shapes; and (3) longitudinal fins on individual tubes. The exchanger having flat (continuous) fins on tubes has been variously referred to as a *plate-fin and tube, plate-finned tube,* and *tube in plate-fin exchanger* in the literature. In order to avoid confusion with a plate-fin exchanger defined above, we will refer to this type as a tube-fin exchanger having flat (plain, wavy, or interrupted) fins. Individually finned tubes are probably more rugged and practical in large tube-fin exchangers. Shell-and-tube exchangers sometimes employ low finned tubes to increase the surface area on the shellside when the shellside heat transfer coefficient is low compared to the tubeside coefficient. The exchanger with flat fins is usually less expensive on a unit heat transfer surface area basis because of its simple and mass-production-type construction features. Longitudinal fins are generally used in condensing applications and for viscous fluids in double pipe heat exchangers.

Tube-fin exchangers can withstand high pressures on the tube side. The highest temperature is again limited by the type of bonding, materials employed, and material thickness. Tube-fin exchangers with an area density of about 3300 m^2/m^3 (1000 ft^2/ft^3) are commercially available. On the fin side, the desired surface area can be employed by using the proper fin
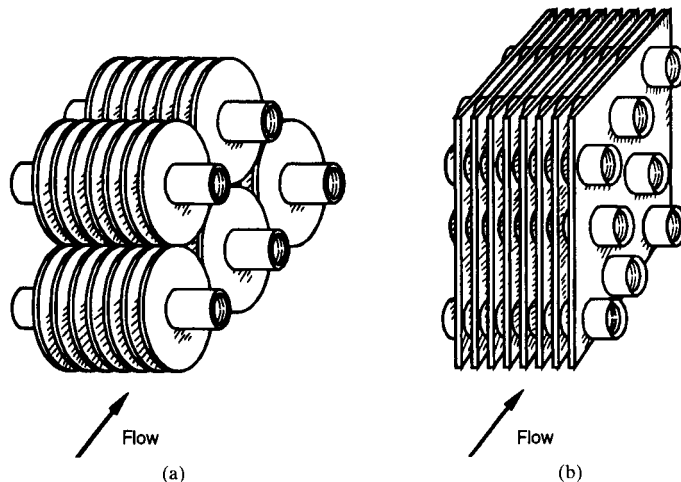

Flow   Flow

(a)   (b)

FIGURE 17.14   (a) Individually finned tubes; (b) flat or continuous fins on an array of tubes.

Helical

Fully cut on helix

Annular

Fully cut along the axis

Studed

Partially cut on helix

Serrated

Slotted wavy helical

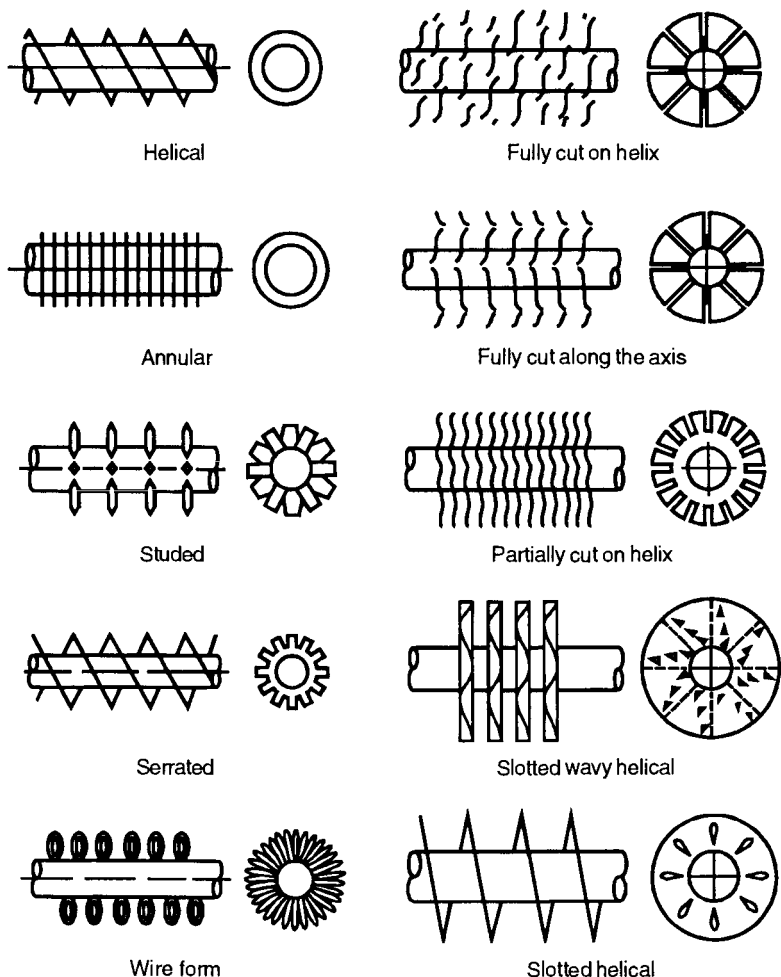Wire form

Slotted helical

FIGURE 17.15   Individually finned tubes.

density and fin geometry. The typical fin densities for flat fins vary from 250 to 800 fins/m (6–20 fins/in), fin thicknesses vary from 0.08 to 0.25 mm (0.003–0.010 in), and fin flow lengths from 25 to 250 mm (1–10 in). A tube-fin exchanger having flat fins with 400 fins/m (10 fins/in) has a surface area density of about 720 m^2/m^3 (220 ft^2/ft^3). These exchangers are extensively used as condensers and evaporators in air-conditioning and refrigeration applications, as condensers in electric power plants, as oil coolers in propulsive power plants, and as air-cooled exchangers (also referred to as a fin-fan exchanger) in process and power industries.

Regenerators.   The regenerator is a storage type exchanger. The heat transfer surface or elements are usually referred to as a matrix in the regenerator. In order to have continuous operation, either the matrix must be moved periodically into and out of the fixed streams of gases, as in a *rotary* regenerator (Fig. 17.17*a*), or the gas flows must be diverted through valves to and from the fixed matrices as in a *fixed-matrix* regenerator (Fig. 17.17*b*). The latter is also sometimes referred to as a *periodic-flow regenerator* or a *reversible heat accumulator.* A third type of regenerator has a fixed matrix (in the disk form) and the fixed stream of gases, but the
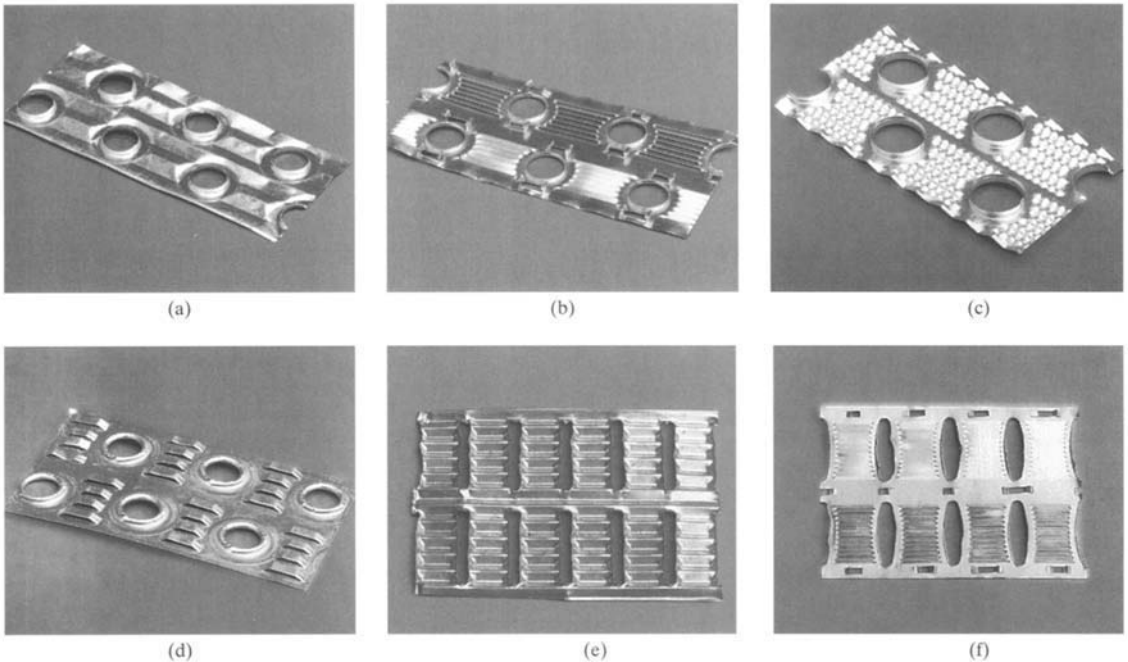
FIGURE 17.16   Flat or continuous fins on an array of tubes: (*a*) wavy fin. (*b*) multilouver fin, (*c*) fin with structured surface roughness (circular dimples), (*d*) parallel louver fin; all four fins with staggered round tubes. (*e*) wavy fin on inline flat tubes, and (*f*) multilouver fin with inline elliptical tubes.

gases are ducted through rotating hoods (headers) to the matrix as shown in Fig. 17.17*c*. This Rothemuhle regenerator is used as an air preheater in some power generating plants. The thermodynamically superior counterflow arrangement is usually employed for regenerators.

The *rotary regenerator* is usually a disk type in which the matrix (heat transfer surface) is in a disk form and fluids flow axially. It is rotated by a hub shaft or a peripheral ring gear drive. For a rotary regenerator, the design of seals to prevent leakages of hot to cold fluids and vice versa becomes a difficult task, especially if the two fluids are at significantly differing pressures. Rotating drives also pose a challenging mechanical design problem.
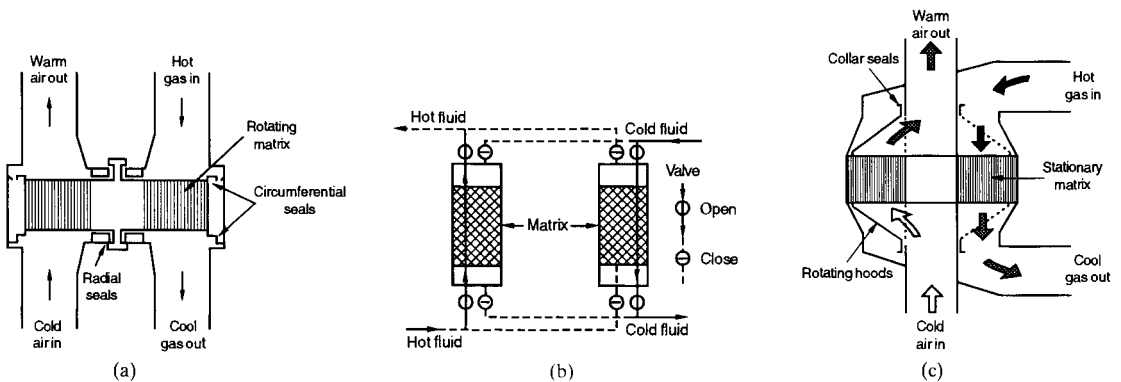
FIGURE 17.17   Regenerators: (*a*) rotary, (*b*) fixed-matrix, and (*c*) rotating hoods.

Major advantages of rotary regenerators follow: For a highly compact regenerator, the cost of the regenerator surface per unit of heat transfer area is usually substantially lower than that for the equivalent recuperator. Another important advantage for a counterflow regenerator compared to a counterflow recuperator is that the design of inlet and outlet headers to distribute the hot and cold gases in the matrix is simple. This is because both fluids flow in different sections (separated by radial seals) of a rotary regenerator. The matrix surface has self-cleaning characteristics for low gas-side fouling because the hot and cold gases flow alternately in the opposite directions in the same fluid passage. Compact surface area density and the counterflow arrangement make the regenerator ideally suited for gas-to-gas heat exchanger applications requiring high exchanger effectiveness, generally exceeding 85 percent. A major disadvantage of a regenerator is an unavoidable carryover of a small fraction of the fluid trapped in the passage to the other fluid stream just after the periodic flow switching. Since fluid contamination (small mixing) is prohibited with liquids, the regenerators are used exclusively for gas-to-gas heat or energy recovery applications. Cross contamination can be minimized significantly by providing a purge section in the disk and using double-labyrinth seals.

Rotary regenerators have been designed for surface area density of up to about 6600 m^2/m^3 (2000 ft^2/ft^3) and exchanger effectiveness exceeding 85 percent for a number of applications. They can employ thinner-stock material, resulting in the lowest amount of material for a given exchanger effectiveness and pressure drop of any heat exchanger known today. The metal rotary regenerators have been designed for continuous operating temperatures up to about 790°C (1450°F) and ceramic matrices for higher-temperature applications; these regenerators are designed up to 400 kPa or 60 psi pressure difference between hot and cold gases. Plastic, paper, and wool are used for regenerators operating below 65°C (150°F) temperatures and one atmospheric pressure. Typical regenerator rotor diameters and rotational speeds are as follows: up to 10 m (33 ft) and 0.5–3 rpm for power plant regenerators, 0.25 to 3 m (0.8 to 9.8 ft) and up to 10 rpm for air-ventilating regenerators, and up to 0.6 m (24 in) and up to 18 rpm for vehicular regenerators. Refer to Shah [1] for the description of the *fixed-matrix regenerator,* also referred to as a *periodic-flow, fixed-bed, valved,* or *stationary* regenerator.

Plate-Type Exchangers. These exchangers are usually built of thin plates (all prime surface). The plates are either smooth or have some form of corrugations, and they are either flat or wound in an exchanger. Generally, these exchangers cannot accommodate very high pressures, temperatures, and pressure and temperature differentials. These exchangers may be further classified as plate, spiral plate, lamella, and platecoil exchangers, as shown in Fig. 17.1. The plate heat exchanger, being the most important of these, is described next.

The *plate-and-frame* or *gasketed plate heat exchanger* (PHE) consists of a number of thin rectangular corrugated or embossed metal plates sealed around the edges by gaskets and held
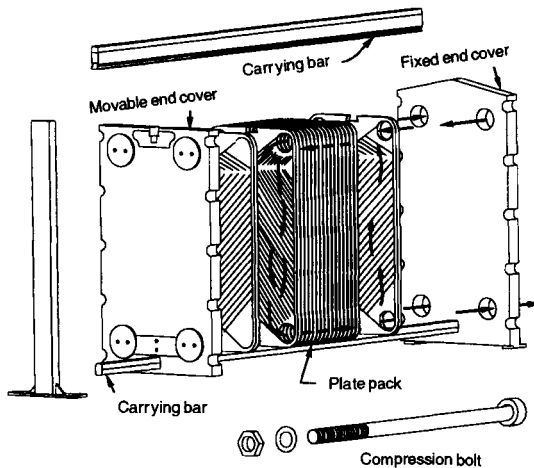

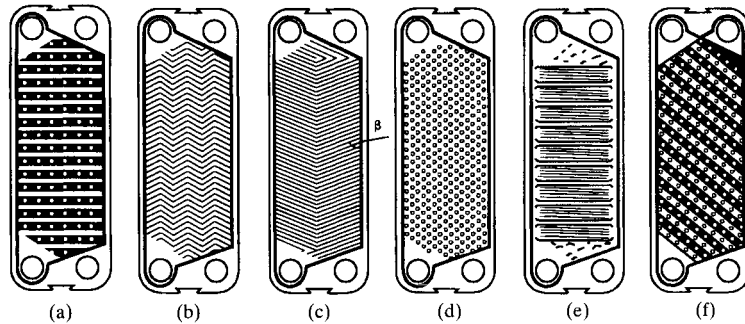FIGURE 17.18 A plate-and-frame or gasketed plate heat exchanger.

FIGURE 17.19 Plate patterns: (*a*) washboard, (*b*) zig-zag, (*c*) chevron or herring-bone, (*d*) protrusions and depressions, (*e*) washboard with secondary corrugations, and (*f*) oblique washboard.

together in a frame as shown in Fig. 17.18. The plate pack with fixed and movable end covers is clamped together by long bolts, thus compressing the gaskets and forming a seal. Typical plate geometries (corrugated patterns) are shown in Fig. 17.19. Sealing between the two fluids is accomplished by elastomeric molded gaskets (typically 5 mm or 0.2 in thick) that are fitted in peripheral grooves mentioned earlier. The most conventional flow arrangement is 1 pass–1 pass counterflow with all inlet and outlet connections on the fixed end cover. By blocking flow through some ports with proper gasketing, either one or both fluids could have more than one pass. Also, more than one exchanger can be accommodated in a single frame with the use of intermediate connector plates such as up to five "exchangers" or sections to heat, cool, and regenerate heat between raw milk and pasteurized milk in a milk pasteurization application.

Typical plate heat exchanger dimensions and performance parameters are given in Table 17.2 [1]. Any metal that can be cold-worked is suitable for PHE applications. The most com-

TABLE 17.2 Plate-and-Frame Exchanger Geometrical, Operational, and Performance Parameters [1]

Unit	
Maximum surface area, m²	2500
Number of plates	3 to 700
Port size, mm	up to 400
Plates	
Thickness, mm	0.5 to 1.2
Size, m²	0.03 to 3.6
Spacing, mm	1.5 to 5
Width, mm	70 to 1200
Length, m	0.6 to 5
Operation	
Pressure, MPa	0.1 to 2.5
Temperature, °C	−40 to 260
Maximum port velocity, m/s	6
Channel flow rates, m³/h	0.05 to 12.5
Maximum unit flow rate, m³/h	2500
Performance	
Temperature approach, °C	as low as 1
Heat exchanger effectiveness, %	up to 93%
Heat transfer coefficients for water-water duties, W/m²K	3000–7000

mon plate materials are stainless steel (AISI 304 or 316) and titanium. Plates made from Incoloy 825, Inconel 625, and Hastelloy C-276 are also available. Nickel, cupronickel, and monel are rarely used. Carbon steel is not used due to low corrosion resistance for thin plates. The heat transfer surface area per unit volume for plate exchangers ranges from 120 to 660 m^2/m^3 (37 to 200 ft^2/ft^3).

Since plate heat exchangers are mainly used for liquid-to-liquid heat exchange applications, the characteristics of these exchangers will be briefly summarized here. The most significant characteristic of a gasketed PHE is that it can easily be taken apart into its individual components for cleaning, inspection, and maintenance. The heat transfer surface area can be readily changed or rearranged through the flexibility of the number of plates, plate type, and pass arrangements. The high turbulence due to plates reduces fouling to about 10 to 25 percent that of a shell-and-tube exchanger. Because of the high heat transfer coefficients, reduced fouling, absence of bypass and leakage streams, and pure counterflow arrangements, the surface area required for a plate exchanger is 1/2 to 1/3 that of a shell-and-tube exchanger for a given heat duty. This would reduce the cost, overall volume, and maintenance space for the exchanger. Also, the gross weight of a plate exchanger is about 1/6 that of an equivalent shell-and-tube exchanger. Leakage from one fluid to the other cannot take place unless a plate develops a hole. Since the gasket is between the plates, any leakage from the gaskets is to the outside of the exchanger. The residence time for fluid particles on a given side is approximately the same for uniformity of heat treatment in applications such as sterilizing, pasteurizing, and cooking. There are no significant hot or cold spots in the exchanger that could lead to the deterioration of heat-sensitive fluids. The volumes of fluids held up in the exchanger are small. This is important with expensive fluids for faster transient response and a better process control. Finally and most importantly, high thermal performance can be achieved in plate exchangers. The high degree of counterflow in PHEs makes temperature approaches of up to 1°C (2°F) possible. The high thermal effectiveness (up to about 93 percent) facilitates economical low-grade heat recovery. Flow-induced vibration, noise, high thermal stresses, and entry impingement problems of shell-and-tube heat exchangers do not exist for plate heat exchangers.

Plate heat exchangers are most suitable for liquid-liquid heat transfer duties that require uniform and rapid heating or cooling, as is often the case when treating thermally sensitive fluids. Special plates capable of handling two-phase fluids (e.g., steam condensation) are available. PHEs are not suitable for erosive duties or for fluids containing fibrous materials. In certain cases, suspensions can be handled; but, to avoid clogging, the largest suspended particle should be at most one-third the size of the average channel gap. Viscous fluids can be handled, but extremely viscous fluids lead to flow maldistribution problems, especially on cooling.

Some other inherent limitations of the plate heat exchangers are due to the plates and gaskets as follows. The plate exchanger is used for a maximum pressure of about 2.5 MPa gauge (360 psig) but usually below 1.0 MPa gauge (150 psig). The gasket materials (except for the recent Teflon-coated type) restrict the use of PHEs in highly corrosive applications; they also limit the maximum operating temperature to 260°C (500°F) but usually below 150°C (300°F) to avoid the use of expensive gasket materials. Gasket life is sometimes limited. Frequent gasket replacement may be needed in some applications. Pinhole leaks are hard to detect. For equivalent flow velocities, pressure drop in a plate exchanger is very high compared to a shell-and-tube exchanger. However, the flow velocities are usually low, and plate lengths are short, so the resulting pressure drops are generally acceptable. Some of the largest units have a total surface area of about 2,500 m^2 (27,000 ft^2) per frame. Large differences in fluid flow rates of two streams cannot be handled in a PHE.

Gasketed plate-and-frame heat exchangers are most common in the dairy, beverage, general food processing, and pharmaceutical industries where their ease of cleaning and the thermal control required for sterilization/pasteurization makes them ideal. They are used in the synthetic rubber industry, paper mills, and petrochemical plants. In addition, they are also used in the process industry for water-water duties (heating, cooling, and temperature control) with stainless steel construction when rather high pressure drops are available.

One of the limitations of gasketed plate heat exchanger is the presence of the gaskets, which restricts their use to compatible fluids (with respect to the gasket material) and limits operating temperatures and pressures. In order to overcome this limitation, a number of *welded plate heat exchanger* designs have surfaced, with a welded pair of plates for one or both fluid sides. However, the disadvantage of such a design is the loss of disassembling flexibility on the fluid sides where the welding is done. Essentially, welding is done around the complete circumference where the gasket is normally placed. A *stacked plate heat exchanger* is another welded plate heat exchanger design from Pacinox in which rectangular plates are stacked and welded at the edges. The physical size limitations of PHEs (1.2 m wide × 4 m long max., 4 × 13 ft) are considerably extended to 1.5 m wide × 20 m long (5 × 66 ft) in this exchanger. A maximum surface area of over 10,000 m^2 or 100,000 ft^2 can be accommodated in one unit. The potential maximum operating temperature is 815°C (1500°F), with an operating pressure of up to 20 MPa (3000 psig) when the stacked plate assembly is placed in a cylindrical pressure vessel. For operating pressures below 2 MPa (300 psig) and operating temperatures below 200°C (400°F), the plate bundle is not contained in a pressure vessel but is bolted between two heavy plates. Some of the applications of this exchanger are catalytic reforming, hydrosulfurization, crude distillation, synthesis converter feed effluent exchanger for methanol, propane condenser, and so on.

A vacuum *brazed plate heat exchanger* is a compact PHE for high-temperature and high-pressure duties, and it does not have gaskets, tightening bolts, frame bars, or carrying and guide bars. It simply consists of stainless steel plates and two end plates brazed together. The brazed unit can be mounted directly on piping without brackets and foundations.

A number of other plate heat exchanger constructions have been developed to address some of the limitations of the conventional PHEs. A double-wall PHE is used to avoid mixing of the two fluids. A wide-gap PHE is used for fluids having high fiber content or coarse particles. A graphite PHE is used for highly corrosive fluids. A flow-flex exchanger has plain fins on one side between plates, and the other side has conventional plate channels and is used to handle asymmetric duties (flow rate ratio of 2 to 1 and higher). A design guide for the selection of these exchangers is presented in Table 17.3, which takes into consideration fluids, operating cost, and maintenance cost [6].
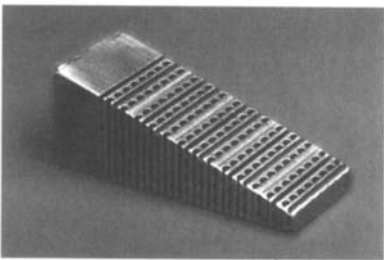

The *printed circuit heat exchanger,* as shown in Fig. 17.20, has only primary heat transfer surface as PHEs. Fine grooves are made in the plate by using the same techniques as those employed for making printed electrical circuits. Very high surface area densities (1000–5000 m^2/m^3 or 300–1520 ft^2/ft^3) are achievable. A variety of materials such as 316 SS, 316L SS, 304 SS, 904L SS, cupronickel, monel, nickel, and superalloys can be used. This exchanger has been successfully used with relatively clean gases, liquids, and phase-change fluids in chemical processing, fuel processing, waste heat recovery, and refrigeration industries. Again, this exchanger is a new construction with limited current special applications.

FIGURE 17.20   A segment of a printed circuit heat exchanger, courtesy of Heatric Ltd, Dorset, UK.

EXCHANGER SINGLE-PHASE HEAT TRANSFER AND PRESSURE DROP ANALYSIS

Our objective is to develop relationships between the heat transfer rate q exchanged between two fluids, heat transfer surface area A, heat capacity rates C of individual fluid streams, overall heat transfer coefficient U, and fluid terminal temperatures. In this section, starting with idealizations for heat exchanger analysis and the thermal circuit associated with a two-fluid exchanger, ε-NTU, P-NTU, and MTD methods used for an exchanger analysis are presented,

TABLE 17.3 A Guide for Selection of Plate Heat Exchangers [6]

	Std. PHE	Flow-Flex PHE	Wide-Gap PHE	Double Wall PHE	Semi-welded PHE	Diabon F graphite PHE	Brazed PHE	Fully welded PHE
Performance data								
Pressure range, full vacuum to MPa (psi)	2.5 (355)	2.0 (285)	0.9 (130)	2.5 (355)	2.5 (355)	0.6 (85)	3.0 (427)	4.0 (570)
Temperature range								
°C (Min)	−30	−30	−30	−30	−30	0	−195	−50
(Max)	+180	+180	+180	+180	+180	+140	+225	+350
Service								
Liquid/liquid	1	1	1	1	1	1	1	1
Gas/liquid	1–3*	1–3*	1–3*	1–3*	1–3*	1–3*	1	1–3*
Gas/gas	1–3*	1–3*	1–3*	1–3*	1–3*	1–3*	1–3*	1–3*
Condensation	1–3*	1–3*	1–3*	1–3*	1–3*	1–3*	1	1–3*
Vaporization	1–3*	1–3*	1–3*	1–3*	1–3*	1–3*	1	1–3*
Nature of media								
Corrosive	1	1	1	1	1	1	3	1
Aggressive	3	3	3	3	1	1	4	1
Viscous	1	1	1	1	1	1	3	1
Heat-sensitive	1	1	1	1	1	1	1	1
Hostile reaction	3	3	3	1	2	3	4	2
Fibrous	4	3	1	4	4	4	4	4
Slurries and suspension	3	2	2	3	3	3	4	4
Fouling	3	2	2	3	3	3	3	3
Inspection								
Corrosion	A	A	A	A	B	A	C	C
Leakage	A	A	A	A	A	A	C	C
Fouling	A	A	A	A	B	A	C	C
Maintenance								
Mechanical cleaning	A	A	A	A	B	A	C	C
Modification	A	A	A	A	A	A	C	C
Repair	A	A	A	A	A	A	C	C

1 = Usually best choice
2 = Often best choice
3 = Sometimes best choice
4 = Seldom best choice
A = Both sides
B = One side
C = No side
* Depending on operating pressures, gas/vapor density, etc.

followed by the fin efficiency concept and various expressions. Finally, pressure drop expressions are outlined for various single-phase exchangers.

Heat Transfer Analysis

Idealizations for Heat Exchanger Analysis.   The energy balances, the rate equations, and the subsequent analyses are subject to the following idealizations.

1. The heat exchanger operates under steady-state conditions (i.e., constant flow rate, and fluid temperatures at the inlet and within the exchanger independent of time).

2. Heat losses to the surroundings are negligible (i.e., the heat exchanger is adiabatic).

3. There are no thermal energy sources and sinks in the exchanger walls or fluids.

4. In counterflow and parallelflow exchangers, the temperature of each fluid is uniform over every flow cross section. From the temperature distribution point of view, in cross-flow exchangers each fluid is considered mixed or unmixed at every cross section depending upon the specifications. For a multipass exchanger, the foregoing statements apply to each pass depending on the basic flow arrangement of the passes; the fluid is considered mixed or unmixed between passes.

5. Either there are no phase changes in the fluid streams flowing through the exchanger or the phase changes (condensation or boiling) occur under one of the following conditions: (a) phase change occurs at a constant temperature as for a single component fluid at constant pressure; the effective specific heat for the phase-changing fluid is infinity in this case, and hence $C_{max} \to \infty$; (b) the temperature of the phase-changing fluid varies linearly with heat transfer during the condensation or boiling. In this case, the effective specific heat is constant and finite for the phase-changing fluid.

6. The specific heats (as well as other fluid properties implicitly used in NTU) of each fluid are constant throughout the exchanger.

7. The velocity and temperature at the entrance of the heat exchanger on each fluid side are uniform.

8. For an extended surface exchanger, the overall extended surface efficiency η_o is considered uniform and constant.

9. The individual and overall heat transfer coefficients are constant (independent of temperature, time, and position) throughout the exchanger, including the case of phase-changing fluid in idealization 5.

10. The heat transfer surface area is distributed uniformly on each fluid side. In a multipass unit, heat transfer surface area is equal in each pass.

11. For a plate-baffled shell-and-tube exchanger, the temperature rise (or drop) per baffle pass is small compared to the overall temperature rise (or drop) of the shell fluid in the exchanger so that the shell fluid can be treated as mixed at any cross section. This implies that the number of baffles is large.

12. The fluid flow rate is uniformly distributed through the exchanger on each fluid side in each pass. No flow maldistribution, flow stratification, flow bypassing, or flow leakages occur in any stream. The flow condition is characterized by the bulk (or mean) velocity at any cross section.

13. Longitudinal heat conduction in the fluid and in the wall is negligible.

Idealizations 1 through 4 are necessary in a theoretical analysis of steady-state heat exchangers. Idealization 5 essentially restricts the analysis to single-phase flow on both sides or on one side with a dominating thermal resistance. For two-phase flows on both sides, many

of the foregoing idealizations are not valid, since mass transfer in phase change results in variable properties and variable flow rates of each phase, and the heat transfer coefficients vary significantly. As a result, the heat exchanger cannot be analyzed using the theory presented here.

If idealization 6 is not valid, divide the exchanger into small segments until the specific heats and/or other fluid properties can be treated as constant. Refer to the section on maldistribution later if idealization 7 is violated. Some investigation is reported in the literature when idealizations 8 through 13 are not valid; this is summarized in the following section. If any of these idealizations are not valid for a particular exchanger application, the best solution is to work directly with either local energy balances and the overall rate equations (see Eqs. 17.1 and 17.2) or their modified form by including a particular effect, and to integrate or numerically analyze them over a small exchanger segment in which all of the idealizations are valid.

Thermal Circuit.   In order to develop relationships among variables for various exchangers, consider a two-fluid exchanger (in Fig. 17.21 a counterflow exchanger is given as an example). Two energy conservation differential equations for an overall adiabatic two-fluid exchanger with any flow arrangement are

$$dq = q''dA = -C_h dT_h = \pm C_c dT_c \tag{17.1}$$

Here dq is heat transfer rate from the hot to cold fluid across the surface area dA; C_h and C_c are the heat capacity rates for the hot and cold fluids, and the $\pm$ sign depends on whether dT_c is increasing or decreasing with increasing dA. The overall rate equation on a local basis is

$$dq = q''dA = U(T_h - T_c)_{loc}dA = U\Delta T dA \tag{17.2}$$

where U is the overall heat transfer coefficient.

Integration of Eqs. 17.1 and 17.2 across the exchanger surface area results in overall energy conservation and rate equations as follows.

$$q = C_h(T_{h,i} - T_{h,o}) = C_c(T_{c,o} - T_{c,i}) \tag{17.3}$$

and
$$q = UA\Delta T_m = \Delta T_m / \mathbf{R}_o \tag{17.4}$$

Here ΔT_m is the true mean temperature difference dependent on the exchanger flow arrangement and degree of fluid mixing within each fluid stream. The inverse of the overall thermal conductance UA is referred to as the overall thermal resistance $\mathbf{R}_o$, which consists of component resistances in series as shown in Fig. 17.22 as follows.
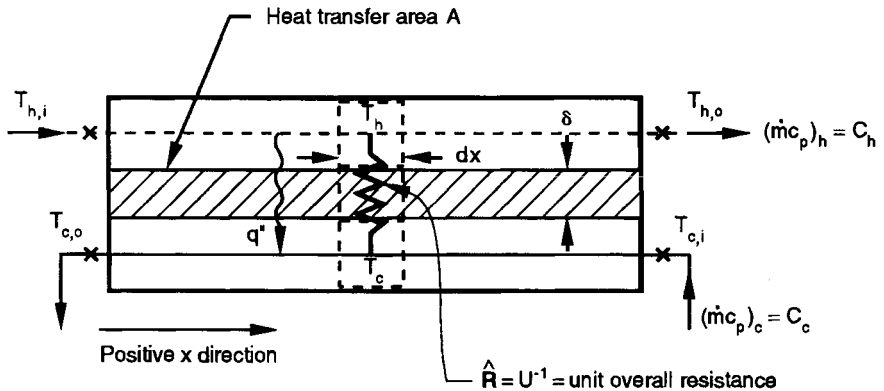

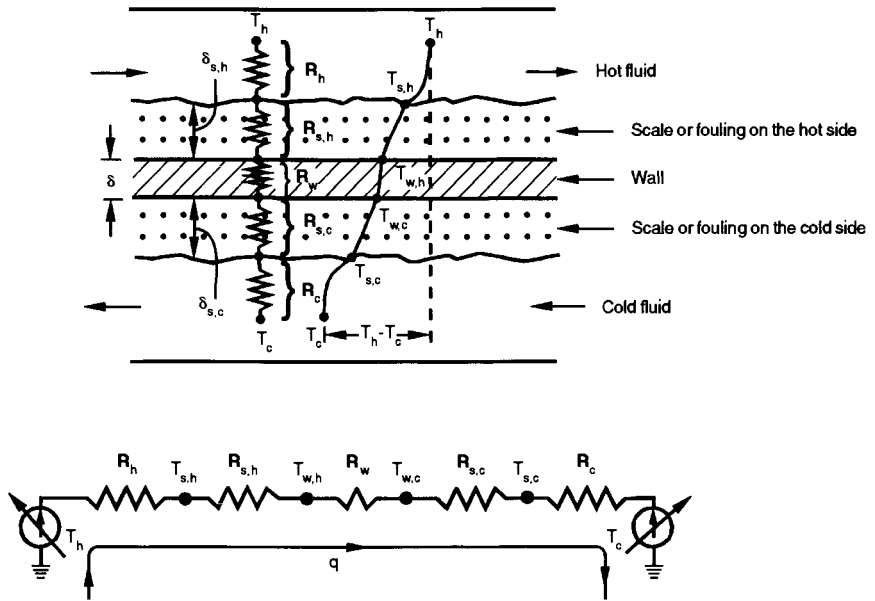**FIGURE 17.21**   Nomenclature for heat exchanger variables.

FIGURE 17.22   Thermal circuit for heat transfer in an exchanger.

$$\mathbf{R}_o = \mathbf{R}_h + \mathbf{R}_{s,h} + \mathbf{R}_w + \mathbf{R}_{s,c} + \mathbf{R}_c \qquad (17.5)$$

where the subscripts *h, c, s,* and *w* denote hot, cold, fouling (or scale), and wall, respectively. In terms of the overall and individual mean heat transfer coefficients, Eq. 17.5 is represented as

$$\frac{1}{U_m A} = \frac{1}{(\eta_o h_m A)_h} + \frac{1}{(\eta_o h_s A)_h} + \mathbf{R}_w + \frac{1}{(\eta_o h_s A)_c} + \frac{1}{(\eta_o h_m A)_c} \qquad (17.6)$$

where η_o is the total surface effectiveness of an extended (fin) surface and is related to the fin efficiency η_f, surface area A_f, and the total (primary plus secondary or finned) surface area A as defined in Eq. 17.24. Note that no fins are shown in the upper sketch of Fig. 17.22; however, η_o is included in the aforementioned various resistance terms in order to make them most general. For all prime surface exchangers (i.e., having no fins or extended surface), $\eta_{o,h}$ and $\eta_{o,c}$ are unity.

A comparison of each respective term of Eqs. 17.5 and 17.6 defines the value of individual thermal resistances. Note $U = U_m$ and $h = h_m$ in Eq. 17.6, since we have idealized constant and uniform individual and overall heat transfer coefficients (the same equation still holds for local U and h values).

The wall thermal resistance $\mathbf{R}_w$ of Eq. 17.5 or 17.6 is given by

$$\mathbf{R}_w = \begin{cases} \delta/A_w k_w & \text{for flat walls with a single layer} \\[2mm] \dfrac{\ln (d_o/d_i)}{2\pi k_w L N_t} & \text{for circular tubes with a single-layer wall} \\[3mm] \dfrac{1}{2\pi L N_t}\left[\sum_j \dfrac{\ln (d_{j+1}/d_j)}{k_{w,j}}\right] & \text{for circular tubes with a multiple-layer wall} \end{cases} \qquad (17.7)$$

where δ is the wall (plate) thickness, A_w is the total wall area for conduction, k_w is the thermal conductivity of the wall material, d_o and d_i are the tube outside and inside diameters, L is the

exchanger length, and N_t is the number of tubes. A flat or plain wall is generally associated with a plate-fin or an all-prime surface plate heat exchanger. In this case, $A_w = L_1 L_2 N_p$ where L_1, L_2, and N_p are the length, width, and total number of separating plates.

If there is any contact or bond resistance present between the fin and tube or plate on the hot or cold fluid side, it is included as an added thermal resistance on the right side of Eq. 17.5 or 17.6. For a heat pipe heat exchanger, additional thermal resistances associated with the heat pipe should be included on the right side of Eq. 17.5 or 17.6; these resistances are evaporator resistance at the evaporator section of the heat pipe, viscous vapor flow resistance inside heat pipe (very small), internal wick resistance at the condenser section of the heat pipe, and condensation resistance at the condenser section.

If one of the resistances on the right-hand side of Eq. 17.5 or 17.6 is significantly higher than the other resistances, it is referred to as the *controlling resistance;* it is considered significantly dominant when it represents more than 80 percent of the total resistance. A reduction in the controlling thermal resistance will have more impact in reducing the exchanger surface area A requirement compared to the reduction in A due to the reduction in other thermal resistances.

UA in Eq. 17.6 may be defined in terms of hot or cold fluid side surface area or wall conduction area as

$$UA = U_h A_h = U_c A_c = U_w A_w \tag{17.8}$$

The knowledge of wall temperature in a heat exchanger is essential to determine localized hot spots, freeze points, thermal stresses, local fouling characteristics, or boiling/condensing coefficients. Based on the thermal circuit of Fig. 17.22, when $\mathbf{R}_w$ is negligible, $T_{w,h} = T_{w,c} = T_w$ is computed from

$$T_w = \frac{T_h + [(\mathbf{R}_h + \mathbf{R}_{s,h})/(\mathbf{R}_c + \mathbf{R}_{s,c})]T_c}{1 + [(\mathbf{R}_h + \mathbf{R}_{s,h})/(\mathbf{R}_c + \mathbf{R}_{s,c})]} \tag{17.9}$$

When there is no fouling on either side ($\mathbf{R}_{s,h} = \mathbf{R}_{s,c} = 0$), Eq. 17.10 reduces to

$$T_w = \frac{T_h/\mathbf{R}_h + T_c/\mathbf{R}_c}{1/\mathbf{R}_h + 1/\mathbf{R}_c} = \frac{(\eta_o hA)_h T_h + (\eta_o hA)_c T_c}{(\eta_o hA)_h + (\eta_o hA)_c} \tag{17.10}$$

Here T_h, T_c, and T_w are local temperatures in this equation.

The ε-NTU, P-NTU, and MTD Methods

If we consider the fluid outlet temperatures or heat transfer rate as dependent variables, they are related to independent variable/parameters of Fig. 17.21 as follows.

$$T_{h,o}, \; T_{c,o}, \; \text{or} \; q = \phi\{T_{h,i}, \; T_{c,i}, \; C_h, \; C_c, \; U, \; A, \; \text{flow arrangement}\} \tag{17.11}$$

Six independent and three dependent variables of Eq. 17.11 for a given flow arrangement can be transferred into two independent and one dependent dimensionless groups; three different methods for design and analysis of heat exchangers are presented in Table 17.4 based on the choice of three dimensionless groups. The relationship among three dimensionless groups is derived by integrating Eqs. 17.1 and 17.2 across the surface area for a specified exchanger flow arrangement. Such expressions are presented later in Table 17.6 for industrially most important flow arrangements. Note that there are other methods such as ψ-P [7] and P_1-P_2 charts [8] in which the important dimensionless groups of three methods of Table 17.4 are delineated; using these charts, the solutions to the rating and sizing problems of heat exchanger design can be obtained graphically straightforward without any iterations. However, the description of these methods will not add any more information from a designer's

TABLE 17.4 General Functional Relationships and Dimensionless Groups for ε-NTU, P-NTU, and LMTD Methods

ε-NTU method	P-NTU method	LMTD method
$q = \varepsilon C_{min}(T_{h,i} - T_{c,i})$	$q = P_1 C_1 |T_{2,i} - T_{1,i}|$	$q = UAF\,\Delta T_{lm}$
$\varepsilon = \phi(NTU, C^*, \text{flow arrangement})$	$P_1 = \phi(NTU_1, R_1, \text{flow arrangement})$	$F = \phi(P_1, R_1, \text{flow arrangement})^\dagger$
$\varepsilon = \dfrac{C_h(T_{h,i} - T_{h,o})}{C_{min}(T_{h,i} - T_{c,i})} = \dfrac{C_c(T_{c,o} - T_{c,i})}{C_{min}(T_{h,i} - T_{c,i})}$	$P_1 = \dfrac{T_{1,o} - T_{1,i}}{T_{2,i} - T_{1,i}}$	$F = \dfrac{\Delta T_m}{\Delta T_{lm}}$
$NTU = \dfrac{UA}{C_{min}} = \dfrac{1}{C_{min}} \displaystyle\int_A U\,dA$	$NTU_1 = \dfrac{UA}{C_1} = \dfrac{|T_{1,o} - T_{1,i}|}{\Delta T_m}$	$LMTD = \Delta T_{lm} = \dfrac{\Delta T_1 - \Delta T_2}{\ln(\Delta T_1/T_2)}$
$C^* = \dfrac{C_{min}}{C_{max}} = \dfrac{(\dot m c_p)_{min}}{(\dot m c_p)_{max}}$	$R_1 = \dfrac{C_1}{C_2} = \dfrac{T_{2,i} - T_{2,o}}{T_{1,o} - T_{1,i}}$	$\Delta T_1 = T_{h,i} - T_{c,o} \qquad \Delta T_2 = T_{h,o} - T_{c,i}$

$^\dagger\ P_1$ and R_1 are defined in the P-NTU method.

viewpoint since the closed-form solutions are presented in Table 17.6 later, and hence these methods will not be discussed. Now we will briefly describe the three methods of Table 17.4.

The ε-NTU Method. In this method, the heat transfer rate from the hot fluid to the cold fluid in the exchanger is expressed as

$$q = \varepsilon C_{min}(T_{h,i} - T_{c,i}) \tag{17.12}$$

Here the exchanger effectiveness ε is an efficiency factor. It is a ratio of the actual heat transfer rate from the hot fluid to the cold fluid in a given heat exchanger of any flow arrangement to the maximum possible heat transfer rate q_{max} thermodynamically permitted. The q_{max} is obtained in a counterflow heat exchanger (recuperator) of infinite surface area operating with the fluid flow rates (heat capacity rates) and fluid inlet temperatures equal to those of an actual exchanger (constant fluid properties are idealized). As noted in Table 17.4, the exchanger effectiveness ε is a function of NTU and C^* in this method. The number of transfer units NTU is a ratio of the overall conductance UA to the smaller heat capacity rate C_{min}. NTU designates the dimensionless heat transfer size or thermal size of the exchanger. It may be interpreted as the C_{min} fluid dimensionless residence time, a temperature ratio, or a modified Stanton number [9]. The heat capacity rate ratio C^* is simply a ratio of the smaller to the larger heat capacity rate for the two fluid streams. Note that $0 \le \varepsilon \le 1$, $0 \le NTU \le \infty$, and $0 \le C^* \le 1$. Graphical results are provided in Figs. 17.23 and 17.24 for a counterflow and an unmixed-unmixed crossflow exchanger as an illustration. The results for many others can be obtained from the closed-form expressions of Table 17.6.

The P-NTU Method. This method represents a variant of the ε-NTU method. The ε-NTU relationship is different depending on whether the shell fluid is the C_{min} or C_{max} fluid in the (stream asymmetric) flow arrangements commonly used for shell-and-tube exchangers. In order to avoid possible errors and confusion, an alternative is to present the temperature effectiveness P as a function of NTU and R, where P, NTU, and R are defined consistently either for the fluid 1 side or fluid 2 side; in Table 17.4, they are defined for the fluid 1 side (regardless of whether that side is the hot or cold fluid side or the shell or tube side). Closed-form $P_1 - NTU_1$ expressions for many industrially useful heat exchanger flow arrangements are provided in Table 17.6, where the fluid 1 side is clearly identified in the sketch for each flow arrangement; it is the shell side in a shell-and-tube exchanger. Note that

$$q = P_1 C_1 |T_{2,i} - T_{1,i}| = P_2 C_2 |T_{1,i} - T_{2,i}| \tag{17.13}$$

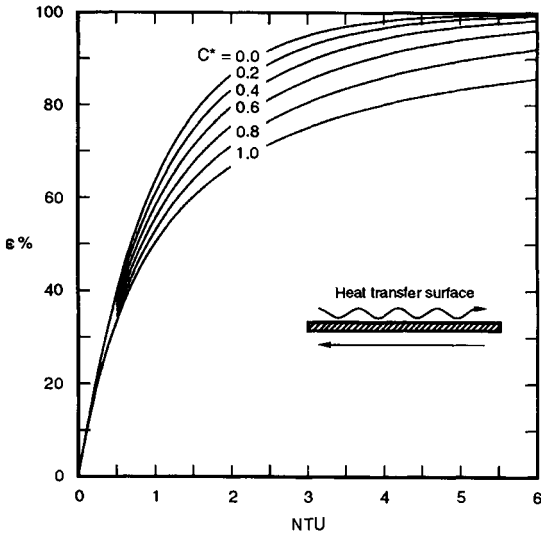$$P_1 = P_2 R_2 \qquad P_2 = P_1 R_1 \tag{17.14}$$

FIGURE 17.23   Heat exchanger effectiveness ε as a function of NTU and C^* for a counterflow exchanger.
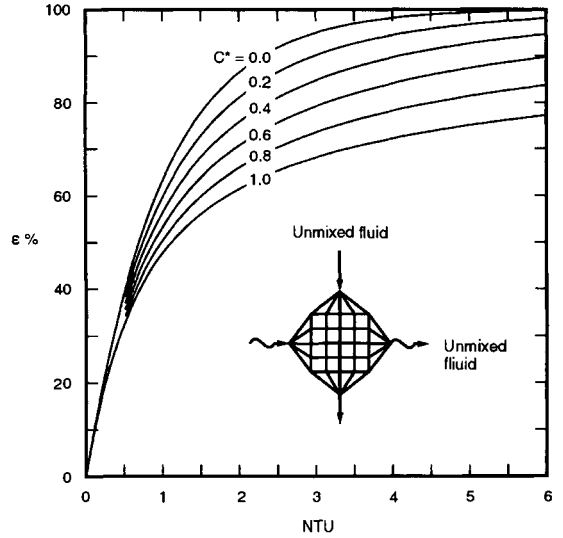

FIGURE 17.24   Heat exchanger effectiveness ε as a function of NTU and C^* for a crossflow exchanger with both fluids unmixed.

$$\text{NTU}_1 = \text{NTU}_2 R_2 \qquad \text{NTU}_2 = \text{NTU}_1 R_1 \qquad (17.15)$$

$$\text{and} \qquad R_1 = 1/R_2 \qquad (17.16)$$

P-NTU results for one of the most common 1-2 TEMA E shell-and-tube exchanger are shown in Fig. 17.25.

In Table 17.6, P-NTU-R results are provided for (1) single-pass counterflow and parallel-flow exchangers, (2) single-pass crossflow exchangers, (3) shell-and-tube exchangers, (4) heat exchanger arrays, and (5) plate heat exchangers. For additional plate exchanger flow arrangements, refer to Ref. 10. For the results of two-pass cross-counterflow or cross-parallelflow exchangers, refer to Ref. 7 for some flow arrangements, and Bačlić [11] for 72 different flow arrangements. Results for some three-pass cross-counterflow and some compound multipass crossflow arrangements are presented in Ref. 7.

The MTD Method.   In this method, the heat transfer rate from the hot fluid to the cold fluid in the exchanger is given by

$$q = UAF\Delta T_{lm} \qquad (17.17)$$

where the log-mean temperature difference correction factor F is a ratio of true (actual) mean temperature difference (MTD) to the log-mean temperature difference (LMTD)

$$\text{LMTD} = \Delta T_{lm} = \frac{\Delta T_1 - \Delta T_2}{\ln (\Delta T_1/\Delta T_2)} \qquad (17.18)$$

Here ΔT_1 and ΔT_2 are defined as

$$\Delta T_1 = T_{h,i} - T_{c,o} \qquad \Delta T_2 = T_{h,o} - T_{c,i} \qquad \text{for all flow arrangements except parallelflow} \qquad (17.19)$$

$$\Delta T_1 = T_{h,i} - T_{c,i} \qquad \Delta T_2 = T_{h,o} - T_{c,o} \qquad \text{for parallelflow} \qquad (17.20)$$

The LMTD represents a true mean temperature difference for counterflow and parallelflow arrangements under the idealizations listed below. Thus the LMTD correction factor F rep-
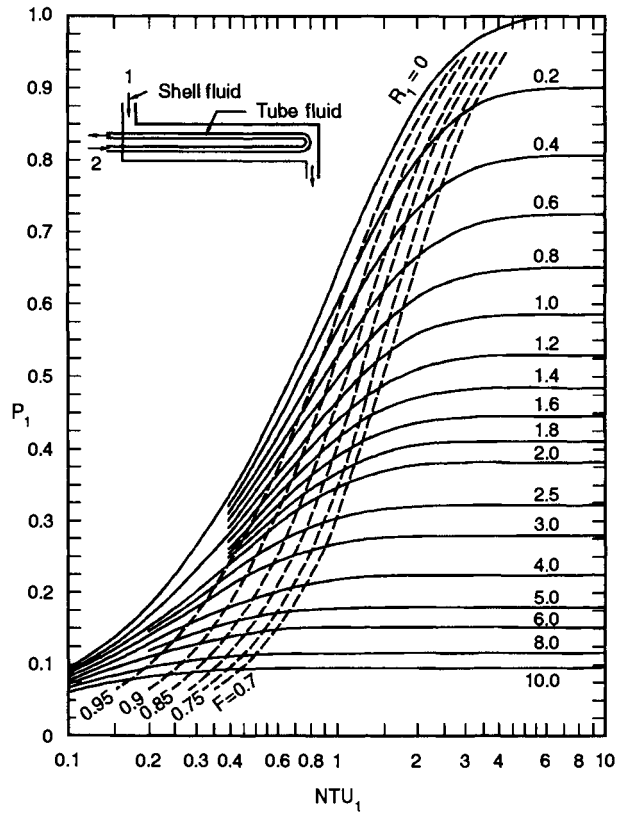
FIGURE 17.25 Temperature effectiveness P_1 as a function of NTU_1 and R_1 for the 1-2 TEMA E shell-and-tube exchanger with shell fluid mixed.
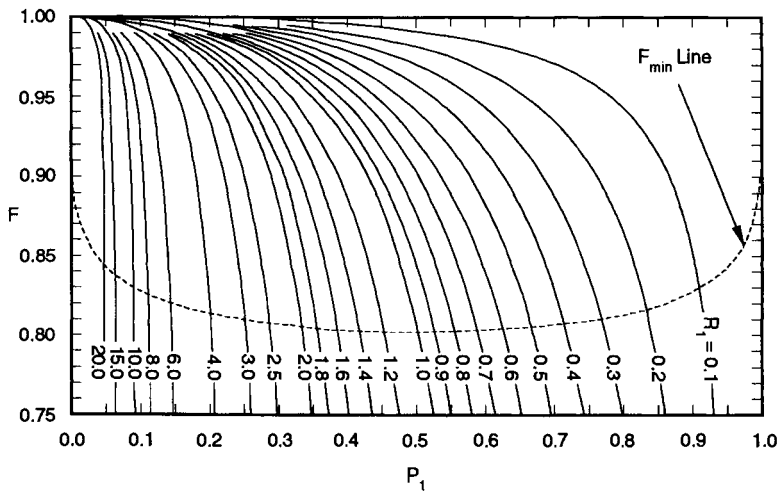

FIGURE 17.26 The LMTD correction factor F as a function of P_1 and R_1 for the 1–2 shell-and-tube exchanger (TEMA E) with shell fluid mixed.

resents a degree of departure for the MTD from the counterflow LMTD; it does not represent the effectiveness of a heat exchanger. For a given flow arrangement, it depends on two dimensionless groups: P_1 and R_1 or P_2 and R_2. (See Fig. 17.26.)

The relationships among the dimensionless groups of the ε-NTU, P-NTU, and MTD methods are presented in Table 17.5. It must be emphasized that closed-form formulas for F factors are available only for (1) a crossflow exchanger with the tube fluid unmixed, shell fluid mixed, (2) a crossflow exchanger with the tube fluid mixed, shell fluid unmixed, and (3) a 1–2 parallel counterflow exchanger (TEMA E). For all other exchanger flow arrangements, one must calculate P_1 first for given NTU_1 and R_1 and use the relationship in Table 17.5 to get the F factor. This is the reason Table 17.6 represents P_1-NTU_1-R_1 formulas, and not the formulas for F factors.

TABLE 17.5 Relationships between Dimensionless Groups of the P-NTU$_1$, LMTD, and ψ-P Methods, and Those of the ε-NTU Method
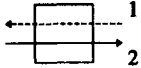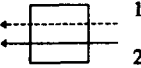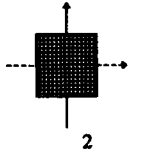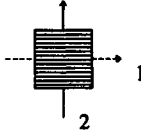
$$P_1 = \frac{C_{min}}{C_1} \varepsilon = \begin{cases} \varepsilon & \text{for } C_1 = C_{min} \\ \varepsilon C^* & \text{for } C_1 = C_{max} \end{cases}$$

$$R_1 = \frac{C_1}{C_2} = \begin{cases} C^* & \text{for } C_1 = C_{min} \\ 1/C^* & \text{for } C_1 = C_{max} \end{cases}$$

$$NTU_1 = NTU\,\frac{C_{min}}{C_1} = \begin{cases} NTU & \text{for } C_1 = C_{min} \\ NTU\,C^* & \text{for } C_1 = C_{max} \end{cases}$$

$$F = \frac{NTU_{cf}}{NTU} = \frac{1}{NTU(1-C^*)} \ln\left[\frac{1-C^*\varepsilon}{1-\varepsilon}\right] \xrightarrow{C^* = 1} \frac{\varepsilon}{NTU(1-\varepsilon)}$$

$$F = \frac{1}{NTU_1(1-R_1)} \ln\left[\frac{1-R_1P_1}{1-P_1}\right] \xrightarrow{R_1 = 1} \frac{P_1}{NTU_1(1-P_1)}$$

$$\psi = \frac{\varepsilon}{NTU} = \frac{P_1}{NTU_1} = \frac{FP_1(1-R_1)}{\ln\left[(1-R_1P_1)/(1-P_1)\right]} \xrightarrow{R_1 = 1} F(1-P_1)$$

Fin Efficiency and Extended Surface Efficiency

Extended surfaces have fins attached to the primary surface on one side of a two-fluid or a multifluid heat exchanger. Fins can be of a variety of geometries—plain, wavy, or interrupted—and can be attached to the inside, outside, or both sides of circular, flat, or oval tubes or parting sheets. Fins are primarily used to increase the surface area (when the heat transfer coefficient on that fluid side is relatively low) and consequently to increase the total rate of heat transfer. In addition, enhanced fin geometries also increase the heat transfer coefficient compared to that for a plain fin. Fins may also be used on the high heat transfer coefficient fluid side in a heat exchanger primarily for structural strength purposes (for example, for high-pressure water flow through a flat tube) or to provide a thorough mixing of a highly viscous liquid (such as for laminar oil flow in a flat or a round tube). Fins are attached to the primary surface by brazing, soldering, welding, adhesive bonding, or mechanical expansion (press fit) or extruded or integrally connected to the tubes. Major categories of extended surface heat exchangers are plate-fin (Fig. 17.10) and tube-fin (Fig. 17.14) exchangers. Note that shell-and-tube exchangers sometimes employ individually finned tubes—low finned tubes (similar to Fig. 17.14a but with low-height fins).
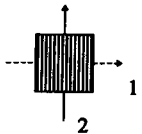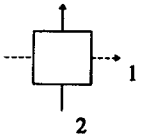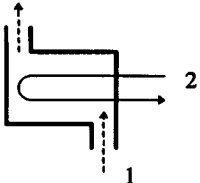
The concept of fin efficiency accounts for the reduction in temperature potential between the fin and the ambient fluid due to conduction along the fin and convection from or to the fin surface depending on the fin cooling or heating situation. The fin temperature effectiveness or *fin efficiency* is defined as the ratio of the actual heat transfer rate through the fin base

TABLE 17.6 P_1–NTU_1 Formulas and Limiting Values P_1 and $R_1 = 1$ and $\text{NTU}_1 \to \infty$ for Various Exchanger Flow Arrangements*

Flow arrangement	Eq. no.	General formula	Value for $R_1 = 1$	Value for $\text{NTU}_1 \to \infty$
Counterflow exchanger, stream symmetric	I.1.1	$P_1 = \dfrac{1 - \exp[-\text{NTU}_1(1 - R_1)]}{1 - R_1\exp[-\text{NTU}_1(1 - R_1)]}$	$P_1 = \dfrac{\text{NTU}_1}{1 + \text{NTU}_1}$	$P_1 \to 1$ for $R_1 \le 1$ $P_1 \to 1/R_1$ for $R_1 \ge 1$
	I.1.2	$\text{NTU}_1 = \dfrac{1}{(1 - R_1)} \ln\left[\dfrac{1 - R_1 P_1}{1 - P_1}\right]$	$\text{NTU}_1 = \dfrac{P_1}{1 - P_1}$	$\text{NTU}_1 \to \infty$
	I.1.3	$F = 1$	$F = 1$	$F = 1$
Parallelflow exchanger, stream symmetric	I.2.1	$P_1 = \dfrac{1 - \exp[-\text{NTU}_1(1 + R_1)]}{1 + R_1}$	$P_1 = \dfrac{1}{2}[1 - \exp(-2\text{NTU}_1)]$	$P_1 \to \dfrac{1}{1 + R_1}$
	I.2.2	$\text{NTU}_1 = \dfrac{1}{1 + R_1} \ln\left[\dfrac{1}{1 - P_1(1 + R_1)}\right]$	$\text{NTU}_1 = \dfrac{1}{2} \ln\left[\dfrac{1}{1 - 2P_1}\right]$	$\text{NTU}_1 \to \infty$
	I.2.3	$F = \dfrac{(R_1 + 1) \ln\left[(1 - R_1 P_1)/(1 - P_1)\right]}{(R_1 - 1) \ln\left[1 - P_1(1 + R_1)\right]}$	$F = \dfrac{2P_1}{(P_1 - 1) \ln(1 - 2P_1)}$	$F \to 0$
Single-pass crossflow exchanger, both fluids unmixed, stream symmetric	II.1	$P_1 = 1 - \exp(\text{NTU}_1)$ $\quad -\exp[-(1 + R_1)\text{NTU}_1]$ $\quad \times \displaystyle\sum_{n=1}^{\infty} R_1^n P_n(\text{NTU}_1)$ $P_n(y) = \dfrac{1}{(n+1)!} \displaystyle\sum_{j=1}^{n} \dfrac{(n+1-j)}{j!} y^{n+j}$	Same as Eq. (II.1) with $R_1 = 1$	$P_1 \to 1$ for $R_1 \le 1$ $P_1 \to 1/R_1$ for $R_1 \ge 1$
Single-pass crossflow exchanger, fluid 1 unmixed, fluid 2 mixed	II.2.1	$P_1 = [1 - \exp(-KR_1)]/R_1$ $K = 1 - \exp(-\text{NTU}_1)$	$P_1 = 1 - \exp(-K)$	$P_1 \to \dfrac{1 - \exp(-R_1)}{R_1}$
	II.2.2	$\text{NTU} = \ln\left[\dfrac{1}{1 + (1/R_1) \ln(1 - R_1 P_1)}\right]$	$\text{NTU}_1 = \ln\left[\dfrac{1}{1 + \ln(1 - P_1)}\right]$	$\text{NTU}_1 \to \infty$
	II.2.3	$F = \dfrac{\ln\left[(1 - R_1 P_1)/(1 - P_1)\right]}{(R_1 - 1) \ln\left[1 + (1/R_1) \ln(1 - R_1 P_1)\right]}$	$F = \dfrac{P_1}{(P_1 - 1) \ln[1 + \ln(1 - P_1)]}$	$F \to 0$

*Table condensed from R. K. Shah and A. Pignotti, *Basic Thermal Design of Heat Exchangers*, National Science Foundation Report, Int-8601771, 1988. In this table, all variables except P_1, R_1, NTU_1, and F are local or dummy variables not necessarily related to those defined in the nomenclature.

TABLE 17.6 P_1–NTU_1 Formulas and Limiting Values P_1 and $R_1 = 1$ and $\mathrm{NTU}_1 \to \infty$ for Various Exchanger Flow Arrangements (*Continued*)

Flow arrangement	Eq. no.	General formula	Value for $R_1 = 1$	Value for $\mathrm{NTU}_1 \to \infty$
	II.3.1	$P_1 = 1 - \exp(-K/R_1)$ $K = 1 - \exp(-R_1 \mathrm{NTU}_1)$	$P_1 = 1 - \exp(-K)$ $K = 1 - \exp(-\mathrm{NTU}_1)$	$P_1 \to 1 - \exp(-1/R_1)$
	II.3.2	$\mathrm{NTU}_1 = \dfrac{1}{R_1} \ln\left[\dfrac{1}{1 + R_1} \ln(1 - P_1) \right]$	$\mathrm{NTU}_1 = \ln\left[\dfrac{1}{1 + \ln(1 - P_1)} \right]$	$\mathrm{NTU}_1 \to \infty$
Single-pass crossflow exchanger, fluid 1 mixed, fluid 2 unmixed	II.3.3	$F = \dfrac{\ln\left[(1 - R_1 P_1)/(1 - P_1)\right]}{(1 - 1/R_1)\ln\left[1 + R_1 \ln(1 - P_1)\right]}$	$F = \dfrac{P_1}{(P_1 - 1)\ln\left[1 + \ln(1 - P_1)\right]}$	$F \to 0$
	II.4	$P_1 = \left[\dfrac{1}{K_1} + \dfrac{R_1}{K_2} - \dfrac{1}{\mathrm{NTU}_1} \right]^{-1}$	$P_1 = \left[\dfrac{2}{K_1} - \dfrac{1}{\mathrm{NTU}_1} \right]^{-1}$	$P_1 \to \dfrac{1}{1 + R_1}$
		$K_1 = 1 - \exp(-\mathrm{NTU}_1)$ $K_2 = 1 - \exp(-R_1 \mathrm{NTU}_1)$		
Single-pass crossflow exchanger, both fluids mixed, stream symmetric				
	III.1.1	$P_1 = \dfrac{2}{1 + R_1 + E \coth(E\mathrm{NTU}_1/2)}$ $E = [1 + R_1^2]^{1/2}$	$P_1 = \dfrac{1}{1 + \coth(\mathrm{NTU}_1/\sqrt{2})/\sqrt{2}}$	$P_1 \to \dfrac{2}{1 + R_1 + E}$
	III.1.2	$\mathrm{NTU}_1 = \dfrac{1}{E}\ln\left[\dfrac{2 - P_1(1 + R_1 - E)}{2 - P_1(1 + R_1 + E)} \right]$	$\mathrm{NTU}_1 = \ln\left[\dfrac{2 - P_1}{2 - 3P_1} \right]$	$\mathrm{NTU}_1 \to \infty$
1-2* TEMA E shell-and-tube exchanger, shell fluid mixed, stream symmetric	III.1.3	$F = \dfrac{E \ln\left[(1 - R_1 P_1)/(1 - P_1)\right]}{(1 - R_1)\ln\left[\dfrac{2 - P_1(1 + R_1 - E)}{2 - P_1(1 + R_1 + E)} \right]}$	$F = \dfrac{P_1/(1 - P_1)}{\ln\left[(2 - P_1)/(2 - 3P_1)\right]}$	$F \to 0$
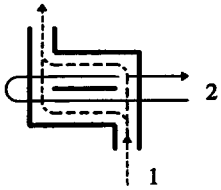
1-2 TEMA E shell-and-tube exchanger, shell fluid divided into two streams individually mixed

III.2

$$P_1 = \frac{1}{R_1}\left[1 - \frac{(2-R_1)(2E+R_1B)}{(2+R_1)(2E-R_1/B)}\right]$$

$$E = \exp(NTU_1)$$

$$B = \exp(-NTU_1 R_1/2)$$

same as 1-1 J shell, Eq. (III.10)

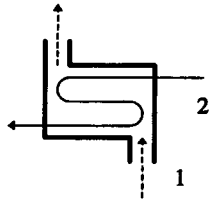$$P_1 = \frac{1}{2}\left[1 - \frac{1+E^{-2}}{2(1+NTU_1)}\right]$$
for $R_1 = 2$

$$P_1 \to \frac{2}{2+R_1}$$
for $R_1 \leq 2$

$$P_1 \to \frac{1}{R_1} \text{ for } R_1 \geq 2$$

1-3 TEMA E shell-and-tube exchanger, shell and tube fluids mixed, one parallelflow and two counterflow passes

III.3

$$P_1 = \frac{1}{R_1}\left[1 - \frac{C}{AC+B^2}\right]$$

$$A = X_1(R_1+\lambda_1)(R_1-\lambda_2)/2\lambda_1 - X_3\delta$$
$$\quad - X_2(R_1+\lambda_2)(R_1-\lambda_1)/2\lambda_2 + 1/(1-R_1)$$

$$B = X_1(R_1-\lambda_2) - X_2(R_1-\lambda_1) + X_3\delta$$

$$C = X_2(3R_1+\lambda_1) - X_1(3R_1+\lambda_2) + X_3\delta$$

$$X_i = \exp(\lambda_i NTU_1/3)/2\delta, \quad i = 1,2,3$$

$$\delta = \lambda_1 - \lambda_2$$

$$\lambda_1 = -\frac{3}{2} + \left[\frac{9}{4} + R_1(R_1-1)\right]^{1/2}$$

$$\lambda_2 = -\frac{3}{2} - \left[\frac{9}{4} + R_1(R_1-1)\right]^{1/2}$$
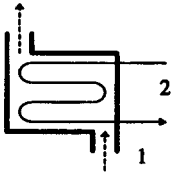
$$\lambda_3 = -R_1$$

Same as Eq. (III.3) with $R_1 = 1$

$$A = -\exp(-NTU_1)/18$$
$$\quad - \exp(NTU_1/3)/2$$
$$\quad + (NTU_1+5)/9$$

$$P_1 \to 1 \text{ for } R_1 \leq 1$$

$$P_1 \to \frac{1}{R_1} \text{ for } R_1 \geq 1$$

1-4 TEMA E shell-and-tube exchanger, shell and tube fluids mixed

III.4

$$P_1 = 4[2(1+R_1) + DA + R_1B]^{-1}$$

$$A = \coth(DNTU_1/4)$$

$$B = \tanh(R_1 NTU_1/4)$$

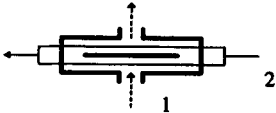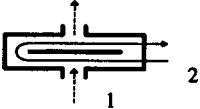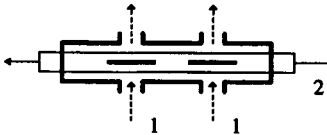$$D = [4+R_1^2]^{1/2}$$

$$P_1 = 4[4 + \sqrt{5}A + B]^{-1}$$

$$A = \coth(\sqrt{5}NTU_1/4)$$

$$B = \tanh(NTU_1/4)$$

$$P_1 \to \frac{4}{2(1+2R_1)+D-R_1}$$

---

* 1-2 means one pass on shellside, two passes on tubeside.

TABLE 17.6 P_1–NTU_1 Formulas and Limiting Values P_1 and $R_1 = 1$ and $NTU_1 \rightarrow \infty$ for Various Exchanger Flow Arrangements (*Continued*)

Flow arrangement	Eq. no.	General formula	Value for $R_1 = 1$	Value for $NTU_1 \rightarrow \infty$
Same as III.4 with $n \rightarrow \infty$	III.5	Eq. (II.4) applies in this limit with $n \rightarrow \infty$	same as for Eq. (II.4)	same as for Eq. (II.4)
  1-1 TEMA G shell-and-tube exchanger, tube fluid split into two streams individually mixed, shell fluid mixed; stream symmetric	III.6	$P_1 = A + B - AB(1 + R_1) + R_1 AB^2$ $A = \dfrac{1}{1 + R_1}\{1 - \exp(-NTU_1(1 + R_1)/2]\}$ $B = (1 - D)/(1 - R_1 D)$ $D = \exp[-NTU_1(1 - R_1)/2]$	Same as Eq. (III.6) with $B = NTU_1/(2 + NTU_1)$ for $R_1 = 1$	$P_1 \rightarrow 1$ for $R_1 \leq 1$ $P_1 \rightarrow \dfrac{1}{R_1}$ for $R_1 \geq 1$
  Overall counterflow 1-2 TEMA G shell-and-tube exchanger; shell and tube fluids mixed in each pass at a cross section	III.7	$P_1 = (B - \alpha^2)/(A + 2 + R_1 B)$ $A = -2R_1(1 - \alpha)^2/(2 + R_1)$ $B = [4 - \beta(2 + R_1)]/(2 - R_1)$ $\alpha = \exp[-NTU_1(2 + R_1)/4]$ $\beta = \exp[-NTU_1(2 - R_1)/2]$	$P_1 = \dfrac{1 + 2NTU_1 - \alpha^2}{4 + 4NTU_1 - (1 - \alpha)^2}$ for $R_1 = 2$ $\alpha = \exp(-NTU_1)$	$P_1 \rightarrow \dfrac{2 + R_1}{R_1^2 + R_1 + 2}$ for $R_1 \leq 2$ $P_1 \rightarrow \dfrac{1}{R_1}$ for $R_1 \geq 2$
  1-1 TEMA H shell-and-tube exchanger, tube fluid split into two streams individually mixed, shell fluid mixed	III.8	$P_1 = E[1 + (1 - BR_1/2)$ $\times (1 - AR_1/2 + ABR_1)]$ $- AB(1 - BR_1/2)$ $A = \dfrac{1}{1 + R_1/2}\{1 - \exp[-NTU_1(1 + R_1/2)/2]\}$ $B = (1 - D)/(1 - R_1 D/2)$ $D = \exp[-NTU_1(1 - R_1/2)/2]$ $E = (A + B - ABR_1/2)/2$	Same as Eq. (III.8) with $B = NTU_1/(2 + NTU_1)$ for $R_1 = 2$	$P_1 \rightarrow \dfrac{4(1 + R_1) - R_1^2}{(2 + R_1)^2}$ for $R_1 \leq 2$ $P_1 \rightarrow \dfrac{1}{R_1}$ for $R_1 \geq 2$
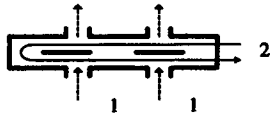
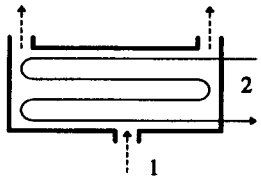|				
  Overall counterflow 1-2 TEMA H shell-and-tube exchanger, shell and tube fluids mixed in each pass at a cross section	III.9	$P_1 = \dfrac{1}{R_1}\left[1 - \dfrac{(1-D)^4}{B - 4G/R_1}\right]$ $B = (1+H)(1+E)^2$ $G = (1-D)^2(D^2+E^2) + D^2(1+E)^2$ $H = [1 - \exp(-2\beta)]/(4/R_1 - 1)$ $E = [1 - \exp(-\beta)]/(4/R_1 - 1)$ $D = [1 - \exp(-\alpha)]/(4/R_1 + 1)$ $\alpha = NTU_1(4+R_1)/8$ $\beta = NTU_1(4-R_1)/8$	Same as Eq. (III.11) with $H = NTU_1$ $E = NTU_1/2$ for $R_1 = 4$	$P_1 \to \left[R_1 + \dfrac{(4-R_1)^3}{(4+R_1)(R_1^3+16)}\right]^{-1}$ for $R_1 \le 4$ $P_1 \to \dfrac{1}{R_1}$ for $R_1 \ge 4$
  1-1 TEMA J shell-and-tube exchanger, shell and tube fluids mixed	III.10	$P_1 = \dfrac{1}{R_1}\left[1 - \dfrac{(2-R_1)(2E+R_1B)}{(2+R_1)(2E-R_1/B)}\right]$ $E = \exp(NTU_1)$ $B = \exp(-NTU_1 R_1/2)$ same as Eq. (III.2)	$P_1 = \dfrac{1}{2}\left[1 - \dfrac{1+E^{-2}}{2(1+NTU_1)}\right]$ for $R_1 = 2$	$P_1 \to \dfrac{2}{2+R_1}$ for $R_1 \le 2$ $P_1 \to \dfrac{1}{R_1}$ for $R_1 \ge 2$
  1-2 TEMA J shell-and-tube exchanger, shell and tube fluids mixed; the results remain the same if fluid 2 is reversed	III.11	$P_1 = \left[1 + \dfrac{R_1}{2} + \lambda B - 2\lambda CD\right]^{-1}$ $B = (A^\lambda + 1)/(A^\lambda - 1)$ $C = \dfrac{A^{(1+\lambda)/2}}{\lambda - 1 + (1+\lambda)A^\lambda}$ $D = 1 + \dfrac{\lambda A^{(\lambda-1)/2}}{A^\lambda - 1}$ $A = \exp(NTU_1)$ $\lambda = (1 + R_1^2/4)^{1/2}$	Same as Eq. (III.11) with $R_1 = 1$	$P_1 \to \left[1 + \dfrac{R_1}{2} + \lambda\right]^{-1}$
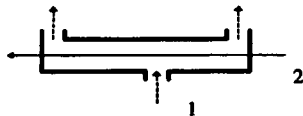
TABLE 17.6 P_1–NTU_1 Formulas and Limiting Values P_1 and $R_1 = 1$ and $NTU_1 \to \infty$ for Various Exchanger Flow Arrangements (*Continued*)*

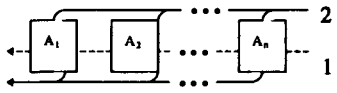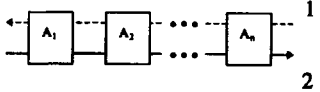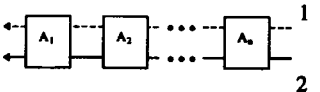| Flow arrangement	Eq. no.	General formula	Value for $R_1 = 1$	Value for $NTU_1 \to \infty$
 1-4 TEMA J shell-and-tube exchanger, shell and tube fluids mixed	III.12	$P_1 = \left[1 + \dfrac{R_1}{4}\left(\dfrac{1+3E}{1+E}\right) + \lambda B - 2\lambda CD\right]^{-1}$ $B = \dfrac{A^\lambda + 1}{A^\lambda - 1}$ $C = \dfrac{A^{(1+\lambda)/2}}{\lambda - 1 + (1+\lambda)A^\lambda}$ $D = 1 + \dfrac{\lambda A^{(\lambda-1)/2}}{A^\lambda - 1}$ $A = \exp(NTU_1)$ $E = \exp(R_1 NTU_1/2)$ $\lambda = (1 + R_1^2/16)^{1/2}$	Same as Eq. (III.12) with $R_1 = 1$	$P_1 \to \left[1 + \dfrac{3R_1}{4} + \lambda\right]^{-1}$
Limit of 1-n TEMA J shell-and-tube exchangers for $n \to \infty$; shell and tube fluids mixed; stream symmetric	III.13	Eq. (II.4) applies in this limit.	Same as for Eq. (II.4)	Same as for Eq. (II.4)
 Parallel coupling of n exchangers; fluid 2 split arbitrarily into n streams	IV.1.1	$P_1 = 1 - \prod_{i=1}^{n}(1 - P_{1,A_i})$	Same as Eq. (IV.1.1)	Same as Eq. (IV.1.1)
	IV.1.2	$\dfrac{1}{R_1} = \sum_{i=1}^{n}\dfrac{1}{R_{1,A_i}}$	$1 = \sum_{i=1}^{n}\dfrac{1}{R_{1,A_i}}$	Same as Eq. (IV.1.2)
	IV.1.3	$NTU_1 = \sum_{i=1}^{n} NTU_{1,A_i}$	Same as Eq. (IV.1.3)	$NTU_1 \to \infty$
 Series coupling of n exchangers, overall counterflow arrangement; stream symmetric if all A_i are stream-symmetric	IV.2.1	$P_1 = \dfrac{\prod_{i=1}^{n}(1 - R_1 P_{1,A_i}) - \prod_{i=1}^{n}(1 - P_{1,A_i})}{\prod_{i=1}^{n}(1 - R_1 P_{1,A_i}) - R_1\prod_{i=1}^{n}(1 - P_{1,A_i})}$	$P_1 = \dfrac{\sum_{i=1}^{n}(P_{1,A_i})/(1 - P_{1,A_i})}{1 + \sum_{i=1}^{n}(P_{1,A_i})/(1 - P_{1,A_i})}$	Same as Eq. (I.1.1) counterflow
	IV.2.2	$R_1 = R_{1,A_i},\ i = 1, \dots, n$	$1 = R_{1,A_i},\ i = 1, \dots, n$	Same as Eq. (IV.2.2)
	IV.2.3	$NTU_1 = \sum_{i=1}^{n} NTU_{1,A_i}$	Same as for Eq. (IV.2.3)	$NTU_1 \to \infty$
	IV.2.4	$F = \dfrac{1}{NTU_1}\sum_{i=1}^{n} NTU_{1,A_i} F_{A_i}$	Same as Eq. (IV.2.4)	Same as Eq. (IV.2.4)
 Series coupling of n exchangers, overall parallelflow arrangement; stream symmetric if all A_i are stream-symmetric	IV.3.1	$P_1 = \dfrac{1}{1+R_1}\left\{1 - \prod_{i=1}^{n}[1 - (1+R_1)P_{1,A_i}]\right\}$	$P_1 = \dfrac{1}{2}\left\{1 - \prod_{i=1}^{n}[1 - 2P_{1,A_i}]\right\}$	Same as Eq. (IV.3.1)
	IV.3.2	$R_1 = R_{1,A_i},\ i = 1, \dots, n$	$1 = R_{1,A_i},\ i = 1, \dots, n$	Same as Eq. (IV.3.2)
	IV.3.3	$NTU_1 = \sum_{i=1}^{n} NTU_{1,A_i}$	Same as Eq. (IV.3.3)	$NTU_1 \to \infty$

Flow arrangement	Eq. no.	General formula	Value for $R_1 = 1$ unless specified differently	Value for $\text{NTU}_1 \to \infty$
1 pass-1 pass parallelflow plate exchanger, stream symmetric	V.1	$P_1 = A$ $A = P_p(\text{NTU}_1, R_1)$ P_1 same as in Eq. (I.2)	$P_1 = \dfrac{1 - \exp(-2\text{NTU}_1)}{2}$	$P_1 = \dfrac{1}{1 + R_1}$
1 pass-1 pass counterflow plate exchanger, stream symmetric	V.2	$P_1 = B$ $B = P_c(\text{NTU}_1, R_1)$ P_1 same as in Eq. (I.1)	$P_1 = \dfrac{\text{NTU}_1}{1 + \text{NTU}_1}$	$P_1 = \begin{cases} 1 & \text{for } R_1 \leq 1 \\[2mm] \dfrac{1}{R_1} & \text{for } R_1 > 1 \end{cases}$
1 pass-2 pass plate exchanger	V.3	$P_1 = \dfrac{1}{2}\left(A + B - \dfrac{1}{2}ABR_1\right)$ $A = P_p(\text{NTU}_1, R_1/2)$ $B = P_c(\text{NTU}_1, R_1/2)$	Same as Eq. (V.3) with $B = \dfrac{\text{NTU}_1}{1 + \text{NTU}_1}$ for $R_1 = 2$	$P_1 = \begin{cases} \dfrac{2}{2 + R_1} & \text{for } R \leq 2 \\[2mm] \dfrac{1}{R_1} & \text{for } R_1 > 2 \end{cases}$
1 pass-3 pass plate exchanger with two end passes in parallelflow	V.4	$P_1 = \dfrac{1}{3}\left[B + A(1 - R_1B/3)(2 - R_1A/3)\right]$ $A = P_p(\text{NTU}_1, R_1/3)$ $B = P_c(\text{NTU}_1, R_1/3)$	Same as Eq. (V.4) with $B = \dfrac{\text{NTU}_1}{1 + \text{NTU}_1}$ for $R_1 = 3$	$P_1 = \begin{cases} \dfrac{9 + R_1}{(3 + R_1)^2} & R_1 \leq 3 \\[2mm] \dfrac{1}{R_1} & R_1 > 3 \end{cases}$
1 pass-3 pass plate exchanger with two end passes in counterflow	V.5	$P_1 = \dfrac{1}{3}\left[A + B(1 - R_1A/3)(2 - R_1B/3)\right]$ $A = P_p(\text{NTU}_1, R_1/3)$ $B = P_c(\text{NTU}_1, R_1/3)$	Same as Eq. (V.5) with $B = \dfrac{\text{NTU}_1}{1 + \text{NTU}_1}$ for $R_1 = 3$	$P_1 = \begin{cases} \dfrac{9 - R_1}{9 + 3R_1} & R_1 \leq 3 \\[2mm] \dfrac{1}{R_1} & R_1 > 3 \end{cases}$

* In all formulas of plate heat exchangers with the number of thermal plates $N \to \infty$ (equation numbers starting with V), the single-pass parallelflow and counterflow temperature effectivenesses are presented in implicit forms. Their explicit forms are as follows, with x and y representing the appropriate values of the number of transfer units and heat capacity rate ratios, respectively.

Single-pass parallelflow

$$P_p(x, y) = \frac{1 - \exp[-x(1 + y)]}{1 + y}$$

$$P_p(x, 1) = [1 - \exp(-2x)]/2$$

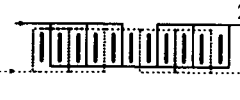$$P_p(\infty, y) = 1/(1 + y)$$

Single-pass counterflow

$$P_c(x, y) = \frac{1 - \exp[-x(1 - y)]}{1 - y \exp[-x(1 - y)]}$$

$$P_c(x, 1) = x/(1 + x)$$

$$P_c(\infty, y) = \begin{cases} 1 & \text{for } y < 1 \\ 1/y & \text{for } y > 1 \end{cases}$$

TABLE 17.6 P_1–NTU_1 Formulas and Limiting Values P_1 and $R_1 = 1$ and $NTU_1 \to \infty$ for Various Exchanger Flow Arrangements (*Continued*)

Flow arrangement	Eq. no.	General formula	Value for $R_1 = 1$ unless specified differently	Value for $NTU_1 \to \infty$
1 pass-4 pass plate exchanger	V.6	$P_1 = (1 - Q)/R_1$ $Q = (1 - AR_1/4)^2(1 - BR_1/4)^2$ $A = P_p(NTU_1, R_1/4)$ $B = P_c(NTU_1, R_1/4)$	Same as Eq. (V.6) with $B = \dfrac{NTU_1}{1 + NTU_1}$ for $R_1 = 4$	$P_1 = \begin{cases} \dfrac{16}{(4 + R_1)^2} & R_1 \le 4 \\ \dfrac{1}{R_1} & R_1 > 4 \end{cases}$
2 pass-2 pass plate exchanger with overall parallelflow and individual passes in parallelflow, stream symmetric	V.7	P_1 same as in Eq. (V.1)	Same as Eq. (V.1)	Same as Eq. (V.1)
2 pass-2 pass plate exchanger with overall parallelflow and individual passes in counterflow, stream symmetric	V.8	$P_1 = B[2 - B(1 + R_1)]$ $B = P_c(NTU_1/2, R_1)$	Same as Eq. (V.8) with $B = \dfrac{NTU_1}{2 + NTU_1}$ for $R_1 = 1$	$P_1 = \begin{cases} 1 - R_1 & R_1 \le 1 \\ \dfrac{R_1 - 1}{R_1^2} & R_1 > 1 \end{cases}$
2 pass-2 pass plate exchanger with overall counterflow and individual passes in parallelflow, stream symmetric	V.9	$P_1 = \dfrac{2A - A^2(1 + R_1)}{1 - R_1 A^2}$ $A = P_p(NTU_1/2, R_1)$	Same as Eq. (V.9)	$P_1 = \dfrac{1 + R_1}{1 + R_1 + R_1^2}$
2 pass-2 pass plate exchanger with overall counterflow and individual passes in counterflow, stream symmetric	V.10	P_1 same as Eq. (V.2)	Same as Eq. (V.2)	Same as Eq. (V.2)

2 pass-3 pass plate exchanger with overall parallelflow	V.11	$P_1 = A + B - (2/9 + D/3)(A^2 + B^2)$ $\quad - (5/9 + 4D/3)AB$ $\quad + D(1+D)AB(A+B)/3$ $\quad - D^2A^2B^2/9$ $A = P_p(\mathrm{NTU}_1/2, D)$ $B = P_c(\mathrm{NTU}_1/2, D)$ $D = 2R_1/3$	Same as Eq. (V.11) with $B = \dfrac{\mathrm{NTU}_1}{2 + \mathrm{NTU}_1}$ for $R_1 = \dfrac{3}{2}$	$P_1 = \begin{cases} \dfrac{9 - 2R_1}{9 + 6R_1} & R_1 \leq \dfrac{3}{2} \\[3mm] \dfrac{4R^2 + 2R_1 - 3}{2R_1^2(3 + 2R_1)} & R_1 > \dfrac{3}{2} \end{cases}$
2 pass-3 pass plate exchanger with overall counterflow	V.12	$P_1 = (A + 0.5B + 0.5C + D)/R_1$ $A = \dfrac{2R_1EF^2 - 2EF + F - F^2}{2R_1E^2F^2 - E^2 - F^2 - 2EF + E + F}$ $B = A(E-1)/F; \ C = (1-A)/E$ $D = R_1E^2C - R_1E + R_1 - C/2$ $E = 1/(2R_1G/3); \ F = 1/(2R_1H/3)$ $G = P_c(\mathrm{NTU}_1/2, 2R_1/3)$ $H = P_p(\mathrm{NTU}_1/2, 2R_1/3)$	Same as Eq. (V.12) with $G = \dfrac{\mathrm{NTU}_1}{2 + \mathrm{NTU}_1}$ for $R_1 = \dfrac{3}{2}$	$P_1 = \begin{cases} \dfrac{27 + 12R_1 - 4R_1^2}{27 + 12R_1 + 4R_1^2} \\[3mm] \qquad\qquad R_1 \leq \dfrac{3}{2} \\[3mm] \dfrac{1}{R_1} \qquad R_1 > \dfrac{3}{2} \end{cases}$
2 pass-4 pass plate exchanger with overall parallelflow	V.13	$P_1 = 2D - (1 + R_1)D^2$ $D = (A + B - ABR_1/2)/2$ $A = P_p(\mathrm{NTU}_1/2, R_1/2)$ $B = P_c(\mathrm{NTU}_1/2, R_1/2)$	Same as Eq. (V.13) with $B = \dfrac{\mathrm{NTU}_1}{2 + \mathrm{NTU}_1}$ for $R_1 = 2$	$P_1 = \begin{cases} \dfrac{4}{(2 + R_1)^2} & R_1 \leq 2 \\[3mm] \dfrac{R_1 - 1}{R_1^2} & R_1 > 2 \end{cases}$
2 pass-4 pass plate exchanger with overall counterflow	V.14	$P_1 = \dfrac{2D - (1 + R_1)D^2}{1 - D^2R_1}$ $D = (A + B - ABR_1/2)/2$ $A = P_p(\mathrm{NTU}_1/2, R_1/2)$ $B = P_c(\mathrm{NTU}_1/2, R_1/2)$	Same as Eq. (V.14) with $B = \dfrac{\mathrm{NTU}_1}{2 + \mathrm{NTU}_1}$ for $R_1 = 2$	$P_1 = \begin{cases} \dfrac{4}{4 + R_1^2} & R_1 \leq 2 \\[3mm] \dfrac{1}{R_1} & R_1 > 2 \end{cases}$

divided by the maximum possible heat transfer rate through the fin base, which would be obtained if the entire fin was at the base temperature (i.e., its material thermal conductivity was infinite). Since most of the real fins are thin, they are treated as one-dimensional (1-D) with standard idealizations used for the analysis [12]. This 1-D fin efficiency is a function of the fin geometry, fin material thermal conductivity, heat transfer coefficient at the fin surface, and the fin tip boundary condition; it is not a function of the fin base or fin tip temperature, ambient temperature, and heat flux at the fin base or fin tip.

The expressions for 1-D fin efficiency formulas for some common fins are presented in Table 17.7. For other fin geometries, refer to Refs. 13 and 14. The fin efficiencies for straight (first and third from the top in Table 17.7) and circular (seventh from the top in Table 17.7) fins of uniform thickness δ are presented in Fig. 17.27 ($r_e/r_o = 1$ for the straight fin).

The fin efficiency for flat fins (Fig. 17.14b) is obtained by a sector method [15]. In this method, the rectangular or hexagonal fin around the tube (Fig. 17.28a and b) or its smallest symmetrical section is divided into N sectors. Each sector is then considered as a circular fin with the radius $r_{e,i}$ equal to the length of the centerline of the sector. The fin efficiency of each sector is subsequently computed using the circular fin formula of Table 17.7. The fin efficiency η_f for the whole fin is then the surface area weighted average of $\eta_{f,i}$ of each sector.

$$\eta_f = \frac{\sum\limits_{i=1}^{N} \eta_{f,i} A_{f,i}}{\sum\limits_{i=1}^{N} A_{f,i}} \tag{17.21}$$

Since the heat flow seeks the path of least thermal resistance, actual η_f will be equal or higher than that calculated by Eq. 17.21; hence Eq. 17.21 yields a somewhat conservative value of η_f.

The η_f values of Table 17.7 or Eq. 17.21 are not valid in general when the fin is thick, is subject to variable heat transfer coefficients or variable ambient fluid temperature, or has temperature depression at the base. For a thin rectangular fin of constant cross section, the fin efficiency as presented in Table 17.7 is given by

$$\eta_f = \frac{\tanh{(m\ell)}}{m\ell} \tag{17.22}$$

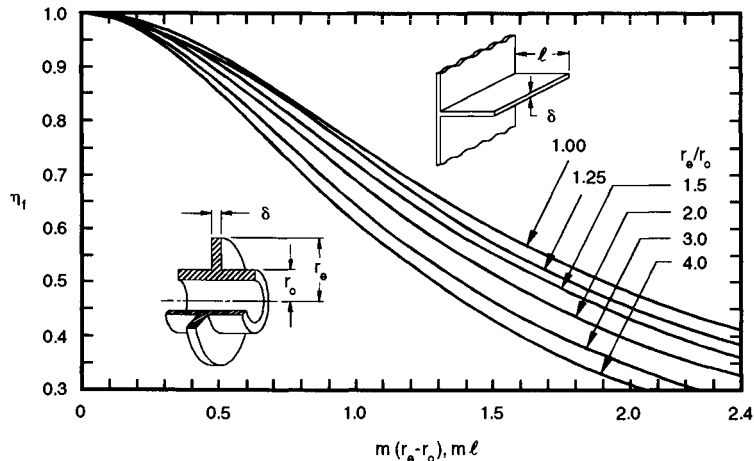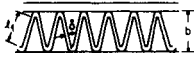where $m = [2h(1 + \delta_f/\ell_f)/k_f\delta_f]^{1/2}$.
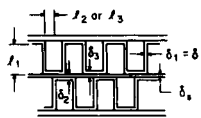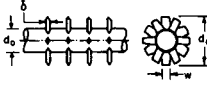
FIGURE 17.27   Fin efficiency of straight and circular fins of uniform thickness.

TABLE 17.7 Fin Efficiency for Plate-Fin and Tube-Fin Geometries of Uniform Fin Thickness

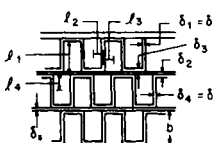| Geometry	Fin efficiency formula $m_i = \left[\dfrac{2h}{k_f \delta_i}\left(1 + \dfrac{\delta_i}{\xi}\right)\right]^{1/2}$ $E_i = \dfrac{\tanh(m_i \ell_i)}{m_i \ell_i}$ $i = 1, 2, 3, 4$
Plain, wavy, or offset strip fin of rectangular cross section	$\eta_f = E_1$ $\ell_1 = \dfrac{b}{2} - \delta_1 \qquad \delta_1 = \delta$
Triangular fin heated from one side	$\eta_f = \dfrac{hA_1(T_0 - T_\infty)\dfrac{\sinh(m_1\ell_1)}{m_1\ell_1} + q_e}{\cosh(m_1\ell_1)\left[hA_1(T_0 - T_\infty) + q_e \dfrac{T_0 - T_\infty}{T_1 - T_\infty}\right]} \qquad \delta_1 = \delta$
Plain, wavy, or louver fin of triangular cross section	$\eta_f = E_1$ $\ell_1 = \dfrac{\ell}{2} \qquad \delta_1 = \delta$
Double sandwich fin	$\eta_f = \dfrac{E_1\ell_1 + E_2\ell_2}{\ell_1 + \ell_2}\,\dfrac{1}{1 + m_1^2 E_1 E_2 \ell_1 \ell_2}$ $\delta_1 = \delta \qquad \delta_2 = \delta_3 = \delta + \delta_s$ $\ell_1 = b - \delta + \dfrac{\delta_s}{2} \qquad \ell_2 = \ell_3 = \dfrac{p_f}{2}$
Triple sandwich fin	$\eta_f = \dfrac{(E_1\ell_1 + 2\eta_{f24}\ell_{24})/(\ell_1 + 2\ell_2 + \ell_4)}{1 + 2m_1^2 E_1 \ell_1 \eta_{f24}\ell_{24}}$ $\eta_{f24} = \dfrac{(2E_2\ell_2 + E_4\ell_4)/(2\ell_2 + \ell_4)}{1 + m_2^2 E_2 E_4 \ell_2 \ell_4/2} \qquad \ell_{24} = 2\ell_2 + \ell_4$ $\delta_1 = \delta_4 = \delta \qquad \delta_2 = \delta_3 = \delta + \delta_s$ $\ell_1 = b - \delta + \dfrac{\delta_s}{2} \qquad \ell_2 = \ell_3 = \dfrac{p_f}{2} \qquad \ell_4 = \dfrac{b}{2} - \delta + \dfrac{\delta_s}{2}$
Pin fin	$\eta_f = \dfrac{\tanh(m\ell)}{m\ell}$ $\ell = \dfrac{b}{2} - d_o \qquad m = \left(\dfrac{4h}{k_f d_o}\right)^{1/2} \qquad \delta = \dfrac{d_o}{2}$
Circular fin	$\eta_f = \begin{cases} a(m\ell_e)^{-b} & \text{for } \Phi > 0.6 + 2.257(r^*)^{-0.445} \\[2mm] \dfrac{\tanh\Phi}{\Phi} & \text{for } \Phi \le 0.6 + 2.257(r^*)^{-0.445} \end{cases}$ $a = (r^*)^{-0.246} \qquad \Phi = m\ell_e(r^*)^n \qquad n = \exp(0.13 m\ell_e - 1.3863)$ $b = \begin{cases} 0.9107 + 0.0893 r^* & \text{for } r^* \le 2 \\ 0.9706 + 0.17125 \ln r^* & \text{for } r^* > 2 \end{cases}$ $m = \left(\dfrac{2h}{k_f \delta}\right)^{1/2} \qquad \ell_e = \ell_f + \dfrac{\delta}{2} \qquad r^* = \dfrac{d_e}{d_o}$
Studded fin	$\eta_f = \dfrac{\tanh(m\ell_e)}{m\ell_e}$ $m = \left[\dfrac{2h}{k_f\delta}\left(1 + \dfrac{\delta}{w}\right)\right]^{1/2} \qquad \ell_e = \ell_f + \dfrac{\delta}{2} \qquad \ell_f = \dfrac{(d_e - d_o)}{2}$
Rectangular fin over circular tubes	See the text.
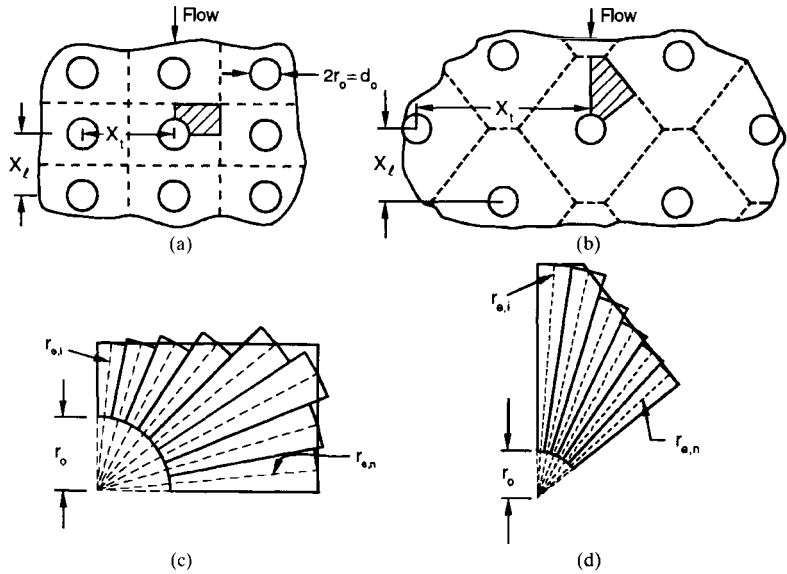
FIGURE 17.28   Flat fin over (a) an inline and (b) staggered tube arrangement; the smallest representative shaded segment of the fin for (c) an inline and (d) a staggered tube arrangement.

For a thick rectangular fin of constant cross section, the fin efficiency (a counterpart of Eq. 17.22) is given by Huang and Shah [12] as

$$\eta_f = \frac{(\mathrm{Bi^+})^{1/2}}{\alpha_f^* \, \mathrm{Bi}} \tanh \left[\alpha_f^* (\mathrm{Bi^+})^{1/2} \right] \qquad (17.23)$$

where $\mathrm{Bi^+} = \mathrm{Bi}/(1 + \mathrm{Bi}/4)$, $\mathrm{Bi} = h\delta_f/2k_f$, $\alpha_f^* = 2\ell/\delta_f$. Equation 17.22 is accurate (within 0.3 percent) for a thick rectangular fin of $\eta_f > 80$ percent; otherwise use Eq. 17.23 for a thick fin.

The nonuniform heat transfer coefficient over the fin surface can lead to significant error in η_f [12] compared to that for a uniform h over the fin surface. However, generally h is obtained experimentally by considering a constant (uniform) value of h over the fin surface. Hence, such experimental h will not introduce significant errors in η_f while designing a heat exchanger, particularly for $\eta_f > 80$ percent. However, one needs to be aware of the impact of nonuniform h on η_f if the heat exchanger test conditions and design conditions are significantly different. Nonuniform ambient temperature has less than a 1 percent effect on the fin efficiency for $\eta_f > 60$ percent and hence can be neglected. The longitudinal heat conduction effect on the fin efficiency is less than 1 percent for $\eta_f > 10$ percent and hence can be neglected. The fin base temperature depression increases the total heat flow rate through the extended surface compared to that with no fin base temperature depression. Hence, neglecting this effect provides a conservative approach for the extended surface heat transfer. Refer to Huang and Shah [12] for further details on the foregoing effects and modifications to η_f for rectangular fins of constant cross sections.

In an extended surface heat exchanger, heat transfer takes place from both the fins ($\eta_f < 100$ percent) and the primary surface ($\eta_f = 100$ percent). In that case, the total heat transfer rate is evaluated through a concept of total surface effectiveness or *extended surface efficiency* η_o defined as

$$\eta_o = \frac{A_p}{A} + \eta_f \frac{A_f}{A} = 1 - \frac{A_f}{A}(1 - \eta_f) \qquad (17.24)$$

where A_f is the fin surface area, A_p is the primary surface area, and $A = A_f + A_p$. In Eq. 17.24, the heat transfer coefficients over the finned and unfinned surfaces are idealized to be equal. Note that $\eta_o \geq \eta_f$ and η_o is always required for the determination of thermal resistances of Eq. 17.6 in heat exchanger analysis.

Extensions of the Basic Recuperator Thermal Design Theory

Nonuniform Overall U. One of the idealizations involved in all of the methods listed in Table 17.4 is that the overall heat transfer coefficient between two fluids is uniform throughout the exchanger and invariant with time. However, the local heat transfer coefficients on each fluid side can vary slightly or significantly due to two effects: (1) changes in the fluid properties or radiation as a result of a rise in or drop of fluid temperatures, and (2) developing thermal boundary layers (referred to as the *length effect*). The first effect due to fluid property variations (or radiation) consists of two components: (1) distortion of velocity and temperature profiles at a given flow cross section due to fluid property variations—this effect is usually taken into account by the so-called property ratio method, with the correction scheme of Eqs. 17.109 and 17.110, and (2) variations in the fluid temperature along the axial and transverse directions in the exchanger depending on the exchanger flow arrangement; this effect is referred to as the *temperature effect*. The resultant axial changes in the overall mean heat transfer coefficient can be significant; the variations in U_{local} could be nonlinear depending on the type of fluid. While both the temperature effect and the thermal entry length effect could be significant in laminar flows, the latter effect is generally not significant in turbulent flow except for low Prandtl number fluids.

It should be mentioned that, in general, the local heat transfer coefficient in a heat exchanger is also dependent upon variables other than the temperature and length effects such as flow maldistribution, fouling, and manufacturing imperfections. Similarly, the overall heat transfer coefficient is dependent upon heat transfer surface geometry, individual Nu (as a function of relevant parameters), thermal properties, fouling effects, temperature variations, temperature difference variations, and so on. However, we will concentrate only on nonuniformities due to temperature and length effects in this section.

In order to outline how to take into account the temperature and length effects, specific definitions of local and mean overall heat transfer coefficients are summarized in Table 17.8 [18]. The three mean overall heat transfer coefficients are important: (1) the traditional U_m defined by Eq. 17.6 or 17.25, (2) $\tilde{U}$ that takes into account only the temperature effect; and (3) $\bar{U}$ that takes into account both effects, with κ providing a correction for the length effect. Note that $U_m(T)$ is traditionally (in the rest of this chapter) defined as

$$\frac{1}{U_m A} = \frac{1}{(\eta_o h_m A)_h} + \mathbf{R}_w + \frac{1}{(\eta_o h_m A)_c} \tag{17.25}$$

where h_m is the mean heat transfer coefficient averaged over the heat transfer surface; $h_{m,h}$ and $h_{m,c}$ are evaluated at the reference temperature T_m for fluid properties; here T_m is usually the arithmetic mean of inlet and outlet fluid temperatures on each fluid side.

Temperature Effect. In order to find whether the variation in UA is significant with the temperature changes, first evaluate UA at the two ends of a counterflow exchanger or a hypothetical counterflow for all other exchanger flow arrangements. If it is determined that the variations in UA are significant for these two points, evaluate the mean value $\tilde{U}$ by integrating the variations in UA by a three-point Simpson method [17, 18] as follows [16]; note that this method also takes into account the variations in c_p with temperature.

1. Hypothesize the given exchanger as a counterflow exchanger and determine individual heat transfer coefficients and enthalpies at three points in the exchanger: inlet, outlet, and a third point designated with a subscript 1/2 within the exchanger. This third point—a central point on the $\ln \Delta T$ axis—is determined by

TABLE 17.8   Definitions of Local and Mean Overall Heat Transfer Coefficients

Symbol	Definition	Meaning	Comments
U	$U = \dfrac{dq}{dA\,\Delta T}$	Local heat flux per unit of local temperature difference	This is the basic definition of the *local* overall heat transfer coefficient.
U_m	$\dfrac{1}{U_m A} = \dfrac{1}{(\eta_o h_m A)_h} + \mathbf{R}_w + \dfrac{1}{(\eta_o h_m A)_c}$	Overall heat transfer coefficient defined using area average heat transfer coefficients on both sides	Individual heat transfer coefficients should be evaluated at respective reference temperatures (usually arithmetic mean of inlet and outlet fluid temperatures on each fluid side).
$\breve{U}$	$\breve{U} = \dfrac{1}{A} \displaystyle\int_A U(A)\, dA$	Overall heat transfer coefficient averaged over: Heat transfer surface area	Overall heat transfer coefficient is either a function of: (1) local position only (laminar gas flow) $\breve{U}$, (2) temperature only (turbulent liquid flow) $\tilde{U}$, or (3) both local position and temperature (a general case) $\overline{\overline{U}}$. $U(T)$ in $\tilde{U}$ represents a position
$\tilde{U}$	$\tilde{U} = (\ln \Delta T_b - \ln \Delta T_a)\left[\displaystyle\int_{\ln \Delta T_a}^{\ln \Delta T_b} \dfrac{d(\ln \Delta T)}{U(T)}\right]^{-1}$	Temperature range	average overall heat transfer coefficient evaluated at a local temperature. Integration should be performed numerically and/ or can be approximated with an evaluation at three points. The
$\overline{\overline{U}}$	$\overline{\overline{U}} = \kappa \tilde{U}$	Local position and temperature range	values of the correction factor κ are presented in Fig. 17.29.

$$\Delta T_{1/2}^* = (\Delta T_1 \Delta T_2)^{1/2} \qquad (17.26)$$

where $\Delta T_1 = (T_h - T_c)_1$ and $\Delta T_2 = (T_h - T_c)_2$ (subscripts 1 and 2 denote terminal points).

2. In order to consider the temperature-dependent specific heats, compute the specific enthalpies i of the C_{max} fluid (with a subscript j) at the third point (referred with 1/2 as a subscript) within the exchanger from the following equation using the known values at each end of a real or hypothetical counterflow exchanger

$$i_{j,1/2} = i_{j,2} + (i_{j,1} - i_{j,2}) \frac{\Delta T_{1/2}^* - \Delta T_2}{\Delta T_1 - \Delta T_2} \qquad (17.27)$$

where $\Delta T_{1/2}^*$ is given by Eq. 17.26. If $\Delta T_1 = \Delta T_2$ (i.e., $C^* = 1$), the quotient in Eq. 17.27 becomes 1/2. If the specific heat does not vary significantly, Eq. 17.27 could also be used for the C_{min} fluid. However, when it varies significantly, as in a cryogenic heat exchanger, the third point calculated for the C_{max} and C_{min} fluid separately by Eq. 17.27 will not be physically located close enough to the others. In that case, compute the third point for the C_{min} fluid by the energy balance as follows:

$$[\dot{m}(i_i - i_{1/2})]_{C_{max}} = [\dot{m}(i_{1/2} - i_o)]_{C_{min}} \qquad (17.28)$$

Subsequently, using the equation of state or tabular/graphic results, determine the temperature $T_{h,1/2}$ and $T_{c,1/2}$ corresponding to $i_{h,1/2}$ and $i_{c,1/2}$. Then

$$\Delta T_{1/2} = T_{h,1/2} - T_{c,1/2} \qquad (17.29)$$

3. The heat transfer coefficient $h_{j,1/2}$ on each fluid side at the third point is evaluated at the following corrected reference temperature for a noncounterflow exchanger.

$$T_{j,1/2.\text{corr}} = T_{j,1/2} + \frac{3}{2}(-1)^j (T_{h,1/2} - T_{c,1/2}) \frac{1 - F}{1 + R_j^{2/3}} \tag{17.30}$$

In Eq. 17.30, the subscript $j = h$ or c (hot or cold fluid), the exponent $j = 1$ or 2, respectively, for the subscript $j = h$ or c, F is the log-mean temperature difference correction factor, and $R_h = C_h/C_c$ or $R_c = C_c/C_h$. The temperatures $T_{h,1/2.\text{corr}}$ and $T_{c,1/2.\text{corr}}$ are used only for the evaluation of fluid properties to compute $h_{h,1/2}$ and $h_{c,1/2}$. The foregoing correction to the reference temperature $T_{j,1/2}$ results in the cold fluid temperature being increased and the hot fluid temperature being decreased.

Calculate the overall conductance at the third point by

$$\frac{1}{U_{1/2}A} = \frac{1}{\eta_{o,h} h_{h,1/2} A_h} + \mathbf{R}_w + \frac{1}{\eta_{o,c} h_{c,1/2} A_c} \tag{17.31}$$

Note that η_f and η_o can be determined accurately at local temperatures.

4. Calculate the apparent overall heat transfer coefficient at this point.

$$U_{1/2}^* A = U_{1/2}A \frac{\Delta T_{1/2}}{\Delta T_{1/2}^*} \tag{17.32}$$

5. Knowing the heat transfer coefficient at each end of the exchanger evaluated at the respective actual temperatures, compute overall conductances according to Eq. 17.31 and find the mean overall conductance for the exchanger (taking into account the temperature dependency of the heat transfer coefficient and heat capacities) from the following equation (Simpson's rule):

$$\frac{1}{\bar{U}A} = \frac{1}{6} \frac{1}{U_1 A} + \frac{2}{3} \frac{1}{U_{1/2}^* A} + \frac{1}{6} \frac{1}{U_2 A} \tag{17.33}$$

6. Finally, the true mean heat transfer coefficient that also takes into account the laminar flow entry length effect is given by:

$$\overline{\overline{U}}A = \bar{U}A \cdot \kappa \tag{17.34}$$

where the entry length effect factor $\kappa \leq 1$ is given in Fig. 17.29.
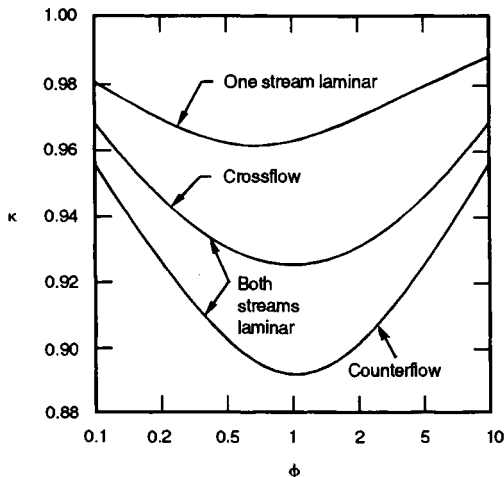

FIGURE 17.29   The length effect correction factor κ for one or both laminar streams as a function of ϕ [17].

Shah and Sekulić [16] recently conducted an analysis of the errors involved with various U averaging methods. They demonstrated that none of the existing methods, including the Roetzel method presented here, can accurately handle a nonlinear temperature variation of U for the surface area determination. The only plausible method in such a case is the numerical approach [16].

If the fluid properties or heat transfer coefficients vary significantly and/or other idealizations built into the ε-NTU or MTD methods are not valid, divide the exchanger into many small segments, and analyze individual small segments with energy balance and rate equations. In such individual small segments, h and other quantities are determined using local fluid properties.

Length Effect.   The heat transfer coefficient can vary significantly in the entrance region of the laminar flow. For hydrodynamically developed and thermally developing flow, the local and mean heat transfer coefficients h_x and h_m for a circular tube or parallel plates are related as [19]

$$h_x = \frac{2}{3} h_m (x^*)^{-1/3} \qquad (17.35)$$

where $x^* = x/(D_h \, \text{Re} \, \text{Pr})$. Using this variation in h on one or both fluid sides, counterflow and crossflow exchangers have been analyzed and the correction factor κ is presented in Fig. 17.29 [17, 18] as a function of ϕ_1 where

$$\phi_1 = \eta_{o2} h_{m,2} A_2 \left[\frac{1}{\eta_{o1} h_{m,1} A_1} + \mathbf{R}_w \right] \qquad (17.36)$$

The value of κ is 0.89 when the exchanger has the thermal resistances approximately balanced and $\mathbf{R}_w = 0$, $\phi_1 = (\eta_o hA)_2/(\eta_o hA)_1 = 1$. Thus when variation in the heat transfer coefficient due to thermal entry length effect is considered, $\overline{U} \lesssim \tilde{U}$ or U_m. The reason for this can be explained easily if one considers thermal resistances connected in series for the problem. For example, consider a very simplified problem with the heat transfer coefficient on each side varying from 80 to 40 W/m^{2}K from entrance to exit and $A_1 = A_2$, $\mathbf{R}_w = 0$, and $\eta_{o1} = \eta_{o2} = 1$. In this case, $h_{m,1} = h_{m,2} = 60$ W/m^{2}K and $U_m = 30$ W/m^{2}K. However, at each end of this counterflow exchanger, $U_1 = U_2 = 26.67$ W/m^{2}K (since $1/U = 1/80 + 1/40$). Hence $\overline{U} = (U_1 + U_2)/2 = 26.67$ W/m^{2}K. Thus $\overline{U}/U_m = 26.67/30 = 0.89$.

Combined Effect.   Specific step-by-step procedures are presented in Ref. 16 to take into account the combined temperature and length effects for counterflow, crossflow, and 1-2N TEMA E shell-and-tube exchangers. In a broader sense, the effect due to fluid property variations (or radiation) consists of two components: (1) distortion of velocity and temperature profiles at a given flow cross section due to fluid property variations, and (2) variations in fluid temperature along the axial and transverse directions in the exchanger. In general, most of the correlations for heat transfer coefficient are experimentally derived at almost constant fluid properties (because generally small temperature differences are maintained during the experiments) or are theoretically/numerically obtained for constant fluid properties. When the temperature differences between the fluid and wall (heat transfer surface) are large, the fluid properties will vary considerably across a given cross section at a local x and will distort both velocity and temperature profiles [20]. In that case, the dilemma is whether to use fluid bulk mean temperature, wall temperature or something in between for fluid properties to determine hs for the constant property correlations. Unless a specific heat transfer correlation includes this effect, it is commonly taken into account by a property ratio method [20] using both fluid bulk mean temperatures and wall temperature. Hence, it must be emphasized that the local heat transfer coefficients at specific points needed in the Simpson method of integration must first be corrected for the local velocity and temperature profile distortions by the property ratio method and then used as local hs for the integration. The net effect on $\tilde{U}$ due to these two temperature effects can be significant, and $\tilde{U}$ can be considerably higher or lower compared to U_m at constant properties.

The individual heat transfer coefficients in the thermal entrance region could be generally high. However, in general they will have less impact on the overall heat transfer coefficient. This is because, when computing U_{loc} by Eq. 17.25, with U_m and h_ms replaced by corresponding local values, its impact will be diminished due to the presence of the other thermal resistances in the series that are controlling (i.e., having low hA). It can also be seen from Fig. 17.29 that the reduction in U_m due to the entry length effect is at most 11 percent, i.e., $\kappa = 0.89$. Usually the thermal entry length effect is significant for laminar gas flow in a heat exchanger.

Unequal Heat Transfer Area in Individual Exchanger Passes.   In a multipass exchanger, it may be preferable to have different heat transfer surface areas in different passes to optimize the exchanger performance. For example, if one pass has two fluids in counterflow and the second pass has two fluids in parallelflow, the overall exchanger performance for a specified total surface area will be higher if the parallelflow pass has a minimum amount of surface area.

Roetzel and Spang [21] analyzed 1-2, 1-3, and 1-2N TEMA E exchangers for unequal heat transfer area in counterflow and parallelflow passes, with the shell inlet either at the stationary head or at the floating head. For a 1-2 TEMA E exchanger, they obtained the following expression for tubeside P_t, NTU_t, and R_t.

$$\frac{1}{P_t} = v + R_t + \frac{1}{NTU_t} \frac{m_1 e^{m_1} - m_2 e^{m_2}}{e^{m_1} - e^{m_2}} \tag{17.37}$$

where

$$m_1, m_2 = \frac{NTU_t}{2} \{\pm[(R_t + 2v - 1)^2 + 4v(1 - v)]^{1/2} - (R_t + 2v - 1)\} \tag{17.38}$$

$$v = \frac{NTU_{pf}}{NTU_t}, \qquad R_t = \frac{C_t}{C_s} \tag{17.39}$$

Here the NTU_{pf} represents the NTU of the parallelflow pass, and NTU_t is the total NTU of the exchanger on the tube side.

Roetzel and Spang [21] showed that Eq. 17.37 represents an excellent approximation for a 1-2N exchanger for $NTU_t \leq 2$ with v not close to zero. If v is close to zero, the appropriate formulas are given in Ref. 21. Refer to Ref. 21 for formulas for unequal passes for 1-3 and 1-2N exchangers. The following are the general observations that may be made from the above results.

- As expected, F factors are higher for $\mathbf{K} > 1.0$ compared to the $\mathbf{K} = 1$ (balanced pass) case for given P and R, where $\mathbf{K} = (UA)_{cf}/(UA)_{pf} = (1 - v)/v$ and the subscripts cf and pf denote counterflow and parallelflow passes, respectively.

- As $\mathbf{K}$ increases, P increases for specified F (or NTU) and R.

- The F factors for the 1-2 exchanger are higher than those for the 1-4 exchanger for specified values of P, R, and $\mathbf{K}$.

- As the number of passes is increased, the F factors (or P) continue to approach to a crossflow exchanger with both fluids mixed, and the advantage of unbalanced passes over balanced passes becomes negligible.

- Although not specifically evaluated, the unbalanced UA (i.e., $\mathbf{K} > 1$) exchanger will have higher total tubeside pressure drop and lower tubeside h compared to those for the balanced UA (i.e., $\mathbf{K} = 1$) exchanger.

Since the analysis was based on the value of $\mathbf{K} = U_{cf}A_{cf}/U_{pf}A_{pf}$, it means that not only the influence of unequal tube pass area can be taken into account, but also the unequal tube side heat transfer coefficient can be taken into account. Similarly, it should be emphasized that the results for nonuniform UA presented in the preceding subsection, if properly interpreted, can

also apply for unequal surface areas in different passes. As noted above, higher exchanger performance can be achieved with higher values of **K** and **K** = U_{cf}/U_{pf} for equal pass areas. Hence, the shell inlet nozzle should be located at the stationary head when heating the tube fluid and at the floating head when cooling the tube fluid. This is because higher temperatures mean higher heat transfer coefficients. It should be emphasized that U_{cf} and U_{pf} represent mean values of U across the counterflow and parallelflow tube passes and not at the inlet and outlet ends.

Spang et al. [22] and Xuan et al. [23] have analyzed 1-N TEMA G (split flow) and 1-N TEMA J (divided flow) shell-and-tube exchangers, respectively, with an arbitrary number of passes N, arbitrary surface area (NTU_i) in each pass, and arbitrary locations of inlet and outlet shellside nozzles in the exchangers. Bačlić et al. [24] have analyzed two-pass cross-counterflow heat exchanger effectiveness deterioration caused by unequal distribution of NTU between passes.

Finite Number of Baffles.   Idealization 11 (see p. 17.27) indicates that the number of baffles used is very large and can be assumed to approach infinity. Under this idealization, the temperature change within each baffle compartment is very small in comparison with the total temperature change of the shell fluid through the heat exchanger. Thus the shell fluid can be considered as uniform (perfectly mixed) at every cross section (in a direction normal to the shell axis). It is with this model that the mean temperature difference correction factor for exchanger effectiveness is normally derived for single-phase exchangers. In reality, a finite number of baffles are used, and the condition stated above can be achieved only partially. Shah and Pignotti [25] have made a comprehensive review and obtained new results as appropriate; they arrived at the following specific number of baffles beyond which the influence of the finite number of baffles on the exchanger effectiveness is not significantly larger than 2 percent.

- $N_b \geq 10$ for 1-1 TEMA E counterflow exchanger
- $N_b \geq 6$ for 1-2 TEMA E exchanger for $NTU_s \leq 2$, $R_s \leq 5$
- $N_b \geq 9$ for 1-2 TEMA J exchanger for $NTU_s \leq 2$, $R_s \leq 5$
- $N_b \geq 5$ for 1-2 TEMA G exchanger for $NTU_s \leq 3$
- $N_b \geq 11$ for 1-2 TEMA H exchanger for $NTU_s \leq 3$

For 1-N TEMA E exchangers, the exchanger effectiveness will depend on the combination of the number of baffles and tube passes [25].

Shell Fluid Bypassing.   Various clearances are required for the construction of a plate-baffled shell-and-tube exchanger. The shell fluid leaks or bypasses through these clearances with or without flowing past the tubes. Three clearances associated with a plate baffle are tube-to-baffle hole clearance, bundle-to-shell clearance, and baffle-to-shell clearance. Various leakage streams associated with these clearances are identified elsewhere.

Gardner and Taborek [26] have summarized the effect of various bypass and leakage streams on the mean temperature difference. As shown in Fig. 17.30, the baffle-to-shell leakage stream E experiences practically no heat transfer; the bundle-to-shell bypass stream C indicates some heat transfer, and the crossflow stream B shows a large temperature change and a possible pinch or temperature cross ($T_{B,0} > T_{t,0}$). The mixed mean outlet temperature $T_{s,0}$ is much lower than the B stream outlet temperature $T_{B,0}$, thus resulting in an indicated temperature difference larger than is actually present; the overall exchanger performance will be lower than the design value. Since the bypass and leakage streams can exceed 30 percent of the total flow, the effect on the mean temperature difference can be very large, especially for close temperature approaches. The Bell-Delaware method of designing shell-and-tube exchangers that includes the effect of leakage and bypass streams is described on p. 17.113.
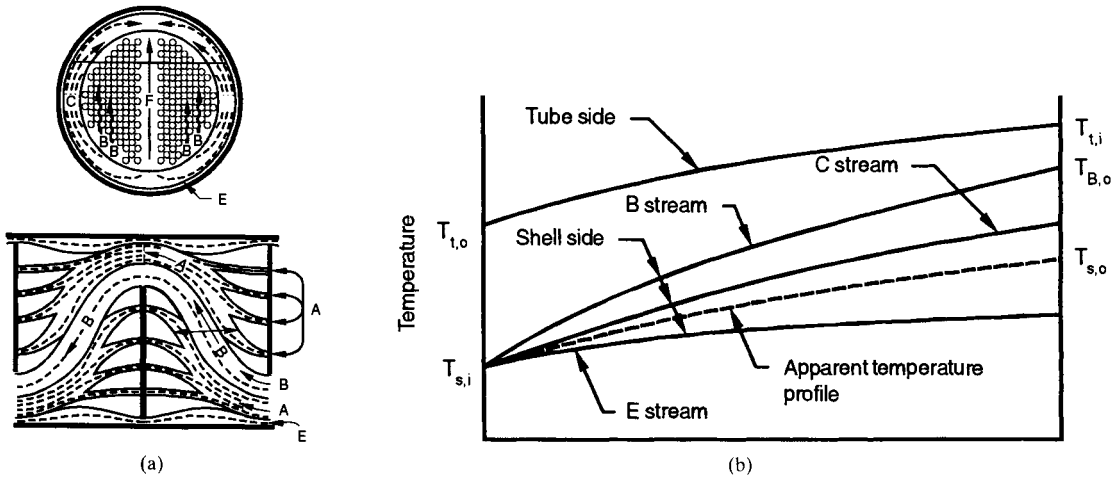
FIGURE 17.30   Effect of bypass and leakage streams on the temperature profile of a shell-and-tube exchanger: (a) streams, (b) temperature profiles.

Longitudinal Wall Heat Conduction Effects.   All three methods discussed in the preceding sections are based on the idealizations of zero longitudinal heat conduction both in the wall and in the fluid in the flow direction. Longitudinal heat conduction in the fluid is negligible for Pe > 10 and $x^* \geq 0.005$ [19], where Pe = Re Pr and $x^* = x/(D_h \text{ Re Pr})$. For most heat exchangers, except for liquid metal exchangers, Pe and x^* are higher than the above indicated values, and hence longitudinal heat conduction in the fluid is negligible.

Longitudinal heat conduction in the wall reduces the exchanger effectiveness and thus reduces the overall heat transfer performance. The reduction in the exchanger performance could be important and thus significant for exchangers designed for effectivenesses greater than about 75 percent. This would be the case for counterflow and single-pass crossflow exchangers. For high-effectiveness multipass exchangers, the exchanger effectiveness per pass is generally low, and thus longitudinal conduction effects for each pass are generally negligible. The influence of longitudinal wall heat conduction on the exchanger effectiveness is dependent mainly upon the longitudinal conduction parameter $\lambda = k_w A_k/LC_{min}$ (where k_w is the wall material thermal conductivity, A_k is the conduction cross-sectional area, and L is the exchanger length for longitudinal conduction). It would also depend on the convection-conductance ratio $(\eta_o hA)^*$, a ratio of $\eta_o hA$ on the C_{min} to that on the C_{max} side, if it varies significantly from unity. The influence of longitudinal conduction on ε is summarized next for counterflow and single-pass crossflow exchangers.

Kroeger [27] analyzed extensively the influence of longitudinal conduction on counterflow exchanger effectiveness. He found that the influence of longitudinal conduction is the largest for $C^* = 1$. For a given C^*, increasing λ decreases ε. Longitudinal heat conduction has a significant influence on the counterflow exchanger size (i.e., NTU) for a given ε when NTU > 10 and $\lambda > 0.005$. Kroeger's solution for $C^* = 1$, $0.1 \leq (\eta_o hA)^* \leq 10$, and NTU ≥ 3 is as follows:

$$\varepsilon = 1 - \cfrac{1}{1 + \text{NTU} \cfrac{1 + \lambda[\lambda\text{NTU}/(1 + \lambda\text{NTU})]^{1/2}}{1 + \lambda\text{NTU}}} \tag{17.40}$$

The results for $1 - \varepsilon$ from this equation are presented in Fig. 17.31a.
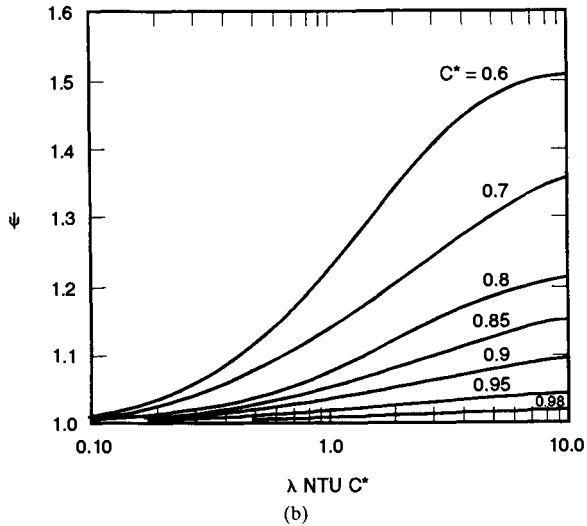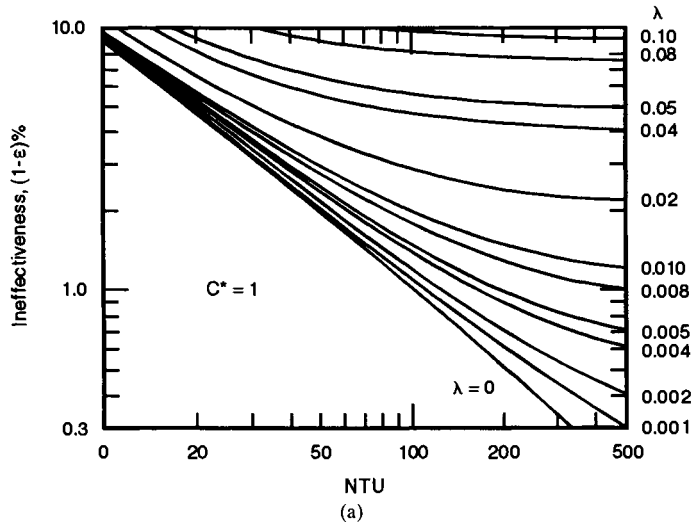
FIGURE 17.31 (*a*) Counterflow exchanger ineffectiveness as a function of NTU and λ for $C^* = 1.0$, (*b*) the parameter ψ for Eq. 17.41.

Kroeger [27] also obtained the detailed results for $1 - \varepsilon$ for $0.8 \leq C^* \leq 0.98$ for the counterflow exchanger. He correlated all his results for $1 - \varepsilon$ for $0.8 \leq C^* \leq 1$ as follows:

$$1 - \varepsilon = \frac{1 - C^*}{\psi \exp(r_1) - C^*} \tag{17.41}$$

where

$$r_1 = \frac{(1 - C^*)\text{NTU}}{1 + \lambda\text{NTU}C^*} \tag{17.42}$$

In Eq. 17.41 the parameter ψ is a function of λ, C^*, and NTU

$$\psi = f(\alpha, C^*) \tag{17.43}$$

where

$$\alpha = \lambda NTU C^* \tag{17.44}$$

The parameter ψ is given in Fig. 17.31b and Ref. 27. For $0.5 < (\eta_o hA)^*/C^* \le 2$, the error introduced in the ineffectiveness is within 0.8 percent and 4.7 percent for $C^* = 0.95$ and 0.8, respectively.

For a crossflow exchanger, temperature gradients in the wall exist in the x and y directions (two fluid flow directions). As a result, two longitudinal conduction parameters λ_h and λ_c are used to take into account the longitudinal conduction effects in the wall. Detailed tabular results are presented in Ref. 15, as reported by Chiou, on the effect of λ_h and λ_c on the exchanger ε for an unmixed-unmixed crossflow exchanger.

ε-NTU$_o$ and Λ-Π Methods for Regenerators

Heat transfer analysis for recuperators needs to be modified for regenerators in order to take into account the additional effects of the periodic thermal energy storage characteristics of the matrix wall and the establishment of wall temperature distribution dependent on $(hA)_h$ and $(hA)_c$. These two effects add two additional dimensionless groups to the analysis to be discussed in the following subsection. All idealizations, except for numbers 8 and 11, listed on p. 17.27, are also invoked for the regenerator heat transfer analysis. In addition, it is idealized that regular periodic (steady-state periodic) conditions are established; wall thermal resistance in the wall thickness (transverse) direction is zero, and it is infinity in the flow direction; no mixing of the fluids occurs during the switch from hot to cold flows or vice versa; and the fluid carryover and bypass rates are negligible relative to the flow rates of the hot and cold fluids. Note that negligible carryover means the dwell (residence) times of the fluids are negligible compared to the hot and cold gas flow periods.

ε-NTU$_o$ and Λ-Π Methods. Two methods for the regenerator heat transfer analysis are the ε-NTU$_o$ and Λ-Π methods [28]. The dimensionless groups associated with these methods are defined in Table 17.9, the relationship between the two sets of dimensionless groups is presented in Table 17.10a, and these dimensionless groups are defined in Table 17.10b for rotary and fixed-matrix regenerators. Notice that the regenerator effectiveness is dependent on four dimensionless groups, in contrast to the two parameters NTU and C^* for recuperators (see Table 17.4). The additional parameters C_r^* and $(hA)^*$ for regenerators denote the dimensionless heat storage capacity rate of the matrix and the convection-conductance ratio of the cold and hot fluid sides, respectively.

Extensive theory and results in terms of the Λ-Π method have been provided by Hausen [29] and Schmidt and Willmott [30]. The ε-NTU$_o$ method has been used for rotary regenerators and the Λ-Π method for fixed-matrix regenerators. In a rotary regenerator, the outlet fluid temperatures vary across the flow area and are independent of time. In a fixed-matrix regenerator, the outlet fluid temperatures vary with time but are uniform across the flow area at any instant of time.* In spite of these subtle differences, if the elements of a regenerator (either rotary or fixed-matrix) are fixed relative to the observer by the selection of the appropriate coordinate systems, the heat transfer analysis is identical for both types of regenerators for arriving at the regenerator effectiveness.

In the Λ-Π method, several different designations are used to classify regenerators depending upon the values of Λ and Π. Such designations and their equivalent dimensionless groups of the ε-NTU$_o$ method are summarized in Table 17.11.

---

* The difference between the outlet temperatures of the heated air (cold fluid) at the beginning and end of a given period is referred to as the temperature swing δT.

TABLE 17.9   General Functional Relationships and Basic Definitions of Dimensionless Groups for ε-NTU$_o$ and Λ-Π Methods for Counterflow Regenerators

ε-NTU$_0$ method	Λ-Π method*
$q = \varepsilon C_{\min}(T_{h,i} - T_{c,i})$	$Q = \varepsilon_h C_h \mathscr{P}_h(T_{hi} - T_{c,i}) = \varepsilon_c C_c \mathscr{P}_c(T_{hi} - T_{c,i})$
$\varepsilon = \phi\{\text{NTU}_0, C^*, C_r^*, (hA)^*\}$	$\varepsilon_r, \varepsilon_h, \varepsilon_c = \phi(\Lambda_m, \Pi_m, \gamma, R^*)$
$\varepsilon = \dfrac{C_h(T_{h,i} - T_{h,o})}{C_{\min}(T_{h,i} - T_{c,i})} = \dfrac{C_c(T_{c,o} - T_{c,i})}{C_{\min}(T_{h,i} - T_{c,i})}$	$\varepsilon_h = \dfrac{Q_h}{Q_{\max,h}} = \dfrac{C_h \mathscr{P}_h(T_{h,i} - \overline{T}_{h,o})}{C_h \mathscr{P}_h(T_{h,i} - T_{c,i})} = \dfrac{T_{h,i} - \overline{T}_{h,o}}{T_{h,i} - T_{c,i}}$
$\text{NTU}_0 = \dfrac{1}{C_{\min}}\left[\dfrac{1}{1/(hA)_h + 1/(hA)_c}\right]$	$\varepsilon_c = \dfrac{Q_c}{Q_{\max,c}} = \dfrac{C_c \mathscr{P}_c(\overline{T}_{c,o} - T_{c,i})}{C_c \mathscr{P}_c(T_{h,i} - T_{c,i})} = \dfrac{\overline{T}_{c,o} - T_{c,i}}{T_{h,i} - T_{c,i}}$
$C^* = \dfrac{C_{\min}}{C_{\max}}$	$\varepsilon_r = \dfrac{Q_h + Q_c}{Q_{\max,h} + Q_{\max,c}} = \dfrac{2Q}{Q_{\max,h} + Q_{\max,c}}$
$C_r^* = \dfrac{C_r}{C_{\min}}$	$\dfrac{1}{\varepsilon_r} = \dfrac{1}{2}\left(\dfrac{1}{\varepsilon_h} + \dfrac{1}{\varepsilon_c}\right)$
$(hA)^* = \dfrac{hA \text{ on the } C_{\min} \text{ side}}{hA \text{ on the } C_{\max} \text{ side}}$	$\dfrac{1}{\Pi_m} = \dfrac{1}{2}\left(\dfrac{1}{\Pi_h} + \dfrac{1}{\Pi_c}\right)$ $\dfrac{1}{\Lambda_m} = \dfrac{1}{2\Pi_m}\left(\dfrac{\Pi_h}{\Lambda_h} + \dfrac{\Pi_c}{\Lambda_c}\right)$
	$\gamma = \dfrac{\Pi_c/\Lambda_c}{\Pi_h/\Lambda_h}$ $R^* = \dfrac{\Pi_h}{\Pi_c}$ $\Lambda_h = \dfrac{(hA)_h}{C_h}$
	$\Lambda_c = \dfrac{(hA)_c}{C_c}$ $\Pi_h \approx \left(\dfrac{hA}{C_r}\right)_h$ $\Pi_c \approx \left(\dfrac{hA}{C_r}\right)_c$

* P_h and P_c represent hot-gas and cold-gas flow periods, respectively, in seconds.

TABLE 17.10(a)   Relationship between Dimensionless Groups of ε-NTU$_0$ and Λ-Π Methods for $C_c = C_{\min}$[†]

$$\varepsilon = \varepsilon_c = \frac{\varepsilon_h}{\gamma} = (\gamma + 1)\frac{\varepsilon_r}{2\gamma} \text{ for } C_c = C_{\min}$$

ε-NTU$_0$	Λ-Π
$\text{NTU}_0 = \dfrac{\Lambda_m(1 + \gamma)}{4\gamma} = \dfrac{\Lambda_c/\Pi_c}{1/\Pi_h + 1/\Pi_c}$	$\Lambda_h = C^*\left[1 + \dfrac{1}{(hA)^*}\right]\text{NTU}_0$
$C^* = \gamma = \dfrac{\Pi_c/\Lambda_c}{\Pi_h/\Lambda_h}$	$\Lambda_c = [1 + (hA)^*]\text{NTU}_0$
$C_r^* = \dfrac{\Lambda_m(1 + \gamma)}{2\gamma\Pi_m} = \dfrac{\Lambda_c}{\Pi_c}$	$\Pi_h = \dfrac{1}{C_r^*}\left[1 + \dfrac{1}{(hA)^*}\right]\text{NTU}_0$
$(hA)^* = \dfrac{1}{R^*} = \dfrac{\Pi_c}{\Pi_h}$	$\Pi_c = \dfrac{1}{C_r^*}[1 + (hA)^*]\text{NTU}_0$

[†] If $C_h = C_{\min}$, the subscripts c and h in this table should be changed to h and c, respectively.

TABLE 17.10(*b*)   Working Definitions of Dimensionless Groups for Regenerators in Terms of Dimensional Variables of Rotary and Fixed-Matrix Regenerators for $C_c = C_{min}$[†]

Dimensionless group	Rotary regenerator	Fixed-matrix regenerator
NTU_0	$\dfrac{h_c A_c}{C_c}\dfrac{h_h A_h}{h_h A_h + h_c A_c}$	$\dfrac{h_c A}{C_c}\dfrac{h_h \mathcal{P}_h}{h_h \mathcal{P}_h + h_c \mathcal{P}_c}$
C^*	$\dfrac{C_c}{C_h}$	$\dfrac{C_c \mathcal{P}_c}{C_h \mathcal{P}_h}$
C_r^*	$\dfrac{M_w c_w \omega}{C_c}$	$\dfrac{M_w c_w}{C_c \mathcal{P}_c}$
$(hA)^*$	$\dfrac{h_c A_c}{h_h A_h}$	$\dfrac{h_c \mathcal{P}_c}{h_h \mathcal{P}_h}$
$\dfrac{1}{\Lambda_m}$	$\dfrac{C_c + C_h}{4}\left(\dfrac{1}{h_h A_h} + \dfrac{1}{h_c A_c}\right)$	$\dfrac{C_c \mathcal{P}_c + C_h \mathcal{P}_h}{4A}\left(\dfrac{1}{h_h \mathcal{P}_h} + \dfrac{1}{h_c \mathcal{P}_c}\right)$
$\dfrac{1}{\Pi_m}$	$\dfrac{M_w c_w \omega}{2}\left(\dfrac{1}{h_h A_h} + \dfrac{1}{h_c A_c}\right)$	$\dfrac{M_w c_w}{2A}\left(\dfrac{1}{h_h \mathcal{P}_h} + \dfrac{1}{h_c \mathcal{P}_c}\right)$
γ	$\dfrac{C_c}{C_h}$	$\dfrac{C_c \mathcal{P}_c}{C_h \mathcal{P}_h}$
R^*	$\dfrac{h_h A_h}{h_c A_c}$	$\dfrac{h_h \mathcal{P}_h}{h_c \mathcal{P}_c}$

[†] If $C_h = C_{min}$, the subscripts *c* and *h* in this table should be changed to *h* and *c*, respectively. The definitions are given for one rotor (disk) of a rotary regenerator or for one matrix of a fixed-matrix regenerator. $\mathcal{P}_h$ and $\mathcal{P}_c$ represent hot-gas and cold-gas periods, respectively, *s*. ω is rotational speed, rev/s.

TABLE 17.11   Designation of Various Types of Regenerators Depending upon the Values of Dimensionless Groups

Terminology	Λ-Π method	ε-NTU_0 method
Balanced regenerators	$\Lambda_h/\Pi_h = \Lambda_c/\Pi_c$ or $\gamma = 1$	$C^* = 1$
Unbalanced regenerators	$\Lambda_h/\Pi_h \neq \Lambda_c/\Pi_c$	$C^* \neq 1$
Symmetric regenerators	$\Pi_h = \Pi_c$ or $R^* = 1$	$(hA)^* = 1$
Unsymmetric regenerators	$\Pi_h \neq \Pi_c$	$(hA)^* \neq 1$
Symmetric and balanced regenerators	$\Lambda_h = \Lambda_c$, $\Pi_h = \Pi_c$	$(hA)^* = 1$, $C^* = 1$
Unsymmetric but balanced regenerators	$\Lambda_h/\Pi_h = \Lambda_c/\Pi_c$	$(hA)^* \neq 1$, $C^* = 1$
Long regenerators	$\Lambda/\Pi > 5$	$C_r^* > 5$

A closed-form solution for a *balanced and symmetric* counterflow regenerator $[C^* = 1, (hA)^* = 1]$ has been obtained by Bačlić [31], valid for all values of C_r^*, as follows.

$$\varepsilon = C_r^* \frac{1 + 7\beta_2 - 24\{B - 2[R_1 - A_1 - 90(N_1 + 2E)]\}}{1 + 9\beta_2 - 24\{B - 6[R - A - 20(N - 3E)]\}} \tag{17.45}$$

where
$$\begin{aligned}
B &= 3\beta_3 - 13\beta_4 + 30(\beta_5 - \beta_6) \\
R &= \beta_2[3\beta_4 - 5(3\beta_5 - 4\beta_6)] \\
A &= \beta_3[3\beta_3 - 5(3\beta_4 + 4\beta_5 - 12\beta_6)] \\
N &= \beta_4[2\beta_4 - 3(\beta_5 + \beta_6)] + 3\beta_5^2 \\
E &= \beta_2\beta_4\beta_6 - \beta_2\beta_5^2 - \beta_3^2\beta_6 + 2\beta_3\beta_4\beta_5 - \beta_4^3 \\
N_1 &= \beta_4[\beta_4 - 2(\beta_5 + \beta_6)] + 2\beta_5^2 \\
A_1 &= \beta_3[\beta_3 - 15(\beta_4 + 4\beta_5 - 12\beta_6)] \\
R_1 &= \beta_2[\beta_4 - 15(\beta_5 - 2\beta_6)] \\
\beta_i &= V_i(2\mathrm{NTU}_o, 2\mathrm{NTU}_o/C_r^*)/(2\mathrm{NTU}_o)^{i-1}, \qquad i = 2, 3, \ldots, 6
\end{aligned} \tag{17.46}$$

and
$$V_i(x, y) = \exp[-(x + y)] \sum_{n=i-1}^{\infty} \binom{n}{i-1}(y/x)^{n/2} I_n(2\sqrt{xy}) \tag{17.47}$$

In these equations, all variables and parameters are local except for NTU_o, C_r^*, and ε. Here I_n represents the modified Bessel function of the first kind and nth order. Shah [32] has tabulated the effectiveness of Eq. 17.46 for $0.5 \leq \mathrm{NTU}_o \leq 500$ and $1 \leq C_r^* \leq \infty$.

Extensive numerical results have been obtained by Lambertson as reported in Ref. 20 for a counterflow regenerator and Theoclitus and Eckrich [33] for a parallelflow regenerator for a wide range of NTU_o, C^*, and C_r^*. Their results for $C^* = 1$ are presented in Figs. 17.32 and 17.33. Note that longitudinal heat conduction in the wall is neglected in these results since infinite thermal resistance is specified for the matrix in the flow direction.

Razelos, as reported in Refs. 15 and 29, proposed the following approximate procedure to calculate the counterflow regenerator effectiveness ε for unbalanced and unsymmetric regenerators for $C_r^* \geq 1$, $0.25 \leq (hA)^* \leq 4$, and the complete range of C^* and NTU_o. For the known values of NTU_o, C^*, and C_r^*, calculate appropriate values of NTU_o and C_r^* for an equivalent balanced regenerator $(C^* = 1)$, designated with a subscript m, as follows:

$$\mathrm{NTU}_{o,m} = \frac{2\mathrm{NTU}_o C^*}{1 + C^*} \tag{17.48}$$
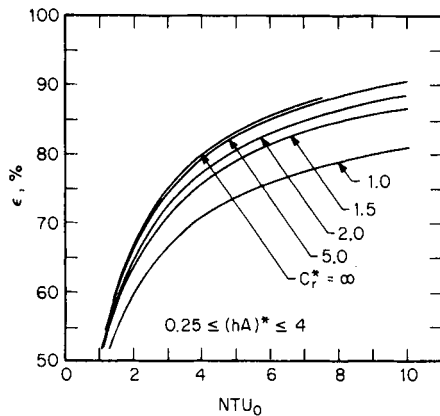

FIGURE 17.32   Counterflow regenerator effectiveness as a function of NTU_o and C_r^* for $C^* = 1$ [20].
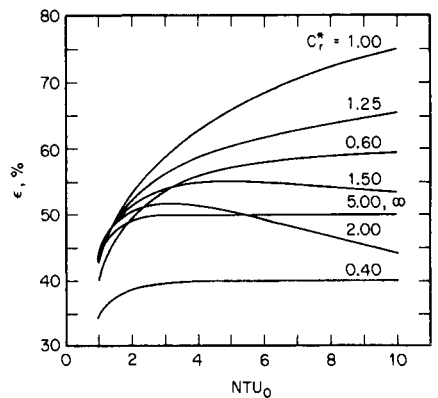
FIGURE 17.33   Parallelflow regenerator effectiveness as a function of NTU_o and C_r^* for $C^* = 1$ and $(hA)^* = 1$ [33].

$$C^*_{r,m} = \frac{2C^*_r C^*}{1 + C^*} \tag{17.49}$$

Then the equivalent balanced regenerator effectiveness ε_r is given by $\varepsilon_r = \varepsilon$ in Eq. 17.45 using the above $NTU_{o,m}$ and $C^*_{r,m}$ for NTU_o and C^*_r in Eq. 17.45. For $C^*_{r,m} < 1$, the regenerator effectiveness can be obtained from Hausen's effectiveness chart in Figs. 13–16 of Ref. 29 or Fig. 5.4 of Ref. 30 using $\Lambda = 2NTU_{o,m}$ and $\Pi = 2NTU_{o,m}/C^*_{r,m}$.

Finally, calculate the desired regenerator effectiveness ε from

$$\varepsilon = \frac{1 - \exp\{\varepsilon_r(C^{*2} - 1)/[2C^*(1 - \varepsilon_r)]\}}{1 - C^* \exp\{\varepsilon_r(C^{*2} - 1)/[2C^*(1 - \varepsilon_r)]\}} \tag{17.50}$$

where $\varepsilon_r = \varepsilon$ of Eq. 17.45 using $NTU_{o,m}$ and $C^*_{r,m}$ of Eqs. 17.48 and 17.49 for NTU_o and C^*_r in Eq. 17.45.

Longitudinal Heat Conduction in Wall. Longitudinal heat conduction in the wall was neglected in deriving the results of the preceding section. However, it may not be negligible, particularly for a high-effectiveness regenerator having a short flow length L and resultant large temperature gradient in the axial direction. It reduces the regenerator effectiveness and the overall heat transfer rate. For example, for regenerators designed for $\varepsilon > 85$ percent, a 1 percent reduction in ε would reduce gas turbine power plant efficiency by about 1 to 5 percent depending upon the load conditions, which could translate into a significant economic penalty. The reduction in ε due to longitudinal conduction in the wall can be 1 percent or higher and hence must be properly considered in the design. Based on extensive numerical results by Bahnke and Howard [20, 34], this effect can be taken into account by an additional parameter λ, referred to as the longitudinal conduction parameter:

$$\lambda = \frac{k_w A_{k,t}}{L C_{\min}} \tag{17.51}$$

where k_w is the thermal conductivity of the matrix wall, and $A_{k,t}$ is the total solid area for longitudinal conduction

$$A_{k,t} = A_{k,c} + A_{k,h} = A_{fr} - A_o = A_{fr}(1 - \sigma) \tag{17.52}$$

Bahnke and Howard's results for $C^* = 1$ can be accurately expressed by

$$\varepsilon = C_\lambda \varepsilon_{\lambda = 0} \tag{17.53}$$

where $\varepsilon_{\lambda = 0}$ is given by Eq. 17.45 and C_λ is given by

$$C_\lambda = \frac{1 + NTU_o}{NTU_o} \left[1 - \frac{1}{1 + NTU_o(1 + \lambda\phi)/(1 + \lambda NTU_o)} \right] \tag{17.54}$$

where

$$\phi = \left[\frac{\lambda NTU_o}{1 + \lambda NTU_o} \right]^{1/2} \tanh \left[\frac{NTU_o}{\{\lambda NTU_o/(1 + \lambda NTU_o)\}^{1/2}} \right] \tag{17.55}$$

$$\approx \left[\frac{\lambda NTU_o}{1 + \lambda NTU_o} \right]^{1/2} \quad \text{for } NTU_o \geq 3 \tag{17.56}$$

Bahnke and Howard's results for $C^* = 1$ and $C^*_r > 5$ are the same as those shown in Fig. 17.31a provided that the abscissa NTU is replaced by NTU_o. The regenerator effectiveness due to longitudinal conduction decreases with increasing values of λ and C^*, with the maximum effect at $C^* = 1$.

For $C^* < 1$, use the following Razelos method to account for the effect of longitudinal conduction in the wall.

1. Compute $NTU_{o,m}$, $C^*_{r,m}$ and $\varepsilon_{r,\lambda=0}$ for an equivalent balanced regenerator using Eqs. 17.48, 17.49, and 17.45, respectively.
2. Compute C_λ from Eq. 17.54 using $NTU_{o,m}$ and λ.
3. Calculate $\varepsilon_{r,\lambda\neq0} = C_\lambda\varepsilon_{r,\lambda=0}$.
4. Finally, ε is determined from Eq. 17.50, with ε_r replaced by $\varepsilon_{r,\lambda\neq0}$.

This procedure yields ε that is accurate within 1 percent for $1 \leq NTU_o \leq 20$ for $C^*_r \geq 1$ when compared to Bahnke and Howard's results.

Influence of Transverse Heat Conduction in Wall. The thermal resistance for heat conduction in the wall thickness direction is considered zero in all of the preceding ε-NTU_o results. This is a good idealization for metal matrices with thin walls. For most rotary regenerators, the thermal resistance in the transverse direction is negligible except possibly for ceramic regenerators.

The wall thermal resistance is evaluated separately during the hot-gas and cold-gas flow periods, since there is no continuous heat flow from the hot gas to the cold gas in the regenerator. Based on the unit area, it is given by [29]

$$\hat{\mathbf{R}}_w = \mathbf{R}_w A = \frac{\delta}{6k_w} \Phi^* \tag{17.57}$$

so that the effective heat transfer coefficients during the hot- and cold-gas flow periods (designated by a superscript bar) are

$$\frac{1}{\bar{h}_h} = \frac{1}{h_h} + \frac{\delta}{6k_w} \Phi^* \qquad \frac{1}{\bar{h}_c} = \frac{1}{h_c} + \frac{\delta}{6k_w} \Phi^* \tag{17.58}$$

where δ is the wall thickness and Φ^* for a plain wall is given by

$$\Phi^* = \begin{cases} 1 - \frac{1}{15}Z & \text{for } Z \leq 5 \tag{17.59} \\ 2.142[0.3 + 2Z]^{-1/2} & \text{for } Z > 5 \tag{17.60} \end{cases}$$

where $Z = (Bi_h/\Pi_h) + (Bi_c/\Pi_c)$ and $Bi_h = h_h(\delta/2)/k_w$, $\Pi_h = h_h A_h/C_{r,h}$, Bi_c and Π_c are defined in a similar manner. The range of Φ^* for Eq. 17.59 is 2/3 to 1, and for Eq. 17.60 from 0 to 2/3. When $Bi \rightarrow 0$, the transverse thermal resistance $\mathbf{R}_w$ of Eq. 17.57 approaches zero. Equations 17.59 and 17.60 are valid for Bi_h and Bi_c lower than 2. For $Bi > 2$, use the numerical results of Heggs et al. [35]. The accuracy of Eqs. 17.59 and 17.60 decreases with increasing Bi/Π and decreasing C^*_r.

The prediction of the temperature swing δT in a fixed-matrix regenerator will not be accurate by the foregoing approximate method. The numerical analysis of the type made by Heggs et al. [35] is essential for accurate δT determination. It may be noted that the δT values of Table 1 of Ref. 35 had a typing error and all should be multiplied by a factor of 10; also all the charts in Fig. 1 of Ref. 35 are poorly drawn, as a result of which the δT values shown are approximate.

Fluid Pressure Leakage and Carryover. In rotary regenerators, fluid mixing from the cold to hot gas stream and vice versa occurs due to fluid pressure and carryover leakages. A comprehensive gas flow network model of pressure leakage and carryover is presented by Shah and Skiepko [36] as shown in Fig. 17.34. A rotary regenerator disk with its housing and radial, peripheral, and axial seals (to prevent leakages) is designated by a boundary indicating an *actual regenerator* in Fig. 17.34; and the regenerator disk or matrix with no leakage streams within its boundary is designated the *internal regenerator;* the hot and cold gas inlet faces are designated the *hot and cold ends.* The high-pressure cold gas (air) can leak through the low-pressure hot gas in a number of ways due to the pressure difference. Also, due to the pressure drop on each gas side in the regenerator, the inlet pressures are going to be higher than the outlet pressures on the respective sides, and hence the cold and hot gases can bypass the
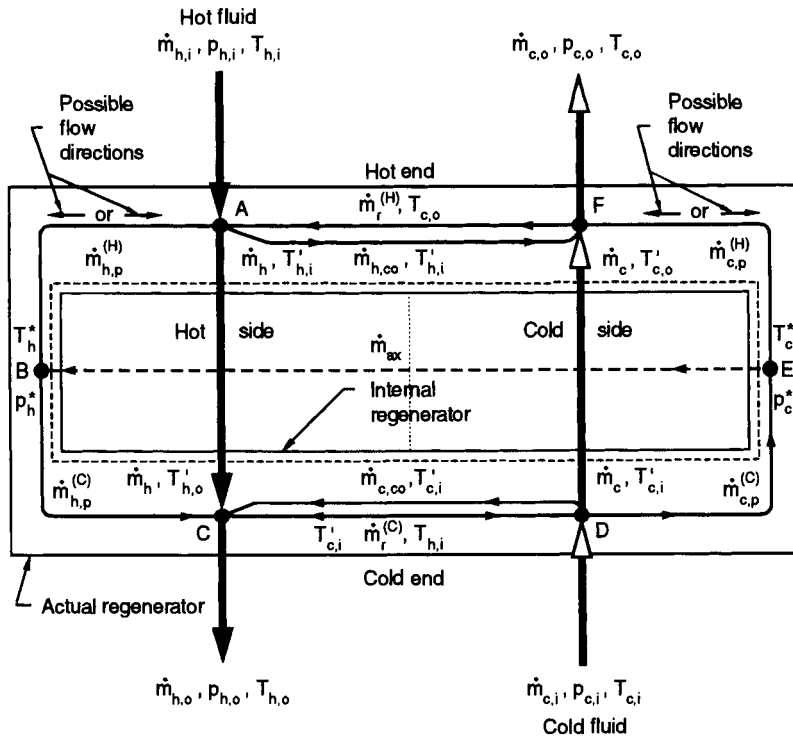
Hot fluid
$\dot{m}_{h,i}$, $p_{h,i}$, $T_{h,i}$

$\dot{m}_{c,o}$, $p_{c,o}$, $T_{c,o}$

Possible flow directions

Possible flow directions

Hot end

$\dot{m}_r^{(H)}$, $T_{c,o}$

— or → A F — or →

$\dot{m}_{h,p}^{(H)}$ $\dot{m}_h$, $T'_{h,i}$ $\dot{m}_{h,co}$, $T'_{h,i}$ $\dot{m}_c$, $T'_{c,o}$ $\dot{m}_{c,p}^{(H)}$

T_h^* Hot side $\dot{m}_{ax}$ Cold side T_c^*

B Internal regenerator E

p_h^* p_c^*

$\dot{m}_{h,p}^{(C)}$ $\dot{m}_h$, $T'_{h,o}$ $\dot{m}_{c,co}$, $T'_{c,i}$ $\dot{m}_c$, $T'_{c,i}$ $\dot{m}_{c,p}^{(C)}$

C $T'_{c,i}$ $\dot{m}_r^{(C)}$, $T_{h,i}$ D

Cold end

Actual regenerator

$\dot{m}_{h,o}$, $p_{h,o}$, $T_{h,o}$

$\dot{m}_{c,i}$, $p_{c,i}$, $T_{c,i}$
Cold fluid

FIGURE 17.34 Regenerator gas flow model with leakages [36].

regenerator matrix on individual sides through the gap between the disk and housing. Various flow leakage streams due to the pressure differences are minimized through the use of radial, peripheral, and axial seals. Because of the mechanical design considerations, there will be finite clearances between the housing and the seals; these clearances will set the leakage flow rates depending on the operating pressures, flow rates and fluid properties. Various leakage flow rate terms designated in Fig. 17.34 are defined in Table 17.12 and are as follows.

- Pressure leakages
  - due to a part of higher pressure gas stream passing through the sealing system, and entering into the lower pressure gas stream: $\dot{m}_r^{(H)}$, $\dot{m}_r^{(C)}$, $\dot{m}_{ax}$.
  - due to a flow bypass from inlet to outlet (through the gap between the housing and disk) on each gas side associated with the pressure drop in the matrix: $\dot{m}_{h,p}^{(H)}$, $\dot{m}_{c,p}^{(H)}$, $\dot{m}_{h,p}^{(C)}$, $\dot{m}_{c,p}^{(C)}$.
- Carryover leakages, when a part of one gas stream trapped into void volumes of the matrix at the end of the period is carried into the other gas stream at the beginning of the following period: $\dot{m}_{h,co}$, $\dot{m}_{c,co}$.

Clearances associated with seals and pressure leakages are considered orifices, and the leakage flow rates are computed using the following ASME orifice formulas with the known seal gap flow areas $A_{o,s}$ as follows.

$$\dot{m}_{\text{seal}} = C_d A_{o,s} Y \sqrt{2\rho\Delta p} \qquad (17.61)$$

Here, the coefficient of discharge $C_d = 0.80$ [36], expansion factor $Y = 1$, and the specific values of Δp and ρ at inlet for each leakage are given in Table 17.12.

TABLE 17.12 Rotary Regenerator Pressure Leakage and Carryover Flow Rates, Δp and Inlet Density for the Orifice Analysis[†]

Leakage terms	Symbols	Pressure drops	Density
Flows through radial seal clearances:			
Flow of the higher pressure cold gas at the hot end	$\dot{m}_r^{(H)}$	$p_{c,o} - p_{h,i}$	$\rho_{c,o}$
Flow of the higher pressure cold gas at the cold end	$\dot{m}_r^{(C)}$	$p_{c,i} - p_{h,o}$	$\rho_{c,i}$
Flows through peripheral seal clearances:			
Flows at the hot end of the disc face			
Flow around inlet to the lower pressure hot gas zone	$\dot{m}_{h,p}^{(H)}$	$p_{h,i} - p_h^*$	$\rho_{h,i}$ if $p_{h,i} > p_h^*$
		$p_h^* - p_{h,i}$	ρ_h^* if $p_{h,i} < p_h^*$
Flow around outlet from the higher pressure cold gas zone	$\dot{m}_{c,p}^{(H)}$	$p_{c,o} - p_c^*$	$\rho_{c,o}$ if $p_{c,o} > p_c^*$
		$p_c^* - p_{c,o}$	ρ_c^* if $p_{c,o} < p_c^*$
Flows at the cold end of the disc face			
Flow around outlet from the lower pressure hot gas zone	$\dot{m}_{h,p}^{(C)}$	$p_h^* - p_{h,o}$	ρ_h^*
Flow around inlet to the higher pressure cold gas zone	$\dot{m}_{c,p}^{(C)}$	$p_{c,i} - p_c^*$	$\rho_{c,i}$
Flow through axial seal clearances:	$\dot{m}_{ax}$	$p_c^* - p_h^*$	ρ_c^*
Gas carryover:			
Carryover of the lower pressure hot gas into cold gas	$\dot{m}_{h,co}$		$\bar{\rho}_h$
Carryover of the higher pressure cold into hot gas	$\dot{m}_{c,co}$		$\bar{\rho}_c$

[†] p_h^* and ρ_h^* are pressure and density at Point B in Fig. 17.34; $\bar{\rho}$ is an average density from inlet to outlet.

Several models have been presented to compute the carryover leakage [15, 36], with the following model as probably the most representative of industrial regenerators.

$$\dot{m}_{co} = A_{fr} \mathbf{N} \bar{\rho} \left[\sum_{i=1}^{n} (L_i \sigma_i) + \Delta L \right] \tag{17.62}$$

where $\mathbf{N}$ is the rotational speed (rev/s) of the regenerator disk, $\bar{\rho}$ is the gas density evaluated at the arithmetic mean of inlet and outlet temperatures, and σ_i and L_i represent the porosity and height of several layers of the regenerator (use σ and L for uniform porosity and a single layer of the matrix) and ΔL represents the height of the header.

Equations 17.61 and 17.62 represent a total of nine equations (see Table 17.12 for nine unknown mass flow rates) that can be solved once the pressures and temperatures at the terminal points of the regenerator of Fig. 17.34 are known. These terminal points are known once the rating of the internal regenerator is done and mass and energy balances are made at the terminal points based on the previous values of the leakage and carryover flow rates. Refer to Shah and Skiepko [36] for further details.

Single-Phase Pressure Drop Analysis

Fluid pumping power is a design constraint in many applications. This pumping power is proportional to the pressure drop in the exchanger in addition to the pressure drops associated with inlet and outlet headers, manifolds, tanks, nozzles, or ducting. The fluid pumping power P associated with the core frictional pressure drop in the exchanger is given by

$$P = \frac{\dot{m}\Delta p}{\rho} \approx \begin{cases} \dfrac{1}{2g_c} \dfrac{\mu}{\rho^2} \dfrac{4L}{D_h} \dfrac{\dot{m}^2}{D_h A_o} f \, \mathrm{Re} & \text{for laminar flow} \quad (17.63a) \\[3mm] \dfrac{0.046}{2g_c} \dfrac{\mu^{0.2}}{\rho^2} \dfrac{4L}{D_h} \dfrac{\dot{m}^{2.8}}{A_o^{1.8} D_h^{0.2}} & \text{for turbulent flow} \quad (17.63b) \end{cases}$$

Only the core friction term is considered in the right-hand side approximation for discussion purposes. Now consider the case of specified flow rate and geometry (i.e., specified $\dot{m}$, L, D_h,

and A_o). As a first approximation, f Re in Eq. 17.63a is constant for fully developed laminar flow, while $f = 0.046\text{Re}^{-0.2}$ is used in deriving Eq. 17.63b for fully developed turbulent flow. It is evident that P is strongly dependent on ρ (P $\propto 1/\rho^2$) in laminar and turbulent flows and on μ in laminar flow, and weakly dependent on μ in turbulent flow. For high-density, moderate-viscosity liquids, the pumping power is generally so small that it has only a minor influence on the design. For a laminar flow of highly viscous liquids in large L/D_h exchangers, pumping power is an important constraint; this is also the case for gases, both in turbulent and laminar flow, because of the great impact of $1/\rho^2$.

In addition, when blowers and pumps are used for the fluid flow, they are generally head-limited, and the pressure drop itself can be a major consideration. Also, for condensing and evaporating fluids, the pressure drop affects the heat transfer rate. Hence, the Δp determination in the exchanger is important. As shown in Eq. 17.177, the pressure drop is proportional to D_h^{-3} and hence it is strongly influenced by the passage hydraulic diameter.

The pressure drop associated with a heat exchanger consists of (1) core pressure drop and (2) the pressure drop associated with the fluid distribution devices such as inlet and outlet manifolds, headers, tanks, nozzles, ducting, and so on, which may include bends, valves, and fittings. This second Δp component is determined from Idelchik [37] and Miller [38]. The core pressure drop may consist of one or more of the following components depending upon the exchanger construction: (1) friction losses associated with fluid flow over heat transfer surface; this usually consists of skin friction, form (profile) drag, and internal contractions and expansions, if any; (2) the momentum effect (pressure drop or rise due to fluid density changes) in the core; (3) pressure drop associated with sudden contraction and expansion at the core inlet and outlet; and (4) the gravity effect due to the change in elevation between the inlet and outlet of the exchanger. The gravity effect is generally negligible for gases. For vertical flow through the exchanger, the pressure drop or rise ("static head") due to the elevation change is given by

$$\Delta p = \pm \frac{\rho_m g L}{g_c} \qquad (17.64)$$

Here the "+" sign denotes vertical upflow (i.e., pressure drop), the "−" sign denotes vertical downflow (i.e., pressure rise or recovery). The first three components of the core pressure drop are now presented for plate-fin, tube-fin, regenerative, and plate heat exchangers. Pressure drop on the shellside of a shell-and-tube heat exchanger is presented in Table 17.31.

Plate-Fin Heat Exchangers.   For the plate-fin exchanger (Fig. 17.10), all three components are considered in the core pressure drop evaluation as follows.

$$\frac{\Delta p}{p_i} = \frac{G^2}{2g_c} \frac{1}{p_i \rho_i} \left[(1 - \sigma^2 + K_c) + f \frac{L}{r_h} \rho_i \left(\frac{1}{\rho}\right)_m + 2\left(\frac{\rho_i}{\rho_o} - 1\right) - (1 - \sigma^2 - K_e) \frac{\rho_i}{\rho_o} \right] \qquad (17.65)$$

where f is the Fanning friction factor, K_c and K_e are flow contraction (entrance) and expansion (exit) pressure loss coefficients, and σ is a ratio of minimum free flow area to frontal area. K_c and K_e for four different long ducts are presented by Kays and London [20] as shown in Fig. 17.35 for which flow is fully developed at the exit. For partially developed flows, K_c is lower and K_e is higher than that for fully developed flows. For interrupted surfaces, flow is never of the fully developed boundary-layer type. For highly interrupted fin geometries, the entrance and exit losses are generally small compared to the core pressure drop, and the flow is well mixed; hence, K_c and K_e for Re → ∞ should represent a good approximation. The entrance and exit losses are important at low values of σ and L (short cores), at high values of Re, and for gases; they are negligible for liquids. The mean specific volume v_m or $(1/\rho)_m$ in Eq. 17.65 is given as follows: for liquids with any flow arrangement, or for a perfect gas with $C^* = 1$ and any flow arrangement (except for parallelflow),
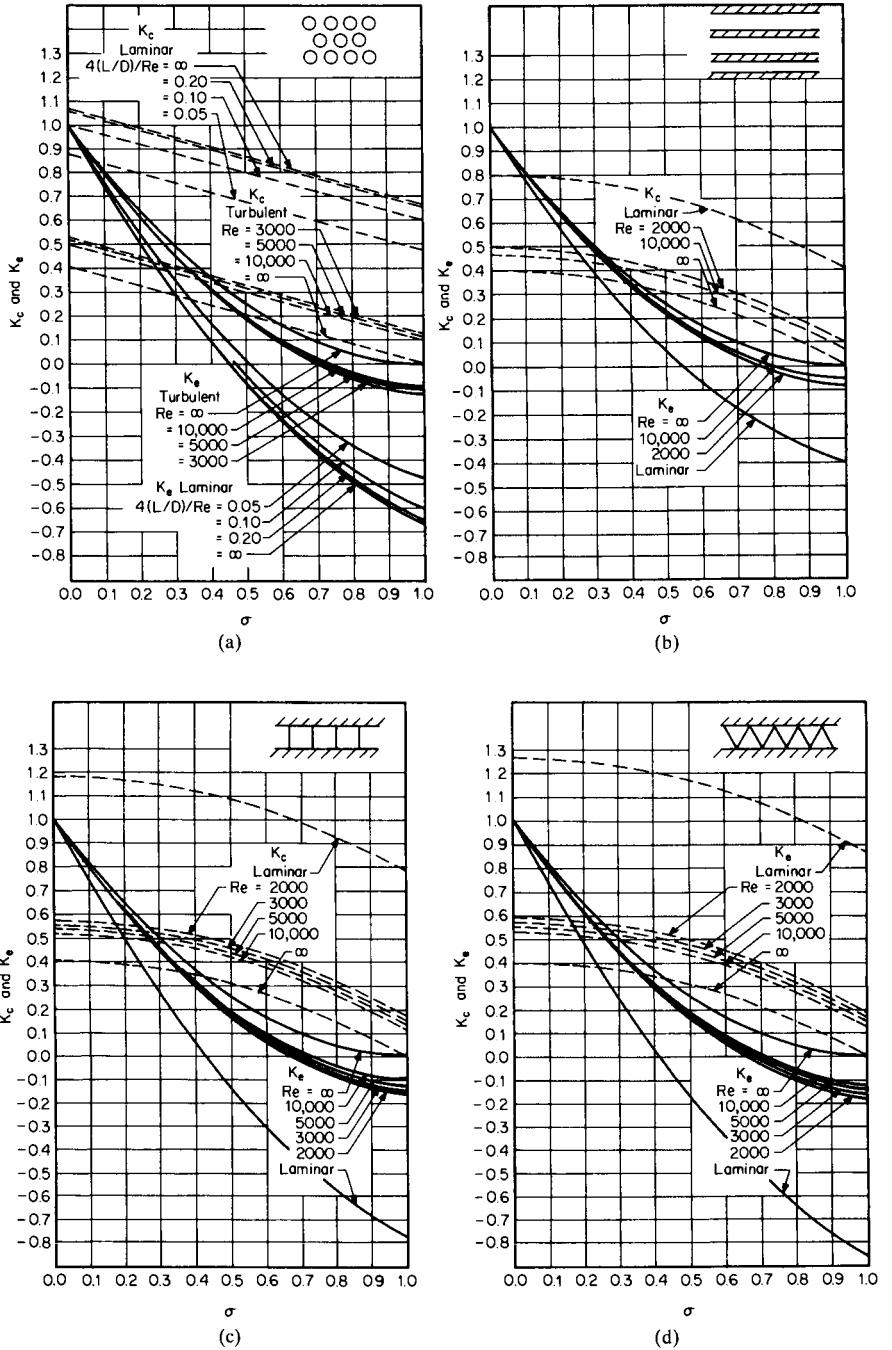
FIGURE 17.35 Entrance and exit pressure loss coefficients: (*a*) circular tubes, (*b*) parallel plates, (*c*) square passages, and (*d*) triangular passages [20]. For each of these flow passages, the fluid flows perpendicular to the plane of the paper into the flow passages.

$$\left(\frac{1}{\rho}\right)_m = v_m = \frac{v_i + v_o}{2} = \frac{1}{2}\left(\frac{1}{\rho_i} + \frac{1}{\rho_o}\right) \tag{17.66}$$

where v is the specific volume in m^3/kg.

For a perfect gas with $C^* = 0$ and any flow arrangement,

$$\left(\frac{1}{\rho}\right)_m = \frac{\tilde{R}}{p_{\text{ave}}} T_{lm} \tag{17.67}$$

Here $\tilde{R}$ is the gas constant in J/(kg K), $p_{\text{ave}} = (p_i + p_o)/2$, and $T_{lm} = T_{\text{const}} + \Delta T_{lm}$, where T_{const} is the mean average temperature of the fluid on the other side of the exchanger; the log-mean temperature difference ΔT_{lm} is defined in Table 17.4. The core frictional pressure drop in Eq. 17.65 may be approximated as

$$\Delta p \approx \frac{4fLG^2}{2g_c D_h}\left(\frac{1}{\rho}\right)_m \approx \frac{4fLG^2}{2g_c \rho_m D_h} \tag{17.68}$$

Tube-Fin Heat Exchangers. The pressure drop inside a circular tube is computed using Eq. 17.65 with proper values of f factors (see equations in Tables 17.14 and 17.16) and K_c and K_e from Fig. 17.35 for circular tubes.

For flat fins on an array of tubes (see Fig. 17.14*b*), the components of the core pressure drop (such as those in Eq. 17.65) are the same with the following exception: the core friction and momentum effect take place within the core with $G = \dot{m}/A_o$, where A_o is the minimum free flow area within the core, and the entrance and exit losses occur at the leading and trailing edges of the core with the associated flow area A_o', so that

$$\dot{m} = GA_o = G'A_o' \qquad \text{or} \qquad G'\sigma' = G\sigma \tag{17.69}$$

where σ' is the ratio of free flow area to frontal area at the fin leading edges and is used in the evaluation of K_c and K_e from Fig. 17.35. The pressure drop for flow normal to a tube bank with flat fins is then given by

$$\frac{\Delta p}{p_i} = \frac{G^2}{2g_c}\frac{1}{p_i \rho_i}\left[f\frac{L}{r_h}\rho_i\left(\frac{1}{\rho}\right)_m + 2\left(\frac{\rho_i}{\rho_o} - 1\right)\right] + \frac{G'^2}{2g_c}\frac{1}{p_i \rho_i}\left[(1 - \sigma'^2 + K_c) - (1 - \sigma'^2 - K_e)\frac{\rho_i}{\rho_o}\right] \tag{17.70}$$

For individually finned tubes as shown in Fig. 17.14*a*, flow expansion and contraction take place along each tube row, and the magnitude is of the same order as that at the entrance and exit. Hence, the entrance and exit losses are generally lumped into the core friction factor. Equation 17.65 for individually finned tubes then reduces to

$$\frac{\Delta p}{p_i} = \frac{G^2}{2g_c}\frac{1}{p_i \rho_i}\left[f\frac{L}{r_h}\rho_i\left(\frac{1}{\rho}\right)_m + 2\left(\frac{\rho_i}{\rho_o} - 1\right)\right] \tag{17.71}$$

Regenerators. For regenerator matrices having cylindrical passages, the pressure drop is computed using Eq. 17.65 with appropriate values of f, K_c, and K_e. For regenerator matrices made up of any porous material (such as checkerwork, wire, mesh, spheres, or copper wool), the pressure drop is calculated using Eq. 17.71, in which the entrance and exit losses are included in the friction factor f.

Plate Heat Exchangers. Pressure drop in a plate heat exchanger consists of three components: (1) pressure drop associated with the inlet and outlet manifolds and ports, (2) pressure drop within the core (plate passages), and (3) pressure drop due to the elevation change. The

pressure drop in the manifolds and ports should be kept as low as possible (generally <10 percent, but it is found as high as 25–30 percent or higher in some designs). Empirically, it is calculated as approximately 1.5 times the inlet velocity head per pass. Since the entrance and exit losses in the core (plate passages) cannot be determined experimentally, they are included in the friction factor for the given plate geometry. The pressure drop (rise) caused by the elevation change for liquids is given by Eq. 17.64. Hence, the pressure drop on one fluid side in a plate heat exchanger is given by

$$\Delta p = \frac{1.5G^2N}{2g_c\rho_i} + \frac{4fLG^2}{2g_cD_e}\left(\frac{1}{\rho}\right)_m + \left(\frac{1}{\rho_o} - \frac{1}{\rho_i}\right)\frac{G^2}{g_c} \pm \frac{\rho_mgL}{g_c} \qquad (17.72)$$

where N is the number of passes on the given fluid side and D_e is the equivalent diameter of flow passages (usually twice the plate spacing). Note that the third term on the right side of the equality sign of Eq. 17.72 is for the momentum effect, which generally is negligible for liquids.

SINGLE-PHASE SURFACE BASIC HEAT TRANSFER AND FLOW FRICTION CHARACTERISTICS

Accurate and reliable surface heat transfer and flow friction characteristics are a key input to the exchanger heat transfer and pressure drop analyses or to the rating and sizing problems (see Fig. 17.36). After presenting the associated nondimensional groups, we will present important experimental methods, analytical solutions, and empirical correlations for some important exchanger geometries.

The dimensionless heat transfer and fluid flow friction (pressure drop) characteristics of a heat transfer surface are simply referred to as the surface basic characteristics or surface basic
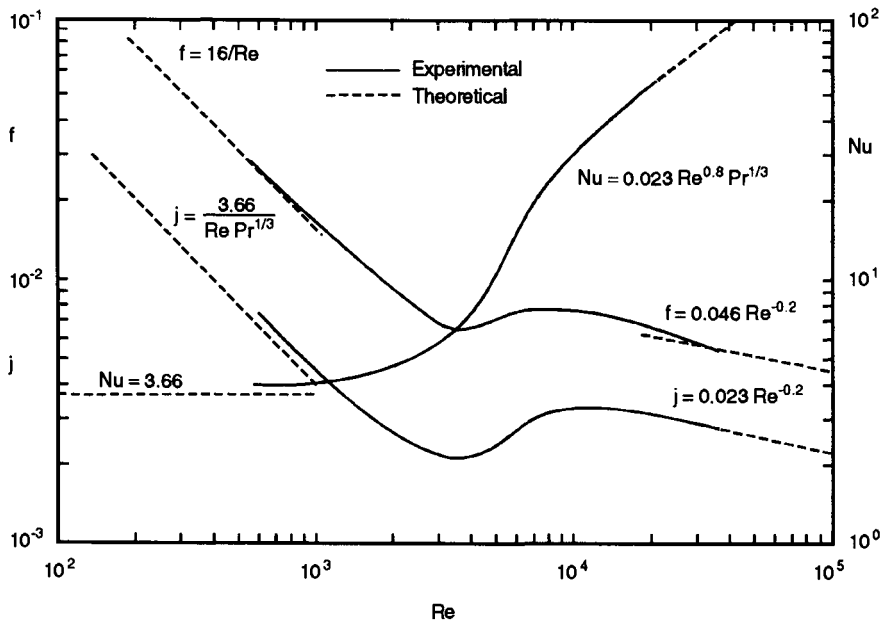

FIGURE 17.36   Basic heat transfer and flow friction characteristics for air flow through a long circular tube.

data.* Generally, the dimensionless experimental heat transfer characteristics are presented in terms of the Colburn factor $j = $ St $Pr^{2/3}$ versus Reynolds number Re, and the theoretical characteristics in terms of Nusselt number Nu versus Re or $x^* = x/(D_h$ Re Pr$)$. The dimensionless pressure drop characteristics are presented in terms of the Fanning friction factor f versus Re or modified friction factor per tube row f_{tb} versus Re_d. These and other important dimensionless groups used in presenting and correlating internal flow forced convection heat transfer are summarized in Table 17.13 with their definition and physical meanings. Where applicable, the hydraulic diameter D_h is used as a characteristic dimension in all dimensionless groups for consistency. However, it must be emphasized that the hydraulic diameter or any other characteristic length does not represent a universal characteristics dimension. This is because the three-dimensional boundary layer and wake effects in noncircular continuous/interrupted flow passages cannot be correlated with a single-length dimension. For some of the dimensionless groups of Table 17.13, a number of different definitions are used in the literature; the user should pay particular attention to the specific definitions used in any research paper before using specific results. This is particularly true for the Nusselt number (where many different temperature differences are used in the definition of h), and for f, Re, and other dimensionless groups having characteristic dimensions different from D_h.

Since the majority of basic data for compact surfaces are obtained experimentally, the dimensionless heat transfer and pressure drop characteristics of these surfaces are presented in terms of j and f versus Re. As an example of these correlating groups, basic heat transfer and flow friction characteristics for air flow in a long circular tube are presented in Fig. 17.36. This figure shows three flow regimes: laminar, transition, and turbulent. This is characteristic of fully developed flow in continuous flow-passage geometries such as a long circular tube and triangular tube. Generally, the compact interrupted surfaces do not have a sharp dip in the transition region (Re ~ 1500–10,000) as shown for the circular tube. Notice that there is a parallel behavior of j versus Re and f versus Re curves, but no such parallelism exists between Nu and f versus Re curves. The parallel behavior of j and f versus Re is useful for: (1) identifying erroneous test data for some specific surfaces for which parallel behavior is expected but indicated otherwise by test results (see Fig. 17.38); (2) identifying specific flow phenomena in which the friction behavior is different from the heat transfer behavior (such as rough surface flow for friction and boundary-layer-type flow for heat transfer in a turbulent flow regime for highly interrupted fin geometries); and (3) predicting the f factors for an unknown surface when the j factors are known by some predictive method. It should be remembered that j versus Re can readily be converted to Nu versus Re curves or vice versa, because $j = $ Nu $Pr^{-1/3}$/Re by definition. Because the values of j, f, and Re are dimensionless, the test data are applicable to surfaces of any hydraulic diameter, provided that complete geometric similarity is maintained.

The limitations of the j versus Re plot, commonly used in presenting compact heat exchanger surface basic data, should be understood. In fully developed laminar flow, as will be discussed, the Nusselt number is theoretically constant, independent of Pr (and also Re). Since $j = $ St $Pr^{2/3} = $ Nu $Pr^{-1/3}$/Re, then j will be dependent upon Pr in the fully developed laminar region, and hence the j factors presented in Chap. 7 of Kays and London [20] for gas flows in the fully developed laminar region should be first converted to a Nusselt number (using Pr = 0.70), which can then be used directly for liquid flows as constant property results. Based on theoretical solutions for thermally developing laminar flow (to be discussed), Nu $\propto$ $(x^*)^{-1/3}$. This means Nu $Pr^{-1/3}$ is independent of Pr, and, hence, j is independent of Pr for thermally developing laminar flows.[†] For fully developed turbulent flow, Nu $\propto$ $Pr^{0.4}$, and, hence,

---

* We will not use the terminology *surface performance data,* since *performance* in industry means a dimensional plot of heat transfer rate and pressure drop as a function of the fluid flow rate for an exchanger. Note that we need to distinguish between the performance of a surface geometry and the performance of a heat exchanger.

[†] If a slope of –1 for the log j-log Re characteristic is used as a criterion for fully developed laminar flow, none of the surfaces (except for long smooth ducts) reported in Chap. 10 of Kays and London [20] would qualify as being in a fully developed laminar condition. Data for most of these surfaces indicate thermally developing flow conditions for which j is almost independent of Pr as indicated (as long as the exponent on Pr is about $-\frac{1}{3}$), and hence the j-Re characteristic should not be converted to the Nu-Re characteristic for the data of Chap. 10, Ref. 20.

TABLE 17.13 Important Dimensionless Groups for Internal Flow Forced Convection Heat Transfer and Flow Friction Useful in Heat Exchanger Design

Dimensionless groups	Definitions and working relationships	Physical meaning and comments
Reynolds number	$\mathrm{Re} = \dfrac{\rho V D_h}{\mu} = \dfrac{G D_h}{\mu}$	A flow modulus proportional to the ratio of inertia force to viscous force
Fanning friction factor	$f = \dfrac{\tau_w}{(\rho V^2/2g_c)}$ $f = \Delta p^* \dfrac{r_h}{L} = \dfrac{\Delta p}{(\rho V^2/2g_c)} \dfrac{r_h}{L}$	The ratio of wall shear (skin frictional) stress to the flow kinetic energy per unit volume; commonly used in heat transfer literature
Apparent Fanning friction factor	$f_{\mathrm{app}} = \Delta p^* \dfrac{r_h}{L}$	Includes the effects of skin friction and the change in the momentum rates in the entrance region (developing flows)
Incremental pressure drop number	$K(x) = (f_{\mathrm{app}} - f_{fd}) \dfrac{L}{r_h}$ $K(\infty) = \text{constant for } x \to \infty$	Represents the excess dimensionless pressure drop in the entrance region over that for fully developed flow
Darcy friction factor	$f_D = 4f = \Delta p^* \dfrac{D_h}{L}$	Four times the Fanning friction factor; commonly used in fluid mechanics literature
Euler number	$\mathrm{Eu} = \Delta p^* = \dfrac{\Delta p}{(\rho V^2/2g_c)}$	The pressure drop normalized with respect to the dynamic velocity head
Dimensionless axial distance for the fluid flow problem	$x^+ = \dfrac{x}{D_h \, \mathrm{Re}}$	The ratio of the dimensionless axial distance (x/D_h) to the Reynolds number; useful in the hydrodynamic entrance region
Nusselt number	$\mathrm{Nu} = \dfrac{h}{k/D_h} = \dfrac{q'' D_h}{k(T_w - T_m)}$	The ratio of the convective conductance h to the pure molecular thermal conductance k/D_h
Stanton number	$\mathrm{St} = \dfrac{h}{G c_p}$ $\mathrm{St} = \dfrac{\mathrm{Nu}}{\mathrm{Pe}} = \dfrac{\mathrm{Nu}}{\mathrm{Re}\,\mathrm{Pr}}$	The ratio of convection heat transfer (per unit duct surface area) to amount virtually transferable (per unit of flow cross-sectional area); no dependence upon any geometric characteristic dimension
Colburn factor	$j = \mathrm{St}\,\mathrm{Pr}^{2/3} = (\mathrm{Nu}\,\mathrm{Pr}^{-1/3})/\mathrm{Re}$	A modified Stanton number to take into account the moderate variations in the Prandtl number for $0.5 \lesssim \mathrm{Pr} \lesssim 10.0$ in turbulent flow
Prandtl number	$\mathrm{Pr} = \dfrac{\nu}{\alpha} = \dfrac{\mu c_p}{k}$	A fluid property modulus representing the ratio of momentum diffusivity to thermal diffusivity of the fluid
Péclet number	$\mathrm{Pe} = \dfrac{\rho c_p V D_h}{k} = \dfrac{V D_h}{\alpha} = \mathrm{Re}\,\mathrm{Pr}$	Proportional to the ratio of thermal energy convected to the fluid to thermal energy conducted axially within the fluid; the inverse of Pe indicates relative importance of fluid axial heat conduction
Dimensionless axial distance for the heat transfer problem	$x^* = \dfrac{x}{D_h \, \mathrm{Pe}} = \dfrac{x}{D_h \, \mathrm{Re}\,\mathrm{Pr}}$	Useful in describing the thermal entrance region heat transfer results
Graetz number	$\mathrm{Gz} = \dfrac{\dot{m} c_p}{k L} = \dfrac{\mathrm{Pe}\,P}{4L} = \dfrac{P}{4 D_h} \dfrac{1}{x^*}$ $\mathrm{Gz} = \pi/(4x^*)$ for a circular tube	Conventionally used in the chemical engineering literature related to x^* as shown when the flow length in Gz is treated as a length variable

$j \propto Pr^{0.07}$. Thus, j is again dependent on Pr in the fully developed turbulent region.* All of the foregoing comments apply to either constant-property theoretical solutions, or almost-constant-property (low-temperature difference) experimental data. The influence of property variations (see p. 17.88) must be taken into account by correcting the aforementioned constant property j or Nu when designing a heat exchanger.

Experimental Methods

Primarily, three different test techniques are used to determine the surface heat transfer characteristics. These techniques are based on the steady-state, transient, and periodic nature of heat transfer modes through the test sections. We will cover here the most common steady-state techniques used to establish the j versus Re characteristics of a recuperator surface. Different data acquisition and reduction methods are used depending upon whether the test fluid is a gas (air) or a liquid. The method used for liquids is generally referred to as the Wilson plot technique. Refer to Ref. 15 for the transient and periodic techniques. Generally, the isothermal steady-state technique is used for the determination of f factors. These test techniques are now described.

Steady-State Test Technique for Gases. Generally, a crossflow heat exchanger is employed as a test section. On one side, a surface for which the j versus Re characteristic is known is employed; a fluid with high heat capacity rate flows on this side. On the other side of the exchanger, a surface for which the j versus Re characteristic is to be determined is employed; the fluid which flows over this unknown-side surface is preferably one that is used in a particular application of the unknown-side surface. Generally, air is used on the unknown side; while steam, hot water, chilled water, or oils having high hAs are used on the known side. A typical test setup used by Kays and London [20] is shown in Fig. 17.37 to provide some ideas on the air-side (unknown-side) components of the test rig. For further details, refer to Ref. 40.

In the experiments, the fluid flow rates on both sides of the exchanger are set constant at predetermined values. Once the steady-state conditions are achieved, fluid temperatures upstream and downstream of the test section on both sides are measured, as well as all pertinent measurements for the determination of the fluid flow rates. The upstream pressure and pressure drop across the core on the unknown side are also recorded to determine the "hot" friction factors.† The tests are repeated with different flow rates on the unknown side to cover the desired range of the Reynolds number.

---

* In 1933 Colburn [39] proposed $j = St\ Pr^{2/3}$ as a correlating parameter to include the effect of Prandtl number based on the then available data for turbulent flow. Based on presently available experimental data, however, the j factor is clearly dependent on Pr for fully developed turbulent flow and for fully developed laminar flow, but not for ideal developing laminar flows.

† The friction factor determined from the Δp measurement taken during the heat transfer testing is referred to as the hot friction factor.
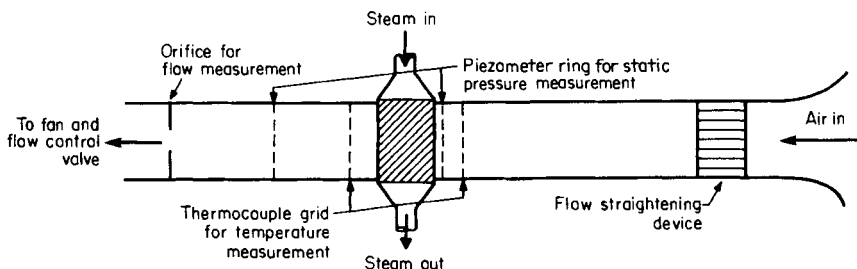

FIGURE 17.37 Schematic of a steam-to-air steady-state heat transfer test rig.

In order to determine the j factor on the unknown side, the exchanger effectiveness ε is determined from the temperature measurements, and the heat capacity rate ratio C^* is determined from individual flow measurements and specific heats. NTU is subsequently computed from the appropriate ε-NTU relationship for the test core flow arrangement (such as Eq. II.1 in Table 17.6). Generally, the test section is a new exchanger core, and fouling resistances are negligible; $\eta_o hA$ on the unknown side is determined from the following thermal resistance equation where UA is found from NTU:

$$\frac{1}{UA} = \frac{1}{(\eta_o hA)_{\text{unknown side}}} + \mathbf{R}_w + \frac{1}{(\eta_o hA)_{\text{known side}}} \tag{17.73}$$

Once the surface area and the geometry are known for the extended surface (if any), h and η_o are computed iteratively using Eqs. 17.73, 17.24, and 17.22 (or an appropriate expression for η_f). Then the j factor is calculated from its definition. The Reynolds number on the unknown side for the test point is determined from its definition for the known mass flow rate and temperature measurements.

The test core is designed with two basic considerations in mind to reduce the experimental uncertainty in the j factors: (1) the magnitudes of thermal resistances on each side as well as of the wall, and (2) the range of NTU.

The thermal resistances in a heat exchanger are related by Eq. 17.73. To reduce the uncertainty in the determination of the thermal resistance of the unknown side (with known overall thermal resistance $1/UA$), the thermal resistances of the exchanger wall and the known side should be kept as small as possible by design. The wall thermal resistance is usually negligible when one of the fluids in the exchanger is air. This may be further minimized through the use of a thin material with high thermal conductivity. On the known side, the thermal resistance is minimized by the use of a liquid (hot or cold water) at high flow rates or a condensing steam (to achieve a high h) or extending the surface area. Therefore, the thermal boundary condition achieved during steady-state testing is generally a close approach to a uniform wall temperature condition.

The NTU range for testing is generally restricted between 0.5 and 3 or between 40 and 90 percent in terms of the exchanger effectiveness. In order to understand this restriction and point out precisely the problem areas, consider the test fluid on the unknown side to be cold air being heated in the test section and the fluid on the known side to be hot water (steam replaced by hot water and its flow direction reversed in Fig. 17.37 to avoid air bubbles). The high NTU occurs at low air flows for a given test core. Both temperature and mass flow rate measurements become more inaccurate at low air flows, and the resultant heat unbalances $(q_w - q_a)/q_a$ increase sharply at low air flows with decreasing air mass flow rate. In this subsection, the subscripts w and a denote water and air sides, respectively. Now, the exchanger effectiveness can be computed in two different ways:

$$\varepsilon = \frac{q_a}{C_a(T_{w,i} - T_{a,i})} \quad \text{or} \quad \varepsilon = \frac{q_w}{C_a(T_{w,i} - T_{a,i})} \tag{17.74}$$

Thus, a large variation in ε will result at low air flows depending upon whether it is based on q_a or q_w. Since ε-NTU curves are very flat at high ε (high NTU), there is a very large error in the resultant NTU, h, and j. The j versus Re curve drops off consistently with decreasing Re, as shown by a dashed line in Fig. 17.38. This phenomenon is referred to as *rollover* or *drop-off* in j. Some of the problems causing the rollover in j are the errors in temperature and air mass flow rate measurements as follows:

FIGURE 17.38 The rollover phenomenon for j versus Re characteristic of a heat exchanger surface at low airflows. The dashed curve indicates the rollover phenomenon; the solid curve represents the accurate characteristics.

1. Basically, the heat transfer coefficients associated with the thermocouple junction or resistance thermometer are quite low at low air flows. Hence, what we measure
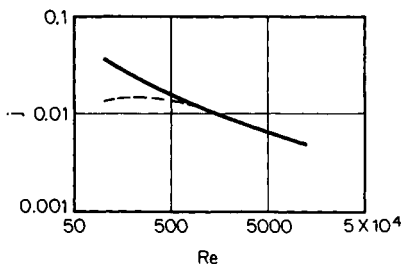
is the junction temperature and not the ambient temperature. Thus, the measured air temperature downstream of the test core $T_{a,o}$ may be too low due to heat conduction along the thermocouple wire. This heat conduction error is not so pronounced for the upstream temperature measurement, since air is at a lower temperature. The measured air temperature upstream of the test core $T_{a,i}$ may be too high due to the radiation effect from the hot core and the hot walls of the wind tunnel because of heat conduction in the duct wall from the hot test core. This error is negligible for the core downstream, since the duct walls are at about the same temperature as the outlet air. Both the aforementioned errors in $T_{a,i}$ and $T_{a,o}$ will decrease the calculated q_a.

2. At low airflows, temperature stratification in the vertical direction would be a problem both upstream and downstream of the test core. Thus it becomes difficult to obtain true bulk mean temperatures $T_{a,i}$ and $T_{a,o}$.

3. On the water side, the temperature drop is generally very small, and hence it will require very accurate instrumentation for ΔT_w measurements. Also, care must be exercised to ensure good mixing of water at the core outlet before ΔT_w is measured.

4. There are generally some small leaks in the wind tunnel between the test core and the point of air mass flow rate measurement. These leaks, although small, are approximately independent of the air mass flow rate, and they represent an increasing fraction of the measured flow rate $\dot{m}_a$ at low air flows. A primary leak test is essential at the lowest encountered test airflow before any testing is conducted.

5. Heat losses to the ambient are generally small for a well-insulated test section. However, they could represent a good fraction of the heat transfer rate in the test section at low airflows. A proper calibration is essential to determine these heat losses.

6. For some test core surfaces, longitudinal heat conduction in the test core surface wall may be important and should be taken into account in the data reduction.

The first five factors cause heat imbalances $(q_w - q_a)/q_a$ to increase sharply at decreasing low air flow rates. In order to minimize or eliminate the rollover in j factors, the data should be reduced based on $q_{ave} = (q_w + q_a)/2$, and whenever possible, by reducing the core flow length (i.e., reducing NTU) by half and then retesting the core.

The uncertainty in the j factors obtained from the steady-state tests ($C^* \approx 0$ case) for a given uncertainty in Δ_2 ($=T_s - T_{a,o}$ or $T_{w,o} - T_{a,o}$) with T_s as condensing steam temperature is given by [15, 40]

$$\frac{d(j)}{j} = \frac{d(\Delta_2)}{\Delta_0} \frac{\text{ntu}_c}{\text{NTU}} \frac{e^{\text{NTU}}}{\text{NTU}} \tag{17.75}$$

Here $\Delta_0 = T_{w,i} - T_{a,i}$ and $\text{ntu}_c/\text{NTU} \approx 1.1$. Thus, a measurement error in the outlet temperature difference [i.e., $d(\Delta_2)$] magnifies the error in j by the foregoing relationship both at high NTU (NTU > 3) and low NTU (NTU < 0.5). The error at high NTU due to the errors in Δ_2 and other factors was discussed above. The error at low NTU due to the error in Δ_2 can also be significant. Hence a careful design of the test core is essential for obtaining accurate j factors.

In addition to the foregoing measurement errors, incorrect j data are obtained for a given surface if the test core is not constructed properly. The problem areas are poor thermal bonds between the fins and the primary surface, gross blockage (gross flow maldistribution) on the air side or water (steam) side, and passage-to-passage nonuniformity (or maldistribution) on the air side. These factors influence the measured j and f factors differently in different Reynolds number ranges. Qualitative effects of these factors are presented in Fig. 17.39 to show the trends. The solid lines in these figures represent the j data of an ideal core having a perfect thermal bond, no gross blockage, and perfect uniformity. The dashed lines represent what happens to j factors when the specified imperfections exist. It is imperative that a detailed air temperature distribution be measured at the core outlet to ensure none of the foregoing problems are associated with the core.
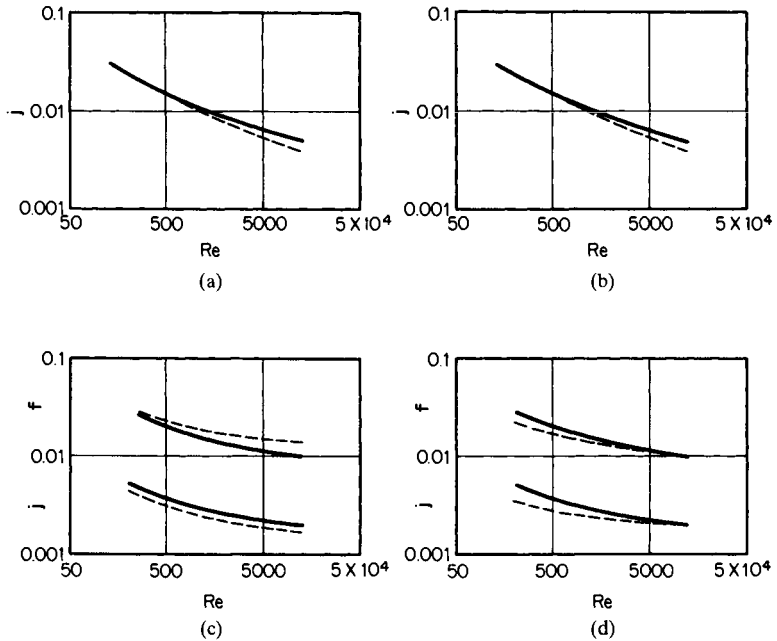
FIGURE 17.39 The influence on measured j data due to (a) poor thermal bond between fins and primary surface, (b) water- (steam-) side gross blockage, (c) air-side blockage, and (d) air-side passage-to-passage nonuniformity. The solid lines are for the perfect core, the dashed lines for the specified imperfect core.

The experimental uncertainty in the j factor for the foregoing steady-state method is usually within ±5 percent when the temperatures are measured accurately to within ±0.1°C (0.2°F) and none of the aforementioned problems exist in the test core. The uncertainty in the Reynolds number is usually within ±2 percent when the mass flow rate is measured accurately within ±0.7 percent.

Wilson Plot Technique for Liquids.   In order to obtain highly accurate j factors, one of the considerations for the design of a test core in the preceding method was to have the thermal resistance on the test fluid (gas) side dominant (i.e., the test fluid side thermal conductance $\eta_o hA$ significantly lower compared to that on the other known side). This is achieved by either steam or hot or cold water at high mass flow rates on the known side. However, if the test fluid is water or another liquid and it has a high heat transfer coefficient, it may not represent a dominant thermal resistance, even if condensing steam is used on the other side. This is because the test fluid thermal resistance may be of the same order of magnitude as the wall thermal resistance. Hence, for liquids, Wilson [41] proposed a technique to obtain heat transfer coefficients h or j factors for turbulent flow in a circular tube.

In this method, liquid (test fluid, unknown side, fluid 1) flows on one side for which j versus Re characteristics are being determined, condensing steam, liquid, or air flows on the other side (fluid 2), for which we may or may not know the j versus Re characteristics. The fluid flow rate on the fluid 2 side and the log-mean average temperature *must* be kept constant (through iterative experimentation) so that its thermal resistance and C_2 in Eq. 17.79 are truly constant. The flow rate on the unknown (fluid 1) side is varied systematically. The fluid flow rates and temperatures upstream and downstream of the test core on each fluid side are measured for each test point. Thus when ε and C^* are known, NTU and UA are computed.

For discussion purposes, consider the test fluid side to be cold and the other fluid side to be hot. UA is given by

$$\frac{1}{UA} = \frac{1}{(\eta_o h A)_c} + \mathbf{R}_{s,c} + \mathbf{R}_w + \mathbf{R}_{s,h} + \frac{1}{(\eta_o h A)_h} \qquad (17.76)$$

Note that $\eta_o = 1$ on the fluid side, which does not have fins. For fully developed turbulent flow through constant cross-sectional ducts, the Nusselt number correlation is of the form

$$\text{Nu} = C_o \, \text{Re}^a \, \text{Pr}^{0.4} \, (\mu_w/\mu_m)^{-0.14} \qquad (17.77)$$

where C_o is a constant and $a = 0.8$ for the Dittus-Boelter correlation. However, note that a is a function of Pr, Re, and the geometry. For example, a varies from 0.78 at Pr = 0.7 to 0.90 at Pr = 100 for Re = 5×10^4 for a circular tube [15]; it also varies with Re for a given Pr. Theoretically, a will vary depending on the tube cross-sectional geometry, particularly for augmented tubes, and is not known a priori. Wilson [41] used $a = 0.82$. The term $(\mu_w/\mu_m)^{-0.14}$ takes into account the variable property effects for liquids; for gases, it should be replaced by an absolute temperature ratio function (see Eq. 17.109). By substituting the definitions of Re, Pr, and Nu in Eq. 17.77 and considering the fluid properties as constant,

$$h_c A_c = A_c (C_o k^{0.6} \rho^{0.82} c_p^{0.4} \mu^{-0.42} D_h^{-0.18})_c V^{0.82} = C_1' V^{0.82} = C_1 V^{0.82}/\eta_{o,c} \qquad (17.78)$$

The test conditions are maintained such that the fouling (scale) resistances $\mathbf{R}_{s,c}$ and $\mathbf{R}_{s,h}$ remain approximately constant though not necessarily zero, although Wilson [41] had neglected them. Since h is maintained constant on the fluid 2 side, the last four terms on the right side of the equality sign of Eq. 17.76 are constant—let us say equal to C_2. Now, substituting Eq. 17.78 in Eq. 17.76, we get

$$\frac{1}{UA} = \frac{1}{C_1 V^{0.82}} + C_2 \qquad (17.79)$$

Equation 17.79 has the form $y = mx + b$ with $y = 1/UA$, $m = 1/C_1$, $x = V^{-0.82}$, and $b = C_2$. Wilson plotted $1/UA$ versus $V^{-0.82}$ on a linear scale as shown in Fig. 17.40. The slope $1/C_1$ and the intercept C_2 are then determined from this plot. Once C_1 is known, h_c from Eq. 17.78 and hence the correlation given by Eq. 17.77 is known.

For this method, the Re exponent of Eq. 17.77 should be known and both resistances on the right side of Eq. 17.79 should be of the same order of magnitude. If C_2 is too small, it could end up negative in Fig. 17.40, depending on the slope due to the scatter in the test data; in this case, ignore the Wilson plot technique and use Eq. 17.76 for the data reduction using the best estimate of C_2. If C_2 is too large, the slope $1/C_1$ will be close to zero and will contain a large experimental uncertainty. If $\mathbf{R}_w$ or $\mathbf{R}_{s,h}$ is too high, $\mathbf{R}_h = 1/(\eta_o h A)_h$ must be kept too low so that C_2 is not very large. However, if $\mathbf{R}_h$ is too low and the hot fluid is a liquid or gas, its temperature drop may be difficult to measure accurately. C_2 can be reduced by increasing h on that side.

The limitations of the Wilson plot technique may be summarized as follows. (1) The fluid flow rate and its log-mean average temperature on the fluid 2 side *must* be kept constant so that C_2 is a constant. (2) The Re exponent in Eq. 17.77 is presumed to be known (such as 0.82 or 0.8). However, in reality it is a function of Re, Pr, and the geometry itself. Since the Re exponent is not known a priori, the Wilson plot technique *cannot* be utilized to determine the constant C_o of Eq. 17.77 for most heat transfer surfaces. (3) All the test data must be in one flow region (e.g., turbulent flow) on fluid 1 side, or the Nu correlation must be expressed by an
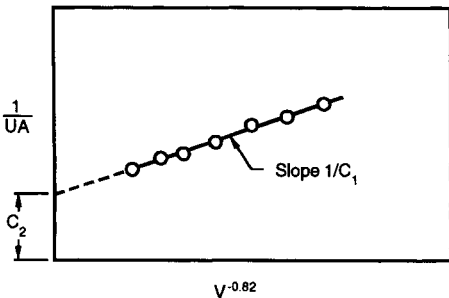

FIGURE 17.40   Original Wilson plot of Eq. 17.79.

explicit equation with only one unknown constant, such as Eq. 17.77 for known exponent a. (4) Fluid property variations and the fin thermal resistance are not taken into consideration on the unknown fluid 1 side. (5) Fouling on either fluid side of the exchanger *must* be kept constant so that C_2 remains constant in Eq. 17.79. Shah [42] discusses how to relax all of the above limitations of the Wilson plot technique except for the third limitation (one flow region for the complete testing); this will be discussed later.

In the preceding case of Eq. 17.79, unknowns are C_1 (means unknown C_o) and C_2. Alternatively, it should be emphasized that if $\mathbf{R}_{s,c}$, $\mathbf{R}_w$, and $\mathbf{R}_{s,h}$ are known a priori, then an unknown C_2 means that only its C_o and a for fluid 2 are unknown. Thus the heat transfer correlation on fluid 2 side can also be evaluated using the Wilson plot technique if the exponents on Re in Eq. 17.77 are known on both fluid sides. The Wilson plot technique thus represents a problem with two unknowns.

For a more general problem (e.g., a shell-and-tube exchanger), consider the Nu correlation on the tube side as Eq. 17.77 with $C_o = C'_t$ and on the shell side as Eq. 17.77 with $C_o = C'_s$ and the Re exponent as d, we can rewrite Eq. 17.76 as follows after neglecting $\mathbf{R}_{s,t} = \mathbf{R}_{s,s} = 0$ for a new/clean exchanger.

$$\frac{1}{UA} = \frac{1}{C_t[\mathrm{Re}^a\ \mathrm{Pr}^{0.4}\ Ak/D_h]_t(\mu_w/\mu_m)_t^{-0.14}} + \mathbf{R}_w + \frac{1}{C_s[\mathrm{Re}^d\ \mathrm{Pr}^{0.4}\ Ak/D_h]_s(\mu_w/\mu_m)_s^{-0.14}} \quad (17.80)$$

where $C_t = \eta_{o,t}C'_t$ and $C_s = \eta_{o,s}C'_s$. Thus, the more general Wilson plot technique has five unknowns (C_t, C_s, a, d, and $\mathbf{R}_w$); Shah [42] discusses the solution procedure.

As mentioned earlier, if one is interested in determining a complete correlation on one fluid side (such as the tube side, Eq. 17.77 without either knowing or not being concerned about the correlation on the other (such as the shell side), it represents a three unknown (C_t, a, and C' of Eq. 17.81) problem. The following procedure is suggested.

1. If the j or Nu versus Re characteristics on the shell side are accurately known, back-calculate the tubeside h from Eq. 17.76 with all other terms known (here, subscripts $c = t$ and $h = s$).

2. If the j or Nu versus Re characteristics on the shell side are *not* known, then the shellside mass flow rate (Reynolds number) and log-mean average temperature *must* be kept constant during the testing. In this case, Eq. 17.80 is manipulated as follows.

$$\left[\frac{1}{UA} - \mathbf{R}_w\right]\left[\frac{\mu_w}{\mu_m}\right]_s^{-0.14} = \frac{1}{C_t}\left\{\frac{(\mu_w/\mu_m)_s^{-0.14}/(\mu_w/\mu_m)_t^{-0.14}}{[\mathrm{Re}^a\ \mathrm{Pr}^{0.4}\ Ak/D_h]_t}\right\} + C' \quad (17.81)$$

where

$$C' = \frac{1}{C_s[\mathrm{Re}^d\ \mathrm{Pr}^{0.4}\ Ak/D_h]_s} = \frac{1}{(\eta_o hA)_s} \quad (17.82)$$

Equation 17.81 has three unknowns, C_t, a, and C', and it represents a variant of the Briggs and Young method [43] for the three-unknown problem. These constants are determined by two successive linear regressions iteratively. The modified Wilson plot of Eq. 17.81 is shown in Fig. 17.41 considering a as known (guessed). In reality, a single plot as shown in Fig. 17.41 is not sufficient. It will require an internal iterative scheme by assuming C' or using it from the previous iteration, computing Nu_s and hence h_s, determining T_w with the measured q, and finally calculating the viscosity ratio functions of Eq. 17.81. Iterations of regression analyses are continued until the successive values of C_t converge within the desired accuracy. Now, with known C', Eq. 17.80 is rearranged as follows.

$$\left[\frac{1}{UA} - \mathbf{R}_w - \frac{C'}{(\mu_w/\mu_m)_s^{-0.14}}\right] \times [\mathrm{Pr}^{0.4}\ Ak/D_h](\mu_w/\mu_m)_t^{-0.14} = \frac{1}{C_t\ \mathrm{Re}_t^a} \quad (17.83)$$

Substituting y_t for the left side of Eq. 17.83 and taking logarithms:

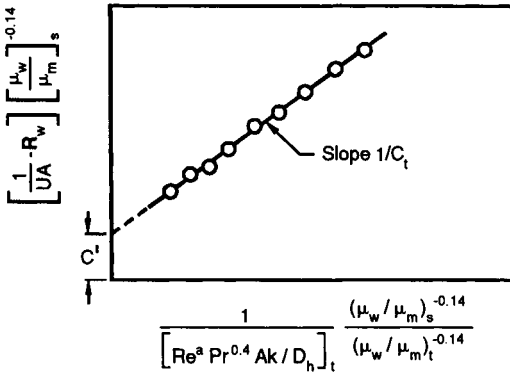$$\ln(1/y_t) = a\ln(\mathrm{Re}_t) + \ln(C_t) \quad (17.84)$$

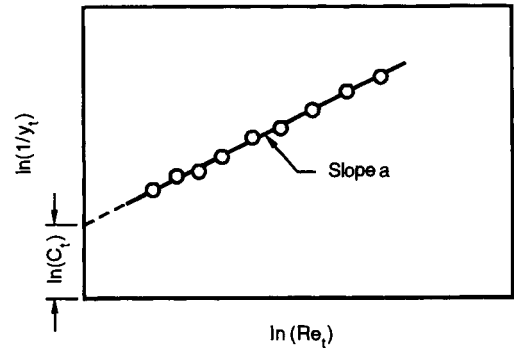**FIGURE 17.41**   A tubeside Wilson plot of Eq. 17.81.

FIGURE 17.42   A tubeside Wilson plot of Eq. 17.84 where y_t is defined by the left side of Eq. 17.83.

Since Eq. 17.84 has a form $Y = mX + b$, C_t and a can be determined from the modified Wilson plot as shown in Fig. 17.42. Note that, here, an internal iterative scheme is not required for the viscosity ratio functions because the shellside C' (correlation) needed to compute the wall temperature is already known from the previous step. Iterations of the modified Wilson plots of Figs. 17.41 and 17.42 are continued until C_t, a, and C' converge within the desired accuracy.

For an accurate determination of C_t and a through the solution of Eq. 17.84, the thermal resistance for the tube side should be dominant for all test points for y_t (of Eq. 17.84) to remain positive. In practice, the purpose of using this modified technique is to determine the tube-side h when its thermal resistance is *not* dominant. If it would have been dominant, use Eq. 17.76 to back-calculate h. If the tube-side resistance cannot be made dominant due to the limitations of test equipment, this method will not yield an accurate tube-side correlation. Hence, a careful design of testing is essential before starting any testing.

If all test points are not in the same flow regime (such as in turbulent flow) for the unknown side of the exchanger using the Wilson plot technique or its variant, use the method recommended in Refs. 15 and 42 to determine h or Nu on the unknown side.

Test Technique for Friction Factors.   The experimental determination of flow friction characteristics of compact heat exchanger surfaces is relatively straightforward. Regardless of the core construction and the method of heat transfer testing, the determination of f is made under steady fluid flow rates with or without heat transfer. For a given fluid flow rate on the unknown side, the following measurements are made: core pressure drop, core inlet pressure and temperature, core outlet temperature for hot friction data, fluid mass flow rate, and the core geometric properties. The Fanning friction factor f is then determined from the following equation:

$$f = \frac{r_h}{L} \frac{1}{(1/\rho)_m} \left[\frac{2g_c \Delta p}{G^2} - \frac{1}{\rho_i} (1 - \sigma^2 + K_c) - 2\left(\frac{1}{\rho_o} - \frac{1}{\rho_i}\right) + \frac{1}{\rho_o} (1 - \sigma^2 - K_e) \right] \qquad (17.85)$$

This equation is an inverted form of the core pressure drop in Eq. 17.65. For the isothermal pressure drop data, $\rho_i = \rho_o = 1/(1/\rho)_m$. The friction factor thus determined includes the effects of skin friction, form drag, and local flow contraction and expansion losses, if any, within the core. Tests are repeated with different flow rates on the unknown side to cover the desired range of the Reynolds number. The experimental uncertainty in the f factor is usually within ±5 percent when Δp is measured accurately within ±1 percent.

Generally, the Fanning friction factor f is determined from isothermal pressure drop data (no heat transfer across the core). The hot friction factor f versus Re curve should be close to the isothermal f versus Re curve, particularly when the variations in the fluid properties are

small, that is, the average fluid temperature for the hot f data is not significantly different from the wall temperature. Otherwise, the hot f data must be corrected to take into account the temperature-dependent fluid properties.

Analytical Solutions

Flow passages in most compact heat exchangers are complex with frequent boundary layer interruptions; some heat exchangers (particularly the tube side of shell-and-tube exchangers and highly compact regenerators) have continuous flow passages. The velocity and temperature profiles across the flow cross section are generally fully developed in the continuous flow passages, whereas they develop at each boundary layer interruption in an interrupted surface and may reach a periodic fully developed flow. The heat transfer and flow friction characteristics are generally different for fully developed flows and developing flows. Analytical results are discussed separately next for developed and developing flows for simple flow passage geometries. For complex surface geometries, the basic surface characteristics are primarily obtained experimentally, as discussed in the previous section; the pertinent correlations are presented in the next subsection.

Analytical solutions for developed and developing velocity/temperature profiles in constant cross section circular and noncircular flow passages are important when no empirical correlations are available, when extrapolations are needed for empirical correlations, or in the development of empirical correlations. Fully developed laminar flow solutions are applicable to highly compact regenerator surfaces or highly compact plate-fin exchangers with plain uninterrupted fins. Developing laminar flow solutions are applicable to interrupted fin geometries and plain uninterrupted fins of short lengths, and turbulent flow solutions to not-so-compact heat exchanger surfaces.

Three important thermal boundary conditions for heat exchangers are ⓣ, ⓗ, and ⓗ②. The ⓣ boundary condition refers to constant wall temperature, both axially and peripherally throughout the passage length. The wall heat transfer rate is constant in the axial direction, while the wall temperature at any cross section is constant in the peripheral direction for the ⓗ boundary condition. The wall heat transfer rate is constant in the axial direction as well as in the peripheral direction for the ⓗ② boundary condition. The ⓗ boundary condition is realized for highly conductive materials where the temperature gradients in the peripheral direction are at a minimum; the ⓗ② boundary condition is realized for very poorly conducting materials for which temperature gradients exist in the peripheral direction. For intermediate thermal conductivity values, the boundary condition will be in between that of ⓗ and ⓗ②. In general, $Nu_{H1} > Nu_T$, $Nu_{H1} \geq Nu_{H2}$, and $Nu_{H2} \gtrsim Nu_T$.

The heat transfer rate in the laminar duct flow is very sensitive to the thermal boundary condition. Hence, it is essential to carefully identify the thermal boundary condition in laminar flow. The heat transfer rate in turbulent duct flow is insensitive to the thermal boundary condition for most common fluids ($Pr > 0.7$); the exception is liquid metals ($Pr < 0.03$). Hence, there is generally no need to identify the thermal boundary condition in turbulent flow for all fluids except liquid metals.
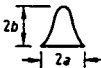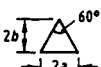
Fully Developed Flows

Laminar Flow. Nusselt numbers for fully developed laminar flow are constant but depend on the flow passage geometry and thermal boundary conditions. The product of the Fanning friction factor and the Reynolds number is also constant but dependent on the flow passage geometry. Fully developed laminar flow problems are analyzed extensively in Refs. 19 and 44; most of the analytical solutions are also presented in closed-form equations in Ref. 44. Solutions for some technically important flow passages are presented in Table 17.14. The following observations may be made from this table: (1) There is a strong influence of flow passage geometry on Nu and f Re. Rectangular passages approaching a small aspect ratio exhibit the highest Nu and f Re. (2) Three thermal boundary conditions have a strong influence on the Nusselt numbers. (3) As $Nu = hD_h/k$, a constant Nu implies the convective heat

transfer coefficient h independent of the flow velocity and fluid Prandtl number. (4) An increase in h can be best achieved either by reducing D_h or by selecting a geometry with a low aspect ratio rectangular flow passage. Reducing the hydraulic diameter is an obvious way to increase exchanger compactness and heat transfer, or D_h can be optimized using well-known heat transfer correlations based on design problem specifications. (5) Since f Re = constant, $f \propto 1/\text{Re} \propto 1/V$. In this case, it can be shown that $\Delta p \propto V$. Many additional analytical results for fully developed laminar flow (Re $\leq$ 2000) are presented in Refs. 19 and 44. For most channel shapes, the mean Nu and f will be within 10 percent of the fully developed value if $L/D_h >$ 0.2Re Pr. The entrance effects, flow maldistribution, free convection, property variation, fouling, and surface roughness all affect fully developed analytical solutions as shown in Table 17.15. Hence, in order to consider these effects in real plate-fin plain fin geometries having fully developed flows, it is best to reduce the magnitude of the analytical Nu by a minimum of 10 percent and increase the value of the analytical f Re by a minimum of 10 percent for design purposes.

Analytical values of L_{hy}^+ and $K(\infty)$ are also listed in Table 17.14. The hydrodynamic entrance length L_{hy} [dimensionless form is $L_{hy}^+ = L_{hy}/(D_h \text{ Re})$] is the duct length required to

TABLE 17.14   Solutions for Heat Transfer and Friction for Fully Developed Laminar Flow through Specified Ducts [19]

Geometry ($L/D_h > 100$)		Nu_{H1}	Nu_{H2}	Nu_T	f Re	$\dfrac{j_{\text{H1}}}{f}$ *	$K(\infty)^\dagger$	$L_{hy}^{+\,\ddagger}$
	$\dfrac{2b}{2a}=\dfrac{\sqrt{3}}{2}$	3.014	1.474	2.39	12.630	0.269	1.739	0.04
	$\dfrac{2b}{2a}=\dfrac{\sqrt{3}}{2}$	3.111	1.892	2.47	13.333	0.263	1.818	0.04
	$\dfrac{2b}{2a}=1$	3.608	3.091	2.976	14.227	0.286	1.433	0.090
		4.002	3.862	3.34	15.054	0.299	1.335	0.086
	$\dfrac{2b}{2a}=\dfrac{1}{2}$	4.123	3.017	3.391	15.548	0.299	1.281	0.085
		4.364	4.364	3.657	16.000	0.307	1.25	0.056
	$\dfrac{2b}{2a}=\dfrac{1}{4}$	5.331	2.94	4.439	18.233	0.329	1.001	0.078
	$\dfrac{2b}{2a}=\dfrac{1}{6}$	6.049	2.93	5.137	19.702	0.346	0.885	0.070
	$\dfrac{2b}{2a}=\dfrac{1}{8}$	6.490	2.94	5.597	20.585	0.355	0.825	0.063
	$\dfrac{2b}{2a}=0$	8.235	8.235	7.541	24.000	0.386	0.674	0.011

* $j_{\text{H1}}/f = \text{Nu}_{\text{H1}}\, \text{Pr}^{-1/3}/(f \text{ Re})$ with Pr = 0.7. Similarly, values of j_{H2}/f and j_T/f may be computed.
† $K(\infty)$ for sine and equilateral triangular channels may be too high [19]; $K(\infty)$ for some rectangular and hexagonal channels is interpolated based on the recommended values in Ref. 19.
‡ L_{hy}^+ for sine and equilateral triangular channels is too low [19], so use with caution. L_{hy}^+ for rectangular channels is based on the faired curve drawn through the recommended value in Ref. 19. L_{hy}^+ for a hexagonal channel is an interpolated value.

TABLE 17.15   Influence of Increase of Specific Variables on Laminar Theoretical Friction Factors and Nusselt Numbers.

Variable	f	Nu
Entrance effect	Increases	Increases
Passage-to-passage nonuniformity	Decreases slightly	Decreases significantly
Gross flow maldistribution	Increases sharply	Decreases
Free convection in a horizontal passage	Increases	Increases
Free convection with vertical aiding flow	Increases	Increases
Free convection with vertical opposing flow	Decreases	Decreases
Property variation due to fluid heating	Decreases for liquids and increases for gases	Increases for liquids and decreases for gases
Property variation due to fluid cooling	Increases for liquids and decreases for gases	Decreases for liquids and increases for gases
Fouling	Increases sharply	Increases slightly
Surface roughness	Affects only if the surface roughness height profile is nonnegligible compared to D_h	Affects only if the surface roughness height profile is nonnegligible compared to D_h

achieve a maximum channel section velocity of 99 percent of that for fully developed flow when the entering fluid velocity profile is uniform. Since the flow development region precedes the fully developed region, the entrance region effects could be substantial, even for channels having fully developed flow along a major portion of the channel. This increased friction in the entrance region and the change of momentum rate is taken into account by the incremental pressure drop number $K(\infty)$ defined by

$$\Delta p = \left[\frac{4f_{fd}L}{D_h} + K(\infty)\right]\frac{G^2}{2g_c\rho} \qquad (17.86)$$

where the subscript fd denotes the fully developed value.

   Transition Flow.   The initiation of transition to turbulent flow, the lower limit of the critical Reynolds number (Re_{cr}), depends on the type of entrance (e.g., smooth versus abrupt configuration at the exchanger flow passage entrance) in smooth ducts. For a sharp square inlet configuration, Re_{cr} is about 10–15 percent lower than that for a rounded inlet configuration. For most exchangers, the entrance configuration would be sharp. Some information on Re_{cr} is provided by Ghajar and Tam [45]. The lower limits of Re_{cr} for various passages with a sharp square inlet configuration vary from about 2000 to 3100 [46]. The upper limit of Re_{cr} may be taken as 10^4 for most practical purposes.

   Transition flow and fully developed turbulent flow Fanning friction factors for a circular duct are given by Bhatti and Shah [46] as

$$f = A + B\,Re^{-1/m} \qquad (17.87)$$

where $A = 0.0054, B = 2.3 \times 10^{-8}, m = -2/3$ for $2100 \leq Re \leq 4000$
$A = 0.00128, B = 0.1143, m = 3.2154$ for $4000 \leq Re \leq 10^7$

Equation 17.87 is accurate within ±2 percent [46]. The transition flow f data for noncircular passages are rather sparse; Eq. 17.87 may be used to obtain fair estimates of f for noncircular flow passages (having no sharp corners) using the hydraulic diameter as the characteristic dimension.

The transition flow and fully developed turbulent flow Nusselt number correlation for a circular tube is given by Gnielinski as reported in Bhatti and Shah [46] as

$$\text{Nu} = \frac{(f/2)(\text{Re} - 1000)\,\text{Pr}}{1 + 12.7(f/2)^{1/2}(\text{Pr}^{2/3} - 1)} \tag{17.88}$$

which is accurate within about ±10 percent with experimental data for $2300 \leq \text{Re} \leq 5 \times 10^6$ and $0.5 \leq \text{Pr} \leq 2000$. For higher accuracies in turbulent flow, refer to the correlations by Petukhov et al. reported by Bhatti and Shah [46]. Churchill as reported in Bhatti and Shah [46] provides a correlation for laminar, transition, and turbulent flow regimes in a circular tube for $2100 < \text{Re} < 10^6$ and $0 < \text{Pr} < \infty$. Since no Nu and j factors are available for transition flow for noncircular passages, Eq. 17.88 may be used to obtain a fair estimate of Nu for noncircular passages (having no sharp corners) using D_h as the characteristic dimension.

Turbulent Flow.   A compendium of available f and Nu correlations for circular and noncircular flow passages are presented in Ref. 46. Table 17.16 is condensed from Ref. 46, summarizing the most accurate f and Nu correlations for smooth circular and noncircular passages.

It is generally accepted that the hydraulic diameter correlates Nu and f for fully developed turbulent flow in circular and noncircular ducts. This is true for the results accurate to within ±15 percent for most noncircular ducts. Exceptions are for those having sharp-angled corners in the flow passage or concentric annuli with inner wall heating. In these cases, Nu and f could be lower than 15 percent compared to the circular tube values. Table 17.16 can be used for more accurate correlations of Nu and f for noncircular ducts.

Roughness on the surface causes local flow separation and reattachment. This generally results in an increase in the friction factor as well as the heat transfer coefficient. A roughness element has no effect on laminar flow, unless the height of the roughness element is not negligible compared to the flow cross section size. However, it exerts a strong influence on turbulent flow. Specific correlations to account for the influence of surface roughness are presented in Refs. 46 and 47.

A careful observation of accurate experimental friction factors for all noncircular smooth ducts reveals that ducts with laminar $f\,\text{Re} < 16$ have turbulent f factors lower than those for the circular tube, whereas ducts with laminar $f\,\text{Re} > 16$ have turbulent f factors higher than those for the circular tube [48]. Similar trends are observed for the Nusselt numbers. If one is satisfied within ±15 percent accuracy, Eqs. 17.87 and 17.88 for f and Nu can be used for noncircular passages with the hydraulic diameter as the characteristic length in f, Nu, and Re; otherwise, refer to Table 17.16 for more accurate results for turbulent flow.

Hydrodynamically Developing Flows

Laminar Flow.   Based on the solutions for laminar boundary layer development over a flat plate and fully developed flow in circular and some noncircular ducts, $f_{\text{app}}\,\text{Re}$ can be correlated by the following equation:
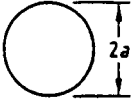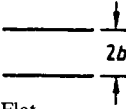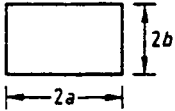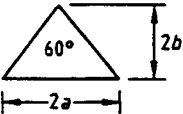
$$f_{\text{app}}\,\text{Re} = 3.44(x^+)^{-0.5} + \frac{K(\infty)/(4x^+) + f\,\text{Re} - 3.44(x^+)^{-0.5}}{1 + C'(x^+)^{-2}} \tag{17.89}$$

where the values of $K(\infty)$, $f\,\text{Re}$, and C' are given in Table 17.17 for three geometries. Here f_{app} is defined the same way as f (see the nomeclature), but Δp includes additional pressure drop due to momentum change and excess wall shear between developing and developed flows.

Turbulent Flow. $f_{\text{app}}\,\text{Re}$ for turbulent flow depends on Re in addition to x^+. A closed-form formula for $f_{\text{app}}\,\text{Re}$ is given in Refs. 46 and 48 for developing turbulent flow. The hydrodynamic entrance lengths for developing laminar and turbulent flows are given by Refs. 44 and 46 as

$$\frac{L_{hy}}{D_h} = \begin{cases} 0.0565\text{Re} & \text{for laminar flow } (\text{Re} \leq 2100) \\ 1.359\text{Re}^{1/4} & \text{for tubulent flow } (\text{Re} \geq 10^4) \end{cases} \tag{17.90}$$

TABLE 17.16 Fully Developed Turbulent Flow Friction Factors and Nusselt Numbers (Pr > 0.5) for Technically Important Smooth-Walled Ducts [44]

Duct geometry and characteristic dimension	Recommended correlations[†]
 Circular $D_h = 2a$	Friction factor correlation for $2300 \leq \mathrm{Re} \leq 10^7$ $$f = A + \frac{B}{\mathrm{Re}^{1/m}}$$ where $A = 0.0054$, $B = 2.3 \times 10^{-8}$, $m = -\frac{2}{3}$ for $2100 \leq \mathrm{Re} \leq 4000$ and $A = 1.28 \times 10^{-3}$, $B = 0.1143$, $m = 3.2154$ for $4000 \leq \mathrm{Re} \leq 10^7$ Nusselt number correlation by Gnielinski for $2300 \leq \mathrm{Re} \leq 5 \times 10^6$: $$\mathrm{Nu} = \frac{(f/2)(\mathrm{Re} - 1000)\,\mathrm{Pr}}{1 + 12.7(f/2)^{1/2}(\mathrm{Pr}^{2/3} - 1)}$$
 Flat $D_h = 4b$	Use circular duct f and Nu correlations. Predicted f are up to 12.5% lower and predicted Nu are within ±9% of the most reliable experimental results.
 Rectangular $D_h = \dfrac{4ab}{a+b}$, $\alpha^* = \dfrac{2b}{2a}$ $\dfrac{D_1}{D_h} = \frac{2}{3} + \frac{11}{24}\,\alpha^*(2 - \alpha^*)$	f factors: (1) substitute D_1 for D_h in the circular duct correlation, and calculate f from the resulting equation. (2) Alternatively, calculate f from $f = (1.0875 - 0.1125\alpha^*)f_c$ where f_c is the friction factor for the circular duct using D_h. In both cases, predicted f factors are within ±5% of the experimental results. Nusselt numbers: (1) With uniform heating at four walls, use circular duct Nu correlation for an accuracy of ±9% for $0.5 \leq \mathrm{Pr} \leq 100$ and $10^4 \leq \mathrm{Re} \leq 10^6$. (2) With equal heating at two long walls, use circular duct correlation for an accuracy of ±10% for $0.5 < \mathrm{Pr} \leq 10$ and $10^4 \leq \mathrm{Re} \leq 10^5$. (3) With heating at one long wall only, use circular duct correlation to get approximate Nu values for $0.5 < \mathrm{Pr} < 10$ and $10^4 \leq \mathrm{Re} \leq 10^6$. These calculated values may be up to 20% higher than the actual experimental values.
 Equilateral triangular $D_h = 2\sqrt{3}a = 4b/3$ $D_1 = \sqrt{3}a = 2b/3\sqrt{3}$	Use circular duct f and Nu correlations with D_h replaced by D_1. Predicted f are within +3% and −11% and predicted Nu within +9% of the experimental values.

[†] The friction factor and Nusselt number correlations for the circular duct are the most reliable and agree with a large amount of the experimental data within ±2% and ±10% respectively. The correlations for all other duct geometries are not as good as those for the circular duct on an absolute basis.

Thermally Developing Flows

Laminar Flow. Thermal entry length solutions with developed velocity profiles are summarized in Refs. 19 and 44 for a large number of practically important flow passage geometries with extensive comparisons.

Shah and London [19] proposed the following correlations for thermal entrance solutions for circular and noncircular ducts having laminar developed velocity profiles and developing temperature profiles.

$$\mathrm{Nu}_{x,T} = 0.427(f\,\mathrm{Re})^{1/3}(x^*)^{-1/3} \tag{17.91}$$

$$\mathrm{Nu}_{m,T} = 0.641(f\,\mathrm{Re})^{1/3}(x^*)^{-1/3} \tag{17.92}$$

TABLE 17.16 Fully Developed Turbulent Flow Friction Factors and Nusselt Numbers (Pr > 0.5) for Technically Important Smooth-Walled Ducts [44] (*Continued*)

Duct geometry and characteristic dimension	Recommended correlations[†]
 Isosceles triangular $D_h = \dfrac{4ab}{a + \sqrt{a^2 + b^2}}$ $\dfrac{D_g}{D_h} = \dfrac{1}{2\pi}\left[3 \ln \cot \dfrac{\theta}{2}\right.$ $\left. + 2 \ln \tan \dfrac{\phi}{2} - \ln \tan \dfrac{\theta}{2}\right]$ where $\theta = (90° - \phi)/2$	For $0 < 2\phi < 60°$, use circular duct f and Nu correlations with D_h replaced by D_g; for $2\phi = 60°$, replace D_h by D_1 (see previous geometry); and for $60° < 2\phi \le 90°$ use circular duct correlations directly with D_h. Predicted f and Nu are within +9% and −11% of the experimental values. No recommendations can be made for $2\phi > 90°$ due to lack of the experimental data.
 Concentric annular $D_h = 2(r_o - r_i),$ $r^* = \dfrac{r_i}{r_0}$ $\dfrac{D_1}{D_h} = \dfrac{1 + r^{*2} + (1 - r^{*2})/\ln r^*}{(1 - r^*)^2}$	f factors: (1) Substitute D_1 for D_h in the circular duct correlation, and calculate f from the resulting equation. (2) Alternatively, calculate f from $f = (1 + 0.0925r^*)f_c$ where f_c is the friction factor for the circular duct using D_h. In both cases, predicted f factors are within ±5% of the experimental results. Nusselt Numbers: In all the following recommendations, use D_h with a wetted perimeter in Nu and Re: (1) Nu at the outer wall can be determined from the circular duct correlation within the accuracy of about ±10% regardless of the condition at the inner wall. (2) Nu at the inner wall cannot be determined accurately regardless of the heating/cooling condition at the outer wall.

[†] The friction factor and Nusselt number correlations for the circular duct are the most reliable and agree with a large amount of the experimental data within ±2% and ±10% respectively. The correlations for all other duct geometries are not as good as those for the circular duct on an absolute basis.
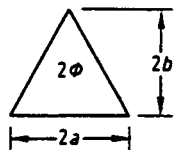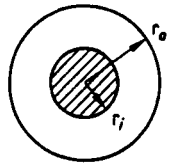
$$\mathrm{Nu}_{x,\mathrm{H1}} = 0.517(f\,\mathrm{Re})^{1/3}(x^*)^{-1/3} \qquad (17.93)$$

$$\mathrm{Nu}_{m,\mathrm{H1}} = 0.775(f\,\mathrm{Re})^{1/3}(x^*)^{-1/3} \qquad (17.94)$$

where f is the Fanning friction factor for fully developed flow, Re is the Reynolds number, and $x^* = x/(D_h\,\mathrm{Re}\,\mathrm{Pr})$. For interrupted surfaces, $x = \ell_{ef}$. Equations 17.91–17.94 are recommended for $x^* < 0.001$.

The following observations may be made from Eqs. 17.91–17.94 and solutions for laminar flow surfaces having developing temperature profiles given in Refs. 19 and 44: (1) the influence of thermal boundary conditions on the convective behavior appears to be of the same order as that for fully developed flow, (2) since Nu $\propto (x^*)^{-1/3} = [x/(D_h\,\mathrm{Re}\,\mathrm{Pr})^{-1/3}]$, then Nu $\propto$ Re$^{1/3} \propto V^{1/3}$—therefore h varies as $V^{1/3}$, (3) since the velocity profile is considered fully devel-

TABLE 17.17 $K(\infty)$, $f\,\mathrm{Re}$, and C' for Use in Eq. 17.89 [19]

	$K(\infty)$	$f\,\mathrm{Re}$	C'
α^*		Rectangular ducts	
1.00	1.43	14.227	0.00029
0.50	1.28	15.548	0.00021
0.20	0.931	19.071	0.000076
0.00	0.674	24.000	0.000029
2Φ		Equilateral triangular duct	
60°	1.69	13.333	0.00053
r^*		Concentric annular ducts	
0	1.25	16.000	0.000212
0.05	0.830	21.567	0.000050
0.10	0.784	22.343	0.000043
0.50	0.688	23.813	0.000032
0.75	0.678	23.967	0.000030
1.00	0.674	24.000	0.000029

oped, $\Delta p \propto V$ as noted earlier; (4) the influence of the duct shape on thermally developed Nu is not as great as that for the fully developed Nu.

The theoretical ratio $\mathrm{Nu}_m/\mathrm{Nu}_{fd}$ is shown in Fig. 17.43 for several passage geometries having constant wall temperature boundary conditions. Several observations may be made from this figure. (1) The Nusselt numbers in the entrance region and hence the heat transfer coefficients could be 2–3 times higher than the fully developed values depending on the interruption length. (2) At $x^* \approx 0.1$, the local Nusselt number approaches the fully developed value, but the value of the mean Nusselt number can be significantly higher for a channel of length $\ell_{ef}^* = x^* = 0.1$. (3) The order of increasing $\mathrm{Nu}_m/\mathrm{Nu}_{fd}$ as a function of channel shape at a given x^*
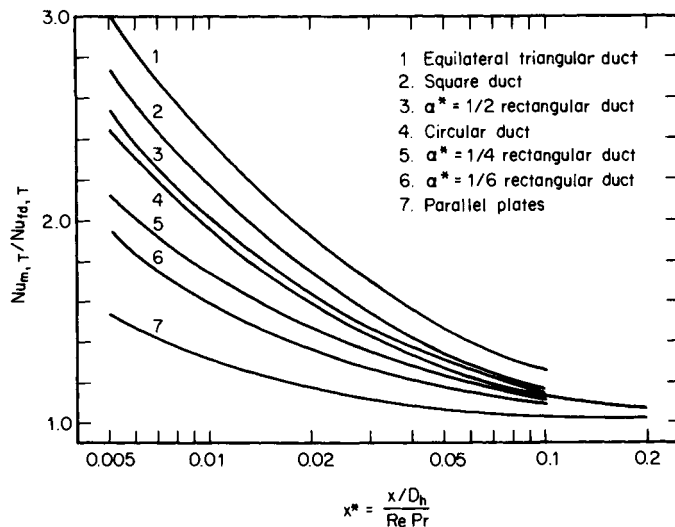

FIGURE 17.43   The ratio of laminar developing to developed Nu for different ducts; the velocity profile developed for both Nu's.

is the opposite of Nu_{fd} in Table 17.14. For a highly interrupted surface, a basic inferior passage geometry for fully developed flow (such as triangular) will not be penalized in terms of low Nu or low h in developing flow. (4) A higher value of Nu_m/Nu_{fd} at $x^* = 0.1$ means that the flow channel has a longer entrance region.

Turbulent Flow. The thermal entry length solutions for smooth ducts for several cross-sectional geometries have been summarized [46]. As for laminar flow, the Nusselt numbers in the thermal region are higher than those in the fully developed region. However, unlike laminar flow, $Nu_{x,T}$ and $Nu_{x,H1}$ are very nearly the same for turbulent flow. The local and mean Nusselt numbers for a circular tube with Ⓣ and Ⓗ boundary conditions are [46]:

$$\frac{Nu_x}{Nu_\infty} = 1 + \frac{c}{10(x/D_h)} \qquad \frac{Nu_m}{Nu_\infty} = 1 + \frac{c}{x/D_h} \tag{17.95}$$

where Nu_∞ stands for the fully developed Nu_T or Nu_H derived from the formulas in Table 17.16, and

$$c = \frac{(x/D_h)^{0.1}}{Pr^{1/6}} \left(0.68 + \frac{3000}{Re^{0.81}} \right) \tag{17.96}$$

This correlation is valid for $x/D_h > 3$, $3500 < Re < 10^5$, and $0.7 < Pr < 75$. It agrees within ± 12 percent with the experimental measurements for $Pr = 0.7$.

Simultaneously Developing Flows

Laminar Flow. In simultaneously developing flow, both the velocity and temperature profiles develop in the entrance region. The available analytical solutions are summarized in Refs. 19 and 44. The theoretical entrance region Nusselt numbers for simultaneously developing flow are higher than those for thermally developing and hydrodynamically developed flow. These theoretical solutions do not take into account the wake effect or secondary flow effect that are present in flow over interrupted heat transfer surfaces. Experimental data indicate that the interrupted heat transfer surfaces do not achieve higher heat transfer coefficients predicted for the simultaneously developing flows. The results for thermally developing flows (and developed velocity profiles) are in better agreement with the experimental data for interrupted surfaces and hence are recommended for design purposes.

Turbulent Flow. The Nusselt numbers for simultaneously developing turbulent flow are practically the same as the Nusselt numbers for the thermally developing turbulent flow [46]. However, the Nusselt numbers for simultaneously developing flow are sensitive to the passage inlet configuration.

Table 17.18 summarizes the dependence of Δp and h on V for developed and developing laminar and turbulent flows. Although these results are for the circular tube, the general functional relationship should be valid for noncircular ducts as a first approximation.

TABLE 17.18 Dependence of Pressure Drop and Heat Transfer Coefficient on the Flow Mean Velocity for Internal Flow in a Constant Cross-Sectional Duct

	$\Delta p \propto V^p$		$h \propto V^q$	
Flow type	Laminar	Turbulent	Laminar	Turbulent
Fully developed	V	$V^{1.8}$	V^0	$V^{0.8}$
Hydrodynamically developing	$V^{1.5}$	$V^{1.8}$	—	—
Thermally developing	V	$V^{1.8}$	$V^{1/3}$	$V^{0.8}$
Simultaneously developing	$V^{1.5}$	$V^{1.8}$	$V^{1/2}$	$V^{0.8}$

Experimental Correlations

Analytical results presented in the preceding section are useful for well-defined constant cross-sectional surfaces with essentially unidirectional flows. The flows encountered in heat exchangers are generally very complex, having flow separation, reattachment, recirculation, and vortices. Such flows significantly affect Nu and f for the specific exchanger surfaces. Since no analytical or accurate numerical solutions are available, the information is derived experimentally. Kays and London [20] and Webb [47] presented many experimental results reported in the open literature. In the following, empirical correlations for only some important surfaces are summarized due to space limitations.

A careful examination of all good data that are published has revealed the ratio $j/f \leq 0.25$ for strip fin, louver fin, and other similar interrupted surfaces. This can be approximately justified as follows. The flow develops along each interruption in such a surface. Based on the Reynolds analogy for fully developed turbulent flow over a flat plate, in the absence of form drag, j/f should be 0.5 for $Pr \approx 1$. Since the contribution of form drag being of the same order of magnitude as the skin friction in developing laminar flows for such an interrupted surface, j/f will be about 0.25. Published data for strip and louver fins are questionable if $j/f > 0.3$. All pressure and temperature measurements and possible sources of flow leaks and heat losses must be checked thoroughly for all those basic data having $j/f > 0.3$ for strip and louver fins.

Bare Tubebanks.   One of the most comprehensive correlations for crossflow over a plain tubebank is presented by Zukauskas [49] as shown in Figs. 17.44 and 17.45 for inline (90° tube layout) and staggered arrangement (30° tube layout) respectively, for the Euler number. These results are valid for the number of tube rows above about 16. For other inline and staggered tube arrangements, a correction factor χ is obtained from the inset of these figures to compute Eu. Zukauskas [49] also presented the mean Nusselt number $Nu_m = h_m d_o/k$ as

$$Nu_m = F_c(Nu_m)_{16 \text{ rows}} \tag{17.97}$$

Values of Nu_m for 16 or more tube rows are presented in Table 17.19 for inline (90° tube layout, Table 17.19*a*) and staggered (30° tube layout, Table 17.19*b*) arrangements. For all expressions in Table 17.19, fluid properties in Nu, Re_d, and Pr are evaluated at the bulk mean temperature and for Pr_w at the wall temperature. The tube row correction factor F_c is presented in Fig. 17.46 as a function of the number of tube rows N_r for inline and staggered tube arrangements.
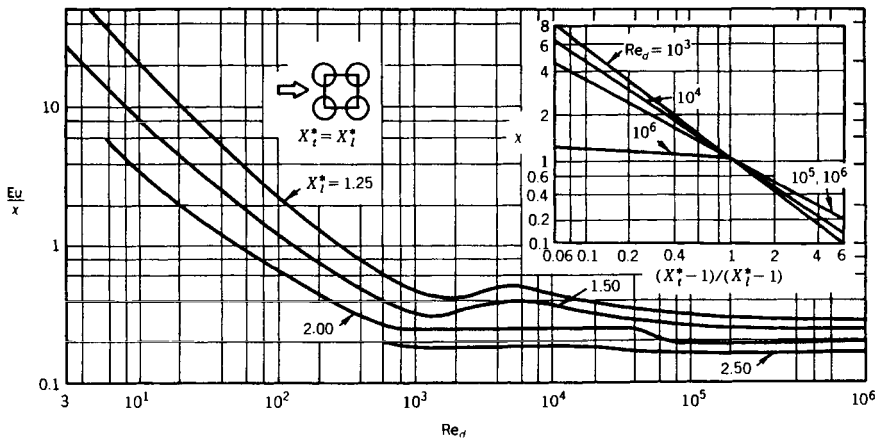
FIGURE 17.44   Friction factors for the inline tube arrangements for $X_t^* = 1.25, 1.5, 2.0,$ and 2.5 where $X_t^* = X_t/d_o$ and $X_l^* = X_l/d_o$ [49].
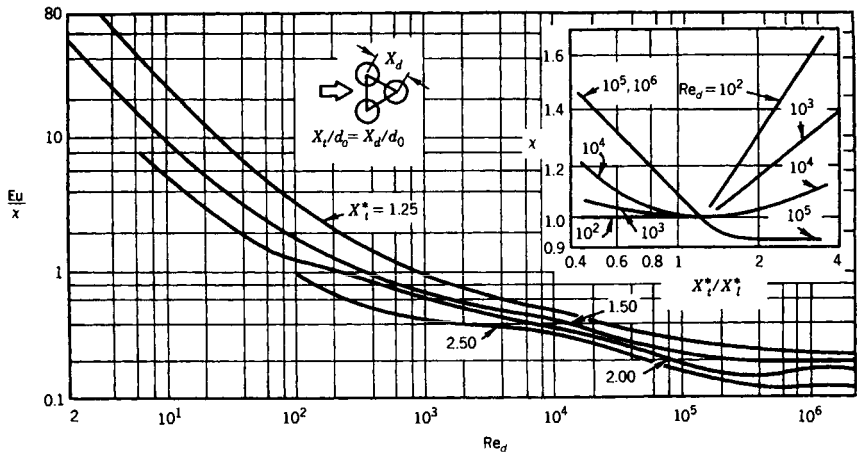
FIGURE 17.45   Friction factors for the staggered tube arrangements for $X_t^* = 1.25, 1.5, 2.0$, and 2.5 where $X_t^* = X_t/d_o$ and $X_t^* = X_t/d_o$ [49].

Plate-Fin Extended Surfaces

Offset Strip Fins.   This is one of the most widely used enhanced fin geometries (Fig. 17.47) in aircraft, cryogenics, and many other industries that do not require mass production. This surface has one of the highest heat transfer performances relative to the friction factor. Extensive analytical, numerical, and experimental investigations have been conducted over the last 50 years. The most comprehensive correlations for j and f factors for the offset strip fin geometry are provided by Manglik and Bergles [50] as follows.

$$j = 0.6522 \text{Re}^{-0.5403} \left(\frac{s}{h'}\right)^{-0.1541} \left(\frac{\delta_f}{\ell_f}\right)^{0.1499} \left(\frac{\delta_f}{s}\right)^{-0.0678} \left[1 + 5.269 \times 10^{-5} \text{Re}^{1.340} \left(\frac{s}{h'}\right)^{0.504} \left(\frac{\delta_f}{\ell_f}\right)^{0.456} \left(\frac{\delta_f}{s}\right)^{-1.055}\right]^{0.1}$$

$$(17.98)$$

TABLE 17.19(a)   Heat Transfer Correlations for Inline Tube Bundles for $n > 16$ [49]

Recommended correlations	Range of Re_d
$\text{Nu} = 0.9\text{Re}_d^{0.4} \text{Pr}^{0.36} (\text{Pr}/\text{Pr}_w)^{0.25}$	$10^0 - 10^2$
$\text{Nu} = 0.52\text{Re}_d^{0.5} \text{Pr}^{0.36} (\text{Pr}/\text{Pr}_w)^{0.25}$	$10^2 - 10^3$
$\text{Nu} = 0.27\text{Re}_d^{0.63} \text{Pr}^{0.36} (\text{Pr}/\text{Pr}_w)^{0.25}$	$10^3 - 2 \times 10^5$
$\text{Nu} = 0.033\text{Re}_d^{0.8} \text{Pr}^{0.4} (\text{Pr}/\text{Pr}_w)^{0.25}$	$2 \times 10^5 - 2 \times 10^6$

TABLE 17.19(b)   Heat Transfer Correlations for Staggered Tube Bundles for $n > 16$ [49]

Recommended correlations	Range of Re_d
$\text{Nu} = 1.04\text{Re}_d^{0.4} \text{Pr}^{0.36} (\text{Pr}/\text{Pr}_w)^{0.25}$	$10^0 - 5 \times 10^2$
$\text{Nu} = 0.71\text{Re}_d^{0.5} \text{Pr}^{0.36} (\text{Pr}/\text{Pr}_w)^{0.25}$	$5 \times 10^2 - 10^3$
$\text{Nu} = 0.35(X_t^*/X_t^*)^{0.2} \text{Re}_d^{0.6} \text{Pr}^{0.36} (\text{Pr}/\text{Pr}_w)^{0.25}$	$10^3 - 2 \times 10^5$
$\text{Nu} = 0.031(X_t^*/X_t^*)^{0.2} \text{Re}_d^{0.8} \text{Pr}^{0.36} (\text{Pr}/\text{Pr}_w)^{0.25}$	$2 \times 10^5 - 2 \times 10^6$

FIGURE 17.46 A correction factor F_c to take into account the tube-row effect for heat transfer for flow normal to bare tubebanks.

FIGURE 17.47 An offset strip fin geometry.

$$f = 9.6243 \text{Re}^{-0.7422}\left(\frac{s}{h'}\right)^{-0.1856}\left(\frac{\delta_f}{\ell_f}\right)^{0.3053}\left(\frac{\delta_f}{s}\right)^{-0.2659}\left[1 + 7.669 \times 10^{-8} \text{Re}^{4.429}\left(\frac{s}{h'}\right)^{0.920}\left(\frac{\delta_f}{\ell_f}\right)^{3.767}\left(\frac{\delta_f}{s}\right)^{0.236}\right]^{0.1}$$
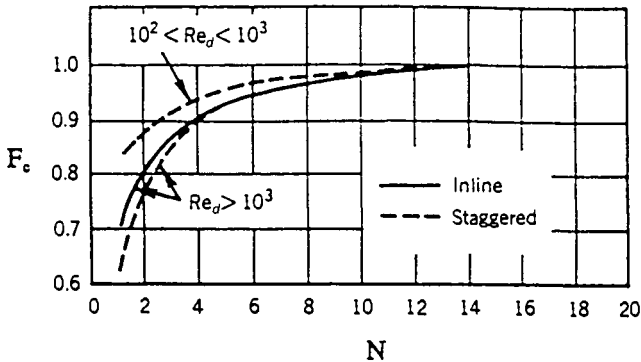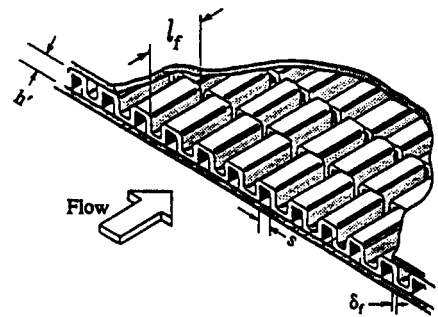
(17.99)

where $$D_h = 4A_o/(A/\ell_f) = 4sh'\ell_f/[2(s\ell_f + h'\ell_f + \delta_f h') + \delta_f s]$$ (17.100)

Geometrical symbols in Eq. 17.100 are shown in Fig. 17.47.

These correlations predict the experimental data of 18 test cores within ±20 percent for $120 \le \text{Re} \le 10^4$. Although all experimental data for these correlations are obtained for air, the j factor takes into consideration minor variations in the Prandtl number, and the above correlations should be valid for $0.5 < \text{Pr} < 15$.

The heat transfer coefficients for the offset strip fins are 1.5 to 4 times higher than those of plain fin geometries. The corresponding friction factors are also high. The ratio of j/f for an offset strip fin to j/f for a plain fin is about 80 percent. If properly designed, the offset strip fin would require substantially lower heat transfer surface area than that of plain fins at the same Δp, but about a 10 percent larger flow area.

Louver Fins. Louver or multilouver fins are extensively used in auto industry due to their mass production manufacturability and lower cost. It has generally higher j and f factors than those for the offset strip fin geometry, and also the increase in the friction factors is in general higher than the increase in the j factors. However, the exchanger can be designed for higher heat transfer and the same pressure drop compared to that with the offset strip fins by a proper selection of exchanger frontal area, core depth, and fin density. Published literature and correlations on the louver fins are summarized by Webb [47] and Cowell et al. [51], and the understanding of flow and heat transfer phenomena is summarized by Cowell et al. [51]. Because of the lack of systematic studies reported in the open literature on modern louver fin geometries, no correlation can be recommended for the design purpose.

Other Plate-Fin Surfaces. Perforated and pin fin geometries have been investigated, and it is found that they do not have superior performance compared to offset strip and louver fin geometries [15]. Perforated fins are now used only in a limited number of applications. They are used as "turbulators" in oil coolers and in cryogenic air separation exchangers as a replacement to the existing perforated fin exchangers; modern cryogenic air separation exchangers use offset strip fin geometries. Considerable research has been reported on vortex generators using winglets [52, 53], but at present neither definitive conclusions are available on the superiority of these surfaces nor manufactured for heat exchanger applications.

Tube-Fin Extended Surfaces.   Two major types of tube-fin extended surfaces are: (1) individually finned tubes, and (2) flat fins (also sometimes referred to as plate fins), with or without enhancements/interruptions on an array of tubes as shown in Fig. 17.14. An extensive coverage of the published literature and correlations for these extended surfaces is provided by Webb [47] and Kays and London [20]. Empirical correlations for some important geometries are summarized below.

Individually Finned Tubes.   In this fin geometry, helically wrapped (or extruded) circular fins on a circular tube as shown in Fig. 17.14*a*, is commonly used in process and waste heat recovery industries. The following correlation for *j* factors is recommended by Briggs and Young (see Webb [47]) for individually finned tubes on staggered tubebanks.

$$j = 0.134 \mathrm{Re}_d^{-0.319} \, (s/\ell_f)^{0.2} (s/\delta_f)^{0.11} \qquad (17.101)$$

where ℓ_f is the radial height of the fin, δ_f is the fin thickness, $s = p_f - \delta_f$ is the distance between adjacent fins, and p_f is the fin pitch. Equation 17.101 is valid for the following ranges: $1100 \leq \mathrm{Re}_d \leq 18{,}000$, $0.13 \leq s/\ell_f \leq 0.63$, $1.01 \leq s/\delta_f \leq 6.62$, $0.09 \leq \ell_f/d_o \leq 0.69$, $0.011 \leq \delta_f/d_o \leq 0.15$, $1.54 \leq X_t/d_o \leq 8.23$, fin root diameter d_o between 11.1 and 40.9 mm, and fin density N_f ($=1/p_f$) between 246 and 768 fins per meter. The standard deviation of Eq. 17.101 with experimental results was 5.1 percent.

For friction factors, Robinson and Briggs (see Webb [47]) recommended the following correlation.

$$f_{tb} = 9.465 \mathrm{Re}_d^{-0.316} \, (X_t/d_o)^{-0.927} (X_t/X_d)^{0.515} \qquad (17.102)$$

Here $X_d = (X_t^2 + X_l^2)^{1/2}$ is the diagonal pitch and X_t and X_l are the transverse and longitudinal tube pitches, respectively. The correlation is valid for the following ranges: $2000 \leq \mathrm{Re}_d \leq 50{,}000$, $0.15 \leq s/\ell_f \leq 0.19$, $3.75 \leq s/\delta_f \leq 6.03$, $0.35 \leq \ell_f/d_o \leq 0.56$, $0.011 \leq \delta_f/d_o \leq 0.025$, $1.86 \leq X_t/d_o \leq 4.60$, $18.6 \leq d_o \leq 40.9$ mm, and $311 \leq N_f \leq 431$ fins per meter. The standard deviation of Eq. 17.102 with correlated data was 7.8 percent.

For crossflow over low-height finned tubes, Rabas and Taborek [54], Ganguli and Yilmaz [55], and Chai [56] have assessed the pertinent literature. A simple but accurate correlation for heat transfer is given by Ganguli and Yilmaz [55] as

$$j = 0.255 \mathrm{Re}_d^{-0.3} \, (d_e/s)^{-0.3} \qquad (17.103)$$

A more accurate correlation for heat transfer is given by Rabas and Taborek [54]. Chai [56] provides the best correlation for friction factors:

$$f_{tb} = 1.748 \mathrm{Re}_d^{-0.233} \left(\frac{\ell_f}{s}\right)^{0.552} \left(\frac{d_o}{X_t}\right)^{0.599} \left(\frac{d_o}{X_l}\right)^{0.1738} \qquad (17.104)$$

This correlation is valid for $895 < \mathrm{Re}_d < 713{,}000$, $20 < \theta < 40°$, $X_t/d_o < 4$, $N_r \geq 4$, and θ is the tube layout angle. It predicts 89 literature data points within a mean absolute error of 6 percent; the range of actual error is from -16.7 to 19.9 percent.

Plain Flat Fins on a Staggered Tubebank.   This geometry, as shown in Fig. 17.14*b*, is used in the air-conditioning/refrigeration industry for cost considerations as well as where the pressure drop on the fin side prohibits the use of enhanced/interrupted flat fins. An inline tubebank is generally not used unless very low finside pressure drop is the essential requirement. The heat transfer correlation for Fig. 17.14*b* for flat plain fins on staggered tubebanks is provided by Gray and Webb (see Webb [47]) as follows for four or more tube rows with the subscript 4.

$$j_4 = 0.14 \mathrm{Re}_d^{-0.328} \, (X_t/X_l)^{-0.502} (s/d_o)^{0.031} \qquad (17.105)$$

For the number of tube rows N_r from 1 to 3, the *j* factor is lower and is given by

$$\frac{j_N}{j_4} = 0.991[2.24 \mathrm{Re}_d^{-0.092} \, (N_r/4)^{-0.031}]^{0.607(4 - N_r)} \qquad (17.106)$$

Gray and Webb hypothesized the friction factor consisting of two components—one associated with the fins and the other associated with the tubes as follows.

$$f = f_f \frac{A_f}{A} + f_t \left(1 - \frac{A_f}{A}\right)\left(1 - \frac{\delta_f}{p_f}\right) \tag{17.107}$$

where

$$f_f = 0.508 \mathrm{Re}_d^{-0.521} \, (X_t/d_o)^{1.318} \tag{17.108}$$

and f_t (defined the same way as f) is the Fanning friction factor associated with the tube and can be determined from Eu of Fig. 17.45 as $f_t = \mathrm{Eu}\, N_r(X_t - d_o)/\pi d_o$. Equation 17.107 correlated 90 percent of the data for 19 heat exchangers within ± 20 percent. The ranges of dimensionless variables of Eqs. 17.107 and 17.108 are $500 \leq \mathrm{Re} \leq 24{,}700$, $1.97 \leq X_t/d_o \leq 2.55$, $1.7 \leq X_l/d_o \leq 2.58$, and $0.08 \leq s/d_o \leq 0.64$.

Influence of Temperature-Dependent Fluid Properties

One of the basic idealizations made in the theoretical solutions for Nu and f is that the fluid properties remain constant throughout the flow field. Most of the experimental j and f data obtained in the preceding section involve small temperature differences so that the fluid properties generally do not vary significantly. In certain heat exchanger applications, fluid temperatures vary significantly. At least two questions arise: (1) Can we use the j and f data obtained for air at 50 to 100°C (100 to 200°F) for air at 500 to 600°C (900 to 1100°F)? (2) Can we use the j and f data obtained with air (such as all data in Ref. 20) for water, oil, and viscous liquids? The answer is yes, by modifying the constant-property j and f data to account for variations in the fluid properties within a heat exchanger. The property ratio method is the most commonly used technique to take into account the fluid property variations in the heat exchanger. In this method, the Nusselt number and friction factors for the variable fluid property case are related to the constant-property values for gases and liquids as follows:

For gases:
$$\frac{\mathrm{Nu}}{\mathrm{Nu}_{cp}} = \left(\frac{T_w}{T_m}\right)^n \qquad \frac{f}{f_{cp}} = \left(\frac{T_w}{T_m}\right)^m \tag{17.109}$$

For liquids:
$$\frac{\mathrm{Nu}}{\mathrm{Nu}_{cp}} = \left(\frac{\mu_w}{\mu_m}\right)^n \qquad \frac{f}{f_{cp}} = \left(\frac{\mu_w}{\mu_m}\right)^m \tag{17.110}$$

Here the subscript cp refers to the constant property variable, and all temperatures in Eq. 17.109 are *absolute*. All of the properties in the dimensionless groups of Eqs. 17.109 and 17.110 are evaluated at the *bulk mean* temperature. The values of the exponents n and m for fully developed laminar and turbulent flows in a circular tube are summarized in Table 17.20 for heating and cooling situations. These correlations, Eqs. 17.109 and 17.110, with exponents from Table 17.20a and b, are derived for the constant heat flux boundary condition. The variable-property effects are generally not important for fully developed flow having constant wall temperature boundary condition, since T_m approaches T_w for fully developed flow. Therefore, in order to take into account minor influence of property variations for the constant wall temperature boundary condition, the correlations of Eqs. 17.109 and 17.110 are adequate.

The Nu and f factors are also dependent upon the duct cross-sectional shape in laminar flow, and are practically independent of the duct shape in turbulent flow. The influence of variable fluid properties on Nu and f for fully developed laminar flow through rectangular ducts has been investigated by Nakamura et al. [57]. They concluded that the velocity profile is strongly affected by the μ_w/μ_m ratio, and the temperature profile is weakly affected by the μ_w/μ_m ratio. They found that the influence of the aspect ratio on the correction factor $(\mu_w/\mu_m)^m$ for the friction factor is negligible for $\mu_w/\mu_m < 10$. For the heat transfer problem, the Sieder-Tate correlation ($n = -0.14$) is valid only in the narrow range of $0.4 < \mu_w/\mu_m < 4$.

TABLE 17.20(a) Property Ratio Method Exponents of Eqs. 17.109 and 17.110 for Laminar Flow

Fluid	Heating	Cooling
Gases	$n = 0.0, m = 1.00$ for $1 < T_w/T_m < 3$	$n = 0.0, m = 0.81$ for $0.5 < T_w/T_m < 1$
Liquids	$n = -0.14, m = 0.58$ for $\mu_w/\mu_m < 1$	$n = -0.14, m = 0.54$ for $\mu_w/\mu_m < 1$

TABLE 17.20(b) Property Ratio Method Correlations or Exponents of Eqs. 17.109 and 17.110 for Turbulent Flow

Fluid	Heating	Cooling
Gases	$Nu = 5 + 0.012Re^{0.83} (Pr + 0.29)(T_w/T_m)^n$ $n = -[\log_{10}(T_w/T_m)]^{1/4} + 0.3$ for $1 < T_w/T_m < 5, 0.6 < Pr < 0.9,$ $10^4 < Re < 10^6$ and $L/D_h > 40$	$n = 0$
	$m = -0.1$ for $1 < T_w/T_m < 2.4$	$m = -0.1$ (tentative)
Liquids	$n = -0.11*$ for $0.08 < \mu_w/\mu_m < 1$ $f/f_{cp} = (7 - \mu_w/\mu_m)/6^\dagger$ or $m = 0.25$ for $0.35 < \mu_w/\mu_m < 1$	$n = -0.25*$ for $1 < \mu_w/\mu_m < 40$ $m = 0.24^\dagger$ for $1 < \mu_w/\mu_m < 2$

* Valid for $2 \leq Pr \leq 140$, $10^4 \leq Re \leq 1.25 \times 10^5$.
† Valid for $1.3 \leq Pr \leq 10$, $10^4 \leq Re \leq 2.3 \times 10^5$.

Influence of Superimposed Free Convection

The influence of superimposed free convection over pure forced convection flow is important when the flow velocity is low, a high temperature difference $(T_w - T_m)$ is employed, or the passage geometry has a large hydraulic diameter D_h. The effect of the superimposed free convection is generally important in the laminar flow of a noncompact heat exchanger; it is quite negligible for compact heat exchangers [19], and hence it will not be covered here. The reader may refer to Ref. 58 for further details.

It should be emphasized that, for laminar flow of liquids in tubes, the influence of viscosity and density variations (buoyancy or free convection effects) must be considered simultaneously for heat exchanger applications. Some correlations and work in this area have been summarized by Bergles [59].

TWO-PHASE HEAT TRANSFER AND PRESSURE DROP CORRELATIONS

Flow Patterns

The *flow pattern* depicts a distinct topology (regarding the spatial and temporal distributions of vapor and liquid phases) of two-phase flow and greatly influences the resulting phenomena of heat transfer and friction. An important feature of a particular flow pattern is the direct relationships of the heat transfer and pressure drop characteristics to the pattern type, leading to an easy identification of important macroscopic heat transfer modes. Consequently, an approach to the selection of appropriate heat transfer and/or pressure drop correlations has to be preceded by an identification of the involved flow patterns.

A particular flow pattern depends upon the flow passage geometry, its orientation, relative magnitudes of flow rates of fluid phases, fluid properties, boundary conditions, and so on. For a heat exchanger designer, several characteristic geometric settings are of special interest: (1) two-phase flow patterns in vertical, horizontal, and inclined flow passages (upward or downward internal flow); and (2) flow patterns in vertical and horizontal flow passages of the shell side of a shell-and-tube heat exchanger (i.e., external crossflow—shellside flow).

Internal Flow

Vertical Ducts.   Typical flow patterns in upward vertical two-phase flow in a tube are presented in Fig. 17.48a. At low vapor qualities and low mass flow rates, the flow usually obeys the bubbly flow pattern. At higher vapor qualities and mass flow rates, slug or plug flow replaces the bubbly flow pattern. Further increase in vapor quality and/or mass flow rates leads to the appearance of the churn, annular, and wispy annular flow patterns.

The prediction of a flow pattern is a very important step in the analysis of a two-phase flow. In a graphical form, flow-pattern maps provide an empirical quantitative set of criteria for predicting flow conditions for a given flow pattern to occur; also, flow pattern maps delineate the boundaries of transitions from one flow regime to another. In Fig. 17.49, a flow pattern map is presented for a vertical upward flow [60, 113]. The map offers only a rough estimation of all the pattern transitions in terms of the so-called superficial momentum fluxes of the vapor and liquid (i.e., $\rho_v j_v^2 = G^2 x^2/\rho_v$ versus $\rho_l j_l^2 = G^2(1-x)^2/\rho_l$). Note that loci of points correspond to the precisely defined pairs of superficial vapor and liquid momentum fluxes, but the corresponding transition boundaries should actually be interpreted as transition regions. The presented map, although not entirely reliable and less sophisticated than some subsequently developed for various situations, still provides a guide for engineering use. Taitel et al. [61] developed semiempirical models for transition between the flow patterns of steady upward gas-liquid flow in vertical tubes. Weisman and Kang [62] developed empirical flow pattern maps for both vertical and upward inclined tubes.

Horizontal Ducts.   The topology of flow patterns in horizontal tubes with a circular cross section has different although analogous structure to that for the upward vertical two-phase flow. In Fig. 17.48b, the major types of the horizontal tube flow patterns are presented.

A flow pattern map for two-phase horizontal tube flow is given in Fig. 17.50. This map, developed by Taitel and Dukler [63], presents the transitions between various flow patterns in terms of three parameters K, F, and T as a function of the Martinelli parameter X, the ratio of the frictional pressure gradients for the gas and liquid phases flowing alone in the duct. All these parameters are defined in the figure caption. The transition between dispersed bubbly flow and intermittent flow (i.e., plug and slug flows, see Fig. 17.48b) is defined with a T versus X curve in Fig. 17.50. The transition between wavy (stratified) and both intermittent and annular (dispersed) flows is defined as an F versus X curve. The transition between stratified (smooth) and wavy flow is defined as a K versus X curve. Finally, the transition between either dispersed bubbly or intermittent flow patterns and annular flow is defined with a constant X line ($X = 1.6$). In addition to the Taitel and Dukler semiempirical map, a number of other flow pattern maps have been proposed, and the corresponding studies of the flow pattern transitions for horizontal two-phase flows have been conducted. An analysis of flow patterns for the entire range of duct inclinations is given by Barnea [64, 65]. An overview of the interfacial and structural stability of separated flow (both stratified and annular) is presented in Ref. 66. The most recent review and flow pattern map for boiling is provided by Kattan et al. [67].

External Flow (Shell Side).

Two-phase flow patterns for flow normal to tube bundles (crossflow), such as on the shell side of a shell-and-tube heat exchanger, are much more complex than those inside a plain circular tube. Consequently, prediction of flow patterns in such situations is very difficult. It is important to note that two-phase shellside flow patterns are substantially less analyzed than those for internal flows. A review of the shellside flow pattern is presented by Jensen [68]. The dominant flow patterns (see Fig. 17.51 [69]) may be assessed

Bubbly Flow   Slug Flow   Churn Flow   Wispy-Annular Flow   Annular Flow

(a)

Bubbly Flow

Plug Flow

Stratified Flow

Wavy Flow

Slug Flow

Annular Flow

(b)
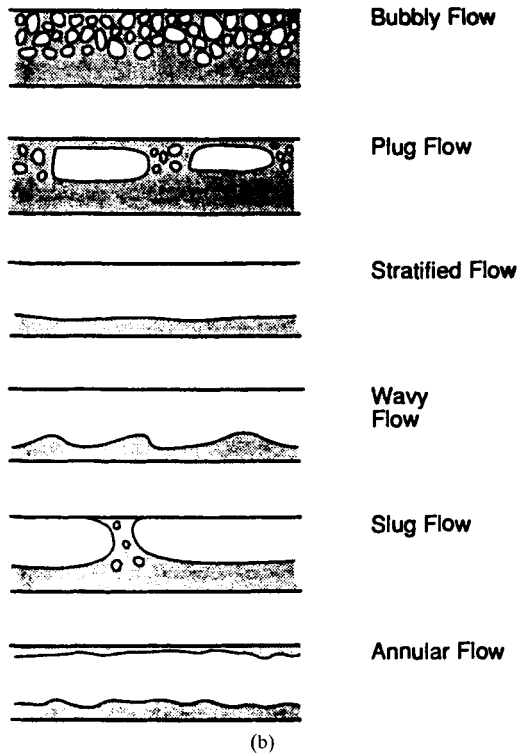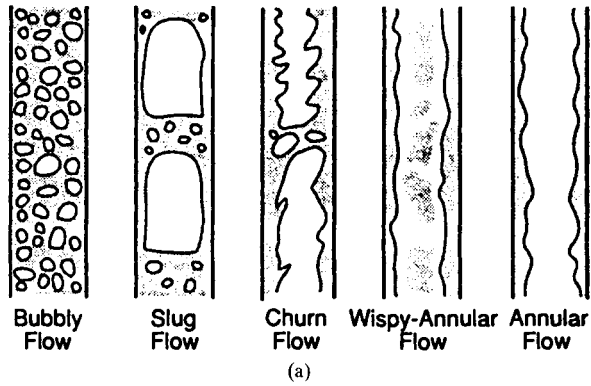
FIGURE 17.48 Flow patterns: (*a*) vertical cocurrent two-phase flow, (*b*) horizontal cocurrent two-phase flow [76].

using the flow pattern map presented in Fig. 17.52 by Grant and Chrisholm [70]. Again, as in the case of flow pattern maps for internal flows, the actual transitions are not abrupt as presented in Fig. 17.52. The flow pattern transitions are given as functions of liquid and gas velocities based on minimum cross-sectional areas and modified by a fluid property parameter to take into account property variations.
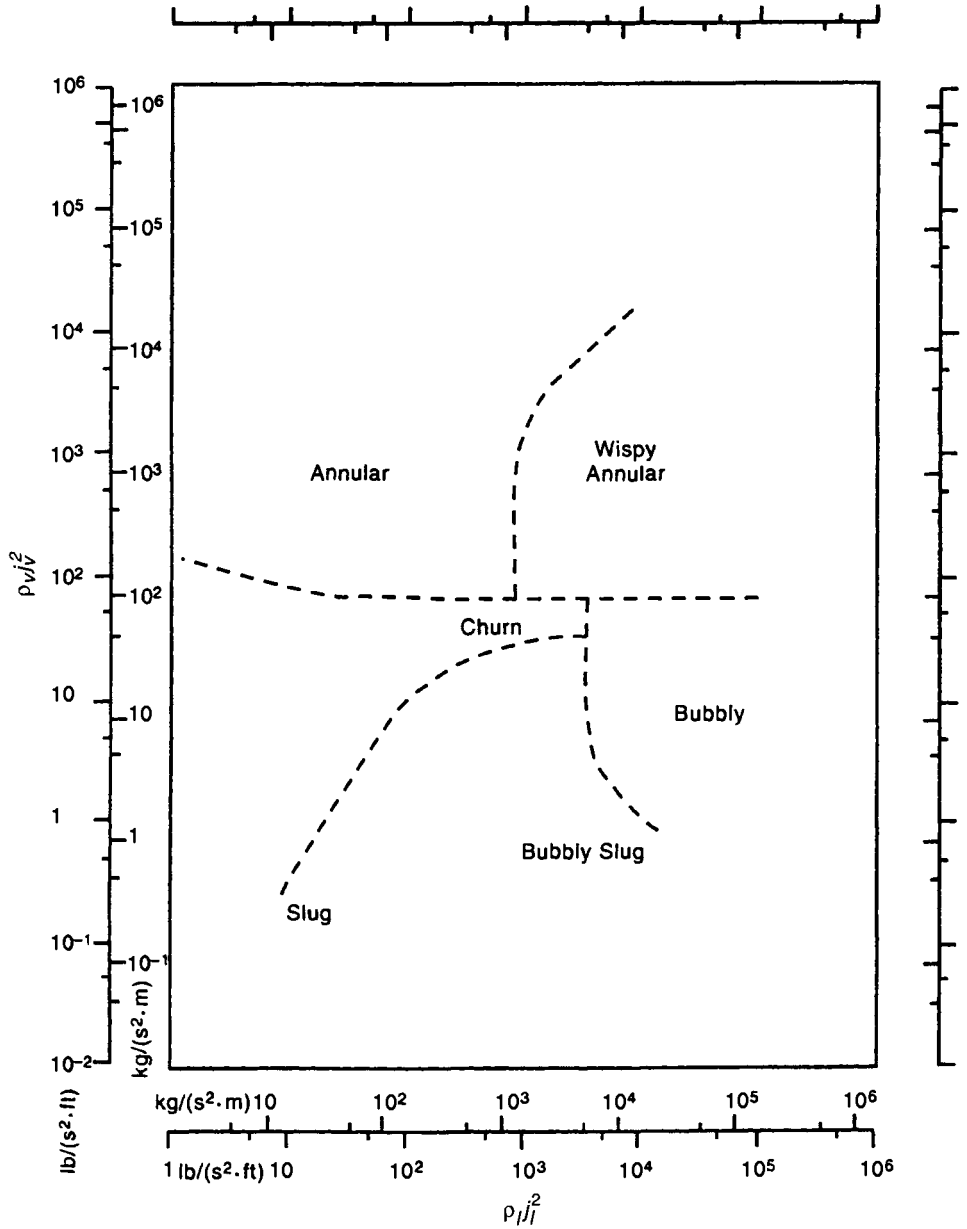
FIGURE 17.49 Flow pattern map for vertical, upward two-phase flow [60].
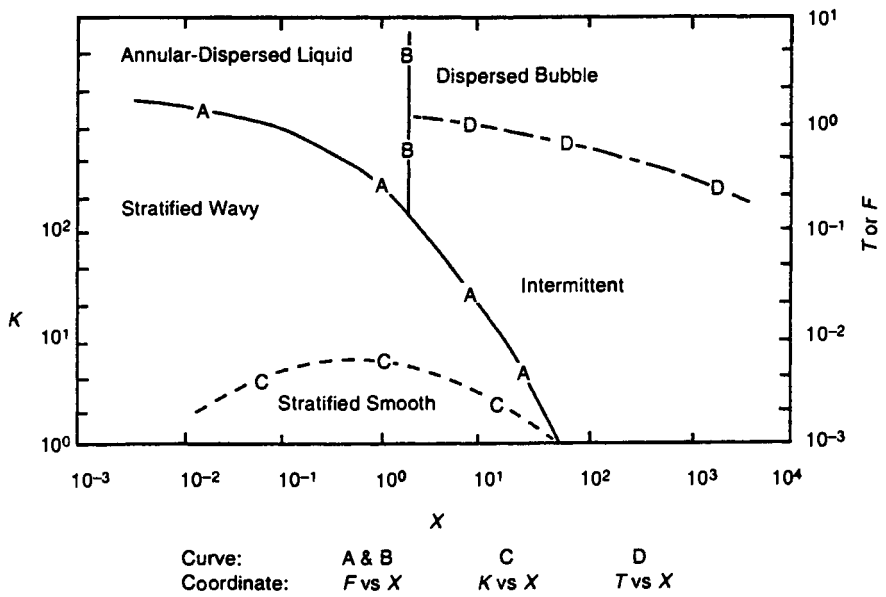
FIGURE 17.50 Flow pattern map for horizontal two-phase flow [63]. $X = [(dp/dz)_l/(dp/dz)_v]^{1/2}$, $K = F(d_i j_l/\nu_l)^{1/2}$, $F = [\rho_v/(\rho_l - \rho_v)]^{1/2} j_v/(d_i g \cos\theta)^{1/2}$, and $T = \{(dp/dz)_l/[(\rho_l - \rho_v)g \cos\theta]\}^{1/2}$ [63].

FIGURE 17.51 Flow patterns in tube bundles: (*a*) spray flow, (*b*) bubbly flow (vertical and horizontal), (*c*) chugging flow (vertical), (*d*) stratified spray flow, (*e*) horizontal stratified flow as defined by Grant and reported in Ref. 69.

17.93
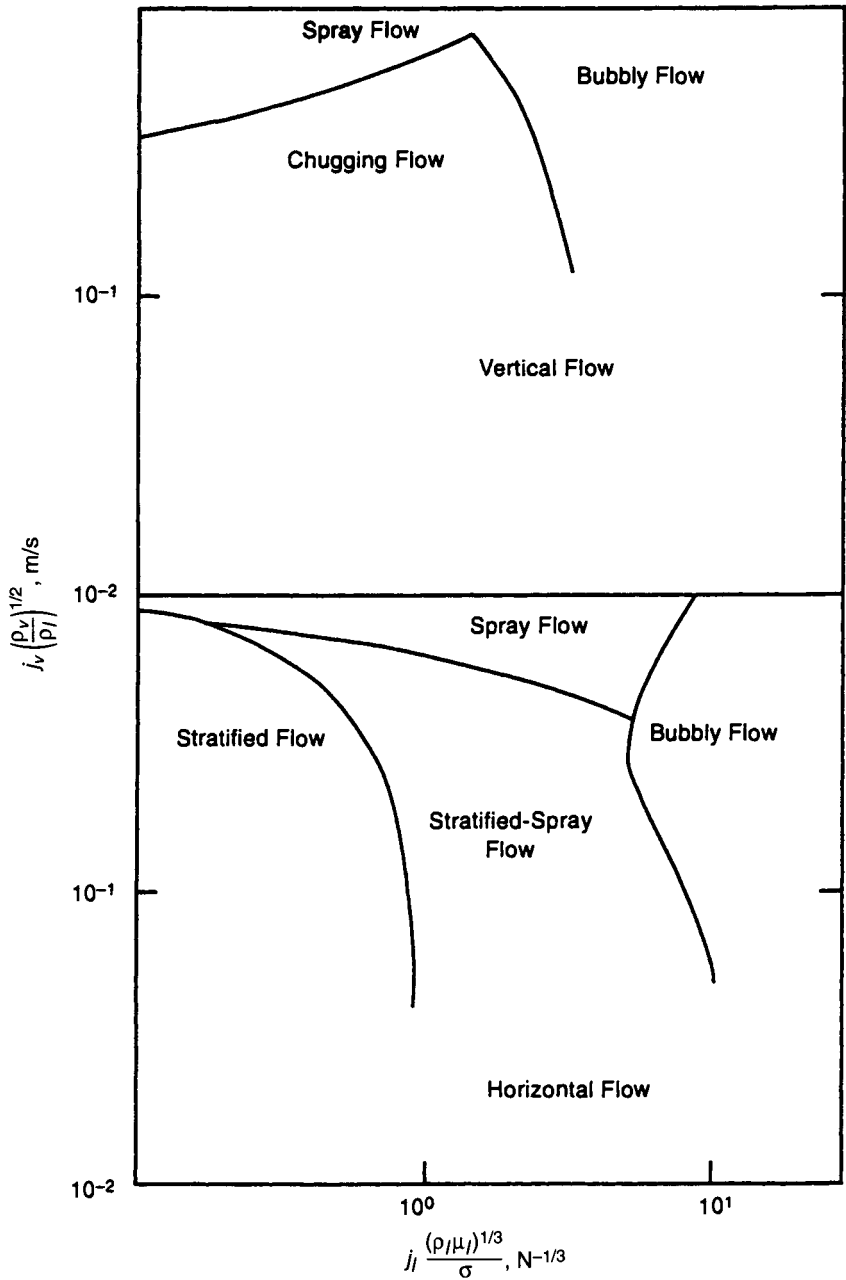
FIGURE 17.52 A flow pattern map for shellside two-phase flow by Grant, as reported in [71].

Two-Phase Pressure Drop Correlations

As a rule, the pressure drop for a two-phase flow is difficult to predict with good accuracy because of the presence of two phases, which results into various pressure drop components of individual phases and their interactions to well-understood, single-phase flows. The total pressure drop in a two-phase flow can be calculated as follows:

$$\Delta p = \Delta p_s + \Delta p_f + \Delta p_m + \Delta p_g \qquad (17.111)$$

Major contributions to the total pressure drop (i.e., the various terms on the right-hand side of the equality sign of Eq. 17.111) depend on losses caused by friction and momentum changes along the two-phase fluid flow path. The list may include the following contributions: (1) pressure drop due to various singularities along the flow path such as an abrupt change in the free flow area, bends, and valves Δp_s (details regarding calculation of this pressure drop are provided in [71]), (2) two-phase friction loss Δp_f, (3) hydrostatic loss (i.e., the gravity loss or static head) Δp_g, and (4) momentum change loss (caused by acceleration or deceleration of the flow) Δp_m. The three dominant contributions are friction (the most difficult to determine accurately), momentum change (can be sizable in both vaporizers and condensers, primarily in vacuum operation), and hydrostatic effects (important only in a nonhorizontal flow). In most geometries, entrance and exit losses of Δp_s are difficult to measure. Hence, in two-phase or multiphase flow, they are often lumped into friction losses.

Analytical expressions for the three dominant pressure drop contributions will be discussed next. The correlations will be presented separately for internal (in-tube) and external (shellside—tube bundle) two-phase flows.

Intube Pressure Drop. The two-phase friction pressure drop can be estimated from the corresponding pressure drop for single-phase flow (with total two-phase fluid flowing as vapor or liquid) and multiplying that pressure drop magnitude with the so-called two-phase friction multiplier denoted as φ^2. The two-phase friction multiplier should be defined for corresponding hypothetical single-phase flows assuming that mass velocities are either equal to the actual respective m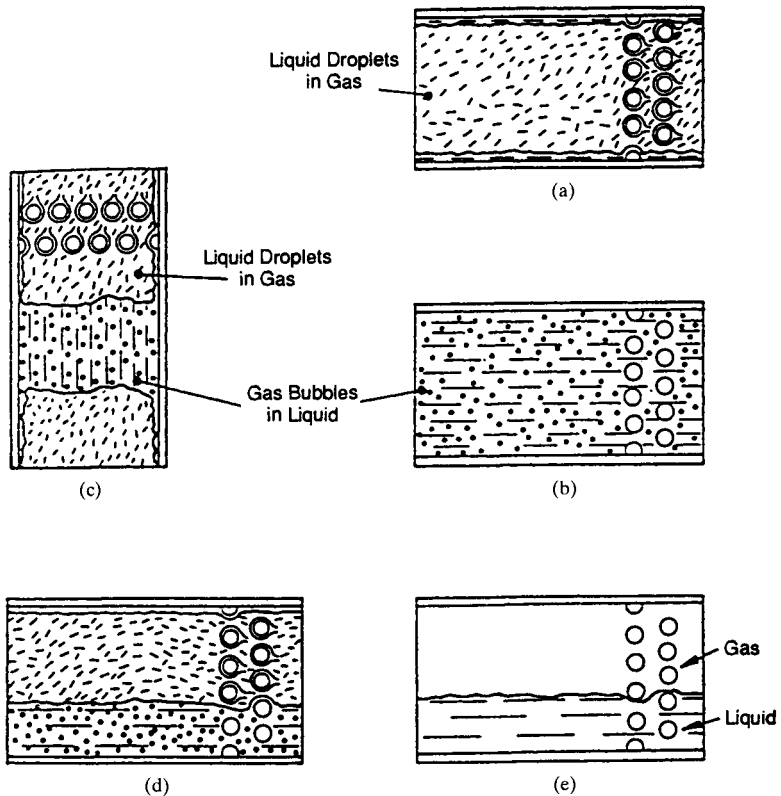ass velocities $[G_l = (1 - x)G, G_v = xG]$, or to the total mass velocity G. For example, the frictional multiplier φ_{lo}^2 represents the ratio of the two-phase frictional pressure gradient and the single-phase (liquid) pressure gradient for a flow with the same total mass velocity as liquid [71]. Therefore, the friction pressure drop can be presented as:

$$\Delta p_f = \Delta p_{f,lo}\varphi_{lo}^2 = f_{lo}\frac{2L}{D_h}\frac{G^2}{g_c\rho_l}\,\varphi_{lo}^2 \qquad \text{or} \qquad \Delta p_f = \Delta p_{f,vo}\varphi_{vo}^2 = f_{vo}\frac{2L}{D_h}\frac{G^2}{g_c\rho_v}\,\varphi_{vo}^2 \qquad (17.112)$$

where f_{lo} and f_{vo} represent the single-phase Fanning friction factor (the total mass flow rate as liquid or vapor, respectively, f_{lo} equal to $16/\mathrm{Re}_{lo}$ for $\mathrm{Re}_{lo} = GD_h/\mu_l < 2000$, and $f_{lo} = 0.079(\mathrm{Re}_{lo})^{-0.25}$ for $\mathrm{Re}_{lo} > 2000$). In Table 17.21, the two most reliable correlations for the friction multiplier are presented, a Friedel correlation [71, 72] for vertical upward and horizontal flow and $\mu_l/\mu_v < 1000$, and the Chisholm correlation [71, 73] for $\mu_l/\mu_v > 1000$ and $G > 100 \text{ kg/m}^2$s. An empirically determined standard deviation for Friedel correlation [72] can be fairly large, up to 50 percent for two-component flows compared with a data bank of 25,000 data points [71]. The standard deviation is smaller for single-component flows, up to 30 percent. However, for small mass fluxes ($G < 100 \text{ kg/m}^2$s), the two correlations given in Table 17.21 are not accurate. The best correlation available for this range of mass fluxes is the well-known Lockhart-Martinelli correlation [74]. This correlation uses φ_l^2 and φ_v^2, fractional multipliers for vapor and liquid phases, based on the single-phase pressure gradients defined by

$$\Delta p_f = \Delta p_{f,l}\varphi_l^2 = \Delta p_{f,v}\varphi_v^2 \qquad (17.113)$$

where φ_l^2 and φ_v^2 are given by Ref. 74 as follows for $\mu_l/\mu_v > 1000$ and $G < 100 \text{ kg/m}^2$s:

$$\varphi_l^2 = \frac{(dp/dz)}{(dp/dz)_l} = 1 + \frac{c}{X} + \frac{1}{X^2} \qquad (17.113a)$$

TABLE 17.21   Frictional Multiplier Correlations*

Correlation	Parameters	Ref.
Friedel correlation $$\varphi_{lo}^2 = E + 3.23 \frac{FH}{Fr^{0.045} We^{0.035}}$$	$$E = (1-x)^2 + x^2 \frac{\rho_l}{\rho_v} \frac{f_{vo}}{f_{lo}} \qquad F = x^{0.78}(1-x)^{0.24}$$ $$H = \left(\frac{\rho_l}{\rho_v}\right)^{0.91} \left(\frac{\mu_v}{\mu_l}\right)^{0.19} \left(1 - \frac{\mu_v}{\mu_l}\right)^{0.7}$$ $$Fr = \frac{G^2}{g D_h \rho_{hom}^2} \qquad We = \frac{G^2 D_h}{\sigma \rho_{hom}}$$ $$\frac{1}{\rho_{hom}} = \frac{x}{\rho_v} + \frac{1-x}{\rho_l}; \qquad \frac{\mu_l}{\mu_v} < 1000$$	71
Chisholm correlation $$\varphi_{lo}^2 = 1 + (Y^2 - 1)[Bx^{n^*}(1-x)^{n^*} + x^{2-n}]$$ $$n^* = \frac{2-n}{2}$$	$Y = (\Delta p_{fvo}/\Delta p_{L,lo})^{1/2}, \quad n = 1/4$ [exponent in $f = C\,Re^n$] $$B = \begin{cases} 4.8 & G < 500 \\ 2400/G & 500 \le G < 1900 \\ 55/G^{1/2} & G \ge 1900 \end{cases} \text{ for } Y \le 9.5$$ $$B = \begin{cases} 520/(YG^{1/2}) & G \le 600 \\ 21/Y & G > 600 \end{cases} \text{ for } 9.5 < Y < 28$$ $$B = 15{,}000/(Y^2 G^{1/2}) \text{ for } Y > 28$$ $$\frac{\mu_l}{\mu_v} > 1000; G > 100$$	71

* The parameters E, F, H, Y, and B are local for this table as defined; other variables in SI units.

$$\varphi_v^2 = \frac{(dp/dz)}{(dp/dz)_v} = 1 + cX + X^2 \qquad (17.113b)$$

In Eqs. 17.113a and 17.113b, the value of c depends on the single-phase regime for liquid and vapor streams as follows: (1) if both liquid and vapor phases are turbulent, $c = 20$; (2) if the liquid phase is turbulent and the vapor phase is viscous (laminar), $c = 10$; (3) if the liquid phase is viscous and the vapor phase is turbulent, $c = 12$; and (4) if both liquid and vapor phases are viscous, $c = 5$.

The momentum pressure drop can be calculated integrating the momentum balance equation [75], thus obtaining:

$$\Delta p_m = \frac{G^2}{g_c}\left[\left(\frac{x^2}{\alpha\rho_v} + \frac{(1-x)^2}{(1-\alpha)\rho_l}\right)_{z=z_2} - \left(\frac{x^2}{\alpha\rho_v} + \frac{(1-x)^2}{(1-\alpha)\rho_l}\right)_{z=z_1}\right] \qquad (17.114)$$

where α represents the void fraction of the vapor (gas) phase. For the homogeneous model, the two-phase flow behaves like a single phase, and the vapor and liquid velocities are equal. A number of correlations for the void fraction exist [76]. An empirical correlation whose general form is valid for several frequently used models is given by Butterworth as reported in [76]:

$$\alpha = \left[1 + A\left(\frac{1-x}{x}\right)^p \left(\frac{\rho_v}{\rho_l}\right)^q \left(\frac{\mu_l}{\mu_v}\right)^r\right]^{-1} \qquad (17.115)$$

where the constants A, p, q, and r depend on the two-phase model and/or empirical data chosen. These constants for a nonhomogeneous model, based on steam-water data, are [76]: $A = 1$, $p = 1$, $q = 0.89$, and $r = 0.18$. For the homogeneous model, $A = p = q = 1$ and $r = 0$. The Lockhart and Martinelli model assumes $A = 0.28$, $p = 0.64$, $q = 0.36$, and $r = 0.07$. For engineering design calculations, the homogeneous model yields the best results where the slip velocity between the phases is small (for bubbly or mist flows).

Finally, the pressure drop caused by the gravity (hydrostatic) effect is:

$$\Delta p_g = \pm \frac{g}{g_c} \sin \theta \int_0^L [\alpha \rho_v + (1 - \alpha)\rho_l] \, dz \tag{17.116}$$

Note that the negative sign (i.e., the pressure recovery) stands for a downward flow in an inclined or vertical fluid flow.

Shellside Pressure Drop. Surprisingly little attention has been devoted in engineering literature to estimate two-phase pressure drop on the shell side of shell-and-tube heat exchangers [77, 78]. In engineering practice, the estimation of the two-phase flow pressure drop can be performed in some situations using modified single-phase flow correlations. This approach is, however, highly unreliable.

In Table 17.22, two correlations are presented for shellside two-phase flow pressure drop estimation, based on modifications of the internal flow correlations. The first correlation uses the modified Chrisholm correlation [69, 79], and the second one [80] employs the modified Lockhart-Martinelli correlation. The first correlation is for horizontal crossflow (crossflow in a baffled horizontal heat exchanger with horizontal or vertical baffle cuts). The second one is for vertical crossflow (upflow in a horizontal tube bundle).

Heat Transfer Correlations for Condensation

The objective of this subsection is to present the most important condensation correlations for design of heat transfer equipment.

Condensation represents a class of vapor-liquid phase change phenomena that usually take place when vapor is cooled below its saturation temperature at a given pressure. In the case of condensation on a heat exchanger surface, the heat transfer interaction between the bulk of the vapor and the surface involves heterogeneous nucleation that leads to a formation

TABLE 17.22   Shellside Two-Phase Pressure Drop Correlations

Correlation	Parameters					Ref.
Chisholm correlation: $\Delta p_f = \Delta p_{f,lo}\varphi_{lo}^2$	Orientation	Flow pattern		n	B	
$\varphi_{lo}^2 = 1 + (Y^2 - 1)[Bx^{(2-n)/2}(1-x)^{(2-n)/2} + x^{2-n}]$	Vertical ↑↓	Spray and bubble		0.37	1	69
	Horizontal	Spray and bubble		0.46	0.75	79
$Y = (\Delta p_{f,vo}/\Delta p_{l,lo})^{1/2}$	Horizontal	Stratified and spray		0.46	0.25	
	Window zone flow					
See Eq. 17.112 for $\Delta p_{f,vo}$ and $\Delta p_{f,lo}$	Vertical ↑↓			0	0.25	
	Horizontal			0	$2/(Y+1)$	

Correlation	Parameters					Ref.
Modified Lockhart-Martinelli correlation: $\Delta p_f = \Delta p_{f,l}\varphi_l^2$ For $\mathrm{Fr}_l > 0.15$:	$C = c_1 \, \mathrm{Fr}_l^{c_2} \ln X_{tt} + c_3 \, \mathrm{Fr}_l^{c_4}$					
$\varphi_l^2 = 1 + \dfrac{C}{X_{tt}} + \dfrac{c_5}{X_{tt}^2}$ For $\mathrm{Fr}_l \leq 0.15$:						
$\varphi_l^2 = 1 + \dfrac{8}{X_{tt}} + \dfrac{1}{X_{tt}^2}$	Flow pattern	c_1	c_2	c_3	c_4	c_5
	Bubble	0.036	1.51	7.79	−0.057	0.774
	Slug ($\mathrm{Fr}_l > 1.15$)	2.18	−0.643	11.6	0.233	1.09
$X_{tt} = \left(\dfrac{1-x}{x}\right)^{0.9}\left(\dfrac{\rho_v}{\rho_l}\right)^{0.5}\left(\dfrac{\mu_l}{\mu_v}\right)^{0.1}$	Spray ($\mathrm{Fr}_l > 1.15$)	0.253	−1.50	12.4	0.207	0.205
$X_{tt} < 0.2$						

(Ref. 80 for the modified Lockhart-Martinelli correlation)

of liquid droplets (dropwise condensation) and/or a liquid layer (filmwise condensation) between the surface and the condensing vapor. The dropwise condensation is desirable because the heat transfer coefficients are an order of magnitude higher than those for film-wise condensation. Surface conditions, though, are difficult for sustaining dropwise condensation. Hence, this mode is not common in practical applications. The heat transfer correlations presented in this section will deal primarily with filmwise condensation (also classified as surface condensation). Refer to Chap. 12 and Refs. 75, 76, 81, and 82 for additional information.

Heat transfer coefficients for condensation processes depend on the condensation models involved, condensation rate, flow pattern, heat transfer surface geometry, and surface orientation. The behavior of condensate is controlled by inertia, gravity, vapor-liquid film interfacial shear, and surface tension forces. Two major condensation mechanisms in film condensation are gravity-controlled and shear-controlled (forced convective) condensation in passages where the surface tension effect is negligible. At high vapor shear, the condensate film may became turbulent.

Now we will present separately heat transfer correlations for external and internal film-wise condensation.

Heat Transfer Correlations for External Condensation.   Although the complexity of condensation heat transfer phenomena prevents a rigorous theoretical analysis, an external condensation for some simple situations and geometric configurations has been the subject of a mathematical modeling. The famous pioneering Nusselt theory of film condensation had led to a simple correlation for the determination of a heat transfer coefficient under conditions of gravity-controlled, laminar, wave-free condensation of a pure vapor on a vertical surface (either flat or tube). Modified versions of Nusselt's theory and further empirical studies have produced a list of many correlations, some of which are compiled in Table 17.23.

Vertical Surfaces.   Condensation heat transfer coefficients for external condensation on vertical surfaces depend on whether the vapor is saturated or supersaturated; the condensate film is laminar or turbulent; and the condensate film surface is wave-free or wavy. Most correlations assume a constant condensation surface temperature, but variable surface temperature conditions are correlated as well as summarized in Table 17.23. All coefficients represent mean values (over a total surface length), that is, $\bar{h} = (1/L) \int_0^L h_{loc}\, dx$.

The first two correlations in Table 17.23 for laminar condensation of saturated vapor with negligible interfacial shear and wave-free condensate surface are equivalent, the difference being only with respect to the utilization of a condensate Reynolds number based on the condensation rate evaluated at distance L. If the assumption regarding the uniformity of the heat transfer surface temperature does not hold, but condensation of a saturated vapor is controlled by gravity only, the heat transfer surface temperature can be approximated by a locally changing function as presented in Table 17.23 (third correlation from the top). This results into a modified Nusselt correlation, as shown by Walt and Kröger [83]. It is important to note that all heat transfer correlations mentioned can be used for most fluids regardless of the actual variation in thermophysical properties as long as the thermophysical properties involved are determined following the rules noted in Table 17.23.

A presence of interfacial waves increases the heat transfer coefficient predicted by Nusselt theory by a factor up to 1.1. An underprediction of a heat transfer coefficient by the Nusselt theory is more pronounced for larger condensate flow rates. For laminar condensation having both a wave-free and wavy portion of the condensate film, the correlation based on the work of Kutateladze as reported in [81] (the fourth correlation from the top of Table 17.23) can be used as long as the flow is laminar.

Film turbulence (the onset of turbulence characterized by a local film Reynolds number range between 1600 and 1800) changes heat transfer conditions depending on the magnitude of the Pr number. For situations when the Prandtl number does not exceed 10, a mean heat transfer coefficient may be calculated using the correlation provided by Butterworth [81] (the fifth correlation from the top of Table 17.23). An increase in the Pr and Re numbers causes an

TABLE 17.23 Heat Transfer Correlations for External Condensation on Vertical Surfaces

Vapor condition*	Liquid-vapor interface	Condensation surface	Correlation	Ref.	Comment[†]
Saturated vapor	Laminar wave-free	$T_w = \text{const.}$	$\bar{h} = 0.943\left[\dfrac{k_l^3\rho_l(\rho_l - \rho_v)gi_{lv}}{\mu_l(T_{sat} - T_w)L}\right]^{1/4}$	81	$i_{lv}, \rho_v \ @ \ T_{sat}$
			$\bar{h} = 1.47\,\dfrac{k_l}{Re_L^{1/3}}\left[\dfrac{\mu_l^2}{\rho_l(\rho_l - \rho_v)g}\right]^{-1/3}$	81	$k_l = [(k_l)_{T_w} + (k_l)_{T_{sat}}]/2;$ $\rho_l = [(\rho_l)_{T_w} + (\rho_l)_{T_{sat}}]/2$
		$T_w = T_{sat} - az^n$ $0 < n < 3$	$\bar{h} = \dfrac{4}{3-n}\left(\dfrac{n+1}{4}\right)^{1/4}\left[\dfrac{k_l^3\rho_l(\rho_l - \rho_g)gi_{lv}}{\mu_l(T_{sat} - T_w)_{z=L}L}\right]^{1/4}$	83	$\mu_l = \dfrac{3\mu_{l,T_w} + \mu_{l,T_{sat}}}{4}$
	Laminar and both wave-free and wavy	$T_w = \text{const.}$	$\bar{h} = \dfrac{Re_L\,k_l[\mu_l^2/\{\rho_l(\rho_l - \rho_v)g\}]^{-1/3}}{1.08Re_L^{1.22} - 5.2}$	81	$Re_L = \dfrac{4\Gamma_L}{\mu_l} < 1600;\ \Gamma_L = \dfrac{\dot{m}}{s}$[†]
	Laminar wave-free, wavy and turbulent		$\bar{h} = \dfrac{Re_L\,k_l[\mu_l^2/\{\rho_l(\rho_l - \rho_v)g\}]^{-1/3}}{8750 + 58Pr^{-0.5}\,(Re_L^{0.75} - 253)}$	81	$Pr \leq 10$
Superheated vapor	Laminar, wavy-free		$\bar{h} = \bar{h}_{sat}\left[1 + \dfrac{c_{p,v}(T_v - T_{sat})}{i_{lv}}\right]^{1/4}$	84	$h_{sat} = \bar{h}$ as given above

* Negligible vapor velocity.

[†] s is the plate width or tube perimeter for a tube.

[†] Thermophysical properties are taken as indicated for all correlations unless indicated otherwise.

increase in the heat transfer coefficient in the turbulent region. The correlation given in Table 17.23 tends to overpredict the heat transfer coefficient for Pr > 10. For further details about treating the existence of turbulence, see Refs. 76 and 78.

It must be noted that predictions of heat transfer coefficients in all mentioned situations may be treated, as a rule, as conservative as long as the correlation is based on the Nusselt theory. Two important additional phenomena, though, are *not* included: vapor superheat and vapor shear effects. The influence of superheating can be included (although the effect is usually small) by the sixth correlation from the top in Table 17.23.

An interfacial shear may be very important in so-called shear-controlled condensation because downward interfacial shear reduces the critical Re number for onset of turbulence. In such situations, the correlations must include interfacial shear stress, and the determination of the heat transfer coefficient follows the Nusselt-type analysis for zero interfacial shear [76]. According to Butterworth [81], data and analyses involving interfacial shear stress are scarce and not comprehensive enough to cover all important circumstances. The calculations should be performed for the local heat transfer coefficient, thus involving step-by-step procedures in any condenser design. The correlations for local heat transfer coefficients are presented in [81] for cases where interfacial shear swamps any gravitational forces in the film or where both vapor shear and gravity are important.

Horizontal and Inclined Surfaces. The Nusselt theory of gravity-controlled film condensation can easily be applied to horizontal or inclined surfaces. Correlations for horizontal single tubes and tube bundles are given in Table 17.24. The first two correlations in the table are valid for negligible vapor shear effect. The correlations predict the mean heat transfer coefficient around the tube circumference at a given location along the tube. The last correlation is for condensing superheated vapor. The correlations for a single tube are conservative. They generally underpredict the heat transfer coefficients by up to 20 percent.

When vapor is moving at a large approaching velocity, the shear stress between the vapor and the condensate surface must be taken into account (i.e., shear forces are large compared to gravity force). A good review of the work devoted to this problem is found in Rose [85], who provided a detailed discussion of film condensation under forced convection. In Table 17.24, a correlation derived by Fuji et al. [86] and suggested by Butterworth [81] is included for the vapor shear effect. The same equation can be applied for a tube bundle. In such a situation, the approach velocity u_v should be calculated at the maximum free-flow area cross section within the bundle.

Film condensation in tube bundles (more commonly used in shell-and-tube heat exchangers) characterize more complex physical conditions compared to condensation on a single tube. The gravity-controlled and surface-shear-stress-influenced condensate films must be modeled in different ways to accommodate combined influences of condensate drain to lower tubes (i.e., condensate inundation) and shear effects. Such a correlation, the fourth correlation from the top of Table 17.24, was proposed by Kern and modified by Butterworth [81].

In the absence of vapor shear effects, the heat transfer coefficient around the lower tubes in a bundle should decrease. However, in general, it is difficult to predict the actual value in a tube bundle depending on the influence of vapor and condensate velocities, turbulence effects, vapor flow direction, tube bundle layout, pressure, heat transfer surface conditions, and so on.

Heat Transfer Correlations for Internal Condensation. Internal condensation processes are complex because a simultaneous motion of both vapor and condensate takes place (in addition to phase change phenomena) in a far more complex manner than for unconfined external condensation. The flow regime can vary substantially. Characteristics of a particular flow pattern involved are extremely important in describing particular heat transfer conditions. Correspondingly, to predict with confidence the heat transfer coefficient for internal film condensation appears to be even more difficult than for external condensation.

Convective condensation in horizontal and vertical tubes is most important with two flow patterns: annular film flow and stratified flow.

TABLE 17.24 Heat Transfer Correlations for External Condensation on Horizontal and Inclined Tubes and Tube Bundles

Vapor condition	Liquid-vapor interface	Condensation surface	Correlation	Ref.	Comment
Saturated vapor	Laminar, no vapor shear	$T_w = $ const. Horizontal, single tube ($\theta = 0$); inclined tube ($\theta \neq 0$)	$\bar{h} = 0.728\left[\dfrac{k_l^3 \rho_l (\rho_l - \rho_v) g \cos\theta\, i_{lv}}{\mu_l (T_{\text{sat}} - T_w) d_o}\right]^{1/4}$	81	i_{lv}, ρ_v @ T_{sat} $k_l = [(k_l)_{T_w} + (k_l)_{T_{\text{sat}}}]/2$; $\rho_l = [(\rho_l)_{T_w} + (\rho_l)_{T_{\text{sat}}}]/2$ $\mu_l = \dfrac{3\mu_{l,T_w} + \mu_{l,T_{\text{sat}}}}{4}$
		$q_w = $ const. Horizontal single tube	$\bar{h} = 0.70\left[\dfrac{k_l^3 \rho_l (\rho_l - \rho_v) g i_{lv}}{\mu_l (T_{\text{sat}} - T_w) d_o}\right]^{1/4}$	86	
	Laminar, vapor shear exists	$T_w = $ const. Single tube	$\bar{h} = 0.728\xi\left[\dfrac{k_l^3 \rho_l (\rho_l - \rho_v) g i_{lv}}{\mu_l (T_{\text{sat}} - T_w) d_o}\right]^{1/4}$	86	$1 < \xi = 1.4\left[\dfrac{u_v^2 (T_{\text{sat}} - T_w) k_l}{\mu_l i_{lv} g d_o}\right]^{1/20} < 1.7$
	Laminar	$T_w = $ const. Horizontal tube bundle	$\bar{h} = \bar{h}_{\text{single,top}} a N^{-b}$	81	$a = 1, b = \frac{1}{6},$ for $N < 10$ $a = 1.24, b = \frac{1}{4},$ for $N \geq 10$
Superheated vapor	Laminar		$\bar{h} = \bar{h}_{\text{sat}}\left[1 + \dfrac{c_{p,v}(T_v - T_{\text{sat}})}{i_{lv}}\right]^{1/4}$	84	$h_{\text{sat}} = \bar{h}$ as given above

Note: $\bar{h}$ is the mean coefficient around the tube perimeter; u_v is the vapor approach velocity.

TABLE 17.25 Heat Transfer Correlations for Internal Condensation in Horizontal Tubes

Stratification conditions	Correlation	Ref.
Annular flow* (Film condensation)	$h_{\text{loc}} = h_l\left[(1-x)^{0.8} + \dfrac{3.8x^{0.76}(1-x)^{0.04}}{(p/p_c)^{0.38}}\right]$	
	where $h_l = 0.023\,\dfrac{k_l}{d_i}\,\text{Re}_l^{0.8}\,\text{Pr}_l^{0.4}$	88
	$\text{Re}_l = \dfrac{Gd_i}{\mu_l}$, $G = $ total mass velocity (all liquid)	
	$100 \le \text{Re}_l \le 63{,}000$	
	$0 \le x \le 1$ $1 \le \text{Pr}_l \le 13$	
Stratified flow	$\bar{h} = 0.728\left[1 + \dfrac{1-x}{x}\left(\dfrac{\rho_v}{\rho_l}\right)^{2/3}\right]^{-(3/4)}\left[\dfrac{k_l^3\rho_l(\rho_l-\rho_g)gi'_{lv}}{\mu_l(T_{\text{sat}}-T_w)d_i}\right]^{1/4}$	76
	where: $i'_{lv} = i_{lv} + 0.68c_{p,l}(T_{\text{sat}} - T_w)$	87

* Valid for horizontal, vertical or inclined tubes of diameters ranging from 7 to 40 mm.

Horizontal Surfaces. For annular film flow, the Nusselt-theory-based correlations usually fail to provide acceptable predictions. This type of flow is shear-dominated flow. This problem has been a subject of extensive research, and numerous correlations can be found in literature [78]. The correlation given by Shah [88] in Table 17.25 is the best, as it is valid for a wide range of fluids and flow conditions. The mean deviation for 474 data points analyzed was found to be 15 percent.

In stratified flow, the stratified layer at the lower part of the tube free-flow area is influenced primarily by shear effects, while a thin film covers the upper portions of the inner tube wall and stratifies under the influence of gravity. The heat transfer conditions in two regions are quite different, but it is a standard practice to correlate heat transfer based on the entire perimeter. In Table 17.25, a correlation based on the modified Nusselt theory is given for stratified flow, developed by Chato [87] and modified by Jaster and Kosky, as reported by Carey [76]. Consult Carey [76] and Butterworth [81] for a detailed analysis of related phenomena. The most recent condensation correlations are given by Dobson and Chato [89].

Vertical Surfaces. If the laminar flow direction is downward and gravity-controlled, heat transfer coefficient for internal condensation inside vertical tubes can be predicted using the correlations for external film condensation—see Table 17.23. The condensation conditions usually occur under annular flow conditions. Discussion of modeling of the downward internal convective condensation is provided in Ref. 76.

For the interfacial shear-controlled flows, annular film flow pattern is established, and the tube orientation is irrelevant. Consequently, the correlations for annular condensation in horizontal tubes can be applied for vertical internal downward flows as well—see Table 17.25.

For an upward flow direction, the shear forces may influence the downward-flow of the condensate, causing an increase of the condensate film thickness. Therefore, the heat transfer coefficient under such conditions shall decrease up to 30 percent compared to the result obtained using the same correlation as the upward-flowing vapor. If the vapor velocity increases substantially, the so-called flooding phenomenon may occur. Under such condition, the shear forces completely prevent the downward condensate flow and flood (block) the tube with the condensate. Prediction of the flooding conditions is discussed by Wallis, as reported by Butterworth [81].

Heat Transfer Correlations for Condensation Under Special Conditions. In a number of practical engineering situations, condensation phenomena may occur under quite different conditions compared to the ones discussed in the preceding subsections. This includes noncir-

cular compact heat exchanger passages, augmented tube geometries, condensation of multi-component vapor mixtures, presence of noncondensable gases, surface tension driven flows, and so on. Also, the appearance of dropwise condensation radically changes heat transfer performance. In all these situations, the conservative approach cannot be applied. For detailed discussion of these factors, one may consult Refs. 76, 78, 81, and 90–93 for details.

Heat Transfer Correlations for Boiling

Vaporization (boiling and evaporation) phenomena have been extensively investigated and reported in the literature [75, 76, 94, 95]. This section is devoted primarily to forced convective boiling and critical heat flux correlations important for heat exchanger design. These correlations are considered for the intube and shellside of a shell-and-tube heat exchanger. Vaporization in both geometries is a very complex process, and the empirical data are the primary source for engineering heat transfer correlations. Over the years, a large number of correlations have been developed; for example, well over 30 correlations are available for saturated flow boiling [96]. We will present now the most accurate correlations (based on experimental data for many fluids) for both intube and shellside forced convective boiling.

Heat Transfer Coefficient Correlations

Intube Forced (Flow) Saturated Boiling. The correlation proposed by Kandlikar [96] is based on empirical data for water, refrigerants, and cryogens. The correlation consists of two parts, the convective and nucleate boiling terms, and utilizes a fluid-dependent parameter.

TABLE 17.26 Heat Transfer Correlations for Boiling

Geometry	Correlation
	$\dfrac{h}{h_l} = c_1 \, \text{Co}^{c_2} \, (25\text{Fr}_{lo})^{c_3} + C_3 \, \text{Bo}^{c_4} \, F_{fl}$
Intube [96]	$h_l = 0.023\text{Re}_l^{0.8} \, \text{Pr}_l^{0.4} \left(\dfrac{k_l}{d_i}\right) \quad \text{Co} = \left(\dfrac{1-x}{x}\right)^{0.8}\left(\dfrac{\rho_v}{\rho_l}\right)^{0.5}$
	$\text{Re}_l = \dfrac{Gd_i(1-x)}{\mu_l} \quad \text{Fr}_{lo} = \dfrac{G^2}{gd_i\rho_l^2} \quad \text{Bo} = \dfrac{q''}{Gi_{lv}}$

c_i	Convective boiling	Nucleate boiling	Fluid	F_{fl}
c_1	1.1360	0.6683	H_2O	1.00
c_2	–0.9	–0.2	R-11	1.30
c_3	667.2	1058.0	R-12	1.50
c_4	0.7	0.7	R-22	2.20
c_5	0.3	0.3	R-113	1.30
Note: $c_5 = 0$ for vertical tubes			R-114	1.24
and $c_5 = 0$ for horizontal tubes			N_2	4.70
for $\text{Fr}_{lo} > 0.04$.			Ne	3.50

Geometry	Correlation
Shellside [68]	$h = Fh_{\text{conv}} + Sh_{NB}$
	h_{conv}, single-phase correlation of a type $\text{Nu} = C\,\text{Re}^n\,\text{Pr}^{0.34}$
	h_{NB}, a nucleate pool boiling correlation [95]
	$F = (\varphi_l^2)^{n/(2-m)}$, m from a single-phase correlation $f = C'\,\text{Re}^{-m}$
	$S = \dfrac{k}{F}\,h_{\text{conv}}X_o\left[1 - \exp\left(-\dfrac{Fh_{\text{conv}}X_o}{k}\right)\right] \qquad X_o = 0.041\left[\dfrac{\sigma}{g(\rho_l - \rho_v)}\right]^{0.5}$
	φ_l^2, friction multiplier, see Table 17.22
	For single-phase correlations, refer to the major section starting on p. 17.66.

The correlation is given in Table 17.26 and can be applied for either vertical (upward and downward) or horizontal intube flow. A mean deviation of slightly less than 16 percent with water and 19 percent with refrigerants has been reported.

Shellside Forced Boiling.   Additional turbulence effects, complex flow fields, and drag effects can significantly increase heat transfer coefficients on the shell side of a tube bundle. A detailed review of the topic is given in Ref. 68.

As in the case of the intube boiling, the shellside boiling is controlled by a trade-off between the convective and nucleate boiling. This has been the reason why a correlation type originally developed for intube boiling has extensively been used for shellside boiling conditions as well. It should be pointed out that the prediction of the heat transfer coefficient on the shell side can easily reach an error margin of 40 percent [68]. One such correlation is presented in Table 17.26 [68].

Critical Heat Flux.   The importance of the critical heat flux (CHF) for engineering practice cannot be overemphasized. A sharp increase of the wall temperature caused by the onset of critical conditions can lead to failure of heat transfer equipment. This is the reason for a large number of correlations in the literature. An instructive overview of the topic is provided in Ref. 76. The critical heat flux conditions in a single tube or on the shell side of the tube bundle are not the same, and the suggestions regarding the use of the most precise correlations are given below.

Intube Forced (Flow) Boiling.   The prediction of the onset of the internal boiling flow is more accurate (the root-mean-square error of correlations is reported to be usually between 7 and 15 percent). The correlation presented in Table 17.27, along with the direction concerning the application for vertical uniformly heated tubes, is proposed by Katto and Ohno [97], as reported by Carey [76]. An explicit information regarding the accuracy of this correlation is not available.

TABLE 17.27   CHF Correlation for a Vertical, Uniformly Heated Tube [97]

CHF correlation
$$q''_{crit} = q''_{co}\left(1 + K_K \frac{i_{l,sat} - i_{in}}{i_{lv}}\right)$$

$\rho^* = \rho_v/\rho_l \geq 0.15$	$\rho^* = \rho_v/\rho_l < 0.15$
$q''_{co} = q''_{co1}$ for $q''_{co1} < q''_{co5}$	$q''_{co} = q''_{co1}$ for $q''_{co1} < q''_{co2}$
$q''_{co} = q''_{co5}$ for $q''_{co1} > q''_{co5} > q''_{co4}$	$q''_{co} = q''_{co2}$ for $q''_{co1} > q''_{co2} < q''_{co3}$
$q''_{co} = q''_{co4}$ for $q''_{co1} > q''_{co5} \leq q''_{co4}$	$q''_{co} = q''_{co3}$ for $q''_{co2} \geq q''_{co3}$
$K_K = K_{K1}$ for $K_{K1} > K_{K2}$	$K_K = K_{K1}$ for $K_{K1} > K_{K2}$
$K_K = K_{K2}$ for $K_{K1} \leq K_{K2} < K_{K3}$	$K_K = K_{K2}$ for $K_{K1} \leq K_{K2}$
$K_K = K_{K3}$ for $K_{K1} \leq K_{K2} \geq K_{K3}$	

$$K_{K1} = \frac{1.043}{4C_K \, \text{We}_K^{-0.043}} \qquad K_{K2} = \frac{5}{6} \frac{0.0124 + d_i/L}{(\rho^*)^{0.133} \, \text{We}_K^{-1/3}} \qquad K_{K3} = 1.12 \frac{1.52 \text{We}_K^{-0.233} + d_i/L}{(\rho^*)^{0.6} \, \text{We}_K^{-0.173}}$$

$$q''_{co1} = C_K Gi_{lv} \, \text{We}_K^{-0.043} \, (L/d_i)^{-1} \qquad q''_{co2} = 0.1 Gi_{lv}(\rho^*)^{0.133} \, \text{We}_K^{-1/3}\left[\frac{1}{1 + 0.0031(L/d_i)}\right]$$

$$q''_{co3} = 0.098 Gi_{lv}(\rho^*)^{0.133} \, \text{We}_K^{-0.433}\left[\frac{(L/d_i)^{0.27}}{1 + 0.0031(L/d_i)}\right] \qquad q''_{co4} = 0.0384 Gi_{lv}(\rho^*)^{0.6} \, \text{We}_K^{-0.173}\left[\frac{1}{1 + 0.28\text{We}_K^{-0.233}(L/d_i)}\right]$$

$$q''_{co5} = 0.234 Gi_{lv}(\rho^*)^{0.513} \, \text{We}_K^{-0.433}\left[\frac{(L/d_i)^{0.27}}{1 + 0.0031(L/d_i)}\right] \qquad \text{We}_K = \frac{G^2 L}{\sigma \rho_l}$$

$$C_K = 0.25 \quad \text{for} \quad \frac{L}{d_i} < 50; \qquad C_K = 0.25 + 0.0009\left[\left(\frac{L}{d_i}\right) - 50\right] \quad \text{for} \quad 50 \leq \frac{L}{d_i} \leq 150; \qquad C_K = 0.34 \quad \text{for} \quad \frac{L}{d_i} > 150$$

Shellside Forced Boiling.   As is the case with the heat transfer coefficient, an accurate prediction of the CHF for shellside boiling is much more difficult than for internal flow. Available experimental data suggest that a correlation presented by Palen and Small in graphical form [98] is very conservative, but it is still the only one available for general use [68].

THERMAL DESIGN FOR SINGLE-PHASE HEAT EXCHANGERS

Exchanger Design Methodology

The problem of heat exchanger design is complex and multidisciplinary [99]. The major design considerations for a new heat exchanger include: process/design specifications, thermal and hydraulic design, mechanical design, manufacturing and cost considerations, and trade-offs and system-based optimization as shown in Fig. 17.53, with possible strong interactions among these considerations as indicated by double-sided arrows. The thermal and hydraulic designs are mainly analytical and the structural design is to some extent. Most of the other major design considerations involve qualitative and experience-based judgments, trade-offs, and compromises. Therefore, there is no unique solution to designing a heat exchanger for given process specifications. Further details on this design methodology are given by Ref. 99.

Two most important heat exchanger design problems are the rating and sizing problems. Determination of heat transfer and pressure drop performance of either an existing exchanger or an already sized exchanger is referred to as the *rating problem.* The objective here is to verify vendor specifications or determine the performance at off-design conditions. The rating problem is also sometimes referred to as the performance problem. In contrast, the design of a new or existing-type exchanger is referred to as the *sizing problem.* In a broad sense, it means the determination of the exchanger construction type, flow arrangement, heat transfer surface geometries and materials, and the physical size of an exchanger to meet the specified heat transfer and pressure drops. However, from the viewpoint of quantitative thermal-hydraulic analysis, we will consider that the selection of the exchanger construction type, flow arrangement, and materials has already been made. Thus, in the sizing problem, we will determine here the physical size (length, width, height) and surface areas on each side of the exchanger. The sizing problem is also sometimes referred to as the design problem.

The step-by-step solution procedures for the rating and sizing problems for counterflow and crossflow single-pass plate-fin heat exchangers have been presented with a detailed illustrative example by Ref. 100. Shah [101] presented further refinements in these procedures as well as step-by-step solution procedures for two-pass cross-counterflow plate-fin exchangers and single-pass crossflow and two-pass cross-counterflow tube-fin exchangers. Also, step-by-step solution procedures for the rating and sizing problems for rotary regenerators [32], heat pipe heat exchangers [102], and plate heat exchangers [103] are available. The well-established step-by-step solution procedures for two-fluid heat exchangers cannot be extended easily when more than two fluids are involved, such as in three-fluid or multifluid heat exchangers [104]. As an illustration, the step-by-step solution procedures will be covered here for a two-fluid single-pass crossflow exchanger.

Extended Surface Heat Exchangers

Rating Problem for a Crossflow Plate-Fin Exchanger.   We will present here a step-by-step solution procedure for the rating problem for a crossflow plate-fin exchanger. Inputs to the rating problem for a two-fluid exchanger are: the exchanger construction, flow arrangement and overall dimensions, complete details on the materials and surface geometries on both sides including their nondimensional heat transfer and pressure drop characteristics (j and f
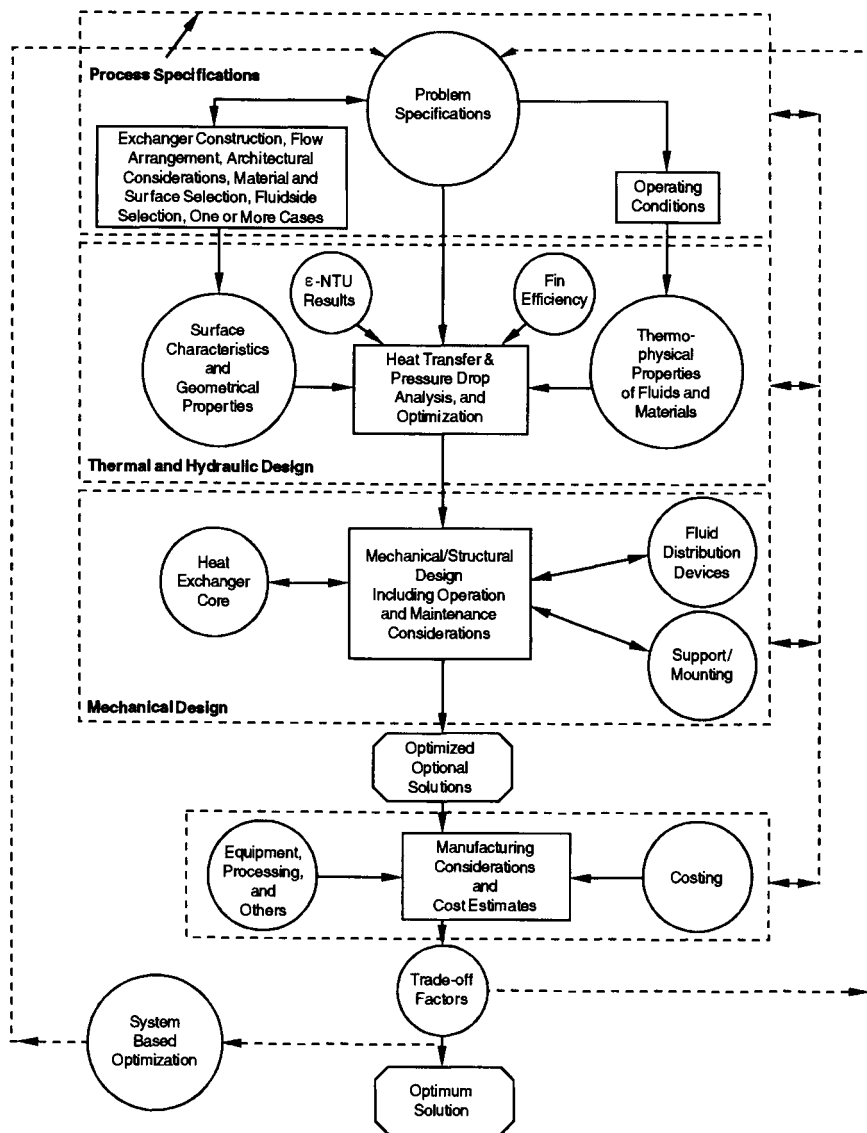
FIGURE 17.53   Heat exchanger overall design methodology.

versus Re), fluid flow rates, inlet temperatures, and fouling factors. The fluid outlet temperatures, total heat transfer rate, and pressure drops on each side of the exchanger are then determined as the rating problem solution.

1. Determine the surface geometrical properties on each fluid side. This includes the minimum free flow area A_o, heat transfer surface area A (both primary and secondary), flow lengths L, hydraulic diameter D_h, heat transfer surface area density β, the ratio of minimum free flow area to frontal area σ, fin length and fin thickness δ_f for fin efficiency determination, and any specialized dimensions used for heat transfer and pressure drop correlations.

2. Compute the fluid bulk mean temperature and fluid thermophysical properties on each fluid side. Since the outlet temperatures are not known for the rating problem, they are estimated initially. Unless it is known from past experience, assume an exchanger effectiveness as 60–75 percent for most single-pass crossflow exchangers or 80–85 percent for single-pass counterflow exchangers. For the assumed effectiveness, calculate the fluid outlet temperatures.

$$T_{h,o} = T_{h,i} - \varepsilon(C_{\min}/C_h)(T_{h,i} - T_{c,i}) \tag{17.117}$$

$$T_{c,o} = T_{c,i} + \varepsilon(C_{\min}/C_c)(T_{h,i} - T_{c,i}) \tag{17.118}$$

Initially, assume $C_c/C_h = \dot{m}_c/\dot{m}_h$ for a gas-to gas exchanger, or $C_c/C_h = \dot{m}_c c_{p,c}/\dot{m}_h c_{p,h}$ for a gas-to-liquid exchanger with very approximate values of c_p for the fluids in question.

For exchangers with $C^* \geq 0.5$ (usually gas-to-gas exchangers), the bulk mean temperatures on each fluid side will be the arithmetic mean of the inlet and outlet temperatures on each fluid side [100]. For exchangers with $C^* < 0.5$ (usually gas-to-gas exchangers), the bulk mean temperature on the $C_{\max}$ side will be the arithmetic mean of inlet and outlet temperatures; the bulk mean temperature on the $C_{\min}$ side will be the log-mean average temperature obtained as follows:

$$T_{m,C_{\min}} = T_{m,C_{\max}} \pm \Delta T_{lm} \tag{17.119}$$

where ΔT_{lm} is the log-mean temperature difference based on the terminal temperatures (see Eq. 17.18); use the plus sign only if the $C_{\min}$ side is hot.

Once the bulk mean temperatures are obtained on each fluid side, obtain the fluid properties from thermophysical property software or handbooks. The properties needed for the rating problem are μ, c_p, k, Pr, and ρ. With this c_p, one more iteration may be carried out to determine $T_{h,o}$ or $T_{c,o}$ from Eq. 17.117 or 17.118 on the $C_{\max}$ side and, subsequently, T_m on the $C_{\max}$ side. Refine fluid properties accordingly.

3. Calculate the Reynolds number $\text{Re} = GD_h/\mu$ and/or any other pertinent dimensionless groups (from the basic definitions) needed to determine the nondimensional heat transfer and flow friction characteristics (e.g., j or Nu and f) of heat transfer surfaces on each side of the exchanger. Subsequently, compute j or Nu and f factors. Correct Nu (or j) for variable fluid property effects [100] in the second and subsequent iterations from the following equations.

For gases:
$$\frac{\text{Nu}}{\text{Nu}_{cp}} = \left[\frac{T_w}{T_m}\right]^n \qquad \frac{f}{f_{cp}} = \left[\frac{T_w}{T_m}\right]^m \tag{17.120}$$

For liquids:
$$\frac{\text{Nu}}{\text{Nu}_{cp}} = \left[\frac{\mu_w}{\mu_m}\right]^n \qquad \frac{f}{f_{cp}} = \left[\frac{\mu_w}{\mu_m}\right]^m \tag{17.121}$$

where the subscript cp denotes constant properties, and m and n are empirical constants provided in Table 17.20a and 17.20b. Note that T_w and T_m in Eqs. 17.120 and 17.121 and in Table 17.20a and 17.20b are absolute temperatures, and T_w is computed from Eq. 17.9.

4. From Nu or j, compute the heat transfer coefficients for both fluid streams.

$$h = \text{Nu}\, k/D_h = jGc_p\, \text{Pr}^{-2/3} \tag{17.122}$$

Subsequently, determine the fin efficiency η_f and the extended surface efficiency η_o:

$$\eta_f = \frac{\tanh ml}{ml}$$

where
$$m^2 = \frac{h\mathbf{P}}{k_f A_k} \tag{17.123}$$

where **P** is the wetted perimeter of the fin surface.

$$\eta_o = 1 - (1 - \eta_f)A_f/A \qquad (17.124)$$

Also calculate the wall thermal resistance $\mathbf{R}_w = \delta/A_w k_w$. Finally, compute overall thermal conductance UA from Eq. 17.6, knowing the individual convective film resistances, wall thermal resistances, and fouling resistances, if any.

5. From the known heat capacity rates on each fluid side, compute $C^* = C_{min}/C_{max}$. From the known UA, determine NTU $= UA/C_{min}$. Also calculate the longitudinal conduction parameter λ. With the known NTU, C^*, λ, and the flow arrangement, determine the crossflow exchanger effectiveness (from either closed-form equations of Table 17.6 or tabular/graphical results from Kays and London [20].

6. With this ε, finally compute the outlet temperatures from Eqs. 17.117 and 17.118. If these outlet temperatures are significantly different from those assumed in step 2, use these outlet temperatures in step 2 and continue iterating steps 2–6 until the assumed and computed outlet temperatures converge within the desired degree of accuracy. For a gas-to-gas exchanger, one or two iterations may be sufficient.

7. Finally compute the heat duty from

$$q = \varepsilon C_{min}(T_{h,i} - T_{c,i}) \qquad (17.125)$$

8. For the pressure drop calculations, first we need to determine the fluid densities at the exchanger inlet and outlet (ρ_i and ρ_o) for each fluid. The mean specific volume on each fluid side is then computed from Eq. 17.66.

Next, the entrance and exit loss coefficients K_c and K_e are obtained from Fig. 17.35 for known σ, Re, and the flow passage entrance geometry.

The friction factor on each fluid side is corrected for variable fluid properties using Eq. 17.120 or 17.121. Here, the wall temperature T_w is computed from

$$T_{w,h} = T_{m,h} - (\mathbf{R}_h + \mathbf{R}_{s,h})q \qquad (17.126)$$

$$T_{w,c} = T_{m,c} + (\mathbf{R}_c + \mathbf{R}_{s,c})q \qquad (17.127)$$

where the various resistance terms are defined by Eq. 17.6.

The core pressure drops on each fluid side are then calculated from Eq. 17.65. This then completes the procedure for solving the rating problem.

Sizing Problem for Plate-Fin Exchangers.   As defined earlier, we will concentrate here to determine the physical size (length, width, and height) of a single-pass crossflow exchanger for specified heat duty and pressure drops. More specifically inputs to the sizing problem are surface geometries (including their nondimensional heat transfer and pressure drop characteristics), fluid flow rates, inlet and outlet fluid temperatures, fouling factors, and pressure drops on each side.

For the solution to this problem, there are four unknowns—two flow rates or Reynolds numbers (to determine correct heat transfer coefficients and friction factors) and two surface areas—for the two-fluid crossflow exchanger. Equations 17.128, 17.129, 17.130 for $q = 1, 2,$ and 17.132 are used to solve iteratively the surface areas on each fluid side: UA in Eq. 17.128 is determined from NTU computed from the known heat duty or ε and C^*; G in Eq. 17.130 represents two equations for fluids 1 and 2 [101]; and the volume of the exchanger in Eq. 17.132 is the same based on the surface area density of fluid 1 (hot) or fluid 2 (cold).

$$\frac{1}{UA} \approx \frac{1}{(\eta_o hA)_h} + \frac{1}{(\eta_o hA)_c} \qquad (17.128)$$

Here, we have neglected the wall and fouling thermal resistances. Defining $\mathrm{ntu}_h = (\eta_o hA)_h/C_h$ and $\mathrm{ntu}_c = (\eta_o hA)_c/C_c$, Eq. 17.128 in nondimensional form is given by

$$\frac{1}{\mathrm{NTU}} = \frac{1}{\mathrm{ntu}_h(C_h/C_{\min})} + \frac{1}{\mathrm{ntu}_c(C_c/C_{\min})} \tag{17.129}$$

$$G_q = \left[\frac{2g_c\Delta p}{\mathrm{Deno}}\right]_q^{1/2} \qquad q = 1, 2 \tag{17.130}$$

where

$$(\mathrm{Deno})_q = \left[\frac{f}{j}\frac{\mathrm{ntu}}{\eta_o}\mathrm{Pr}^{2/3}\left(\frac{1}{\rho}\right)_m + 2\left(\frac{1}{\rho_o} - \frac{1}{\rho_i}\right) + (1 - \sigma^2 + K_c)\frac{1}{\rho_i} - (1 - \sigma^2 - K_e)\frac{1}{\rho_o}\right]_q \tag{17.131}$$

$$V = \frac{A_1}{\alpha_1} = \frac{A_2}{\alpha_2} \tag{17.132}$$

In the iterative solutions, one needs ntu_h and ntu_c to start the iterations. These can be determined either from the past experience or by estimations. If both fluids are gases or liquids, one could consider that the design is balanced (i.e., the thermal resistances are distributed approximately equally on the hot and cold sides). In that case, $C_h = C_c$, and

$$\mathrm{ntu}_h \approx \mathrm{ntu}_c \approx 2\mathrm{NTU} \tag{17.133}$$

Alternatively, if we have liquid on one side and gas on the other side, consider 10 percent thermal resistance on the liquid side, i.e.

$$0.10\left(\frac{1}{UA}\right) = \frac{1}{(\eta_o hA)_{\mathrm{liq}}} \tag{17.134}$$

Then, from Eqs. 17.128 and 17.129 with $C_{\mathrm{gas}} = C_{\min}$, we can determine the ntu on each side as follows.

$$\mathrm{ntu}_{\mathrm{gas}} = 1.11\mathrm{NTU}, \qquad \mathrm{ntu}_{\mathrm{liq}} = 10C^*\mathrm{NTU} \tag{17.135}$$

Also note that initial guesses of η_o and j/f are needed for the first iteration to solve Eq. 17.131. For a good design, consider $\eta_o = 0.80$ and determine approximate value of j/f from the plot of j/f versus Re curve for the known j and f versus Re characteristics of each fluid side surface. The specific step-by-step design procedure is as follows.

1. In order to compute the fluid bulk mean temperature and the fluid thermophysical properties on each fluid side, determine the fluid outlet temperatures from the specified heat duty.

$$q = (\dot{m}c_p)_h(T_{h,i} - T_{h,o}) = (\dot{m}c_p)_c(T_{c,o} - T_{c,i}) \tag{17.136}$$

or from the specified exchanger effectiveness using Eqs. 17.117 and 17.118. For the first time, estimate the values of c_p.

For exchangers with $C^* \geq 0.5$, the bulk mean temperature on each fluid side will be the arithmetic mean of inlet and outlet temperatures on each side. For exchangers with $C^* < 0.5$, the bulk mean temperature on the $C_{\max}$ side will be the arithmetic mean of the inlet and outlet temperatures on that side, the bulk mean temperature on the $C_{\min}$ side will be the log-mean average as given by Eq. 17.119. With these bulk mean temperatures, determine c_p and iterate one more time for the outlet temperatures if warranted. Subsequently, determine μ, c_p, k, Pr, and ρ on each fluid side.

2. Calculate C^* and ε (if q is given) and determine NTU from the ε-NTU expression, tables, or graphical results for the selected crossflow arrangement (in this case, it is unmixed-unmixed crossflow, Table 17.6). The influence of longitudinal heat conduction, if any, is ignored in the first iteration, since we don't know the exchanger size yet.

3. Determine ntu on each side by the approximations discussed with Eqs. 17.133 and 17.135 unless it can be estimated from the past experience.

4. For the selected surfaces on each fluid side, plot j/f versus Re curve from the given surface characteristics, and obtain an approximate value of j/f. If fins are employed, assume $\eta_o = 0.80$ unless a better value can be estimated.

5. Evaluate G from Eq. 17.130 on each fluid side using the information from steps 1–4 and the input value of Δp.

6. Calculate Reynolds number Re, and determine j and f for this Re on each fluid side from the given design data for each surface.

7. Compute h, η_f, and η_o using Eqs. 17.122–17.124. For the first iteration, determine U_1 on the fluid 1 side from the following equation derived from Eqs. 17.6 and 17.132.

$$\frac{1}{U_1} = \frac{1}{(\eta_o h)_1} + \frac{1}{(\eta_o h_s)_1} + \frac{\alpha_1/\alpha_2}{(\eta_o h_s)_2} + \frac{\alpha_1/\alpha_2}{(\eta_o h)_2} \tag{17.137}$$

where $\alpha_1/\alpha_2 = A_1/A_2$, $\alpha = A/\mathbf{V}$ and $\mathbf{V}$ is the exchanger total volume, and subscripts 1 and 2 denote the fluid 1 and 2 sides. For a plate-fin exchanger, α's are given by [20, 100]:

$$\alpha_1 = \frac{b_1 \beta_1}{b_1 + b_2 + 2\delta} \qquad \alpha_2 = \frac{b_2 \beta_2}{b_1 + b_2 + 2\delta} \tag{17.138}$$

Note that the wall thermal resistance in Eq. 17.137 is ignored in the first iteration. In the second and subsequent iterations, compute U_1 from

$$\frac{1}{U_1} = \frac{1}{(\eta_o h)_1} + \frac{1}{(\eta_o h_s)_1} + \frac{\delta A_1}{k_w A_w} + \frac{A_1/A_2}{(\eta_o h_s)_2} + \frac{A_1/A_2}{(\eta_o h)_2} \tag{17.139}$$

where the necessary geometry information A_1/A_2 and A_1/A_w is determined from the geometry calculated in the previous iteration.

8. Now calculate the core dimensions. In the first iteration, use NTU computed in step 2. For subsequent iterations, calculate longitudinal conduction parameter λ and other dimensionless groups for a crossflow exchanger. With known ε, C^*, and λ, determine the correct value of NTU using either a closed-form equation or tabulated/graphical results [10]. Determine A_1 from NTU using U_1 from previous step and known $C_{\min}$.

$$A_1 = \text{NTU} C_{\min}/U_1 \tag{17.140}$$

and hence
$$A_2 = (A_2/A_1)A_1 = (\alpha_2/\alpha_1)A_1 \tag{17.141}$$

A_o is derived from known $\dot{m}$ and G as

$$A_{o1} = (\dot{m}/G)_1 \qquad A_{o2} = (\dot{m}/G)_2 \tag{17.142}$$

so that
$$A_{fr,1} = A_{o1}/\sigma_1 \qquad A_{fr2} = A_{o2}/\sigma_2 \tag{17.143}$$

where σ_1 and σ_2 are generally specified for the surface or can be computed for plate-fin surfaces from [20, 100]:

$$\sigma_1 = \frac{b_1 \beta_1 D_{h,1}/4}{b_1 + b_2 + 2\delta} \qquad \sigma_2 = \frac{b_2 \beta_2 D_{h,2}/4}{b_1 + b_2 + 2\delta} \tag{17.144}$$
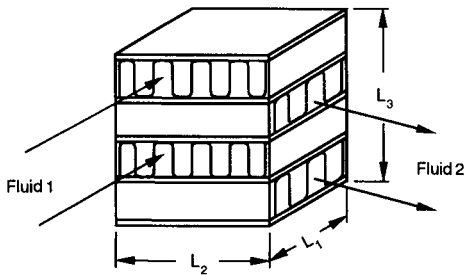
FIGURE 17.54 A single-pass crossflow exchanger.

Now compute the fluid flow lengths on each side (see Fig. 17.54) from the definition of the hydraulic diameter of the surface employed on each side.

$$L_1 = \left(\frac{D_h A}{4 A_o}\right)_1, \qquad L_2 = \left(\frac{D_h A}{4 A_o}\right)_2 \qquad (17.145)$$

Since $A_{fr,1} = L_2 L_3$ and $A_{fr,2} = L_1 L_3$, we can obtain

$$L_3 = \frac{A_{fr,1}}{L_2} \qquad \text{or} \qquad L_3 = \frac{A_{fr,2}}{L_1} \qquad (17.146)$$

Theoretically, L_3 calculated from both expressions of Eq. 17.146 should be identical. In reality, they may differ slightly due to the round-off error. In that case, consider an average value for L_3.

9. Now compute the pressure drop on each fluid side, after correcting f factors for variable property effects, in a manner similar to step 8 of the rating problem for the crossflow exchanger.

10. If the calculated values of Δp are close to input specifications, the solution to the sizing problem is completed. Finer refinements in the core dimensions such as integer numbers of flow passages may be carried out at this time. Otherwise, compute the new value of G on each fluid side using Eq. 17.65 in which Δp is the input specified value and f, K_c, K_e, and geometrical dimensions are from the previous iteration.

11. Repeat (iterate) steps 6–10 until both heat transfer and pressure drops are met as specified. It should be emphasized that, since we have imposed no constraints on the exchanger dimensions, the above procedure will yield L_1, L_2, and L_3 for the selected surfaces such that the design will meet the heat duty and pressure drops on both fluid sides exactly.

Shell-and-Tube Heat Exchangers

The design of a shell-and-tube heat exchanger is more complex than the plate-fin and tube-fin exchangers. There are many variables associated with the geometry (i.e., shell, baffles, tubes, front and rear end, and heads) and operating conditions including flow bypass and leakages in a shell-and-tube heat exchanger [5]. There are no systematic quantitative correlations available to take into account the effect of these variables on the exchanger heat transfer and pressure drop. As a result, the common practice is to presume the geometry of the exchanger and determine the tube (shell) length for the sizing problem or do the rating calculations for the given geometry to determine the heat duty, outlet temperatures, and pressure drops. Hence, effectively, the rating calculations are done for the determination of the heat duty or the exchanger length; in both cases, the basic exchanger geometry is specified. The design calculations are essentially a series of iterative rating calculations made on an assumed design and modified as a result of these calculations until a satisfactory design is achieved.

The following is a step-by-step procedure for the "sizing" problem in which we will determine the exchanger (shell-and-tube) length.

The key steps of the thermal design procedure for a shell-and-tube heat exchanger are as follows:

1. For a given (or calculated) heat transfer rate (required duty), compute (or select) the fluid streams inlet and/or outlet temperatures using overall energy balances and specified (or selected) fluid mass flow rates.

2. Select a preliminary flow arrangement (i.e., a type of the shell-and-tube heat exchanger based on the common industry practice).

TABLE 17.28   Shell-and-Tube Overall Heat Transfer Coefficient, Modified from Ref. 115

Cold-side fluid	Hot-side fluid U, W/(m²K)*							
	Gas @ 10^5 Pa	Gas @ 2×10^6 Pa	Process H_2O	Organic liquid[†]	Viscous liquid[‡]	Condensing steam	Condensing hydrocarbon	Condensing hydrocarbon and inert gas
Gas @ 10^5 Pa	55	93	102	99	63	107	100	86
Gas @ 2×10^6 Pa	93	300	429	375	120	530	388	240
H_2O, treated	105	484	938	714	142	1607	764	345
Organic liquid[†]	99	375	600	500	130	818	524	286
High-viscosity liquid[‡]	68	138	161	153	82	173	155	124
H_2O, boiling	105	467	875	677	140	1432	722	336
Organic liquid, boiling[§]	99	375	600	500	130	818	524	286

* Based on data given in [G.F. Hewit, A.R. Guy, and R. Marsland, Heat Transfer Equipment, Ch. 3 in *A User Guide on Process Integration for the Efficient Use of Energy*, eds. B. Linnhoff et al., The IChemE, Rugby, 1982]. Any such data, including the data given in this table, should be used with caution. The numbers are based on empirical data and should be considered as mean values for corresponding data ranges. Approximate values for boiling and condensation are given for convenience.
† Viscosity range 1 to 5 mPa s.
‡ Viscosity range > 100 mPa s.
§ Viscosity typically < 1 mPa s.

3. Estimate an overall heat transfer coefficient using appropriate empirical data (see, for example, Table 17.28).

4. Determine a first estimate of the required heat transfer area using Eq. 17.17 (i.e., using a first estimate of the log-mean temperature difference ΔT_{lm} and the correction factor F, the estimated overall heat transfer coefficient U, and given heat duty q). Good design practice is to assume $F = 0.8$ or a higher value based on past practice. Based on the heat transfer area, the mass flow rates, and the process conditions, select suitable types of exchangers for analysis (see Refs. 106 and 109). Determine whether a multipass exchanger is required.

5. Select tube diameter, length, pitch, and layout. Calculate the number of tubes, the number of passes, shell size, and baffle spacing. Select the tentative shell diameter for the chosen heat exchanger type using manufacturer's data. The preliminary design procedure presented on p. 17.116 can be used to select these geometrical parameters.

6. Calculate heat transfer coefficients and pressure drops using the Bell-Delaware Method [105] or the stream analysis method [106].

7. Calculate a new value of the overall heat transfer coefficient.

8. Compare the calculated values for the overall heat transfer coefficient (obtained in step 7) with the estimated value of the overall heat transfer coefficient (step 3), and similarly calculated pressure drops (obtained in step 6) with allowable values for pressure drops.

9. Inspect the results and judge whether the performance requirements have been met.

10. Repeat, if necessary, steps 5 to 9 with an estimated change in design until a final design is reached that meets, for instance, specified q and Δp, requirements. If it cannot, then one may need to go back to step 2 for iteration. At this stage, an engineer should check for meeting TEMA standards, ASME Pressure Vessel Codes (and/or other pertinent standards and/or codes as appropriate), potential operating problems, cost, and so on; if the design change is warranted, iterate steps 5 to 9 until the design meets thermal/hydraulic and other requirements.

This step-by-step procedure is consistent with overall design methodology and can be executed as a straightforward manual method or as part of a computer routine. Although the actual design has been frequently carried out using available sophisticated commercial soft-

ware, a successful designer ought to know all the details of the procedure in order to interpret and assess the results from the commercial software.

The central part of thermal design procedure involves determination of heat transfer and pressure drops. A widely utilized, most accurate method in the open literature is the well-known Bell-Delaware method [105] that takes into account various flow characteristics of the complex shellside flow. The method was developed originally for design of fully tubed E-shell heat exchangers with nonenhanced tubes based on the experimental data obtained for an exchanger with geometrical parameters closely controlled. It should be noted that this method can be applied to the broader range of applications than originally intended. For example, it can be used to design J-shell or F-shell heat exchangers. Also, an external low-finned tubes design can easily be considered [105, 106].

Bell-Delaware Method.   Pressure drop and heat transfer calculations (the step 6 of the above thermal design procedure) constitute the key part of design. Tubeside calculations are straightforward and should be executed using available correlations for internal forced convection. The shellside calculations, however, must take into consideration the effect of various leakage streams (A and E streams in Fig. 17.30) and bypass streams (C and F streams in Fig. 17.30) in addition to the main crossflow stream B through the tube bundle. Several methods have been in use over the years, but the most accurate method in the open literature is the above mentioned Bell-Delaware method. This approach is based primarily on limited experimental data. The set of correlations discussed next constitutes the core of the Bell-Delaware method.

Heat Transfer Coefficients.   In this method, an actual heat transfer coefficient on the shellside h_s is determined, correcting the ideal heat transfer coefficient h_{ideal} for various leakage and bypass flow streams. The h_{ideal} is determined for pure crossflow in an ideal tubebank, assuming the entire shellside stream flows across the tubebank at or near the centerline of the shell. The correction factor is defined as a product of five correction factors $J_1, J_2, \ldots J_5$ that take into account, respectively, the effects of:

- Baffle cut and baffle spacing ($J_1 = 1$ for an exchanger with no tubes in the window and increases to 1.15 for small baffle cuts and decreases to 0.65 for large baffle cuts)
- Tube-to-baffle and baffle-to-shell leakages (A and E streams, Fig. 17.30); a typical value of J_2 is in the range of 0.7–0.8
- Tube bundle bypass and pass partition bypass (C and F streams, Fig. 17.30); a typical value of J_3 is in the range 0.7–0.9
- Laminar flow temperature gradient buildup (J_4 is equal to 1.0 except for shellside Reynolds numbers smaller than 100)
- Different central versus end baffle spacings (J_5 usually ranges from 0.85 to 1.0)

A complete set of equations and parameters for the calculation of the shellside heat transfer coefficient is given in Tables 17.29 and 17.30.

A combined effect of all five corrections can reduce the ideal heat transfer coefficient by up to 60 percent. A comparison with a large number of proprietary experimental data indicates the shellside h predicted using all correction factors is from 50 percent too low to 200 percent too high with a mean error of 15 percent low (conservative) at all Reynolds numbers.

Pressure Drops.   Shellside pressure drop has three components: (1) pressure drop in the central (crossflow) section Δp_c, (2) pressure drop in the window area Δp_w, and (3) pressure drop in the shell side inlet and outlet sections, $\Delta p_{i\text{-}o}$. It is assumed that each of the three components is based on the total flow and that each component can be calculated by correcting the corresponding ideal pressure drops.

The ideal pressure drop in the central section Δp_{bi} assumes pure crossflow of the fluid across the ideal tube bundle. This pressure drop should be corrected for: (a) leakage streams (A and E, Fig. 17.30; correction factor R_ℓ), and (b) bypass flow (streams C and F, Fig. 17.30;

TABLE 17.29 The Heat Transfer Coefficient on the Shell Side, Bell-Delaware Method

Shell-side heat transfer coefficient h_s	
$$h_s = h_{ideal}J_1J_2J_3J_4J_5$$	

$h_{ideal} = j_i c_p G_s \, \mathrm{Pr}_s^{-2/3} \, \phi_s$

$j_i = j_i(\mathrm{Re}_s, \text{tube layout, pitch})$

$$\phi_s = \begin{cases} (\mu_s/\mu_w)^{0.14} & \text{for liquid} \\ 1 & \text{for gas (cooled)} \\ (T_s/T_w)^{0.25} & \text{for gas (heated)} \end{cases}$$

$\mu_w = \mu_{T_w}, \; T_s = \overline{T}_s, \; T_s \text{ and } T_w \text{ in } [K]$

$$G_s = \frac{\dot{m}_s}{A_{mb}} \qquad \mathrm{Re}_s = \frac{d_o G_s}{\mu_s}$$

$j_i = j$ from Figs. 17.55–17.57 or alternately from correlations as those given in Table 17.19*

$J_1 = 0.55 + 0.72F_c$

F_c from Table 17.30

$J_2 = 0.44(1 - r_s) + [1 - 0.44(1 - r_s)] \exp(-2.2r_{lm})$

$$r_s = \frac{A_{sb}}{A_{sb} + A_{tb}} \qquad r_{lm} = \frac{A_{sb} + A_{tb}}{A_{mb}}$$

A_{sb}, A_{tb}, A_{mb} from Table 17.30

$$r_b = \frac{A_{ba}}{A_{mb}} \qquad N_{ss}^+ = \frac{N_{ss}}{N_{tcc}}$$

$J_3 = 1$ for $N_{ss}^+ \geq \frac{1}{2}$
$J_3 = \exp\{-Cr_b[1 - (2N_{ss}^+)^{1/3}]\}$ for $N_{ss}^+ < \frac{1}{2}$

A_{ba}, N_{ss}, N_{tcc} from Table 17.30
$C = 1.35$ for $\mathrm{Re}_s \leq 100$
$C = 1.25$ for $\mathrm{Re}_s > 100$

$$J_4 = \begin{cases} 1 & \mathrm{Re}_s > 100 \\ (10/N_c)^{0.18} & \mathrm{Re}_s \leq 20 \end{cases}$$

$N_c = N_{tcc} + N_{tcw}$
N_{tcw} from Table 17.30
Linear interpolation for $20 < \mathrm{Re}_s < 100$

$$J_5 = \frac{N_b - 1 + (L_i^+)^{(1-n)} + (L_o^+)^{(1-n)}}{N_b - 1 + L_i^+ + L_o^+}$$

$$L_i^+ = \frac{L_{bi}}{L_{bc}} \qquad L_o^+ = \frac{L_{bo}}{L_{bc}} \qquad N_b = \frac{L_{ti}}{L_{bc}} - 1$$

$L_{bi}, L_{bo}, L_{bc},$ and L_{ti} from Table 17.30
$n = 0.6$ (turbulent flow)

* A number of accurate correlations such as those given in Table 17.19 are available. Traditionally, the diagrams such as those given in Figs. 17.55–17.57 have been used in engineering practice.

correction factor R_b). The ideal window pressure drop Δp_w has also to be corrected for both baffle leakage effects. Finally, the ideal inlet and outlet pressure drops Δp_{i-o} are based on an ideal crossflow pressure drop in the central section. These pressure drops should be corrected for bypass flow (correction factor R_b) and for effects of uneven baffle spacing in inlet and outlet sections (correction factor R_s). Typical correction factor ranges are as follows:

- Baffle leakage effects (i.e., tube-to-baffle and baffle-to-shell leakages, A and E streams, Fig. 17.30); a typical value of R_ℓ is in the range of 0.4–0.5
- Tube bundle and pass partition bypass flow effects (i.e., streams C and F, Fig. 17.30); a typical value of R_b is in the range of 0.5–0.8
- The inlet and outlet baffle spacing effects correction factor R_s, in the range of 0.7–1

The complete set of equations, including the correcting factors, is given in Table 17.31.
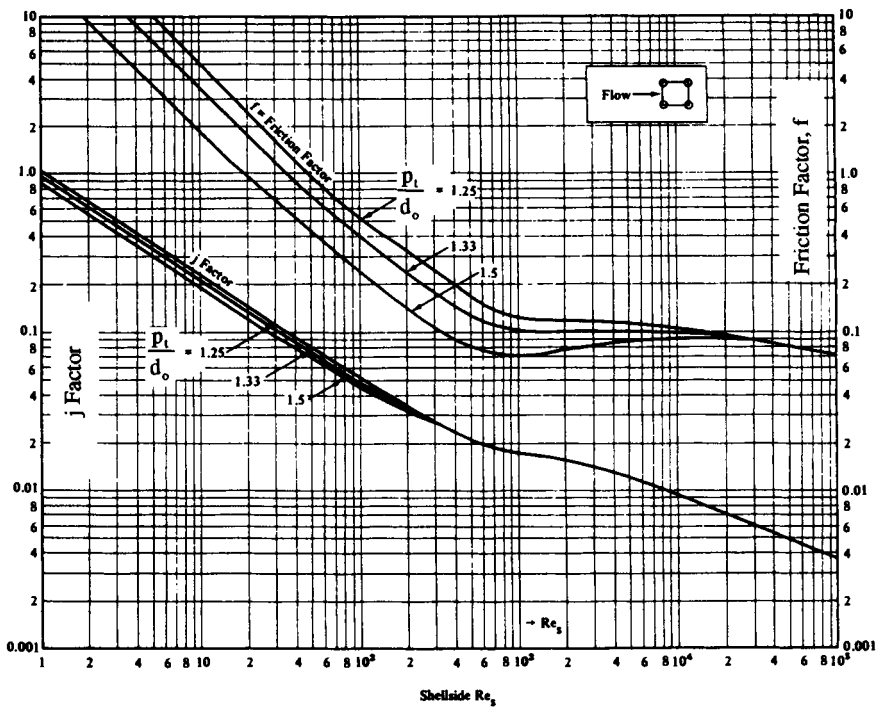
FIGURE 17.55 Colburn factors and friction factors for ideal crossflow in tube bundles, 90° inline layout [106].
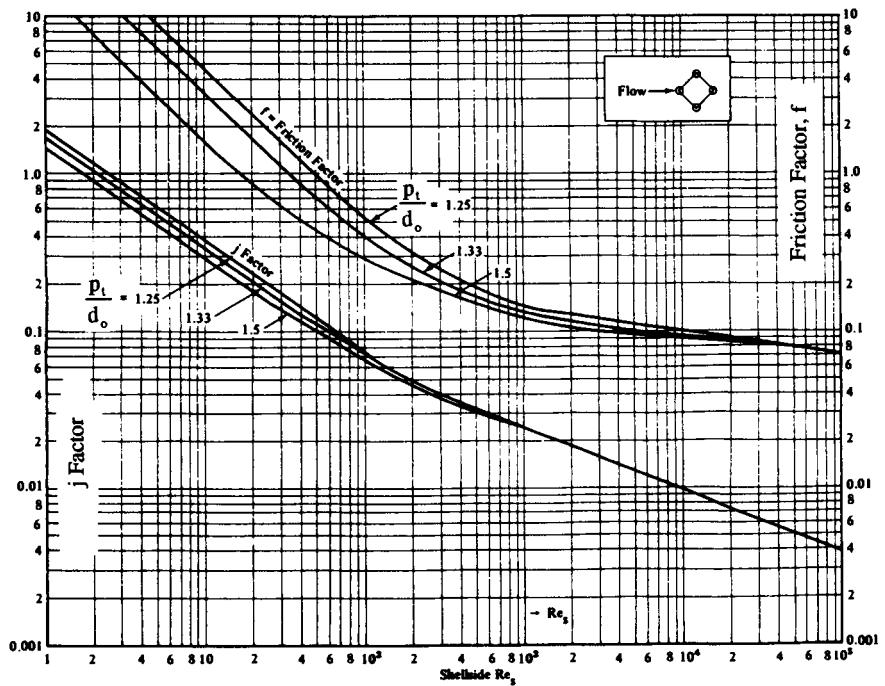

FIGURE 17.56 Colburn factors and friction factors for ideal crossflow in tube bundles, 45° staggered layout [106].
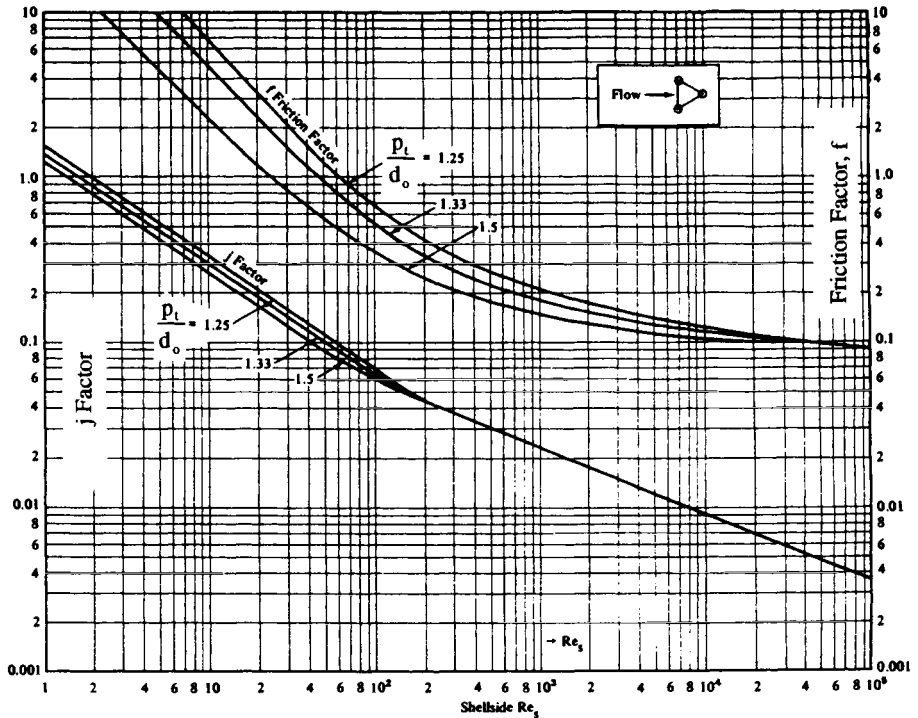
FIGURE 17.57 Colburn factors and friction factors for ideal crossflow in tube bundles, 30° staggered layout [106].

The combined effect of pressure drop corrections reduces the ideal total shellside pressure drop by 70–80 percent. A comparison with a large number of proprietary experimental data indicate shellside Δp from about 5 percent low (unsafe) at $Re_s > 1000$ to 100 percent high at $Re_s < 10$. The tubeside pressure drop is calculated using Eq. 17.65 for single-phase flow.

Preliminary Design. A state-of-the-art approach to design of heat exchangers assumes utilization of computer software, making any manual method undoubtedly inferior. For a review of available computer software, consult Ref. 107. The level of sophistication of the software depends on whether the code is one-, two-, or three-dimensional. The most complex calculations involve full-scale CFD (computational fluid dynamics) routines. The efficiency of the software though is not necessarily related to the complexity of the software because of a need for empirical data to be incorporated into design and sound engineering judgment due to the lack of comprehensive empirical data. The design of shell-and-tube heat exchangers is more accurate for a variety of fluids and applications by commercial software than any other heat exchanger type [108] because of its verification by extensive experimental data.

A successful design based on the Bell-Delaware method obviously depends to a great extent on the experience and skills of the designer. An important component of the experience is an ability to perform a preliminary estimate of the exchanger configuration and its size. A useful tool in accomplishing this task is an approximate sizing of a shell-and-tube heat exchanger. Brief details of this procedure according to Ref. 109 follow. The procedure is based on the MTD method.

TABLE 17.30   Shell-and-Tube Geometric Characteristics to Accompany Tables 17.29 and 17.31

Shellside geometry*
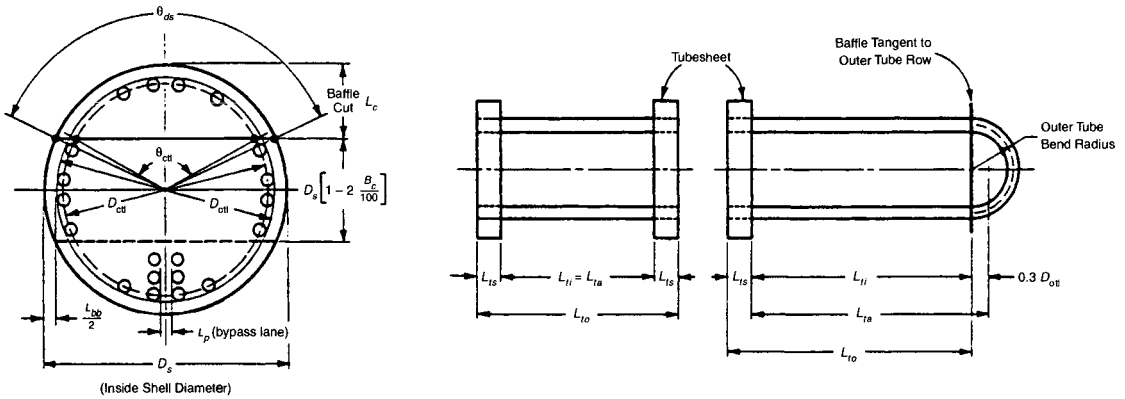
$$A_{mb} = L_{bc}\left[L_{bb} + \frac{D_{ctl}}{p_{t,\text{eff}}}(p_t - d_o)\right] \qquad D_{ctl} = D_{otl} - d_o \qquad p_{t,\text{eff}} = \xi p_t \qquad \begin{array}{l} \xi = 1 \text{ for } 30° \text{ and } 90° \\ \xi = 0.707 \text{ for } 45° \text{ layout} \end{array}$$

$$F_c = 1 - 2F_w \qquad F_w = \frac{\theta_{ctl}}{360°} - \frac{\sin\theta_{ctl}}{2\pi} \qquad \theta_{ctl} = 2\cos^{-1}\left[\frac{D_s}{D_{ctl}}\left(1 - 2\frac{B_c}{100}\right)\right] \qquad B_c = \frac{\text{Baffle cut}}{D_s} \times 100$$

$$A_{sb} = \pi D_s \frac{L_{sb}}{2} \frac{360° - \theta_{ds}}{360°} \qquad \text{see Ref. 5 for allowable } L_{sb} \text{ and } L_{tb} \qquad \theta_{ds} = 2\cos^{-1}\left[1 - 2\frac{B_c}{100}\right]$$

$$A_{tb} = \frac{\pi}{4}\left[(d_o + L_{tb})^2 - d_o^2\right]N_t(1 - F_w) \qquad A_{ba} = L_{bc}[(D_s - D_{otl}) + L_{pl}] \qquad L_{pl} = \begin{cases} 0 & \text{standard} \\ \frac{1}{2}d_o & \text{estimation} \end{cases}$$

$$N_{tcc} = \frac{D_s}{X_t}\left(1 - 2\frac{B_c}{100}\right) \qquad N_{tcw} = 0.8\frac{L_{cp}}{X_t} \qquad N_{ss} = 1 \text{ per 4 or 6 tube rows crossed}$$

$$A_w = A_{wg} - A_{wt} \qquad A_{wg} = \frac{\pi}{4}D_s^2\left(\frac{\theta_{ds}}{360°} - \frac{\sin\theta_{ds}}{2\pi}\right) \qquad A_{wt} = N_t F_w \frac{\pi d_o^2}{4}$$

Note: Specification of the shell-side geometry provided in this table follows (with a few exceptions) the notation adopted in Ref. 7. Somewhat different approach is provided in Ref. 105. Refer to Ref. 106 for further details.
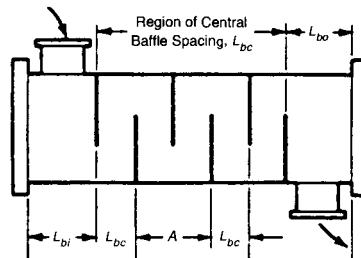
* A proper set of units should be used for calculating data in Tables 17.29, 17.30, and 17.31. If using SI units, refer for further details to Ref. 106; if using U.S. Engineering units, refer to Ref. 5.

TABLE 17.31   Shellside Pressure Drop, Bell-Delaware Method

Shellside pressure drop Δp_s^*	
$\Delta p_s = \Delta p_c + \Delta p_w + \Delta p_{i-o}$	

$\Delta p_c = \Delta p_{bi}(N_b - 1)R_b R_l$

$N_b = \dfrac{L_{ti}}{L_{bc}} - 1$

$\Delta p_{bi} = 2fN_{tcc}\dfrac{G_s^2}{g_c\rho_s}\,\phi_s$

L_{ti}, L_{bc} from Table 17.30;
f from Figs. 17.55–17.57[†]

$f = f(\text{Re}_s, \text{tube layout, pitch})$

Re_s, G_s, ϕ_s, N_{ss}^+ defined in
Table 17.29

$R_b = \exp\{-\mathbf{D}r_b[1 - (2N_{ss}^+)^{1/3}]\}$ for $N_{ss}^+ < 1/2$

N_{tcc} from Table 17.30
r_b, r_{lm}, r_s from Table 17.29

$R_l = \exp[-1.33(11 + r_s)(r_{lm})^p]$

$p = [-0.15(1 + r_s) + 0.8]$

$\mathbf{D} = 4.5$ for $\text{Re}_s \leq 100$; $\mathbf{D} = 3.7$ for $\text{Re}_s > 100$

$R_b = 1$ at $N_{ss}^+ \geq \frac{1}{2}$

$\Delta p_w = \begin{cases} N_b(2 + 0.6N_{tcw})\dfrac{G_w^2}{2g_c\rho_s}R_l & \text{for Re}_s \geq 100 \\[2ex] N_b\left[26\dfrac{G_w\mu_s}{\rho_s}\left(\dfrac{N_{tcw}}{p_t - d_o} + \dfrac{L_{bc}}{D_w^2}\right) + 2(10^{-3})\dfrac{G_w^2}{2g_c\rho_s}\right]R_l & \\ & \text{for Re} < 100 \end{cases}$

N_{tcw}, L_{bc}
from Table 17.30

$G_w = \dfrac{\dot{m}_s}{(A_{mb}A_w)^{1/2}}$

A_{mb}, A_w from Table 17.30

$D_w = \dfrac{4A_w}{\pi d_o F_w N_t + \pi D_s\dfrac{\theta_{ds}}{360}}$

$\Delta p_{i-o} = \Delta p_{bi}\left(1 + \dfrac{N_{tcw}}{N_{tcc}}\right)R_b R_s$

N_{tcc}, L_{bo}, L_{bi}, and L_{bc}
from Table 17.30

$R_s = \left(\dfrac{L_{bc}}{L_{bo}}\right)^{2-n} + \left(\dfrac{L_{bc}}{L_{bi}}\right)^{2-n}$ $n = \begin{cases} 1.0 & \text{laminar flow} \\ 0.2 & \text{turbulent flow} \end{cases}$

* Note regarding the units: Δp in Pa or psi; A_{mb} and A_w in mm² or in²; p_t, d_o, and D_w in mm or in. See notes in Table 17.30.
† A number of accurate correlations such as those given in Table 17.19 are available. Traditionally, the diagrams such as those given in Figs. 17.55–17.57 have been used in engineering practice.

1. Determine the heat load. If both streams are single phase, calculate the heat load q using Eq. 17.3. If one of the streams undergoes a phase change, calculate $q = \dot{m}i$ where $\dot{m}$ = mass flow rate of that stream and i = specific enthalpy of phase change.

2. Determine the logarithmic mean temperature difference using Eq. 17.18.

3. Estimate the log-mean temperature difference correction factor F. For a single TEMA E shell with an arbitrary even number of tubeside passes, the correction factor should be $F > 0.8$. The correction factor F should be close to 1 if one stream changes its temperature only slightly in the exchanger. F should be close to 0.8 if the outlet temperatures of the two streams are equal. Otherwise, assume $F = 0.9$.

4. Estimate the overall heat transfer coefficient (use Table 17.28 with judgment or estimate the individual heat transfer coefficients and wall resistance [109], and afterwards calculate the overall heat transfer coefficient using Eq. 17.6).

5. Calculate the total outside tube heat transfer area (including fin area) using $A = A_p + A_f$.

6. Determine the set of heat exchanger dimensions that will accommodate the calculated total heat transfer area for a selected shell diameter and length using the diagram given in Fig. 17.58. The diagram in Fig. 17.58 corresponds to plain tubes with a 19-mm outside

diameter on a 23.8-mm equilateral triangular tube layout. The extension of this diagram to other shell/bundle/tube geometries requires determination of a corrected effective total heat transfer area using the procedure outlined in Ref. 109. The abscissa in Fig. 17.58 is the effective tube length of a single straight section. The effective length is from tubesheet to tubesheet for a straight tube exchanger and from tubesheet to tangent line for a U-tube bundle. The dashed lines show the approximate locus of shells with a given effective tube length-to-shell diameter ratio. The solid lines are the inside diameters of the shell. The proper selection of the combination of parameters and the effective tube length depends on the particular requirements and given conditions and is greatly influenced by the designer's experience. For a good design, the L/D ratio for the shell is kept between 6 and 15 to optimize the cost of the shell (diameter) and the tubeside pressure drop (tube length).

The thermal design and some aspects of the mechanical design of a shell-and-tube heat exchanger are empirically based, as discussed above. However, there are many criteria for mechanical selection [5], many experience-based criteria that can avoid or minimize operating problems [155], and other design considerations such as identification of thermodynamic irreversibilities [15, 110], thermoeconomic considerations [111], system optimization, and process integration [112]. In industrial applications, thermoeconomic optimization should be
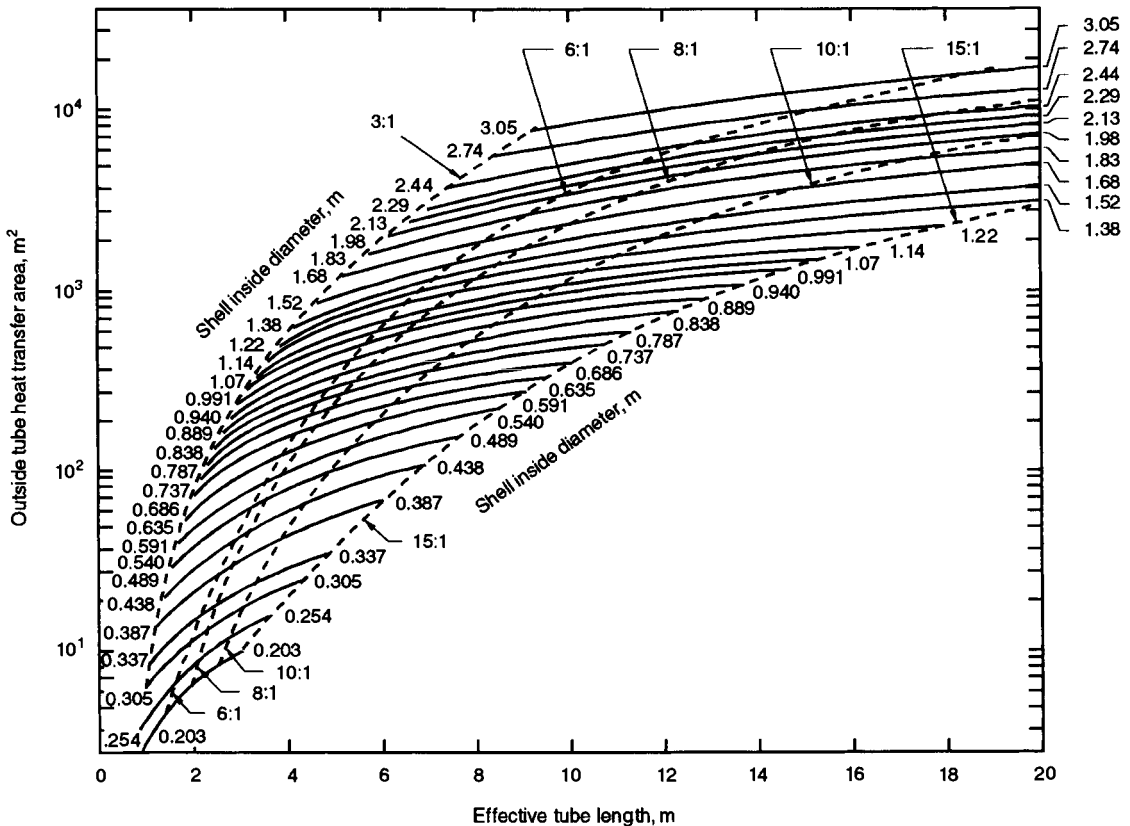

FIGURE 17.58 Heat transfer area as a function of the tube length and shell inside diameter for 19.0-mm outside diameter plain tubes on a 23.8-mm equilateral tube layout, fixed tubesheet, one tubeside pass, and fully tubed shell [109].

carried out at the system level, but individual irreversibilities of the heat exchanger expressed in terms of their monetary values must be identified [15]. All these clearly demonstrate the complexity of heat exchanger thermal design.

THERMAL DESIGN FOR TWO-PHASE HEAT EXCHANGERS

Most common heat exchangers operating under two-phase and multiphase flow conditions are condensers and vaporizers. See Fig. 17.2 for further classification.

The variety of phase-change conditions, the diversity of heat exchanger constructions, and the broad ranges of operating conditions prevent a thorough and complete presentation of design theory and design considerations in a limited space. The objective of this section, though, is to summarize the key points regarding thermal design and to present design guidelines for the most frequently utilized two-phase flow heat exchangers.

Condensers

In a condenser, the process stream (single component or multicomponent with or without noncondensable gases) is condensed to a liquid with or without desuperheating and/or subcooling. The diversity of major design features of various condensers is very broad, as can be concluded from many different applications presented in Fig. 17.2b. Consequently, various aspects of condenser operation as well as their various design characteristics cannot be presented in a unified fashion. Important aspects of condenser operation involve, but are not restricted to: (1) the character of the heat transfer interaction (direct or indirect contact type); (2) the geometry of the heat transfer equipment (shell-and-tube, extended surface, plate, and so on); (3) the number of components in the condensing fluid (single or multicomponent); (4) desuperheating, condensation, and subcooling; and (5) the presence of noncondensable gas in the condensing fluid (partial condensation).

Primary objectives for accomplishing the condensation process vary depending on a particular application, but common features of a vapor-liquid phase-change lead to certain general similarities in thermal design procedure. Nonetheless, thermal design of a condenser does not necessarily follow a standardized procedure, and it greatly depends on a condenser type and the factors mentioned above.

In indirect contact type condensers, two fluid streams are separated by a heat transfer surface. A shell-and-tube condenser is one of the most common type. For example, surface condensers are the turbine exhaust steam condensers used in power industry. In another condenser, a boiler feedwater is heated with a superheated steam on the shell side, causing desuperheating, condensing, and subcooling of the steam/water. In process industry, condensation of either single or multicomponent fluids (with or without noncondensable gases) may occur inside or outside the tubes, the tubes being either horizontal or vertical. Extended surface condensers are used both in power and process industries (including cryogenic applications) and are designed either as tube-fin or plate-fin exchangers. If the metal plate substitutes a tube wall to separate the two fluids (the condensing vapor and the coolant) in all primary surface condensers, the resulting design belongs to the family of plate condensers (plate-and-frame, spiral plate, and printed circuit heat exchangers).

In direct contact condensers, a physical contact of the working fluids (a saturated or superheated vapor and a liquid) occurs, allowing for the condensation to be accomplished simultaneously with the mixing process. The fluids can be subsequently separated only if they are immiscible. Direct contact is generally characterized with a very high heat transfer rate per unit volume. The classification of indirect and direct contact heat exchangers is discussed in more detail in Ref. 2.

Thorough discussion of various topics related to condensers and their characteristics is provided in Refs. 113–115.

Indirect Contact Type Condensers

Thermal Design.   Sizing or rating of an indirect contact condenser involves the very same heat transfer rate equation, Eq. 17.4, that serves as a basis for the thermal design of a single-phase recuperator. In the case of a condenser, however, both the overall heat transfer coefficient and the fluid temperature difference vary considerably along and across the exchanger. Consequently, in the design of a condenser, the local heat transfer rate equation, Eq. 17.2:

$$dq = U\Delta T dA \tag{17.147}$$

may be supplemented with an approximate equation:

$$q = \breve{U}\Delta T_m A \tag{17.148}$$

where

$$\breve{U} = \frac{1}{A} \int_A U \, dA \tag{17.149}$$

and/or

$$\Delta T_m = \frac{q}{\int_A U \, dA} \tag{17.150}$$

or alternately, the integration of Eq. 17.147 must be rigorously executed.

Now, the problem is how to determine the mean overall heat transfer coefficient and the corresponding mean temperature difference, Eqs. 17.149 and 17.150.

In practice, calculation has to be performed by dividing the condenser's total heat transfer load in an appropriate number of heat duty zones and subsequently writing auxiliary energy balances based on enthalpy differences for each zone. One must simultaneously establish the corresponding temperature variation trends, corresponding zonal mean overall heat transfer coefficients, and mean temperature differences. As a result, one can calculate the heat transfer surface for each zone using Eq. 17.148. Total heat transfer area needed for design is clearly equal to the sum of the heat transfer areas of all zones. In a limit, for a very large number of zones, the total heat transfer area is equal to:

$$A = \int_q \frac{dq}{U\Delta T} \tag{17.151}$$

Modern computer codes for designing heat exchangers evaluate Eq. 17.151 numerically, utilizing local overall heat transfer coefficients and local fluid temperature differences.

A method based on this simple set of propositions leads to the formulation of the thermal evaluation method as suggested by Butterworth [113]. This method is convenient for a preliminary design of E- and J-type shell-and-tube condensers. The complete design effort must include a posteriori the determination of pressure drop and corresponding corrections of saturation temperature and should ultimately end with an economic assessment based on, say, capital cost. The thermal evaluation method can be summarized for the shell side of a shell-and-tube condenser having a single tube pass as follows:

1. Construct an exchanger operating diagram. The plot provides the local shellside fluid equilibrium temperature T_s as a function of the corresponding fluid specific enthalpy (see Fig. 17.59). A correlation between the shellside and tubeside fluid enthalpies is provided by the enthalpy balance, therefore the tubeside temperature dependence T_t can be presented as well. The local equilibrium temperature is assumed to be the temperature of the stream well mixed at the point in question. Note that this step does not involve an estimation of the overall heat transfer coefficient.
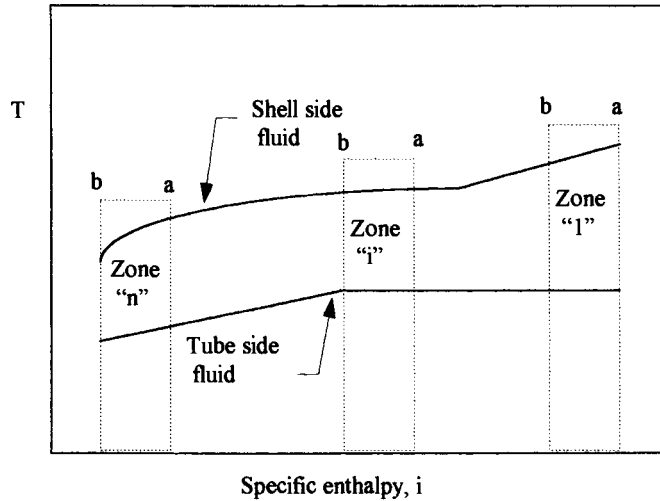
FIGURE 17.59   Operating diagram of a condenser.

2. Divide the exchanger operating diagram into N zones, $\{a, b\}_i$, for which both corresponding temperatures vary linearly with the shellside enthalpy. Here, a_i and b_i denote terminal points of the zone i.

3. Determine logarithmic mean temperature differences for each zone:

$$\Delta T_m = \Delta T_{lm,i} = \frac{\Delta T_{a,i} - \Delta T_{b,i}}{\ln (\Delta T_{a,i}/\Delta T_{b,i})} \qquad (17.152)$$

4. Calculate the overall heat transfer coefficient for each zone using an appropriate set of heat transfer correlations and an appropriate correlation from Table 17.32. More specifically, if a linear dependence between U and A can be assumed, an arithmetic mean between the terminal U values should be used as a mean value. If both U and T vary linearly with q, the mean U value should be calculated from a logarithmic mean value of the $U\Delta T$ product as indicated in Table 17.32. Next, if both $1/U$ and T vary linearly with q, the third equation for the mean U value from Table 17.32 should be used. Finally, if U is not a linear function of either A or q, the mean value should be assessed following the procedure described in the section starting on p. 17.47.

TABLE 17.32   Mean (Zonal) Overall Heat Transfer Coefficient

Conditions	Mean overall heat transfer coefficient
$\breve{U}$ vs. A linear within the zone $a - b$	$\breve{U} = \dfrac{U_a + U_b}{2}$
$\breve{U}$ and ΔT vs. A linear within the zone $a - b$	$\breve{U} = \dfrac{U_a\Delta T_b - U_b\Delta T_a}{\Delta T_{lm} \ln \left(\dfrac{U_a\Delta T_b}{U_b\Delta T_a} \right)}$
$\dfrac{1}{\breve{U}}$ and ΔT vs. A linear within the zone $a - b$	$\dfrac{1}{\breve{U}} = \dfrac{1}{U_a} \left(\dfrac{\Delta T_{lm} - \Delta T_b}{\Delta T_a - \Delta T_b} \right) + \dfrac{1}{U_b} \left(\dfrac{\Delta T_a - \Delta T_{lm}}{\Delta T_a - \Delta T_b} \right)$
$\breve{U}$ vs. A nonlinear within the zone $a - b$	See text on p. 17.47

5. Calculate heat transfer area for each zone:

$$A_i = \frac{\dot{m}_s \Delta i_i}{\bar{U}_i \Delta T_{lm,i}} \qquad (17.153)$$

6. The total heat transfer area is then:

$$A = \sum_{i=1}^{i=N} A_i \qquad (17.154)$$

This procedure is applicable to either countercurrent or cocurrent condensers (the difference being only the enthalpy balances in formal writing). The use of the exchanger operating diagram can also be utilized for shellside E-type condensers with more than one tube pass (i.e., 2, 4, and more passes); see Ref. 113 for details. As it was already pointed out, this method does not cover the complete set of design requirements (i.e., the pressure drop considerations must be included into the analysis). The preliminary design obtained by using the described method should be corrected as necessary, repeating the procedure for different assumed geometries, calculating the pressure drops, and evaluating mechanical and economic aspects of the design.

A modern approach to the design of condensers inevitably involves the use of complex numerical routines. An overview of numerical methods is provided in Ref. 117.

Overall Design Considerations and Selection of Condenser Types. Regardless of the particular thermal design method involved, a designer should follow an overall design procedure as outlined by Mueller for preliminary sizing of shell-and-tube condensers [114]: (1) determine a suitable condenser type following specific selection guidelines (see Table 17.33), (2) determine the heat load, (3) select coolant temperatures and calculate mean temperatures, (4) estimate the overall heat transfer coefficient, (5) calculate the heat transfer area, (6) select geometric characteristics of heat transfer surfaces (e.g., for a shell-and-tube heat exchanger, select the tube size, pitch, length, the number of tubes, shell size, and baffling), (7) compute pressure drops on both sides, and (8) refine the sizing process in an iterative procedure (as a rule using a computer). The final design has to be accompanied by mechanical design and thermoeconomic optimization.

Pressure drops on both sides of a condenser are usually externally imposed constraints and are calculated using the procedures previously described (see text starting on p. 17.62 for single-phase and p. 17.95 for two-phase). However, such calculated pressure drops for two-phase flow have a much larger uncertainty than those for single-phase conditions.

Comprehensive guidelines regarding the condenser selection process are given in Ref. 114 and are briefly summarized in Table 17.33. Most tubeside (condensation on tubeside) condensers with horizontal tubes are single-pass or two-pass shell-and-tube exchangers. They are acceptable in partial condensation with noncondensables. The tube layout is governed by the coolant side conditions. Tubeside condensers with vertical downflow have baffled shell sides, and the coolant flows in a single-pass countercurrent to the vapor. The vapor in such settings condenses, usually with an annular flow pattern. If the vapor condenses in upflow, the important disadvantage may be the capacity limit influenced by flooding. Shellside condensers with horizontal tubes can be baffled or the crossflow type. In the presence of noncondensables, the baffle spacing should be made variable. If the shellside pressure drop is a severe constraint, J-shell and X-shell designs are preferable. Tubes on the vapor side are often enhanced with low-height fins. The tube side can have multipasses. Vertical shellside condensers usually do not have baffled shell sides, and as a rule, vapor is in downflow.

Design procedures for condensers with noncondensables and multicomponent mixtures are summarized in Ref. 2.

Direct Contact Condensers

Thermal Design. A unified approach to the design of direct contact condensers does not exist. A good overview of direct contact condensation phenomena is provided in Ref. 115.

TABLE 17.33 Selection Guidelines for Condensers (Modified from Ref. 112)

	Tubeside condensation — High and intermediate pressures. Noncorrosive or corrosive vapor. High temperature (> 400°C). Severe vapor fouling. Good control of venting. Poor for pressures below 3 kPa.						Shellside condensation — Intermediate pressure. Noncorrosive vapor. Severe coolant or moderate vapor fouling. Can handle freezing condensate. Tube vibration problems. Multipassing and variable baffle spacing can be used for total condensation. Good venting control.								Direct contact condensation — Design information is limited. If coolant is condensate, then an external cooler is required. With water coolant, there may be pollution problems. Applicable for very low or intermediate pressure, very corrosive vapor, and severe or moderate coolant fouling.	
	Horizontal Possible slugging of condensate for total condensation.		**Vertical** Tubesheet vents required.				**Horizontal** Can use finned or enhanced tubes.				**Vertical** Can use a falling-water film but possible venting problems for total condensation.					
			Downflow Handles dirty or polymerizing vapors.		**Upflow** Flooding. Hot condensate return and removal of small amounts of low boilers for total condensation.		**Cross "X"** Possible venting problems for total condensation.		**Baffled** Multipassing and variable baffle spacing can be used for a partial condensation case.		**Downflow** Multipassing and variable baffle spacing and falling-water film can be used for a partial condensation case.		**Upflow** For partial condensation, no known practical application.			
	Total	Partial	Total	Partial	Total	Partial	Total	Partial	Total	Partial	Total	Partial	Total	Partial	Total	Partial
SCV¹	G² ●³	G ●	G ●	G ●	F ☺	X ⊠	G ☺	P ☺	G ☺	P ☺	G ☺	F ☺	G ⊗	P ☺	G ☺	X ⊠
MCV	F ☺	P ☺	G ☺	G ☺	F ⊗	X ⊠	G ☺	F ☺	G ☺	P ⊗	G ⊗	P ☺	F ⊗	X ⊠	P ⊗	F ⊗
SC	P ⊠	G ☺	G ☺	G ●	X ⊠	X ⊠	F ⊗	G ☺	P ⊗	G ☺	F ☺	F ●	X ⊠	X ⊠	X ⊠	F ☺
Δp high	G ☺	G ☺	G ⊗	G ⊗	X ⊗	P ⊗	G ☺	G ☺	G ☺	G ☺	G ⊗	G ⊗	X ⊗	X ⊗	X ⊠	X ⊠
Δp low	P	P	P	G	G	F	G	G	F	P	G	G	F	F	G	G
C liquid	G	G	G	G	G	G	G	G	G	G	G	G	G	G	G	G
C gas	G	G	G	G	G	G	G	G	G	G	G	G	G	G	X	X
C boiling	G	G	G	G	G	G	X	X	X	X	G	G	G	G	X	X

¹SCV - Single-component vapor; MCV - Multicomponent vapor; SC - Subcooled condensate; Δp - Pressure drop; C - Coolant.

²Acceptability: G - good; F - fair; P - poor; X - not acceptable or not recommended.

³ Predictability: ● - average (~25%); ☺ - fair (< 50%); ⊗ - poor (50+%); ⊠ - no method or not recommended.

Physical conditions greatly depend on the aggregate state of the continuous phase (vapor in spray and tray condensers, liquid in pool-type condensers, and liquid film on the solid surface in packed bed condensers). Design of the most frequently used spray condensers, featuring vapor condensation on the water droplets, depends on the heat and mass transfer phenomena involved with saturated vapor condensation in the presence of the subcooled liquid droplets of changing mass. The process is very complex. For further details on the problems involved, consult Refs. 116 and 118. Such designs involve a substantial input of empirical data.

The key process variables are the time required for a spray drop of a particular size to reach prescribed distance and the quantity of heat received by droplets from the vapor. The initial size of a droplet obviously influences the size of a heat exchanger. Subsequent transient heat and mass transfer processes of vapor condensation on a droplet of changing size has a key role in the exchanger operation. Initial droplet sizes and their distribution is controlled by design of spray nozzles. Thermofluid phenomena models involve a number of idealizations; the following are important: (1) heat transfer is controlled by transient conduction within the droplet as a solid sphere, (2) droplet size is uniform and surface temperature equal to the saturation temperature, and (3) droplets are moving relative to the still vapor. Although these idealizations seem to be too radical, the models developed provide at least a fair estimate for the initial design. In Table 17.34, compiled are the basic relations important for contact condensation of saturated vapor on the coolant liquid. Generally, guidelines for design or rating a direct contact condenser do not exist and each design should be considered separately. A good overview of the calculations involved is provided in Ref. 118.

TABLE 17.34   Direct Contact Condensation Thermofluid Variables

	Correlation	Parameters
Liquid drop residence time	$\mathrm{Fo} = -\dfrac{1}{\pi^2}\ln\left[1-\left(\dfrac{T-T_i}{T_{\mathrm{sat}}-T_i}\right)^2\right]$	$\mathrm{Fo} = \dfrac{4\alpha\tau}{D^2} \qquad \alpha = \dfrac{k_l}{\rho_l c_{p,l}}$
Drop travel distance, m	$L = 0.06\,\dfrac{D^{1.84}}{\Gamma}\,(V_i^{0.84}-V^{0.84})$	$\Gamma = v_v^{0.84}\,\dfrac{\rho_v}{\rho_l}$
Drop velocity, m/s	$V = \left(V_i^{-0.16}+3.23\,\dfrac{\Gamma\tau}{D^{1.84}}\right)^{-1/0.16}$	
Heat transfer rate	$q = (\dot{m}c_p)_l(T-T_i)$	
Condensate mass flow rate	$\dot{m}_v = \dfrac{q}{i_{lv}}$	

Vaporizers

Heat exchangers with liquid-to-vapor phase change constitute probably the most diverse family of two-phase heat exchangers with respect to their functions and applications (see Fig. 17.2). We will refer to them with the generic term *vaporizer* to denote any member of this family. Therefore, we will use a single term to denote boilers, steam and vapor generators, reboilers, evaporators, and chillers. Design methodologies of these vaporizers differ due to construction features, operating conditions, and other design considerations. Hence, we will not be able to cover them here but will emphasize only a few most important thermal design topics for evaporators.

Thermal Design.   The key steps of an evaporator thermal design procedure follow the heat exchanger overall design methodology. For a two-phase liquid-vapor heat exchanger, the procedure must accommodate the presence of phase change and corresponding variations of

local heat transfer characteristics, the same two major features discussed for condensers. The procedure should, at least in principle, include the following steps:

1. Select an appropriate exchanger type following the analysis of the vaporizer function, and past experience if any. The selection influences both heat transfer and nonheat transfer factors such as: heat duty, type of fluids, surface characteristics, fouling characteristics, operating conditions (operating pressure and design temperature difference), and construction materials. For example, a falling-film evaporator should be used at pressures less than 1 kP (0.15 psi). At moderate pressures (less than 80 percent of the corresponding reduced pressure), the selection of a vaporizer type does not depend strongly on the pressure, and other criteria should be followed. For example, if heavy fouling is expected, a vertical tubeside thermosiphon may be appropriate.

2. Estimate thermofluid characteristics of liquid-vapor phase change and related heat transfer processes such as circulation rate in natural or forced internal or external fluid circulation, pressure drops, and single- and two-phase vapor-liquid flow conditions. The initial analysis should be based on a rough estimation of the surface area from the energy balance.

3. Determine local overall heat transfer coefficient and estimate corresponding local temperature difference (the use of an overall logarithmic mean temperature difference based on inlet and outlet temperatures is, in general, not applicable).

4. Evaluate (by integration) the total heat transfer area, and subsequently match the calculated area with the area obtained for a geometry of the selected equipment.

5. Evaluate pressure drops. The procedure is inevitably iterative and, in practice, ought to be computer-based.

6. Determine design details such as the separation of a liquid film from the vapor (i.e., utilization of baffles and separators).

Important aspects in thermal design of evaporators used in relation to concentration and crystallization in the process/chemical industry can be summarized as follows [119]:

1. The energy efficiency of the evaporation process (i.e., the reduction of steam consumption by adequate preheating of feed by efficient separation, managing the presence of noncondensable gases, avoiding high concentrations of impurities, and proper selection of take-off and return of the liquid)

2. The heat transfer processes

3. The means by which the vapor and liquid are separated

Preliminary thermal design is based on the given heat load, estimated overall heat transfer coefficient, and temperature difference between the saturation temperatures of the evaporating liquid and condensing vapor. The guidelines regarding the preliminary estimation of the magnitude of the overall heat transfer coefficient are provided by Smith [119]; also refer to Table 17.28 for shell-and-tube heat exchangers.

Problems that may be manifested in the operation of evaporators and reboilers are numerous: (1) corrosion and erosion, (2) flow maldistribution, (3) fouling, (4) flow instability, (5) tube vibration, and (6) flooding, among others. The final design must take into account some or all of these problems in addition to the thermal and mechanical design.

A review of thermal design of reboilers (kettle, internal, and thermosiphon), and an overview of important related references is provided by Hewitt at al. [115]. It should be pointed out that a computer-based design is essential. Still, one must keep in mind that the results greatly depend on the quality of empirical data and correlations. Thermal design of kettle and internal reboilers, horizontal shellside and vertical thermosiphon reboilers, and the useful guidelines regarding the special design considerations (fouling, flow regime consideration, dryout, overdesign, vapor separation, etc.) are provided in Ref. 2.

Finally, it should be noted that nuclear steam generators and waste heat boilers, although working in different environments, both represent modern unfired steam raisers (i.e., steam generators) that deserve special attention. High temperatures and operating pressures, among the other complex issues, impose tough requirements that must be addressed in design. The basic thermal design procedure, though, is the same as for other vapor-liquid heat exchangers [120, 121].

FLOW-INDUCED VIBRATION

In a tubular heat exchanger, interactions between fluid and tubes or shell include the coupling of fluid flow-induced forces and an elastic structure of the heat exchanger, thus causing oscillatory phenomena known under the generic name *flow-induced vibration* [122]. Two major types of flow-induced vibration are of a particular interest to a heat exchanger designer: tube vibration and acoustic vibration.

Tube vibrations in a tube bundle are caused by oscillatory phenomena induced by fluid (gas or liquid) flow. The dominant mechanism involved in tube vibrations is the *fluidelastic instability* or *fluidelastic whirling* when the structure elements (i.e., tubes) are shifted elastically from their equilibrium positions due to the interaction with the fluid flow. The less dominant mechanisms are vortex shedding and turbulent buffeting.

Acoustic vibrations occur in fluid (gas) flow and represent standing acoustic waves perpendicular to the dominant shellside fluid flow direction. This phenomenon may result in a loud noise.

A key factor in predicting eventual flow-induced vibration damage, in addition to the above mentioned excitation mechanisms, is the natural frequency of the tubes exposed to vibration and damping provided by the system. Tube vibration may also cause serious damage by fretting wear due to the collision between the tube-to-tube and tube-to-baffle hole, even if resonance effects do not take place.

Flow-induced vibration problems are mostly found in tube bundles used in shell-and-tube, duct-mounted tubular and other tubular exchangers in nuclear, process, and power industries. Less than 1 percent of such exchangers may have potential flow-induced vibration problems. However, if it results in a failure of the exchanger, it may have a significant impact on the operating cost and safety of the plant.

This subsection is organized as follows. The tube vibration excitation mechanism (the fluidelastic whirling) will be considered first, followed by acoustic phenomena. Finally, some design-related guidelines for vibration prevention will be outlined.

Tube Vibration

Fluidelastic Whirling.   A displacement of a tube in a tube bundle causes a shift of the flow field, and a subsequent change of fluid forces on the tubes. This change can induce instabilities, and the tubes will start vibrating in oval orbits. These vibrations are called the fluidelastic whirling (or the fluidelastic instability). Beyond the critical intertube flow velocity V_{crit}, the amplitude of tube vibrations continues to increase exponentially with increasing flow velocity. This phenomenon is recognized as the major cause of tube vibrations in the tubular heat exchangers. The critical velocity of the complex phenomenon is correlated semiempirically as follows [122].

$$\frac{V_{crit}}{f_n d_o} = \mathbf{C} \left(\frac{\delta_o M_{eff}}{\rho_s d_o^2} \right)^a$$

(17.155)

where δ_o represents the logarithmic decrement, ρ_s is shellside fluid density, and M_{eff} is the virtual mass or the effective mass per unit tube length given by

$$M_{\text{eff}} = \frac{\pi}{4}(d_o^2 - d_i^2)\rho_t + \frac{\pi}{4}d_i^2\rho_{f_t} + \frac{\pi}{4}d_o^2 C_m \rho_s \qquad (17.156)$$

The effective mass per unit tube length, M_{eff}, includes the mass of the tube material per unit length, the mass of the tubeside fluid per unit tube length, and the hydrodynamic mass per

unit tube length (i.e., the mass of the shellside fluid displaced by a vibrating tube per unit tube length). In the hydrodynamic mass per unit tube length, ρ_s is the shellside fluid density and C_m is the added mass (also virtual mass or hydrodynamic mass) coefficient provided in Fig. 17.60. In addition to the known variables, two additional coefficients ought to be introduced: the coefficient **C** (also referred to as the *threshold instability constant* [130, 154] or *fluidelastic instability parameter* [154]) and the exponent *a*. Both coefficient **C** and exponent *a* can be obtained by fitting experimental data for the critical flow velocity as a function of the so-called *damping parameter* (also referred to as *mass damping*), the bracketed quantity on the right side of Eq. 17.155. The coefficient **C** is given in Table 17.35 as a function of tube bundle layout under the condition that exponent *a* take the value of 0.5 as predicted by the theory of fluidelastic instability developed by Connors [124] and for the damping parameter greater than 0.7. If the damping parameter is smaller than 0.7, a least-square curve fit of available data gives $\mathbf{C}_{\text{mean}} = 3.9$, and $a = 0.21$ (the statistical lower bound $\mathbf{C}_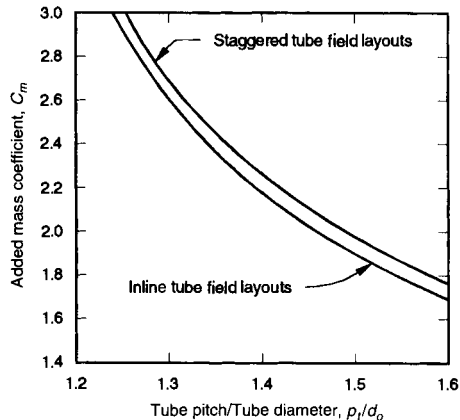{90\%}$ being 2.7) [122]. The smallest coefficient $\mathbf{C}_{\text{mean}}$ in Table 17.35 corresponds to the 90° tube layout, thus implying this layout has the smallest critical velocity (the worst from the fluidelastic whirling point of view) when other variables remain the same. The same correlation with different coefficients and modified fluid density can be applied for two-phase flow [125]. It should be noted that the existing models cannot predict the fluidelastic whirling with the accuracy better than the one implied by a standard deviation of more than 30 percent of existing experimental data [126].

FIGURE 17.60   Upper bound of added mass coefficient C_m [128].

TABLE 17.35   Coefficient **C** in Eq. 17.155 [122]

C	Tube pattern					
	30°	60°	45°	90°	All	Single tube row
$\mathbf{C}_{\text{mean}}$	4.5	4.0	5.8	3.4	4.0	9.5
$\mathbf{C}_{90\%}$	2.8	2.3	3.5	2.4	2.4	6.4

Acoustic Vibrations

This mechanism produces noise and generally does not produce tube vibration. It is one of the most common forms of flow-induced vibration in shell-and-tube exchangers for high velocity shellside gas flows in large exchangers. When a forcing frequency (such as the frequency of vortex shedding, turbulent buffeting, or any periodicity) coincides with the natural frequency of a fluid column in a heat exchanger, a coupling occurs. The kinetic energy in the flow stream is converted into acoustic pressure waves; this results in a possibility of standing wave vibration, also referred to as acoustic resonance or acoustic vibration, creating an intense, low-frequency, pure-tone noise. Particularly with a gas stream on the shell side, the sound pressure

in a tube array may reach the level of 160–176 dB, the values up to 40 dB lower outside the heat exchanger shell [122]. Acoustic vibration could also increase shellside pressure drop through the resonant section and cause severe vibration and fatigue damage to the shell (or casing), connecting pipes, and floor. If the frequency of the standing wave coincides with the tube natural frequency, tube failure may occur.

Now we will briefly describe two additional mechanisms: vortex shedding and turbulent buffeting. It should be noted that these mechanisms could cause tube vibrations, but their influence on a tube bundle is less critical compared to the fluidelastic instabilities described earlier.

Vortex Shedding.   A tube exposed to an incident crossflow above critical Reynolds numbers provokes an instability in the flow and a simultaneous shedding of discrete vorticities alternately from the sides of the tube. This phenomenon is referred to as *vortex shedding*. Alternate shedding of the vorticities produces harmonically varying lift and drag forces that may cause movement of the tube. When the tube oscillation frequency approaches the tube natural frequency within about ±20 percent, the tube starts vibrating at its natural frequency. This results in the vortex shedding frequency to shift to the tube's natural frequency (lock-in mechanism) and causes a large amplification of the lift force. The vortex shedding frequency is no more dependent upon the Reynolds number. The amplitude of vibration grows rapidly if the forcing frequency coincides with the natural frequency. This can result in large resonant amplitudes of the tube oscillation, particularly with liquid flows, and possible damage to tubes.

Vortex shedding occurs for Re numbers above 100 (the Re number is based on the upstream fluid velocity and tube outside diameter). In the region $10^5 < Re < 2 \times 10^6$, vortex shedding has a broad band of shedding frequencies. Consequently, the regular vortex shedding does not exist in this region.

The vortex shedding frequency f_v for a tubebank is calculated from the Strouhal number

$$Sr = \frac{f_v d_o}{V_c} \tag{17.157}$$

where Sr depends on tube layouts as given in Fig. 17.61. The Strouhal number is nearly independent of the Reynolds number for Re > 1000.

The reference crossflow velocity V_c in gaps in a tube row is difficult to calculate since it is not based on the minimum free flow area. The local crossflow velocity in the bundle varies from span to span, from row to row within a span, and from tube to tube within a row [5]. In general, if the flow is not normal to the tube, the crossflow velocity in Eq. 17.157 is to be interpreted as the normal component (crossflow) of the free stream velocity [154]. Various methods may be used to evaluate reference crossflow velocity. In Table 17.36, a procedure is given for the determination of the reference crossflow velocity according to TEMA Standards [5]. The calculated velocity takes into account fluid bypass and leakage which are related to heat exchanger geometry. This method of calculation is valid for single-phase shellside fluid with single segmental baffles in TEMA E shells.

Turbulent Buffeting.   Turbulent buffeting refers to unsteady forces developed on a body exposed to a highly turbulent flow. The oscillatory phenomenon in turbulent flow on the shell side (when the shellside fluid is gas) is characterized by fluctuating forces with a dominant frequency as follows [123, 154]:

$$f_{tb} = \frac{V_c d_o^2}{X_l X_t} \left[3.05 \left(1 - \frac{d_o}{X_t} \right)^2 + 0.28 \right] \tag{17.158}$$

The correlation was originally proposed for tube-to-diameter ratios of 1.25 and higher. It should be noted that the turbulent buffeting due to the oncoming turbulent flow is important
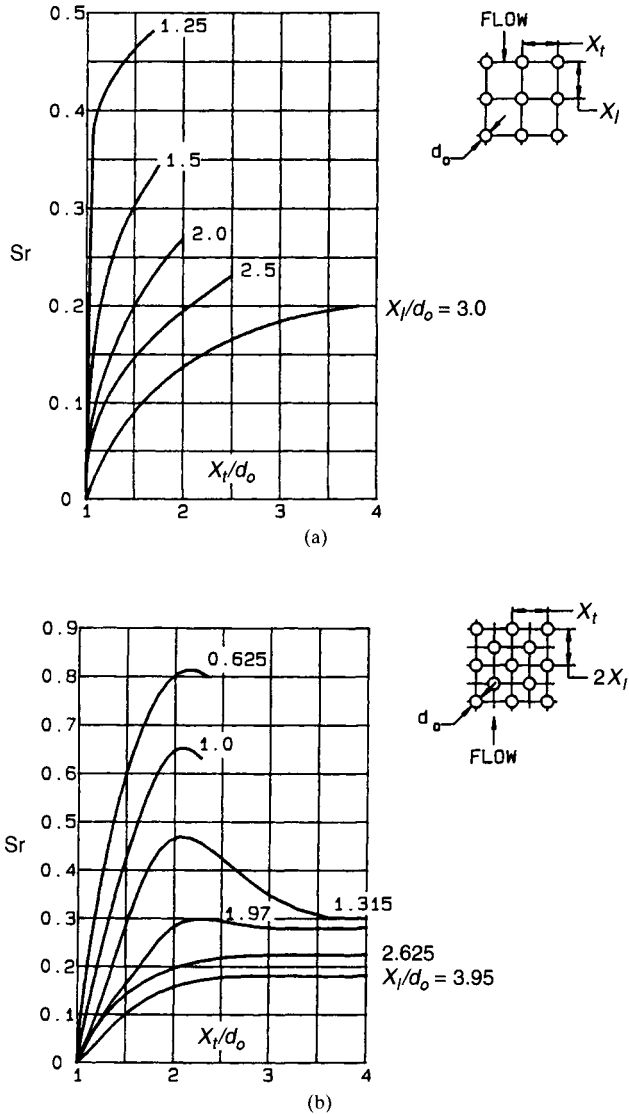
FIGURE 17.61   Vortex shedding Strouhal numbers for tube patterns:
(a) 90°, (b) 30°, 45°, 60° [5].

only for gases at high Reynolds numbers. The reference crossflow velocity in Eq. 17.158 should be calculated using the procedure presented in Table 17.36.

Tube Bundle Natural Frequency.   Elastic structures vibrate at different natural frequencies. The lowest (fundamental) natural frequency is the most important. If the vortex shedding or turbulent buffeting frequency is lower than the tube fundamental natural frequency, it will not create the resonant condition and the tube vibration problem. Hence, the knowledge of the fundamental natural frequency is sufficient in most situations if f_n is found to be higher than f_v or f_{tb}. Higher than the third harmonic is generally not important for flow-

TABLE 17.36 Reference Crossflow Velocity in Tube Bundle Gaps [5]*

Reference crossflow velocity V_c

$$V_c = \frac{F_h}{M}\frac{\dot{m}_s}{a_x \rho_s}\left[\frac{m}{s}\right]; \quad \dot{m}_s\left[\frac{kg}{s}\right]; \quad \rho_s\left[\frac{kg}{m^3}\right]; \quad a_x = C_a L_{bc} D_{otl} \ [m^2]$$

$$F_h = \left[1 + N_h\left(\frac{D_s}{p_t}\right)^{1/2}\right]^{-1}$$

$$N_h = f_1 C_7 + f_2 \Psi + f_3 E \qquad f_1 = \frac{(C_1 - 1)^{3/2}}{C_1^{1/2}} \qquad f_2 = \frac{C_2}{C_1^{3/2}}$$

$$f_3 = C_3 C_1^{1/2} \qquad C_1 = \frac{D_s}{D_{otl}} \qquad C_2 = \frac{d_1 - d_o}{d_o} \qquad C_3 = \frac{D_s - D_{baff}}{D_s}$$

$$C_7 = C_4\left(\frac{p_t}{p_t - d_o}\right)^{3/2} \qquad \Psi = C_5 C_8 \frac{D_s}{L_{bc}}\left(\frac{d_o}{p_t}\right)^2 \frac{p_t}{p_t - d_o}$$

$$E = C_6 \frac{p_t}{p_t - d_o}\frac{D_s}{L_{bc}}\left(1 - \frac{L_c}{D_s}\right)$$

See below for C_4, C_5, and C_6.

L_c/D_s	0.10	0.15	0.20	0.25	0.30	0.35	0.40	0.45	0.50
C_8	0.94	0.90	0.85	0.80	0.74	0.68	0.62	0.54	0.49

A linear interpolation C_8 vs. L_c/D_s is permitted

$$M = \left[1 - \frac{0.7 L_{bc}}{D_s}\left(M_w^{-0.6} - 1\right)\right]^{-1}$$

$$M_w = m C_1^{1/2} \qquad C_a = \left(\frac{p_t - d_o}{p_t}\right)$$

C_i	30°	60°	90°	45°
C_4	1.26	1.09	1.26	0.90
C_5	0.82	0.61	0.66	0.56
C_6	1.48	1.28	1.38	1.17
m	0.85	0.87	0.93	0.80

*In Ref. 5, U.S. Engineering units are used.

induced vibration in heat exchangers. For vortex shedding, the resonant condition can be avoided if the vortex shedding frequency is outside ±20 percent of the natural frequency of the tube.

Determination of natural frequency of an elastic structure can be performed analytically (for simple geometries) [127] and/or numerically (for complex structures) using finite element computer programs (such as NASTRAN, MARC, and ANSYS) or proprietary computer programs.

Straight Tube. A tube of a shell-and-tube heat exchanger with fluid flowing in it and a flow of another fluid around it is hardly a simple beam structure. Consequently, the natural frequency of the ith mode of a straight tube rigidly fixed at the ends in the tubesheets and supported at the intermediate baffles can be calculated using a semiempirical equation as follows:

$$f_{n,i} = \frac{\lambda_i^2}{2\pi}\left(\frac{EI}{M_{eff} L^4}\right)^{1/2} \qquad (17.159)$$

where E represents modulus of elasticity, I is area moment of inertia, and M_{eff} is the effective mass of the tube per unit length defined by Eq. 17.156. Length L in Eq. 17.159 is the tube unsupported span length. The coefficient λ_i^2 is the so-called frequency constant which is a function of the mode number i, the number of spans N, and the boundary conditions. The frequency constant for the fundamental frequency $i = 1$ of an N-span beam with clamped ends, pinned intermediate supports, and variable spacing in the outermost spans is presented in Fig. 17.62 [127].
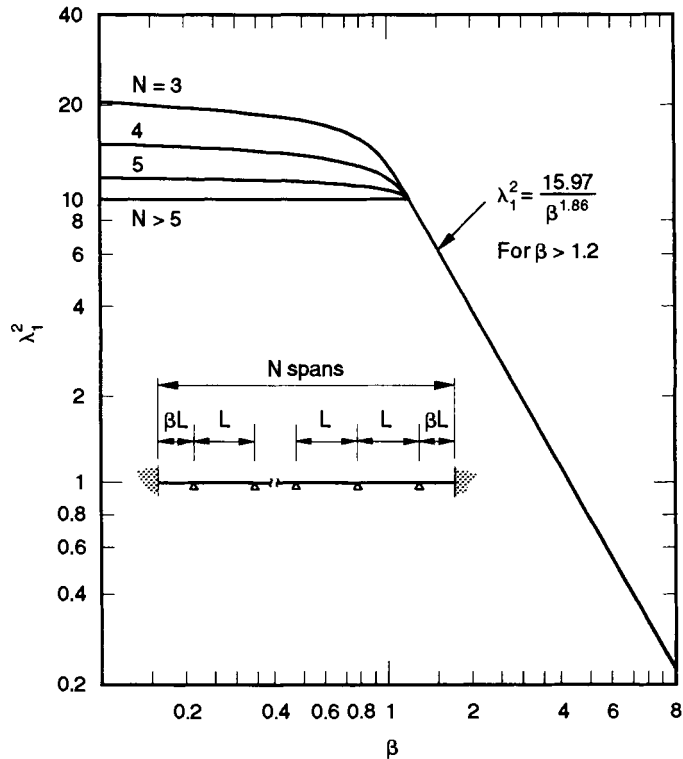
FIGURE 17.62   Frequency constant λ_1^2 for the fundamental frequency of an N span beam for Eq. 17.159 [127].

Various factors influence the tube natural frequency in a shell-and-tube heat exchanger as summarized in Table 17.37. In general, the natural frequency of an unsupported span is influenced primarily by the geometry, elastic properties, inertial properties, span shape, boundary conditions, and axial loading of the tube.

U Tube.   It is more difficult to predict correctly the natural frequency of U tubes than the natural frequency of a straight tube. The fundamental natural frequency can be calculated following the suggestion from TEMA standards [5]:

$$f_n = \frac{C_u}{R^2}\left(\frac{EI}{M_{\text{eff}}}\right)^{1/2} \tag{17.160}$$

where C_u represents the U-tube natural frequency constant, which depends on the span geometry, and R is the mean bend radius. The numerical values of C_u for four characteristic U-bend geometries are given in Fig. 17.63 [5].

Damping Characteristics.   Damping causes vibrations to decay in an elastic structure and depends on the vibration frequency, the material of the elastic structure, the geometry, and the physical properties of the surrounding fluid (in the case of a shell-and-tube heat exchanger, the surrounding fluid is the shell fluid).

The quantitative characteristic of damping is the logarithmic decrement δ_o. It is defined as $\delta_o = \ln(x_n/x_{n+1})$, where x_n and x_{n+1} are the successive midspan amplitudes of a lightly damped structure in free decay. The magnitude of the damping factor is within the range of 0.03 and 0.01 [122]. Statistical analysis of damping factor values compiled by Pettigrew et al. [128] reveals the data as follows. For a heat exchanger tubing in air, the average damping factor is

TABLE 17.37 Influence of Design Factors on the Tube Fundamental Natural Frequency (Modified from Ref. 155)

Influential factor	Variation trend		Comments
	Factor	Frequency	
Length of tube span (unsupported)	↑	↓	The most significant factor.
Tube outside diameter	↑	↑	
Tube wall thickness	↑	↑	A very weak dependence.
Modulus of elasticity	↑	↑	
Number of tube spans	↑	↓	The rate of decrease diminishes with a large number of tube spans.
Tube-to-baffle hole clearance	↑	↓	f_n increases only if there is a press fit and the clearance is very small.
Number of tubes in a bundle	↑	↓	
Baffle spacing	↑	↓	
Baffle thickness	↑	↑	A weak dependence only if the tube-to-baffle clearance is tight.
Tensile stress in tubes	↑	↑	Important in a fixed tubesheet exchanger.
Compressive stress in tubes	↑	↓	A slight decrease; under high compressive loads, high decrease.

0.069 with the standard deviation of 0.0145. For a heat exchanger tubing in water, the average damping factor is 0.0535 with the standard deviation of 0.0110. TEMA standards [5] suggest empirical correlations for δ_o that depend on the fluid thermophysical properties, the outside diameter of the tube, and the fundamental natural frequency and effective mass of the tube.

Acoustic Natural Frequencies. The natural frequencies of transverse acoustic modes in a cylindrical shell can be calculated as follows [122]:

$$f_{a,i} = \frac{c_{\text{eff}}}{\pi} \frac{a_i}{D_s} \qquad i = 1, 2 \tag{17.161}$$

where
$$c_{\text{eff}} = \frac{c_o}{(1 + \sigma)^{1/2}} \qquad \text{with } c_o = \left(\frac{\gamma}{\rho \kappa_T}\right)^{1/2} \tag{17.162}$$

Here c_{eff} represents the effective speed of sound, c_o is the actual speed of sound in free space, γ is the specific heat ratio, and κ_T is the isothermal compressibility of the fluid. A fraction of shell volume occupied by tubes, *solidity* σ can be easily calculated for a given tube pattern. For example, $\sigma = 0.9069 (d_o/p_t)^2$ for an equilateral triangular tube layout, and $\sigma = 0.7853 (d_o/p_t)^2$ for a square layout. Coefficients a_i are the dimensionless sound frequency parameters associated with the fundamental diametrical acoustic mode of a cylindrical volume. For the fundamental mode $a_1 = 1.841$, and, for the second mode, $a_2 = 3.054$ [122].

According to Chenoweth [130], acoustic vibration is found more often in tube bundles with a staggered rather than inline layout. It is most common in bundles with the rotated square (45°) layout.

Prediction of Acoustic Resonance. The procedure for prediction of the onset of acoustic resonance is as follows [122]:

1. Determine the first two natural frequencies of acoustic vibration using Eqs. 17.161 and 17.162. Note that failure to check the second mode may result in the onset of acoustic resonance.
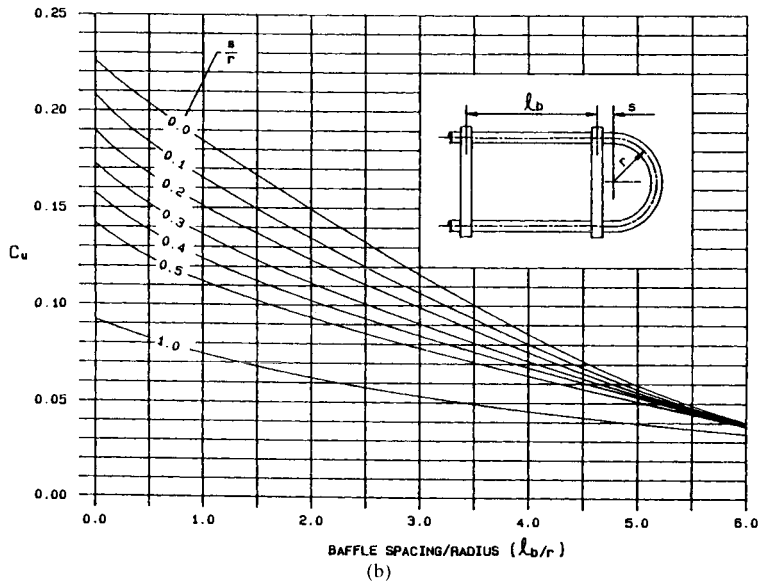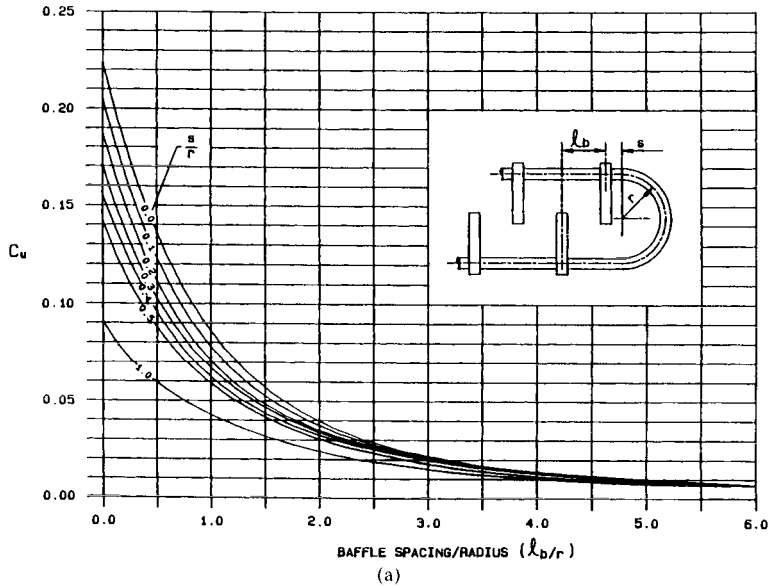
FIGURE 17.63 U-tube frequency constants for geometries shown in (a) and (b) [5].

2. Determine the vortex shedding frequency using Eq. 17.157 and turbulent buffeting frequency using Eq. 17.158. Also compute the natural frequency f_n of the tubes by using Eq. 17.159 or 17.160.

3. Determine the onset of the resonance margin as follows:

$$(1 - \alpha')(f_v \text{ or } f_{tb}) < f_{a,i} < (1 + \alpha'')(f_v \text{ or } f_{tb}) \tag{17.163}$$
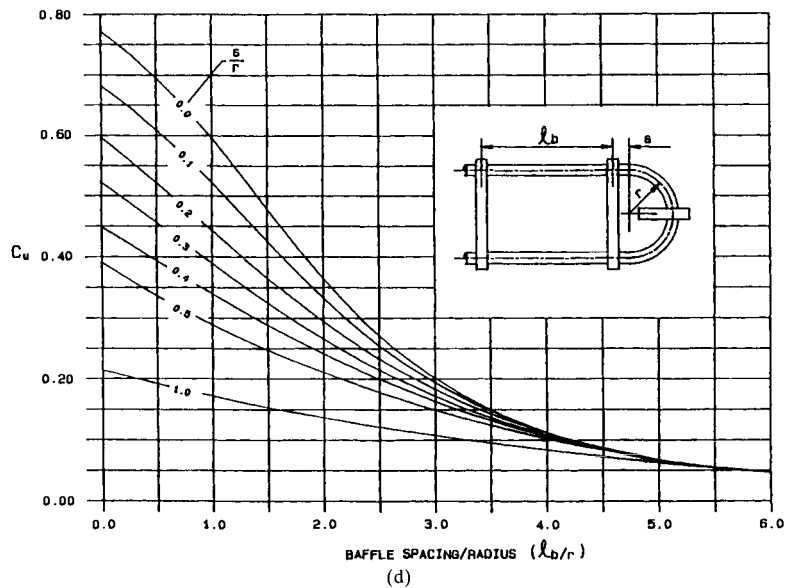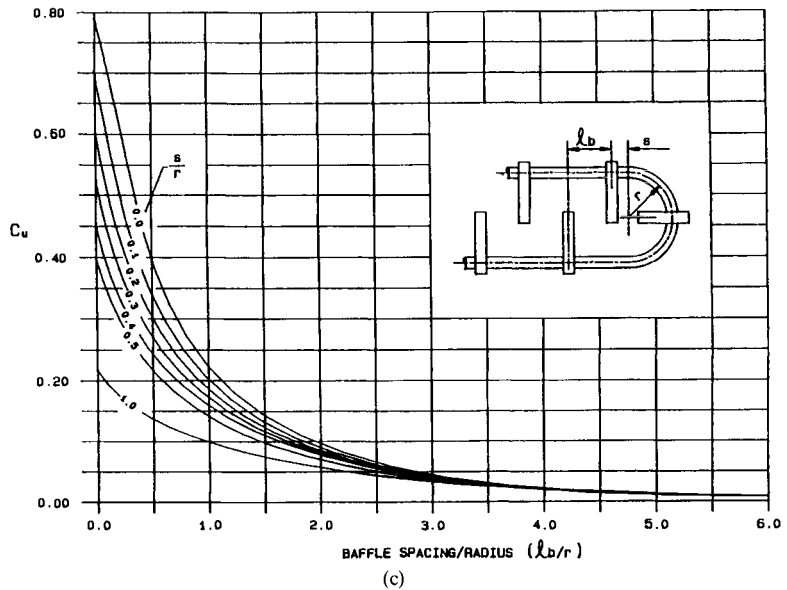
FIGURE 17.63 (*Continued*)   U-tube frequency constants for geometries shown in (*c*) and
(*d*) [5].

where the coefficients $\alpha' = \alpha'' = 0.2$ as recommended by TEMA Standards [5] (i.e., f_v or f_{tb}
within ±20 percent of $f_{a,i}$). Some measurements [129] suggest different values for this mar-
gin, $\alpha' = 0.19$ and $\alpha'' = 0.29$, and the maximum values being 0.4 and 0.48, respectively.

The acoustic frequency of an ith mode should be within the margin defined by Eq. 17.163
for resonance to occur. TEMA Standards [5] suggest somewhat different conditions. In addi-

tion to Eq. 17.163, TEMA recommends that the reference crossflow velocity (Table 17.36) must be above certain values involving an additional parameter that depends on the Reynolds and Strouhal numbers and the tube bundle geometry. For details, refer to Ref. 5.

Design Guidelines for Vibration Mitigation

Three major modes of tube failure deserve to be mentioned [122]:

- Fatigue due to repeated bending (i.e., if the stress level in the tube at the tubesheet joint is above the fatigue limit, a circumferential crack will grow about the tube periphery).
- Large-amplitude vibration, resulting in clashing of adjacent tubes at midspan, which will wear flats in neighboring tubes, leading to thinning of the tube walls with eventual splitting (collision damage).
- If there is clearance between a tube and its support, large amplitude tube motion can wear a groove in the tube at a support, in particular if the baffles are thin or harder than the tubes or there is a large baffle-to-tube clearance (baffle damage).

Heat exchanger vibrations can be reduced either by increasing the tube bundle natural frequency or reducing excitation mechanisms. Methods to accomplish that and eventually prevent vibration and potential damage can be summarized as follows [130]:

- Reducing the longest unsupported span length
- Reducing the shellside velocities by increasing tube pitch or using TEMA X- or J-shell styles
- Reducing nozzle velocities by adding annular distributors and/or a support plate at the centerline of the nozzles and/or vapor belts
- Changing the baffle type (multisegmental baffle, RODbaffle type bundle)
- Adding deresonating plates in the exchanger bundle to break the acoustic waves

FLOW MALDISTRIBUTION

A standard idealization of the basic heat exchanger theory is that the fluid flow rate is distributed uniformly through the exchanger on each side of the heat transfer surface. However, in practice, flow maldistribution is more common and can reduce the idealized performance significantly.

Flow maldistribution can be induced by (1) heat exchanger geometry (mechanical design features such as the basic geometry, manufacturing imperfections, and tolerances), and (2) heat exchanger operating conditions (such as viscosity or density-induced maldistribution, multiphase flow, and fouling phenomena). Geometry-induced flow maldistribution can be classified into (a) gross flow maldistribution, (b) passage-to-passage maldistribution, and (c) manifold-induced maldistribution. The most important flow maldistributions caused by operating conditions is the viscosity-induced maldistribution and associated flow instability.

Various problems related to flow maldistribution phenomena including flow instabilities are discussed extensively in the literature. Refer to Mueller and Chiou [131] for a review.

Geometry-Induced Flow Maldistribution

A class of maldistribution phenomena that are a consequence of geometric characteristics of fluid flow passages are called geometry-induced flow maldistributions. This type of maldistribution is closely related to heat exchanger construction and fabrication (such as header

design and heat exchanger core fabrication, including brazing in compact heat exchangers). This maldistribution is inherent to a particular heat exchanger in question and cannot be influenced significantly by modifying operating conditions.

Gross Flow Maldistribution.   The major feature of the gross flow maldistribution is that the nonuniform flow happens at the macroscopic level (due to poor header design or blockage of some flow passages in manufacturing operation) and that it does not depend on the local heat transfer surface geometry. This class of maldistribution causes (1) a significant increase in heat exchanger pressure drop and (2) some reduction in heat transfer rate. In order to predict the magnitude of these effects, the nonuniformity is modeled in the literature as one-dimensional or two-dimensional. Some specific results are presented next.

One-Dimensional Flow Nonuniformity.   In this case, the gross flow maldistribution is restricted predominantly to one dimension across the free flow area. A method for predicting the performance of a heat exchanger with this type of nonuniformity is quite straightforward for heat exchangers with simple flow arrangements [100]. The key idea in quantifying the influence of the flow maldistribution on the effectiveness of a heat exchanger involves three interrelated idealizations:

1. The total heat transfer rate in a real heat exchanger with one-dimensional flow maldistribution is equal to the sum of heat transfer rates that would be exchanged in an arbitrary but previously defined number (N) of hypothetical, smaller units, having the same flow arrangement but without the maldistribution.

2. Each of the units defined by idealization 1 obeys the set of standard idealizations of the basic heat exchanger theory listed on p. 17.27.

3. The sum of the heat capacity rates for all smaller units is equal to the total heat capacity rates of the real maldistributed heat exchanger.

With these auxiliary assumptions, the temperature effectiveness of a heat exchanger can be calculated using the following equations after the maldistributed fluid stream is divided into N individual uniform fluid streams:

1. For counterflow and parallelflow arrangements:

$$P_{ms} = \frac{1}{C_{ms}} \sum_{n=1}^{N} C_{ms,n} P_{ms,n} \tag{17.164}$$

2. For crossflow exchanger (mixed-unmixed) with nonuniformity on the unmixed side only:

$$P_{ms} = \frac{1}{C_{ms}} \left[P_{ms,1} C_{ms,1} + \sum_{n=2}^{N} P_{ms,n} C_{ms,n} \prod_{k=1}^{n-1} \left(1 - \frac{P_{ms,k} C_{ms,k}}{C_s} \right) \right] \tag{17.165}$$

where P and C represent temperature effectiveness and heat capacity rate, respectively, and the subscript ms denotes maldistributed fluid stream side.

The method is proposed only for the counterflow, parallelflow and crossflow arrangement with one fluid unmixed throughout. Analytical expressions for temperature effectivenesses are provided in Table 17.6 for the uniform flow case and are used for individual N hypothetical units. The heat capacity rate of the maldistributed fluid in the nth subheat exchanger, as in a counterflow arrangement, is given by

$$C_{ms,n} = \left(\frac{V_n}{V_m} \right)_{ms} \left(\frac{A_{o,n}}{A_o} \right)_{ms} C_{ms} \tag{17.166}$$

where V_m represents the mean flow velocity, A_o is the minimum free flow area for the whole exchanger, and the subscript n represents the quantities for the nth exchanger. The heat capacity rate for other fluid in the nth heat exchanger can be calculated using the same equa-

tion, Eq. 17.166, but with the velocity ratio equal to 1 (due to uniform flow on that side) and other variables defined for that side of the heat exchanger.

The influence of gross flow maldistribution is shown in Fig. 17.64 for a balanced ($C^* = 1$) counterflow heat exchanger in terms of the performance (effectiveness) deterioration factor, $\Delta \varepsilon^*$. It can be seen that, for a particular value of V_{max}/V_m and given NTU, the greatest reduction in the heat exchanger effectiveness occurs when the velocity function is a two-step function over the flow area. The effect of flow maldistribution increases with NTU. Note that the reduction in the temperature effectiveness obtained using Eqs. 17.164 and 17.165 is valid regardless of whether the maldistributed fluid is the hot, cold, C_{max}, or C_{min} fluid.

Tubeside maldistribution in a counterflow shell-and-tube heat exchanger studied in [132] led to the following major conclusions:

- For $C_s/C_t = 0.1$, the performance loss is negligible for large flow nonuniformities for NTU < 2.

- For $C_s/C_t > 1$, a loss can be noticed but diminishes for NTU > 2.

- $C_s/C_t = 1$ is the worst case at large NTUs (NTUs based on the shell fluid heat capacity rate).

Fleming [133] and Chowdhury and Sarangi [134] have studied various models of flow maldistribution on the tube side of a counterflow shell-and-tube heat exchanger. It is concluded that high NTU heat exchangers are more susceptible to maldistribution effects. According to Mueller [135], the well-baffled 1-1 counterflow shell-and-tube heat exchanger (tube side nonuniform, shell side mixed) is affected the least by flow maldistribution. Shell-and-tube heat exchangers that do not have mixing of the uniform fluid (tube side nonuniform, shell side unmixed; or tube side uniform, shell side nonuniform in crossflow) are affected more by flow maldistribution. According to Ref. 136, the radial flow variations of the mismatched air side and gas side reduce the regenerator effectiveness significantly.

Two-Dimensional Flow Nonuniformity. The two-dimensional flow maldistribution has been analyzed only for a crossflow exchanger. In a series of publications as summarized in Refs. 131 and 137, Chiou has studied the effects of flow maldistribution on an unmixed-
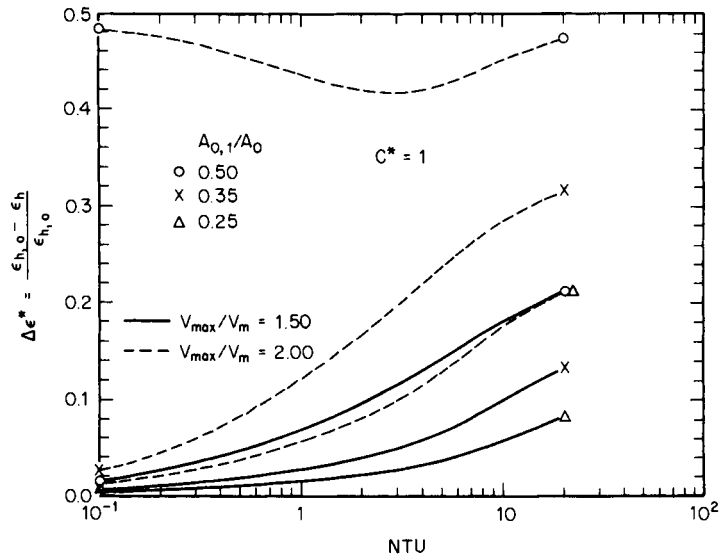

FIGURE 17.64 Reduction in heat exchanger effectiveness caused by gross flow maldistribution [100].

unmixed crossflow single-pass heat exchanger with flow maldistribution on one and both sides. If the flow maldistribution is present only on one side, the following general conclusions were obtained:

- For flow maldistribution on the C_{max} fluid side, the exchanger thermal performance deterioration factor $\Delta\varepsilon^*$ approaches a single value of 0.06 for all $C^* < 1$ if NTU approaches zero. The performance deterioration factor decreases as NTU increases. For a balanced heat exchanger ($C^* = 1$), the exchanger thermal performance deterioration factor continually increases with NTU.

- For flow maldistribution on the C_{min} fluid side, the thermal performance deterioration factor first increases and then decreases as NTU increases.

- If flow nonuniformities are present on both sides, the performance deterioration factor can be either larger or smaller than that for the case where flow nonuniformity is present only on one side, and there are no general guidelines about the expected trends.

A study of the influence of two-dimensional nonuniformities in inlet fluid temperatures [138] indicates that there is a smaller reduction in the exchanger effectiveness for the nonuniform inlet temperature than that for the nonuniform inlet flow. For various nonuniform flow models studied, the inlet nonuniform flow case showed a decrease in the effectiveness of up to 20 percent; whereas, for the nonuniform inlet temperature case, a decrease in the effectiveness of up to 12 percent occurred with even an increase in the effectiveness for some cases of the nonuniform inlet temperature.

Passage-to-Passage Flow Maldistribution.   Compact heat exchangers are highly susceptible to passage-to-passage flow maldistribution. Neighboring passages are never geometrically identical because of manufacturing tolerances. It is especially difficult to control precisely the passage size when small dimensions are involved (e.g., a rotary regenerator with $D_h = 0.5$ mm or 0.020 in). Since differently sized and shaped passages exhibit different flow resistances and the flow seeks a path of least resistance, a nonuniform flow through the matrix results. This phenomena usually causes a slight reduction in pressure drop, while the reduction in heat transfer rate may be significant. The influence is of particular importance for continuous flow passages at low Re numbers.

A theoretical analysis for passage-to-passage flow maldistribution was conducted for the so-called plate-spacing and fin-spacing-type nonuniformities influenced by manufacturing tolerances. In the analysis, the actual nonuniform surface is idealized as containing an equal number of large and small passages relative to the nominal passage dimensions. The models include: (a) the two-passage model [139], (b) the three-passage model, and (c) the N-passage model [140]. Both triangular and rectangular passage cross sections were studied. The influence of the fin curvature was studied in Ref. 141.

In the N-passage model, there are N differently sized passages of the same basic shape, either rectangular or triangular. In Fig. 17.65a, a reduction in NTU for rectangular passages is shown when 50 percent of the flow passages are large ($c_2 > c_r$) and 50 percent of the passages are small ($c_1 < c_r$) compared to the nominal passages. The results are presented for the passages having a nominal aspect ratio α_c^* of 1, 0.5, 0.25, and 0.125 for the Ⓗ and Ⓣ boundary conditions and for a reference NTU of 5.0. Here, a percentage loss in NTU and the channel deviation parameter δ_c are defined as

$$\text{NTU}^*_{cost} = \left(1 - \frac{\text{NTU}_e}{\text{NTU}_r}\right) \times 100 \qquad (17.167)$$

$$\delta_c = 1 - \frac{c_1}{c_r} \qquad (17.168)$$

where NTU_e is the effective NTU when a two-passage model passage-to-passage nonuniformity is present, and NTU_r is the reference or nominal NTU. It can be seen from Fig.

(a)

(b)
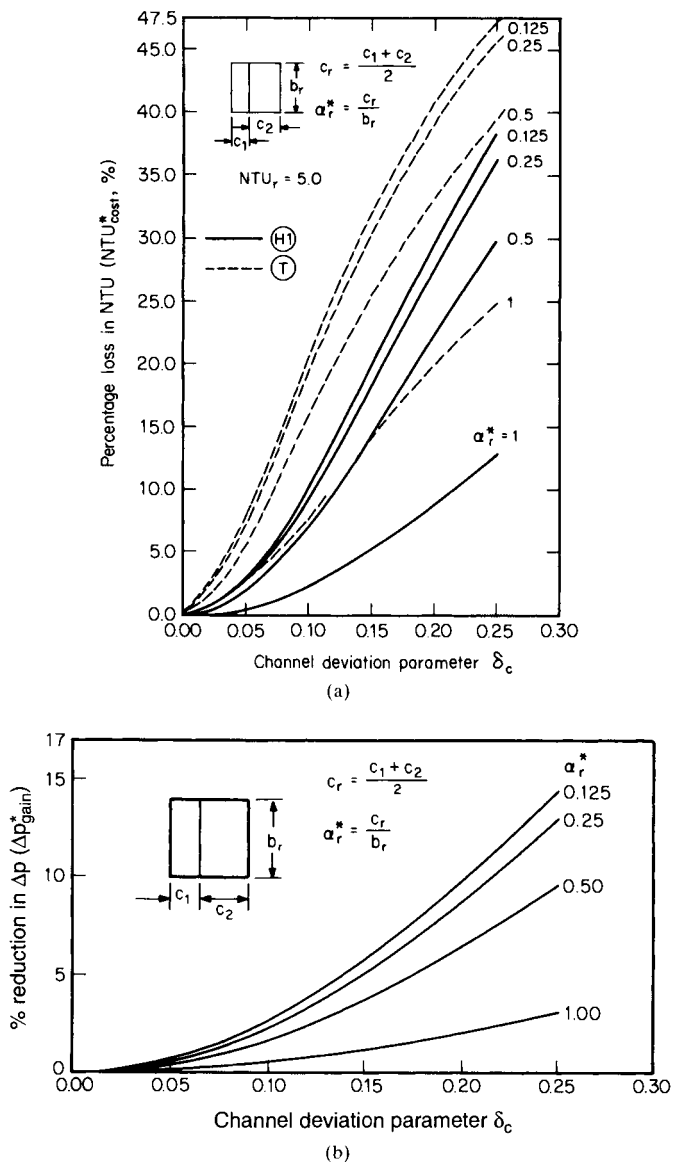
FIGURE 17.65   (a) Percentage loss in NTU as a function of δ_c, α_r^*, and thermal boundary conditions for two-passage nonuniformities in rectangular passages. (b) Percentage reduction in Δp as a function of δ_c and α_r^* for two-passage nonuniformities in rectangular passages.

17.65a that a 10 percent channel deviation (which is common for a highly compact surface) results in a 10 and 21 percent reduction in NTU_{H1} and NTU_T, respectively, for $\alpha_r^* = 0.125$ and $NTU_r = 5.0$. In contrast, a gain in the pressure drop due to the passage-to-passage nonuniformity is only 2.5 percent for $\delta_c = 0.10$ and $\alpha_r^* = 0.125$, as found from Fig. 17.65b. Here, Δp_{gain}^* (reduction in Δp) is defined as:

$$\Delta p^*_{\text{gain}} = \left(1 - \frac{\Delta p_{\text{actual}}}{\Delta p_{\text{nominal}}}\right) \times 100 \qquad (17.169)$$

The results of Figs. 17.65a and b are also applicable to an N-passage model in which there are N differently sized passages in a normal distribution about the nominal passage size. The channel deviation parameter needs to be modified for this case to

$$\delta_c = \left[\sum_{i=1}^{N} \chi_i \left(1 - \frac{c_i}{c_r}\right)^2\right]^{1/2} \qquad (17.170)$$

Here, χ_i is the fractional distribution of the ith shaped passage. For $N = 2$ and $\chi_i = 0.5$, Eq. 17.170 reduces to Eq. 17.168.

The following observations may be made from Fig. 17.65a and additional results presented in [140]: (1) The loss in NTU is more significant for the Ⓣ boundary condition than for the Ⓗ boundary condition. (2) The loss in NTU increases with higher nominal NTU. (3) The loss in NTU is much more significant compared to the gain in Δp at a given δ_c. (4) The deterioration in performance is the highest for the two-passage model compared to the N-passage model with $N > 2$ for the same value of c_{max}/c_r.

Results similar to those in Fig. 17.65a and b are summarized in Fig. 17.66 for the N-passage model of nonuniformity associated with equilateral triangular passages. In this case, the definition of the channel deviation parameter δ_c is modified to

$$\delta_c = \left[\sum_{i=1}^{N} \chi_i \left(1 - \frac{r_{h,i}}{r_{h,r}}\right)^2\right]^{1/2} \qquad (17.171)$$

Manifold Induced Flow Maldistribution. Manifolds can be classified as two basic types: simple dividing flow and combining flow. When interconnected by lateral branches, these manifolds result into the parallel and reverse-flow systems, as shown in Fig. 17.67a and b; these were investigated by Bajura and Jones [142] and Datta and Majumdar [143]. A few general conclusions from these studies are as follows:

- To minimize flow maldistribution, one should limit to less than unity the ratio of flow area of lateral branches (exchanger core) to flow area of the inlet header (area of pipe before lateral branches).

- A reverse-flow manifold system provides more uniform flow distribution than a parallel-flow manifold system.

- In a parallel-flow manifold system, the maximum flow occurs through the last port and, in the reverse-flow manifold system, the first port.

- The flow area of a combining-flow header should be larger than that for the dividing-flow header for a more uniform flow distribution through the core in the absence of heat transfer within the core. If there is heat transfer in lateral branches (core), the flow areas should be adjusted first for the density change, and then the flow area of the combining header should be made larger than that calculated previously.

- Flow reversal is more likely to occur in parallel-flow systems that are subject to poor flow distribution.

Flow Maldistribution Induced by Operating Conditions

Operating conditions (temperature differences, number of phases present, etc.) inevitably influence thermophysical properties (viscosity, density, quality, onset of oscillations) of the flowing fluids, which, in turn, may cause various flow maldistributions, both steady and transient in nature.
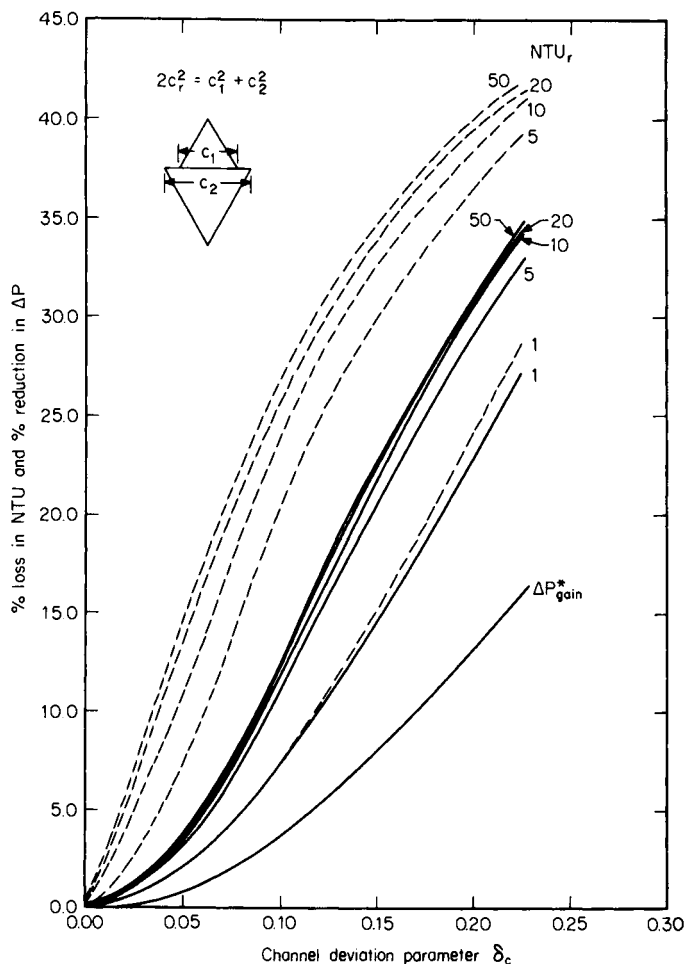
FIGURE 17.66 Percentage loss in NTU and percentage reduction in Δp as functions of δ_c for N-passage nonuniformities in equilateral triangular passages.

Viscosity-Induced Flow Maldistribution. Viscosity-induced flow instability and maldistribution are results of large changes in fluid viscosity within the exchanger as a result of different heat transfer rates in different tubes (flow passages). The possibility for an onset of an instability phenomenon is present whenever one or more fluids are liquids and the viscous liquid is cooled. Flow maldistribution and flow instability are more likely in laminar flow ($\Delta p \propto \mu$) as compared to the turbulent flow ($\Delta p \propto \mu^{0.2}$). Mueller [144] has proposed a procedure for determining the pressure drop or mass flow rate (in a single-tube laminar flow cooler) above which the possibility of flow maldistribution that produces flow instability within a multitubular heat exchanger is eliminated. Putnam and Rohsenow [145] investigated the flow instability phenomenon that occurs in noninterconnected parallel passages of laminar flow heat exchangers.

If a viscous liquid stream is cooled, the viscosity of the liquid may either vary along the flow path influenced by the local bulk fluid temperature $\mu(T)$, or it may stay invariant, defined by the constant wall temperature $\mu_w(T_w)$. The total pressure drop between the inlet
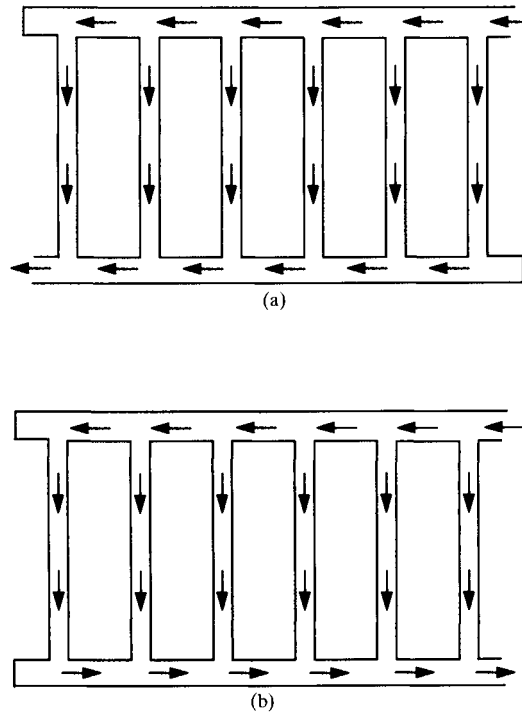
FIGURE 17.67   Manifold systems: (*a*) parallel flow, (*b*) reverse flow.

and outlet of the flow passage could be approximated as a sum of the two terms that are based on the two viscosity regions defined by an axial location x below which μ is dependent on T and beyond which μ is dependent only on the wall temperature. Assume that one can define an average viscosity μ_m such that, when used in the standard pressure drop equation, gives the true pressure drop for the tube section between the tube inlet and the location x. From x to the tube exit $(x = L)$, the viscosity is μ_w. The pressure drop in the second zone should be calculated using viscosity μ_w. The total pressure drop is equal to the sum of the two above mentioned pressure drops. It can be shown [144] that the pressure drop calculated in such a manner behaves as shown in Fig. 17.68 as a function of the flow rate. The analysis is based on: (1) fully developed laminar flow in the tube, (2) the viscosity, which is the only fluid property that can vary along the flow path, (3) the only frictional pressure drop contribution significant, and (4) the wall temperature, which is constant and lower than the fluid inlet temperature. There will be no flow-maldistribution-induced instability in a multitubular cooler if the mass flow rate per tube, assuming uniform distribution $\dot{m}_m$ is greater than $\dot{m}_{min}$ in Fig. 17.68.

Mueller [144] proposed the following procedure to determine the maximum pressure drop, Δp_{max}, above which the flow-maldistribution-induced instability would not be possible. The case considered is for a viscous liquid of a known inlet temperature being cooled as it flows through the length of a tube of known constant temperature T_w.

1. From viscosity data, determine the slope m of curve $\ln (\mu)$ versus $1/T$ where T is temperature on the absolute temperature scale.

2. With known m and the inlet (μ_i) and wall (μ_w) viscosities, determine the average viscosity (μ_m) using Fig. 17.69. This figure is based on the assumption that the fluid reaches the wall
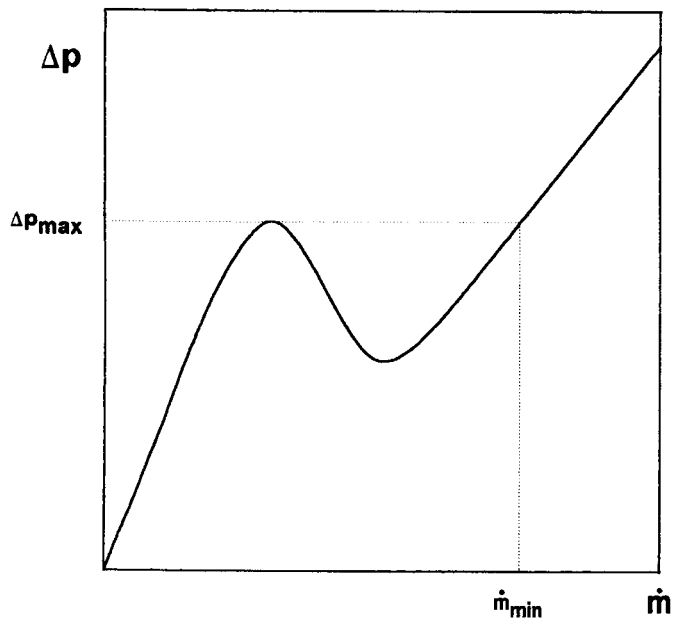
FIGURE 17.68   Pressure drop versus mass flow rate for a single flow passage in laminar liquid flow cooling [144].
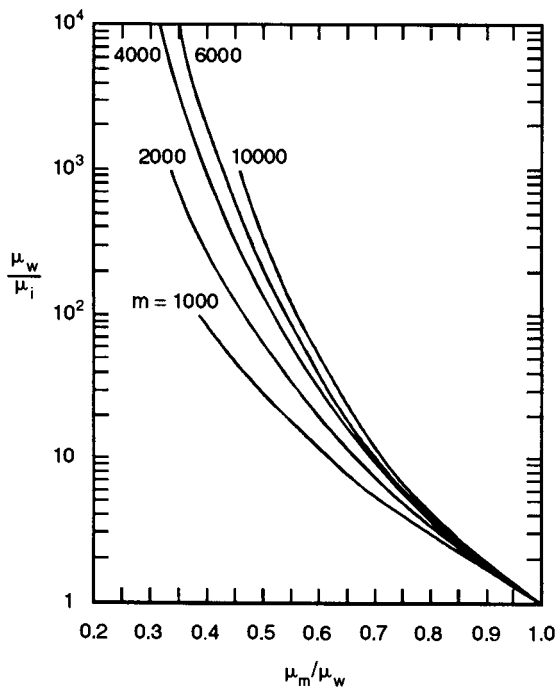
FIGURE 17.69   Viscosity ratio chart for various slopes m of $[\mu = Be^{m/T}]$ [144].

temperature within the tube. If the fluid exit temperature is still larger than the wall temperature, the average viscosity should be modified. The details are provided in Ref. 144.

3. With these viscosities, determine x from

$$x = \frac{L/2}{1 - (\mu_m/\mu_w)} \tag{17.172}$$

4. Calculate the mass flow rate from

$$\text{Gz} = \frac{kL}{\dot{m}c_p} \approx 0.4 \tag{17.173}$$

5. Calculate the maximum pressure drop from

$$\Delta p_{\max} = \frac{128}{\pi g_c \rho D_h^4} \dot{m}\mu_w \left[x + \frac{x^2}{L}\left(\frac{\mu_m}{\mu_w} - 1\right) \right] \tag{17.174}$$

If the pressure drop is found to be less than calculated by Eq. 17.174, the fluid flow length should be increased (either increasing the duct length or considering a multipass design) to eliminate the flow instability.

The preceding method can be used to calculate the pressure drop magnitudes for various tubes in a multitube unit and consequently to visualize the eventual flow maldistribution instability. For further details regarding the procedure, refer to Ref. 144.

Flow Maldistribution in Heat Exchangers with Phase Change. Two-phase flow maldistribution may be caused and/or influenced by phase separation, oscillating flows, variable pressure drops (density-wave instability), flow reversals, and other flow instabilities. For a review of pertinent literature, refer to Ref. 131.

Flow maldistribution problems in condensers may be severe and should not be underestimated [146]. Most problems with flow maldistribution in condensers, though, can be resolved through good venting and condensate drainage [2].

The flow maldistribution problem in evaporators is most severe when the major part of the pressure drop occurs in the two-phase heated region and cannot be prevented in some cases (reboilers and evaporators). However, in most heat exchangers with such problems, the economic penalty for maldistribution is small, and deterioration of the thermal performance is slightly affected [115]. The flow instabilities can be controlled by restricting the liquid circulation [2]. Falling film evaporators are particularly prone to flow maldistribution. This effect can be reduced through design modifications (the top tube plate must be exactly horizontal, addition of inserts into the top of each tube must be secured, etc.) [120].

Mitigation of Flow Maldistribution

Flow maldistribution in a heat exchanger may be reduced through modifications in the existing design or taken into account by incorporating its effect in the design methodology. Most gross flow maldistributions may result in minor performance reduction (smaller than 5 percent for NTU < 4 [131] in shell-and-tube heat exchangers). At high NTUs (NTU > 10), the performance loss may be substantially larger. The passage-to-passage maldistribution may result in a significant reduction in heat transfer performance, particularly for laminar flow exchangers.

Any action in mitigating flow maldistribution must be preceded by an identification of possible reasons that may cause the performance deterioration and/or may affect mechanical characteristics of the heat exchanger. The possible reasons that affect the performance are [131, 147]: (1) deterioration in the heat exchanger effectiveness and pressure drop characteristics, (2) fluid freezing, as in viscous flow coolers, (3) fluid deterioration, (4) enhanced fouling, and (5) mechanical and tube vibration problems (flow-induced vibrations as a consequence of flow instabilities, wear, fretting, erosion, corrosion, and mechanical failure).

No generalized recommendations can be made for mitigating negative consequences of flow maldistribution. Most of the problems must be solved by intelligent designs and on an individual basis. A few broad guidelines regarding various heat exchanger types follow.

In shell-and-tube heat exchangers, inlet axial nozzles on the shell side may induce gross flow maldistribution. Placing an impingement perforated baffle about halfway to the tubesheet will break up the inlet jet stream [131]. It is speculated also that a radial nozzle may eliminate jet impingement. The shell inlet and exit baffle spaces are regions prone to flow maldistribution. An appropriate design of the baffle geometry (for example the use of double segmental or disk-and-doughnut baffles) may reduce this maldistribution.

Flow maldistribution is often present in phase-change applications. A common method to reduce the flow maldistribution in condensers is to use a vent condenser or increase the number of tubeside passes [131]. To minimize the negative influence of flow maldistribution, one should reduce the pressure drop downstream of the vaporizer tube bundle and throttle the inlet stream to prevent oscillations. Also, for reboilers and vaporizers, the best solution is to use a vertical exchanger with the two-phase fluid to be vaporized entering on the shell side through annular distributor [147]. Rod-type baffles should be used whenever appropriate. Prevention of maldistribution in air-cooled condensers includes the following measures [115]: (1) selective throttling of the vapor flow to each tube row, (2) use of a downstream condenser to eliminate the effects of inert gas blanketing by having a definite stream flow through each tube row, and (3) matching the heat transfer characteristics of each tube row so as to produce uniform heat transfer rate through each tube row.

FOULING AND CORROSION

Fouling and corrosion, both operation-induced effects, should be considered for the design of a new heat exchanger as well as subsequent exchanger operation. Fouling represents an undesirable accumulation of deposits on heat transfer surface. Fouling is a consequence of various mass, momentum, and transfer phenomena involved with heat exchanger operation. The manifestations of these phenomena, though, are more or less similar. Fouling results in a reduction in thermal performance and an increase in pressure drop in a heat exchanger. Corrosion represents mechanical deterioration of construction materials of a heat exchanger under the aggressive influence of flowing fluid and the environment in contact with the heat exchanger material. In addition to corrosion, some other mechanically induced phenomena are important for heat exchanger design and operation, such as fretting (corrosion occurring at contact areas between metals under load subjected to vibration and slip) and fatigue (a tendency of a metal to fracture under cyclic stressing).

In order to understand the influence of fouling on compact heat exchanger performance, the following equations for h and Δp are derived from the equations presented earlier for fully developed gas flow in a circular or noncircular tube:

$$h = \begin{cases} \dfrac{\mathrm{Nu}\, k}{D_h} \text{ with Nu} = \text{constant} & \text{for laminar flow} \\[2em] \dfrac{k}{D_h}\left[0.022\left(\dfrac{4L\dot{m}}{A\mu}\right)^{0.8} \mathrm{Pr}^{0.5}\right] & \text{for turbulent flow} \end{cases}$$
(17.175)

and

$$\Delta p = \begin{cases} \dfrac{1}{D_h^3}\left[\dfrac{1}{2g_c}\dfrac{\mu}{\rho}\dfrac{16L^2}{A}\dot{m}(f\,\mathrm{Re})\right] & \text{for laminar flow} \\[2em] \dfrac{1}{D_h^3}\left[\dfrac{0.046}{2g_c}\dfrac{\mu^{0.2}}{\rho}\dfrac{(4L)^{2.8}}{A^{1.8}}\dot{m}^{1.8}\right] & \text{for turbulent flow} \end{cases}$$
(17.176)

For constant $\dot{m}$, L, A, and fluid properties, from Eqs. 17.175 and 17.176,

$$h \propto \frac{1}{D_h} \qquad \Delta p \propto \frac{1}{D_h^3} \qquad\qquad (17.177)$$

Since $A = \pi D_h L$, Δp is proportional to D_h^{-4} and $D_h^{-4.8}$ in laminar and turbulent flows, respectively. As fouling will reduce the flow area A_o and hence the passage D_h, it will increase h to some extent, but the pressure drop is increased more strongly. The thermal resistance of the fouling film will generally result in an overall reduction in heat transfer in spite of a slight increase in h.

The ratio of pressure drops of fouled (Δp_F) and clean exchanger (Δp_C) for constant mass flow rate is given by [151]:

$$\frac{\Delta p_F}{\Delta p_C} = \frac{f_F}{f_C}\left(\frac{D_{h,C}}{D_{h,F}}\right)\left(\frac{u_{m,F}}{u_{m,C}}\right)^2 = \frac{f_F}{f_C}\left(\frac{D_{h,C}}{D_{h,F}}\right)^5 \qquad\qquad (17.178)$$

If we consider that fouling does not affect friction factor (i.e., the friction factor under clean conditions f_C is equal to the friction factor under fouled conditions f_F) and the reduction in the tube inside diameter due to fouling is only 10 to 20 percent, the resultant pressure drop increase will be approximately 60 percent and 250 percent, respectively, according to Eq. 17.178, regardless of whether the fluid is liquid or gas (note that $h \propto 1/D_h$ and $\Delta p \propto 1/D_h^5$ for fully developed turbulent flow and constant mass flow rate). At the same time, the slight increase in h will not increase the overall heat transfer coefficient because of the additional thermal resistance of the fouling layers.

Fouling in liquids and two-phase flows has a significant detrimental effect on heat transfer with some increase in fluid pumping power. In contrast, fouling in gases reduces heat transfer somewhat (5–10 percent in general) but increases pressure drop and fluid pumping power significantly (up to several hundred percent). Thus, although the effect of fouling on the pressure drop is usually neglected with liquid flows, it can be significant for heat exchangers with gas flows.

Fouling

General Considerations. The importance of fouling phenomena stems from the fact that the fouling deposits increase thermal resistance to heat flow. According to the basic theory, the heat transfer rate in the exchanger depends on the sum of thermal resistances between the two fluids, Eq. 17.5. Fouling on one or both fluid sides adds the thermal resistance $\mathbf{R}_s$ to the overall thermal resistance and, in turn, reduces the heat transfer rate (Eq. 17.4). Simultaneously, hydraulic resistance increases because of a decrease in the free flow area. Consequently, the pressure drops and the pumping powers increase (Eq. 17.63).

Fouling is an extremely complex phenomena characterized by a combined heat, mass, and momentum transfer under transient conditions. Fouling is affected by a large number of variables related to heat exchanger surfaces, operating conditions, and fluids. In spite of the complexity of the fouling process, a general practice is to include the effect of fouling on the exchanger thermal performance by an empirical fouling factor $r_s = 1/h_s$. The problem, though, is that this straightforward procedure will not (and cannot) reflect a real transient nature of the fouling process. Current practice is to use fouling factors from TEMA [5] or modified recent data by Chenoweth [148]. See Table 17.38. However, probably a better approach is to eliminate the fouling factors altogether in the design of an exchanger and thus avoid overdesign [149]. This is because overdesign reduces the flow velocity and promotes more fouling.

Types of Fouling Mechanisms. The nature of fouling phenomena greatly depends on the fluids involved as well as on the various parameters that control the heat transfer phenomena and the fouling process itself. There are six types of liquid-side fouling mechanisms: (1) precipitation (or crystallization) fouling, (2) particulate fouling, (3) chemical reaction fouling, (4)

TABLE 17.38   Fouling Resistances of Various Liquid Streams (Adapted from Ref. 148)

Fluid	Fouling resistance $r_s \times 10^4$ (m²K/W)	Comments
Liquid water streams		
Seawater	1.75–3.5	$T_{out,max} = 43°C$
Brackish water	3.5–5.3	$T_{out,max} = 43°C$
Treated cooling tower water	1.75–3.5	$T_{out,max} = 49°C$
Artificial spray pond	1.75–3.5	$T_{out,max} = 49°C$
Closed loop treated water	1.75	
River water	3.5–5.3	*Operating conditions for all water streams:*
Engine jacket water	1.75	For tubeside flow, the velocity for the
Distilled water or closed cycle		streams is at least 1.2 m/s for tubes of
condensate	0.9–1.75	nonferrous alloy and 1.8 m/s for ferrous
Treated boiler feedwater	0.9	alloys. For shellside fluid, the velocity is
Boiler blowdown water	3.5–5.3	at least 0.6 m/s. Heat transfer surface
		temperatures are below 71°C.
Industrial liquid streams		
No. 2 fuel oil	3.5	
No. 6 fuel oil	0.9	
Transformer oil, engine lube oil	1.75	
Refrigerants, hydraulic fluid, ammonia	1.75	
Industrial organic HT fluids	1.75–3.5	
Ammonia (oil bearing)	5.3	
Methanol, ethanol, ethylene glycol		
solutions	3.5	
Process liquid streams		
MEA and DEA solutions	3.5	
DEG and TEG solutions	3.5	
Stable side draw and bottom products	1.75–3.5	
Caustic solutions	3.5	
Crude oil refinery streams:		
temperature, °C		
120	3.5–7	Assumes that the crude oil is desalted
120 to 180	5.3–7	at approximately 120°C and the tubeside
180 to 230	7–9	velocity of the stream is 1.25 m/s or
>230	9–10.5	greater.
Petroleum streams		
Lean oil	3.5	
Rich oil	1.75–3.5	
Natural gasoline, liquefied		
petroleum gases	1.75–3.5	
Crude and vacuum unit gases and vapors		The values listed in this table are typical
Atmospheric tower overhead		values that reflect current trends to longer
vapors, naphthas	1.7	periods before cleaning. It is recognized
Vacuum overhead vapors	3.5	that fouling resistances are not known
Crude and vacuum liquids		with precision. Actual applications may
Gasoline	3.5	require substantially different values.
Naphtha, light distillates,		
kerosine, light gas oil	3.5–5.3	
Heavy gas oil	5.3–9	
Heavy fuel oil	5.3–12.3	
Vacuum tower bottoms	17.6	
Atmospheric tower bottoms	12.3	

TABLE 17.38   Fouling Resistances of Various Liquid Streams (Adapted from Ref. 148) (*Continued*)

Fluid	Fouling resistance $r_s \times 10^4$ (m^{2}K/W)	Comments
Cracking and coking unit streams		
Overhead vapors, light liquid products	3.5	
Light cycle oil	3.5–5.3	
Heavy cycle oil, light coker gas oil	5.3–7	
Heavy coker gas oil	7–9	
Bottoms slurry oil	5.3	
Catalytic reforming, hydrocracking, and		
hydrodesulfurization streams		
Reformer charge, reformer effluent	2.6	Depending on charge characteristics and
Hydrocharger charge and effluent	3.5	storage history, charge fouling resistance
Recycle gas, liquid product over 50°C	1.75	may be many times larger.
Liquid product 30°C to 50°C (API)	3.5	
Light ends processing streams		
Overhead vapors, gases, liquid products	1.75	
Absorption oils, reboiler streams	3.5–5.3	
Alkylation trace acid streams	3.5	
Visbreaker		
Overhead vapor	5.3	
Visbreaker bottoms	17.5	
Naphtha hydrotreater		
Feed	5.3	
Effluent, naphthas	3.5	
Overhead vapor	2.6	
Catalytic hydrodesulfurizer		
Charge	7–9	
Effluent, HT separator overhead,		
liquid products	3.5	
Stripper charge	5.3	
HF alky unit		
Alkylate, depropanizer bottoms	5.3	
Main fractional overhead, and feed	5.3	
Other process streams	3.5	
Industrial gas or vapor streams		
Steam (non-oil-bearing)	9	The original data for fouling resistance are
Exhaust steam (oil-bearing)	2.6–3.5	given in U.S. Customary units with single-
Refrigerant (oil-bearing)	3.5	digit accuracy. The conversion into SI
Compressed air	1.75	units has as a consequence that the
Ammonia	1.75	apparent accuracy seems greater than the
Carbon dioxide	3.5	intent of the original data.
Coal flue gas	17.5	
Natural gas flue gas	9	
Chemical process streams		
Acid gas	3.5–5.3	
Solvent vapor	1.75	
Stable overhead products	1.75	
Natural gas processing streams		
Natural gas	1.75–3.5	
Overheat products	1.75–3.5	

corrosion fouling, (5) biological fouling, and (6) freezing (solidification) fouling. Only biological fouling does not occur in gas-side fouling, since there are no nutrients in the gas flows. In reality, more than one fouling mechanism is present in many applications, and the synergistic effect of these mechanisms makes the fouling even worse than predicted or expected.

In precipitation fouling, the dominant mechanism is the precipitation of dissolved substances on the heat transfer surface. The deposition of solids suspended in the fluid onto the heat transfer surface is a major phenomenon involved with particulate fouling. If the settling occurs due to gravity, the resulting particulate fouling is called *sedimentation fouling*. Chemical reaction fouling is a consequence of deposition of material produced by chemical reactions in which the heat transfer surface material is *not* a reactant. Corrosion of the heat transfer surface may produce products that foul the surface or promote the attachment of other foulants. Biological fouling results from the deposition, attachment, and growth of macro- or microorganisms to the heat transfer surface. Finally, freezing fouling is due to the freezing of a liquid or some of its constituents or the deposition of solids on a subcooled heat transfer surface as a consequence of liquid-solid or gas-solid phase change in a gas stream.

It is obvious that one cannot talk about a single, unified theory to model the fouling process. However, it is possible to extract a few parameter sets that would most probably control any fouling process. These are: (1) the physical and chemical properties of a fluid, (2) fluid velocity, (3) fluid and heat transfer surface temperatures, (4) heat transfer surface properties, and (5) the geometry of the fluid flow passage. For a given fluid-surface combination, the two most important design variables are the fluid flow velocity and heat transfer surface temperature. In general, higher-flow velocities may cause less foulant deposition and/or more pronounced deposit erosion, but, at the same time, it may accelerate the corrosion of the surface by removing the heat transfer surface material. Higher surface temperatures promote chemical reaction, corrosion, crystal formation (with inverse solubility salts), and polymerization, but they also reduce biofouling, prevent freezing, and precipitation of normal solubility salts. Consequently, it is frequently recommended that the surface temperature be maintained low.

Before considering any technique for minimizing fouling, the heat exchanger should be designed to minimize or eliminate fouling. For example, direct-contact heat exchangers are very convenient for heavily fouling liquids. In fluidized bed heat exchangers, the bed motion scours away the fouling deposit. Plate-and-frame heat exchangers can be easily disassembled for cleaning. Compact heat exchangers are not suitable for fouling service unless chemical cleaning or thermal baking is possible. When designing a shell-and-tube heat exchanger, the following are important in reducing or cleaning fouling. The heavy fluid should be kept on the tube side for cleanability. Horizontal heat exchangers are easier to clean than vertical ones. The geometric features of fluid flow passages should reduce to minimum stagnant and low-velocity shellside regions. On the shell side, it is easier to mechanically clean square or rotated square tube layouts with an increased tube pitch than the other types of tube layouts.

Single-Phase Liquid-Side Fouling.   Single-phase liquid-side fouling is most frequently caused by: (1) precipitation of minerals from the flowing liquid, (2) deposition of various particles, (3) biological fouling, and (4) corrosion fouling. Other fouling mechanisms are also present. More important, though, is the synergistic effect of more than one fouling mechanism present. The qualitative effects of some of the operating variables on these fouling mechanisms are shown in Table 17.39 [2].

The quantitative effect of fouling on heat transfer can be estimated by utilizing the concept of fouling resistance and calculating the overall heat transfer coefficient (Eq. 17.6) under both fouling and clean conditions. An additional parameter for determining this influence, used frequently in practice, is the so-called cleanliness factor. It is defined as a ratio of an overall heat transfer coefficient determined for fouling conditions and an overall heat transfer coefficient determined for clean (fouling-free) operating conditions. The effect of fouling on pressure drop can be determined by the reduced free flow area due to fouling and the change in the friction factor, if any, due to fouling.

TABLE 17.39 Influence of Operating Variables on Liquid-Side Fouling [2]

Operating variables	Precipitation	Freezing	Particulate	Chemical	Corrosion	Biological
Temperature	↑↓	↓	↑↓ ↔	↑↓	↑↓	↑↓ ↔
Velocity	↓ ↔	↑↓	↓	↓	↑↓ ↔	↑↓
Supersaturation	↑	↑	O	O	O	O
pH	↑	O	↑↓	O	↑↓	↑↓
Impurities	O	↓	O	O	O	O
Concentration	↑	↑	↑	O	O	O
Roughness	↑	↑	↑ ↔	O	↑ ↔	↑
Pressure	↔	↔	O	↑	↑	↑↓
Oxygen	↔	↔	O	↑	↑	↑↓

When the value of an operating variable is increased, it increases (↑), decreases (↓), or has no effect (↔) on the specific fouling mechanism listed. Circles (O) indicate that no influence of these variables has been reported in the literature.

Prevention and Reduction of Liquid-Side Fouling.   Among the most frequently used techniques for reduction of liquid-side fouling is the online utilization of chemical inhibitors/additives. The list of additives includes: (1) dispersants to maintain particles in suspension, (2) various compounds to prevent polymerization and chemical reactions, (3) corrosion inhibitors or passivators to minimize corrosion, (4) chlorine and other biocide/germicides to prevent biofouling, and (5) softeners, acids, and poliphosphates to prevent crystallization. Finally, an efficient mechanical removal of particles can be performed by filtration. An extensive review of fouling control measures is provided in Ref. 150.

Heat transfer surface cleaning techniques can be applied either online or off-line. Online techniques (usually used for tubeside applications) include various mechanical techniques (flow-driven or power-driven rotating brushes, acoustic/mechanical vibration, chemical feeds, flow reversal, etc.). Off-line techniques include chemical cleaning, mechanical cleaning by circulating particulate slurry, and thermal baking to melt frost/ice deposits.

Single-Phase Gas-Side Fouling.   Gas-side fouling may be caused by precipitation (scaling), particulate deposition, corrosion, chemical reaction, and freezing. Formation of hard scale from the gas flow occurs if the sufficiently low temperature of the heat transfer surface forces salt compounds to solidity. Acid vapors, high-temperature removal of oxide layer by molten ash, or salty air at low temperatures may promote corrosion fouling. An example of particulate deposition is accumulation of plant residues. An excess of various chemical substances such as sulfur, vanadium, and sodium initiates various chemical reaction fouling problems. Formation of frost and various cryodeposits are typical examples of freezing fouling on the gas side. An excellent overview of gas-side fouling of heat transfer surfaces is given by Marner [151]. Qualitative effects of some of the operating variables on gas-side fouling mechanisms is presented in Table 17.40 [2].

Control of fouling should be attempted first before any cleaning method is attempted. The fouling control procedure should be preceded by: (1) verification of the existence of fouling, (2) identification of the feature that dominates the foulant accumulation, and (3) characterization of the deposit.

Prevention and Reduction of Gas-Side Fouling.   The standard techniques for reduction and/or prevention of fouling on the gas side are: (1) techniques for removal of potential residues from the gas, (2) additives for the gas side fluid, (3) surface cleaning techniques, and (4) adjusting design up-front to minimize fouling. Details regarding various techniques for gas-side fouling prevention, mitigation, and accommodation are given in Ref. 152.

Fouling Under Phase Change Conditions.   Fouling is common on the water side in a boiler. Large heat fluxes are subsequently reduced, and elevated wall temperatures may cause tube

TABLE 17.40 Influence of Operating Variables on Gas-Side Fouling [2]

Operating variables	Particulate	Freezing	Chemical	Corrosion
Temperature	↑↓	↓	↑	↑↓ ↔
Velocity	↑↓ ↔	↓	↑↓ ↔	↑ ↔
Impurities	O	↓	O	O
Concentration	↑	↑	O	↑
Fuel-air ratio	↑	O	↑	O
Roughness	↑ ↔	O	O	↑ ↔
Oxigen	↔	↔	↑	O
Sulphur	O	O	↑	↑

When the value of an operating variable is increased, it increases (↑), decreases (↓), or has no effect (↔) on the specific fouling mechanism listed. Circles (O) indicate that no influence of these variables has been reported in the literature.

wall rupture. The most frequently used technique for preventing water-side fouling is the water treatment. Strict guidelines are developed for the quality of water [150]. Among the most difficult problems caused by fouling in boilers is the particulate fouling—especially deposition of iron oxide particles and various inorganic salts. In addition, corrosion fouling can be intensified by the presence of oxygen. Various factors that influence fouling in such conditions are: (1) local thermal conditions (heat flux magnitude), (2) concentration of suspended particles, (3) fluid characteristics (velocity, chemical properties), and (4) heat transfer surface characteristics.

The prevention of iron-oxide-induced corrosion can be accomplished by mechanical filtration of iron oxide, by the use of additives (iron oxide dispersants), and by adding inhibitors for corrosion. Standard procedures for reduction of corrosion in boilers include deaeration of the feedwater and the use of additives such as sodium sulfite.

It was reported [95] that fouling on low-finned tubes in reboilers may occur at a reduced rate compared to plain tubes. Also, the use of porous enhancements (porous coatings, high flux tube) demonstrates strong resistance to fouling.

Corrosion

Single-component corrosion types, important for heat exchanger design and operation, are as follows: (1) uniform attack corrosion, (2) galvanic corrosion, (3) pitting corrosion, (4) stress corrosion cracking, (5) erosion corrosion, (6) deposit corrosion, and (7) selective leaching [153].

Uniform corrosion is a form of corrosion caused by a chemical or electrochemical reaction between the metal and the fluid in contact with it over the entire exposed metal surface. It is usually easy to notice corroded areas attacked by uniform corrosion. This type of corrosion can be suppressed by applying adequate inhibitors, coatings, or cathodic protection. *Galvanic corrosion* is caused by an electric potential difference between two electrically dissimilar metals in the system in the presence of an electrolyte (such as water in a heat exchanger). It may occur at tube-to-tubesheet junctions as well as at the tube-to-baffle hole and baffle-to-shell contacts. Reduction of this type of electrochemical corrosion can be accomplished by selecting dissimilar materials to be as close as possible to each other on the galvanic series list for pairs of components in the system. In addition, insulation of dissimilar metals, application of coatings, addition of inhibitors, and installation of a third metal that is anodic to both metals in the galvanic contact may be used to minimize galvanic corrosion. *Pitting corrosion* is a form of localized autocatalytic corrosion due to pitting that results in holes in the metal. Pits caused by pitting corrosion are usually at places where the metal surface has surface deformities and scratches. This corrosion type is difficult to control. Materials that show pitting should not be

used to build heat exchanger components. Adding inhibitors is not always efficient. *Stress corrosion* is a form of corrosion that involves cracks caused by simultaneous presence of the tensile stress and a corrosive medium. Cold working parts and U-bends in shell-and-tube heat exchangers are the locations where corrosion may take place in combination with an existing stress. The best prevention of stress-corrosion cracking is an appropriate selection of material, reduction of tensile stresses in the construction, elimination of the critical environmental components (for example demineralization or degasification), cathodic protection, and addition of inhibitors. *Erosion corrosion* is a form of surface corrosion due to the errosion of the heat transfer surface due to high-velocity fluid with or without particulates (e.g., fluid velocity greater than 2 m/s or 6 ft/sec for water flow over an aluminum surface) and the subsequent corrosion of the exposed surface. The erosion corrosion is more common at the inlet end of a heat exchanger flow passage. The selection of the correct material less prone to erosion and an adequate velocity range for a working fluid may reduce erosion and cavitation effects. For example, stainless steel 316 can sustain three times the water velocity flowing inside tubes compared to steel or cooper. Also, design modifications, coatings, and cathodic protection should be considered. *Deposit corrosion* (also called *crevice corrosion*) is a form of localized physical deterioration of a metal surface in shielded areas (i.e., in stagnant fluid flow regions) often caused by deposits of dirt and corrosion products. Stagnant areas (such as various gaps) may also be attacked by localized corrosion. Fouling and various deposits influence corrosion at shielded areas if the combination of fluid and heat exchanger surface material is inappropriate. The best prevention of this type of corrosion is a design in which the stagnation areas of the fluid flow and sharp corners are reduced to a minimum. Design should be adjusted for complete drainage, and, if possible, welding should be used instead of rolling in tubes in tubesheets. *Selective leaching* is a selective removal of one metal constituent from an alloy by corrosion. Additives to an alloy, such as arsenic or tin, may reduce the onset of the removal of a constituent from the alloy, thus solving the problem with selective leaching.

CONCLUDING REMARKS

The content presented in this chapter shows clearly the diversity and complexity of topics related to heat exchangers. Space limitation, however, has prevented the authors from thoroughly covering many equally important aspects of design and operation of heat exchangers (refer to Fig. 17.53). Let us briefly summarize some of the issues that should attract considerable attention of an engineer and/or researcher but are not discussed in this text.

The mechanical design of a heat exchanger is a very important consideration for trouble-free operation for the design life. Some of the important considerations are the desired structural strength and fatigue characteristics (based on the operating pressures, temperature, corrosiveness, and chemical reaction of fluids with material), proper selection of the materials and the method of bonding of various components, and problems during operation (such as transients, dynamic instability, freezing, and erosion). Also, the design and operational problems should be addressed for the flow distribution devices (headers, tanks, manifolds, nozzles, or inlet-outlet pipes), heat exchanger installation, maintenance (such as cleaning, repair, serviceability, and general inspection), shipping limitations, and so on. Heat exchangers must also comply with the applicable local, state, national, and/or international codes and standards. The details regarding these considerations can be found in Refs. 4, 5, and 154–156.

Manufacturing considerations are at least as important as the desired thermal and mechanical performance. These include the actual manufacturing of the components of a heat exchanger, the processing considerations (putting together assembly/exchanger), the manufacturing equipment (tools, furnaces, machines) and space, the stacking and bonding of exchangers (brazing, soldering, welding, or mechanical expansion), and leak-free mounting (joining) of headers, tanks, manifolds, pipes, and so on. A variety of references are scattered in the literature on this topic [157]. Basic information on brazing can be found in Ref. 158.

Process integration and system synthesis require a skillful manipulation of system components. For example, heat exchanger network synthesis requires the utilization of very specialized methods of analysis [111, 112]. The search for an efficient system operation requires a multidisciplinary approach that will inevitably involve simultaneous utilization of heat transfer theory and thermal and mechanical design skills as well as specific thermodynamic considerations and economic evaluation. The optimal design of a system cannot be achieved without careful thermo-economic considerations at both system and component (i.e., heat exchanger) levels.

The overall total lifecycle cost for a heat exchanger may be categorized as the capital and operating costs. The capital (total installed) cost includes the costs associated with design, materials, manufacturing (machinery, labor, and overhead), testing, shipping, installation, and depreciation. The operating cost consists of the costs associated with fluid pumping power, warranty, insurance, maintenance, repair, cleaning, lost production/downtime due to failure, and energy cost associated with the utility (steam, fuel, water) in conjunction with the exchanger in the network. Costing information is generally proprietary to industry, and very little information is published in the open literature [159].

Operation and exploitation of a heat exchanger, even in situations when the device is not operating in an unsteady mode such as rotary regenerators, should require considerations of transients and corresponding heat exchanger response. Erratic operation, startups and shutdowns, and/or requirements for optimal control of systems (in which heat exchangers represent important components) are some of the reasons why time-dependent behavior should be studied.

The variety of heat exchanger design types emphasized in the text often prevents unification of the analysis methods and design strategies. This text is primarily devoted to the most frequently used heat exchanger types—recuperators and regenerators. Those interested in the details of design and operation of agitated vessels, multifluid heat exchangers, micro heat exchanger applications, or cryogenic and/or various new heat exchangers design introduced by development of new energy sources and/or emerging technologies (such as solar collectors, high temperature applications, and bioengineering) should consult specialized literature.

NOMENCLATURE

Symbols used only once and/or symbols used only within the context of a specific topic are, as a rule, defined in the text, table, and/or figure.

Unless clearly specified, a regenerator in the nomenclature means either a rotary or a fixed-matrix regenerator.

Symbol, Definition, Units

A	Total heat transfer surface area (both primary and secondary, if any) on one side of a direct transfer type exchanger, total heat transfer surface area of all matrices of a regenerator, m^2, ft^2
A_{cross}	Cross-sectional area of the channel, m^2, ft^2
A_{ba}	Bypass area of one baffle, m^2, ft^2
A_c	Total heat transfer area (both primary and secondary, if any) on the cold side of an exchanger, m^2, ft^2
A_f	Fin or extended surface area on one side of the exchanger, m^2, ft^2
A_{fr}	Frontal or face area on one side of an exchanger, m^2, ft^2
A_h	Total heat transfer surface area (both primary and secondary, if any) on the hot side of an exchanger, m^2, ft^2

A_k	Total wall cross-sectional area for longitudinal conduction (subscripts c, h, and t denote cold side, hot side, and total (hot + cold) for a regenerator), m^2, ft^2
A_{mb}	Minimum flow area at centerline of one baffle, m^2, ft^2
A_o	Minimum free flow (or open) area on one side of an exchanger, m^2, ft^2
A_p	Primary surface area on one side of an exchanger, m^2, ft^2
A_{sb}	Shell-to-baffle leakage area, m^2, ft^2
A_{tb}	Tube-to-baffle leakage area, m^2, ft^2
A_w	Total wall area for heat conduction from the hot fluid to the cold fluid, or total wall area for transverse heat conduction (in the matrix wall thickness direction), m^2, ft^2
A_{wg}	Gross window area, m^2, ft^2
A_{wt}	Window area occupied by tubes, m^2, ft^2
a_i	Sound frequency parameter, dimensionless
B_c	Baffle cut, percent of diameter, dimensionless
Bo	Boiling number (defined in Table 17.26), dimensionless
Bi	Biot number, $Bi = (h\delta_f/2k_f)$ dimensionless
b	Plate spacing, distance between two plates (fin height) in a plate-fin heat exchanger, m, ft
C	Flow stream heat capacity rate with a subscript c or h, $\dot{m}c_p$, W/°C, Btu/hr °F
C^*	Heat capacity rate ratio, C_{min}/C_{max}, dimensionless
C_m	Added mass coefficient (Eq. 17.156 and Fig. 17.60), dimensionless
C_{max}	Maximum of C_c and C_h, W/°C, Btu/hr °F
C_{min}	Minimum of C_c and C_h, W/°C, Btu/hr °F
C_{ms}	Heat capacity rate of the maldistributed stream, W/°C, Btu/hr °F
Co	Convection number (defined in Table 17.26), dimensionless
C_s	Heat capacity rate of the fluid stream that is not maldistributed, W/°C, Btu/hr °F
C_u	U-tube natural frequency constant (Eq. 17.160 and Fig. 17.63), dimensionless
C_r	Heat capacity rate of a regenerator, $M_w c_w \mathbf{N}$ or $M_w c_w / \mathcal{P}_t$, for the hot and cold side matrix heat capacity rates, $C_{r,h}$ and $C_{r,c}$, W/°C, Btu/hr °F
C_r^*	Total matrix heat capacity rate ratio, C_r/C_{min}, $C_{r,h}^* = C_{r,h}/C_h$, $C_{r,c}^* = C_{r,c}/C_c$, dimensionless
$\mathbf{C}$	Coefficient (Eq. 17.155 and Table 17.35), dimensionless
c_{eff}	Effective speed of sound (defined by Eq. 17.162), m/s, ft/s
c_p	Specific heat of fluid at constant pressure, J/kg °C,[†] Btu/lbm °F
c_w	Specific heat of wall material, J/kg °C, Btu/lbm °F
c_o	Speed of sound in free space (defined by Eq. 17.162), m/s, ft/s
D	Diameter of a spherical drop, m, ft
D_{baff}	Baffle diameter, m, ft
D_{ctl}	Diameter, $D_{otl} - d_o$ (defined in Table 17.30), m, ft
D_h	Hydraulic diameter of flow passages, $4r_h$, $4A_o/P$, $4A_o L/A$, or $4\sigma/\alpha$, m, ft
D_{otl}	Diameter of the outer tube limit (defined in Table 17.30), m, ft

---

[†] J = joule = newton × meter = watt × second; newton = N = kg·m/s²; pascal = Pa = N/m².

D_s	Shell diameter, m, ft
D_w	Equivalent diameter in window, m, ft
d_e	Fin tip diameter of a disk (radial) fin, m, ft
d_i	Tube inside diameter, m, ft
d_o	Tube (or pin) outside diameter, m, ft
d_1	Tube hole diameter in baffle, m, ft
E	Modulus of elasticity, Pa, lbf/ft^2
Eu	N-row average Euler number, $\Delta p/(\rho V_m^2 N_r/2g_c)$ or $\rho\Delta p g_c/(N_r G^2/2)$, dimensionless
F	Log-mean temperature difference correction factor (defined by Eq. 17.17 and Table 17.4), dimensionless
F	Parameter, $[\rho_v/(\rho_l - \rho_v)]^{1/2} j_v/(d_i g \cos\theta)^{1/2}$, dimensionless
Fo	Liquid drop Fourier number, $4\alpha\tau/D^2$, dimensionless
Fr	Froude number, $G^2/(gD_h\rho_{\text{hom}}^2)$, dimensionless
Fr$_{\text{lo}}$	Froude number with all flow as liquid, $G^2/(gd_i\rho_l^2)$, dimensionless
f	Fanning friction factor, $\tau_w/(\rho V_m^2/2g_c)$, $\rho\Delta p g_c D_h/(2LG^2)$, dimensionless
f_a	Acoustic frequency, Hz, 1/s
f_n	Tube natural frequency, Hz, 1/s
f_{tb}	Turbulent buffeting frequency, Hz, 1/s
f_v	Vortex shedding frequency, Hz, 1/s
G	Mass velocity, based on the minimum free area, $\dot{m}/A_o$, based on the total flow rate for two-phase flow, kg/m^{2}s, lbm/hr ft^2
g	Acceleration due to gravity, m/s^2, ft/s^2
g_c	Proportionality constant in Newton's second law of motion, $g_c = 1$ and dimensionless in SI units, $g_c = 32.174$ lbm ft/lbf s^2
H	Velocity head or velocity pressure, Pa, lbf/ft^2 (psi)
Ⓗ	Thermal boundary condition referring to constant axial wall as well as peripheral heat flux with wall temperature
Ⓗ₁	Thermal boundary condition referring to constant axial wall heat flux with constant peripheral wall temperature
Ⓗ₂	Thermal boundary condition referring to constant axial wall heat flux with constant peripheral wall heat flux
h	Heat transfer coefficient, W/m^2 K, Btu/hr ft^2 °F
h_e	Heat transfer coefficient at the fin tip, W/m^2 K, Btu/hr ft^2 °F
$(hA)^*$	Convection conductance ratio (defined in Table 17.10b), dimensionless
I	Area moment of inertia, m^4, ft^4
i	Specific enthalpy on per unit mass basis, J/kg; Btu/lbm
i_{lv}	Specific enthalpy of phase change, J/kg, Btu/lbm
J_i	Correction factor for the heat transfer coefficient, $i = 1, 2, \ldots, 5$ (defined in Table 17.29), dimensionless
j	Fluid superficial velocity (volume flow rate of the respective phase divided by cross section area), m/s, ft/s
j	Colburn factor, St Pr$^{2/3}$, dimensionless
K	Pressure loss coefficient, $\Delta p/(\rho V^2/2g_c)$, dimensionless

$K(\infty)$	Incremental pressure drop number for fully developed flow, see Eq. 17.86 for definition, dimensionless
K_c	Contraction loss coefficient for flow at heat exchanger entrance (Eq. 17.65 and Fig. 17.35), dimensionless
K_e	Expansion loss coefficient for flow at heat exchanger exit (Eq. 17.65 and Fig. 17.35), dimensionless
k	Thermal conductivity, for fluid if no subscript, W/m K, Btu/hr ft °F
k_f	Thermal conductivity of the fin material, W/m K, Btu/hr ft °F
k_w	Thermal conductivity of the matrix (wall) material, W/m K, Btu/hr ft °F
L	Fluid flow (core) length on one side of an exchanger, span length for flow-induced vibration analysis, m, ft
L	Drop travel distance, m, ft
L_{bb}	Bundle bypass diameter gap (see Table 17.30), m, ft
L_{bc}	Central baffle spacing, m, ft
L_{bi}	Inlet baffle spacing, m, ft
L_{bo}	Outlet baffle spacing, m, ft
L_c	Distance from baffle cut to shell inside diameter, m, ft
L_{cp}	Distance of penetration, m, ft
L_f	Fin flow length on one side of a heat exchanger, $L_f \le L$, m, ft
L_p	Bypass lane (defined in Table 17.30), m, ft
L_{pl}	Tube lane partition bypass width (defined in Table 17.30), m, ft
L_{pp}	Tube pitch parallel to the flow, the same as X_l, m, ft
L_{sb}	Diametral clearance, shell to baffle (defined in Table 17.30), m, ft
L_{ti}	Tube length between the tubesheet and baffle tangent to the outer tube row, m, ft
L_{tb}	Diametral clearance, tube to baffle, m, ft
L_1	Flow (core) length for fluid 1 of a two-fluid heat exchanger, m, ft
L_2	Flow (core) length for fluid 2 of a two-fluid heat exchanger, m, ft
L_3	No-flow height (stack height) of a two-fluid heat exchanger, m, ft
L_c	Height from baffle cut to shell inside diameter, m, ft
ℓ	Fin length for heat conduction from primary surface to either fin tip or midpoint between plates for symmetric heating, ℓ with this meaning used only in the fin analysis, m, ft
ℓ_b	Baffle spacing (defined in Fig. 17.63), m, ft
ℓ_{ef}	Effective flow length between major boundary layer disturbances, distance between interruptions, m, ft
ℓ_f	Fin height for individually finned tubes = $(d_e - d_o)/2$, offset strip fin length (see Fig. 17.47), m, ft
M_{eff}	Effective mass per unit tube length (defined by Eq. 17.156), kg/m, lbm/ft
m	Fin parameter $(2h/k_f\delta_f)^{1/2}$, 1/m, 1/ft
$\dot{m}$	Fluid mass flow rate, $\rho V_m A_o$, kg/s, lbm/hr
N	Number of zones or sections in a numerical analysis, number of hypothetical units of a maldistributed heat exchanger, dimensionless
N, N_r	Number of tube rows in the flow direction, dimensionless

N	Rotational speed for a rotary regenerator, rev/s, rpm
N_b	Number of baffles, dimensionless
N_c	Effective number of tube rows, $= N_{tcc} + N_{tcw}$, dimensionless
N_p	Number of separating plates in a plate-fin exchanger
N_p	Number of fluid 1 passages
N_{ss}	Number of pairs of sealing strips, dimensionless
N_{ss}^+	Parameter, N_{ss}/N_{tcc}, dimensionless
N_t	Total number of tubes in an exchanger
N_{tcc}	Effective number of tube rows in the crossflow zone (between baffle tips), dimensionless
N_{tcw}	Effective number of tube rows in the window zone, dimensionless
Nu	Nusselt number, hD_h/k, dimensionless
NTU	Number of heat transfer units, UA/C_{min}, it represents the total number of transfer units in a multipass unit, dimensionless
NTU^*_{cost}	Reduction in NTU (defined by Eq. 17.167), dimensionless
NTU_1	Number of heat transfer units based on fluid 1 heat capacity rate, UA/C_1; similarly, $\text{NTU}_2 = UA/C_2$, dimensionless
NTU_o	Modified number of transfer units for a regenerator (defined in Table 17.9), dimensionless
n, n_p	Number of exchanger passes
ntu_c	Number of heat transfer units based on the cold side $(\eta_o hA)_c/C_c$, dimensionless
ntu_h	Number of heat transfer units based on the hot side $(\eta_o hA)_h/C_h$, dimensionless
ntu_n	Number of heat transfer units based on the nominal side, dimensionless
P	Temperature effectiveness of the fluid 1 and 2 with subscripts 1 and 2 (defined in Table 17.4), dimensionless
$\mathbf{P}$	Wetted perimeter of exchanger passages on one side, $\mathbf{P} = A/L = A_{fr}\beta$, m, ft
$\mathscr{P}$	Fluid pumping power, $\dot{m}\Delta p/\rho$, W, hp
Pe	Péclet number, Re Pr, dimensionless
Pr	Prandtl number, $\mu c_p/k$, $V_m D_h/\alpha$, dimensionless
p	Fluid static pressure, Pa, lbf/ft^2 (psi)
p_f	Fin pitch, m, ft
p_t	Tube pitch, center-to-center distance between tubes, m, ft
Δp	Fluid static pressure drop on one side of a heat exchanger core, Pa, lbf/ft^2 (psi)
Δp_{bi}	Fluid static pressure drop associated with an ideal crossflow section between two baffles, Pa, lbf/ft^2 (psi)
Δp_c	Fluid static pressure drop associated with the tube bundle central section (crossflow zone), Pa, lbf/ft^2 (psi)
Δp_{gain}	Pressure drop reduction due to passage-to-passage nonuniformity, Pa, lbf/ft^2 (psi)
Δp_{i-o}	Fluid static pressure drop associated with inlet and outlet sections, Pa, lbf/ft^2 (psi)
Δp_s	Shellside pressure drop (defined in Table 17.31), Pa, lbf/ft^2 (psi)
Δp^*	$= \Delta p/(\rho V_m^2/2g_c)$, dimensionless
Δp_w	Fluid static pressure drop associated with an ideal window section, Pa, lbf/ft^2 (psi)

q	Total or local (whatever appropriate) heat transfer rate in an exchanger, or heat "duty," W, Btu/hr
q''	Heat flux, heat transfer rate per unit surface area, q/A, W/m^2, Btu/hr ft^2
q_e	Heat transfer rate through the fin tip, W, Btu/hr
q_0	Heat transfer rate at the fin base, W, Btu/hr
q_w	Heat flux at the wall, W/m^2, Btu/hr ft^2
$\mathbf{R}$	Thermal resistance based on the surface area A; $\mathbf{R} = 1/UA$ = overall thermal resistance in a two-fluid exchanger, $\mathbf{R}_h = 1/(\eta_o hA)_h$ = hot side film resistance (between the fluid and the wall), $\mathbf{R}_c$ cold-side film resistance, $\mathbf{R}_s$ scale or fouling resistance, and $\mathbf{R}_w$ wall thermal resistance; definitions found after Eqs. 17.4 and 17.5, K/W, hr °F/Btu
R	Heat capacity rate ratio (defined in Table 17.4), dimensionless
R	Mean bend radius in Section on Flow-Induced Vibration, m, ft
R_i	Pressure drop correction factor; $i = \ell$ for baffle leakage effects, $i = b$ for bypass flow effects, $i = s$ for baffle spacing effects
Re	Reynolds number based on the hydraulic diameter, GD_h/μ, dimensionless
Re$_d$	Reynolds number based on the tube outside diameter, $V_m d_o/\nu$, dimensionless
Re$_L$	Reynolds number based on the plate width for condensation, $4\Gamma_l/\mu_l$; also Reynolds number defined in Table 17.25, dimensionless
r	Radial coordinate in the cylindrical coordinate system, m, ft
r	Tube bend radius (defined in Fig. 17.63), m, ft
r_h	Hydraulic radius, $A_o L/A$ or $D_h/4$, m, ft
Sr	Strouhal number, $f_v d_o/V_c$, dimensionless
St	Stanton number, h/Gc_p, St$_o = U/Gc_p$, dimensionless
s	Plate width or tube perimeter, m, ft
T	Temperature, °C, °F, K, R
Ⓣ	Thermal boundary condition referring to constant wall temperature, both axially and peripherally
T_∞	Ambient fluid temperature, °C, °F
T_ℓ	Temperature of the fin tip, °C, °F
T_m	Fluid bulk mean temperature, °C, °F
T_0	Temperature of the fin base, °C, °F
T_w	Wall temperature, °C, °F
ΔT	Local temperature difference between two fluids, $T_h - T_c$, °C, °F
ΔT_{lm}	Log-mean temperature difference (Table 17.4 and Eq. 17.18), °C, °F
ΔT_m	True mean temperature difference, q/UA, °C, °F
U, U_m	Overall heat transfer coefficient (defined by Eqs. 17.4 and 17.6); the subscript m represents mean value when local U is variable, W/m^{2}K, Btu/hr ft^2 °F
V	Fluid mean axial velocity, V_m occurs at the minimum free flow area in the exchanger unless specified, m/s, ft/s; a special function in Eq. 17.47, dimensionless
$\mathbf{V}$	Exchanger total volume, m^3, ft^3
V_c	Reference crossflow velocity in gaps in a tube row (defined in Table 17.36), m/s, ft/s
v	Specific volume, $1/\rho$, m^3/kg, ft^3/lbm

We	Weber number, $G^2 D_h/(\sigma\rho_{\text{hom}})$ or $G^2 L/(\sigma\rho_l)$, dimensionless
X	Martinelli parameter $[(dp/dz)_l/(dp/dz)_v]^{1/2}$, dimensionless
X^*	Axial distance, x/L, dimensionless
X_ℓ	Longitudinal tube pitch, m, ft
X_t	Transverse tube pitch, m, ft
X_{tt}	Martinelli parameter for turbulent-turbulent flow, $[(1-x)/x]^{0.9}(\rho_v/\rho_l)^{0.5}(\mu_l/\mu_v)^{0.1}]$, dimensionless
x, y, z	Cartesian coordinates, m, ft
x	Quality (dryness fraction), dimensionless
x_n	Midspan amplitude, m, ft
x^+	Axial distance, x/D_h Re, dimensionless
x^*	Axial distance, x/D_h Re Pr, dimensionless

Greek Symbols

α	Ratio of total heat transfer area on one side of an exchanger to the total volume of an exchanger, $A/\mathbf{V}$, m²/m³, ft²/ft³
α	Fluid thermal diffusivity, $k/\rho c_p$, m²/s, ft²/s
α	Void fraction (defined by Eq. 17.115), dimensionless
α^*	Aspect ratio of rectangular ducts, a ratio of small to large side, dimensionless
α_f^*	Fin aspect ratio, $2\ell/\delta_f$, dimensionless
β	Heat transfer surface area density, a ratio of total heat transfer area on one side of a plate-fin exchanger to the volume between the plates on that side, m²/m³, ft²/ft³
β	Span length fraction at terminal ends (defined in Fig. 17.65), dimensionless
Γ_L	Amount of condensate produced per unit width of the surface, kg/s m, lbm/s ft
γ	Specific heat ratio, c_p/c_v, dimensionless
δ	Wall or primary surface (plate) thickness, m, ft
δ_c	Channel deviation parameter based on the passage width (defined by Eqs. 17.168, 17.170, and 17.171), dimensionless
δ_f	Fin thickness, at the root if not of constant cross section, m, ft
δ_o	Logarithmic decrement, $\ln(x_n/x_{n+1})$, dimensionless
ε	Heat exchanger effectiveness (defined in Table 17.4), it represents an overall exchanger effectiveness for a multipass unit, dimensionless
ε_p	Heat exchanger effectiveness per pass, dimensionless
ε_r	Regenerator effectiveness of a single matrix (defined in Table 17.9), dimensionless
ζ	Damping factor, $\delta_o/2\pi$, dimensionless
η_f	Fin efficiency (defined by Eq. 17.22), dimensionless
η_o	Overall surface efficiency of total heat transfer area on one side of the extended surface heat exchanger, see Eq. 17.24 for the definition, dimensionless
θ	Tube inclination angle, rad, deg
κ	Length effect correction factor, dimensionless
κ_T	Isothermal compressibility, 1/Pa, ft²/lbf
Λ	Reduced length for a regenerator (defined in Table 17.9), dimensionless
Λ_m	Mean reduced length (defined in Table 17.9), dimensionless

λ Longitudinal wall conduction parameter based on the total conduction area, $\lambda = k_w A_{k,t}/C_{\min}L$, $\lambda_c = k_w A_{k,c}/C_c L$, $\lambda_h = k_w A_{w,h}/C_h L$, dimensionless

λ_i Frequency constant (defined by Eq. 17.159 and λ_1 in Fig. 17.62), $i = 1, 2, \ldots$, dimensionless

μ Fluid dynamic viscosity, Pa·s, lbm/hr ft

ν Fluid kinematic viscosity, m^2/s, ft^2/s

Π Reduced period for a regenerator (defined in Table 17.9), dimensionless

Π_m Harmonic mean reduced period (defined in Table 17.9), dimensionless

ρ Fluid density, kg/m^3, lbm/ft^3

σ Ratio of free flow area to frontal area, A_o/A_{fr}, also the volumetric porosity for regenerators $= r_h \alpha$, dimensionless

σ Solidity of a tube bundle on the shell side, dimensionless

σ Surface tension, N/m, lbf/ft

τ Time variable, s

τ_w Equivalent fluid shear stress at wall, Pa, lbf/ft^2 (psi)

$\phi(\ )$ Denotes a function of; a parameter defined by Eq. 17.36, dimensionless

φ Friction multiplier of respective phases in two-phase flow (defined in Table 17.21 and Eq. 17.113a and b), dimensionless

ψ $\Delta T_m/(T_{h,i} - T_{c,i})$, also a parameter in Fig. 17.31 and Eq. 17.41, dimensionless

Subscripts

a Air side

a Terminal point of the heat exchanger zone

ave   Average

b Bulk

b Terminal point of a heat exchanger zone

c Cold fluid side

cf Counterflow

conv   Single phase convection correlation

cp Constant properties

crit   Critical heat flux (CHF) conditions

f Fin

f Two-phase friction

g Gas side or gas phase

h Hot fluid side

h Hydrostatic effect

hom   Homogeneous

H   Constant axial wall heat flux boundary condition

i Inlet to the exchanger

ideal   Ideal heat transfer conditions

l Liquid phase

lo Total two-phase mass flow rate in the channel flowing as liquid

loc   Local value

lm	Logarithmic mean
m	Mean or bulk mean
m	Momentum
max	Maximum
min	Minimum
NB	Nucleate boiling
n	Nominal or reference passage
o	Overall
o	Outlet
p	Pass
pf	Parallelflow
s	Scale or fouling when used as a subscript with the thermal resistance
s	Shell side
sat	Saturation
T	Constant wall temperature boundary condition
t	Tubeside
tb	Turbulent baffeting
tube	Tube side
v	Vapor phase
w	Wall or properties at the wall temperature
x	Local value at section x along the flow length
1	One section (inlet or outlet) of the exchanger
1	Reduced size passage side
2	Other section (outlet or inlet) of the exchanger
∞	Free stream

Superscripts

‾   Mean value (in Table 17.23, denotes mean over the total length; in Table 17.24, denotes mean over the tube perimeter)

REFERENCES

1. R. K. Shah, "Heat Exchangers," in *Encyclopedia of Energy Technology and the Environment*, edited by A. Bisio and S. G. Boots, pp. 1651–1670, John Wiley & Sons, New York, 1994.
2. R. K. Shah and A. C. Mueller, "Heat Exchange," in *Ullmann's Encyclopedia of Industrial Chemistry*, Unit Operations II, Vol. B3, Chapter 2, pp. 2-1-2-108, VCH Publishers, Weinheim, Germany, 1989.
3. G. Walker, *Industrial Heat Exchangers—A Basic Guide*, 2d ed., Hemisphere, Washington, DC, 1990.
4. G. F. Hewitt, coordinating ed., *Hemisphere Handbook of Heat Exchanger Design*, Hemisphere, Washington, DC, 1989.
5. Tubular Exchanger Manufacturers Association, *Standards of TEMA*, 7th ed., New York, 1988.
6. K. K. Shankarnarayanan, Plate Heat Exchangers, *Proc. Symposium on Heat Exchangers*, Paper IT-3, Indira Gandhi Centre for Atomic Research, Kalpakkam 603102, India, February 1996.
7. R. K. Shah and A. C. Mueller, "Heat Exchanger Basic Thermal Design Methods," in *Handbook of Heat Transfer Applications*, 2d ed., W. M. Rohsenow, J. P. Hartnett, and E. N. Ganić (eds.), Chapter 4, Part 1, pp. 1–77, 1985.

8. W. Roetzel and B. Spang, "Verbessertes Diagramm zur Berechnung von Wärmeübertragern (Improved Chart for Heat Exchanger Design)," *Wärme-und Stofübertragung,* Vol. 25, pp. 259–264, 1990.

9. R. K. Shah, "Heat Exchanger Basic Design Methods," in *Low Reynolds Number Flow Heat Exchangers,* S. Kakaç, R. K. Shah, and A. E. Bergles (eds.), Hemisphere/McGraw-Hill, Washington, DC, 1982.

10. S. G. Kandlikar and R. K. Shah, "Asymptotic Effectiveness-NTU Formulas for Multipass Plate Heat Exchangers," *ASME J. Heat Transfer,* Vol. 111, pp. 314–321, 1989.

11. B. S. Bačlić, "ε-N$_{tu}$ Analysis of Complicated Flow Arrangements," in *Compact Heat Exchangers—A Festschrift for A. L. London,* R. K. Shah, A. D. Kraus, and D. Metzger (eds.), pp. 31–90, Hemisphere, New York, 1990.

12. L. J. Huang and R. K. Shah, "Assessment of Calculation Methods for Efficiency of Straight Fins of Rectangular Profile," *Int. J. Heat Fluid Flow,* Vol. 13, pp. 282–293, 1992.

13. D. Q. Kern and A. D. Kraus, *Extended Surface Heat Transfer,* McGraw-Hill, New York, 1972.

14. R. K. Shah, "Temperature Effectiveness of Multiple Sandwich Rectangular Plate-Fin Surfaces," *ASME J. Heat Transfer,* Vol. 93C, pp. 471–473, 1971.

15. R. K. Shah, "Compact Heat Exchangers," in *Handbook of Heat Transfer Applications,* 2d ed., W. M. Rohsenow, J. P. Hartnett, and E. N. Ganić (eds.), Chapter 4, Part III, pp. 4-174–4-312, McGraw-Hill, New York, 1985.

16. R. K. Shah and D. P. Sekulić, "Nonuniform Overall Heat Transfer Coefficient in Conventional Heat Exchanger Design Theory Revisited," *ASME J. Heat Transfer,* Vol. 120, May 1998.

17. W. Roetzel and B. Spang, "Design of Heat Exchangers, Section Cb: Heat Transfer," *VDI Heat Atlas,* VDI-Verlag GmbH, Dusseldorf, 1993.

18. R. K. Shah, "Nonuniform Heat Transfer Coefficients for Heat Exchanger Thermal Design," in *Aerospace Heat Exchanger Technology 1993,* R. K. Shah and A. Hashemi (eds.), pp. 417–445, Elsevier Science, Amsterdam, 1993.

19. R. K. Shah and A. L. London, *Laminar Flow Forced Convection in Ducts,* supplement 1 to *Advances in Heat Transfer,* Academic Press, New York, 1978.

20. W. M. Kays and A. L. London, *Compact Heat Exchangers,* 3d ed., McGraw-Hill, New York, 1984.

21. W. Roetzel and B. Spang, "Thermal Calculation of Multipass Shell and Tube Heat Exchangers," *Chem. Eng. Res. Des.,* Vol. 67, pp. 115–120, 1989.

22. B. Spang, Y. Xuan, and W. Roetzel, "Thermal Performance of Split-Flow Heat Exchangers," *Int. J. Heat Mass Trans.,* Vol. 34, pp. 863–874, 1991.

23. Y. Xuan, B. Spang, and W. Roetzel, "Thermal Analysis of Shell and Tube Exchangers with Divided-Flow Pattern," *Int. J. Heat Mass Trans.,* Vol. 34, pp. 853–861, 1991.

24. B. Bačlić, F. E. Romie, and C. V. Herman, "The Galerkin Method for Two-pass Crossflow Heat Exchanger Problem," *Chem. Eng. Comm.,* Vol. 70, pp. 177–198, 1988.

25. R. K. Shah and A. Pignotti, "The Influence of a Finite Number of Baffles on the Shell-and-Tube Heat Exchanger Performance," *Heat Transfer Eng.,* Vol. 18, No. 1, pp. 82–94, 1997.

26. K. Gardner and J. Taborek, "Mean Temperature Difference: A Reappraisal," *AIChE J.,* Vol. 23, pp. 777–786, 1977.

27. P. G. Kroeger, "Performance Deterioration in High Effectiveness Heat Exchangers Due to Axial Heat Conduction Effects," *Advances in Cryogenics Engineering,* Vol. 12, pp. 363–372, Plenum, New York, 1967; condensed from a paper presented at the 1966 Cryogenic Engineering Conference, Boulder, Colorado.

28. R. K. Shah, "Thermal Design Theory for Regenerators," in *Heat Exchangers: Thermal-Hydraulic Fundamentals and Design,* S. Kakaç, A. E. Bergles, and F. Mayinger (eds.), pp. 721–763, Hemisphere/McGraw-Hill, Washington, DC, 1981.

29. H. Hausen, *Heat Transfer in Counterflow, Parallel Flow and Cross Flow,* 2d ed., McGraw-Hill, New York, 1983.

30. F. W. Schmidt and A. J. Willmott, *Thermal Energy Storage and Regeneration,* Chaps. 5–9, Hemisphere/McGraw-Hill, Washington, DC, 1981.

31. B. S. Bačlić, "The Application of the Galerkin Method to the Solution of the Symmetric and Balanced Counterflow Regenerator Problem," *ASME J. Heat Transfer,* Vol. 107, pp. 214–221, 1985.

32. R. K. Shah, "Counterflow Rotary Regenerator Thermal Design Procedures," *Heat Transfer Equipment Design,* R. K. Shah, E. C. Subbarao, and R. A. Mashelkar (eds.), pp. 267–296, Hemisphere Publishing Corp., Washington, DC, 1988.

33. G. Theoclitus and T. L. Eckrich, "Parallel Flow through the Rotary Heat Exchanger," *Proc. 3rd Int. Heat Transfer Conf.,* Vol. I, pp. 130–138, 1966.

34. G. D. Bahnke and C. P. Howard, "The Effect of Longitudinal Heat Conduction on Periodic-Flow Heat Exchanger Performance," *ASME J. Eng. Power,* Vol. 86A, pp. 105–120, 1964.

35. P. J. Heggs, L. S. Bansal, R. S. Bond, and V. Vazakas, "Thermal Regenerator Design Charts Including Intraconduction Effects," *Trans. Inst. Chem. Eng.,* Vol. 58, pp. 265–270, 1980.

36. R. K. Shah and T. Skiepko, "Influence of Leakage Distribution on the Thermal Performance of a Rotary Regenerator," in *Experimental Heat Transfer, Fluid Mechanics and Thermodynamics 1997,* M. Giot, F. X. Mayinger, and G. P. Celata (eds.), Edizioni ETS, Pisa, Italy, 1997.

37. I. E. Idelchik, *Handbook of Hydraulic Resistance,* 3d ed., CRC Press, Boca Raton, FL, 1994.

38. D. S. Miller, *Internal Flow Systems,* 2d ed., BHRA (Information Services), Cranfield, UK, 1990.

39. A. P. Colburn, "A Method of Correlating Forced Convection Heat Transfer Data and a Comparison with Fluid Friction," *Trans. AIChE,* Vol. 29, pp. 174–210, 1933; reprinted in *Int. J. Heat Mass Trans.,* Vol. 7, pp. 1359–1384, 1964.

40. W. M. Kays and A. L. London, "Heat Transfer and Flow Friction Characteristics of Some Compact Heat Exchanger Surfaces—Part I: Test System and Procedure," *Trans. ASME,* Vol. 72, pp. 1075–1085, 1950; also "Description of Test Equipment and Method of Analysis for Basic Heat Transfer and Flow Friction Tests of High Rating Heat Exchanger Surfaces," TR No. 2, Department of Mechanical Engineering, Stanford University, Stanford, 1948.

41. E. E. Wilson, "A Basis for Rational Design of Heat Transfer Apparatus," *Trans. ASME,* Vol. 37, pp. 47–82, 1915.

42. R. K. Shah, "Assessment of Modified Wilson Plot Techniques for Obtaining Heat Exchanger Design Data," *Heat Transfer 1990, Proc. of 9th Int. Heat Transfer Conf.,* Vol. 5, pp. 51–56, 1990.

43. D. E. Briggs and E. H. Young, "Modified Wilson Plot Techniques for Obtaining Heat Transfer Correlations for Shell-and-Tube Heat Exchangers," *Chem. Eng. Progr. Symp. Ser. No. 92,* Vol. 65, pp. 35–45, 1969.

44. R. K. Shah and M. S. Bhatti, "Laminar Convective Heat Transfer in Ducts," in *Handbook of Single-Phase Convective Heat Transfer,* Chapter 3, John Wiley, New York, 1987.

45. A. J. Ghajar and L. M. Tam, "Heat Transfer Measurements and Correlations in the Transition Region for a Circular Tube with Three Different Inlet Configurations," *Exp. Thermal and Fluid Sci.,* Vol. 8, pp. 79–90, 1994.

46. M. S. Bhatti and R. K. Shah, "Turbulent and Transition Convective Heat Transfer in Ducts," in *Handbook of Single-Phase Convective Heat Transfer,* Chapter 4, John Wiley, New York, 1987.

47. R. L. Webb, *Principles of Enhanced Heat Transfer,* John Wiley, New York, 1994.

48. R. K. Shah and M. S. Bhatti, "Assessment of Correlations for Single-Phase Heat Exchangers," in *Two-Phase Flow Heat Exchangers: Thermal Hydraulic Fundamentals and Design,* S. Kakaç, A. E. Bergles, and E. O. Fernandes (eds.), pp. 81–122, Kluwer Academic Publishers, Dordrecht, Netherlands, 1988.

49. A. Zukauskas, "Convective Heat Transfer in Cross Flow," *Handbook of Single-Phase Convective Heat Transfer,* S. Kakaç, R. K. Shah, and W. Aung (eds.), Chapter 6, John Wiley, New York, 1987.

50. R. M. Manglik and A. E. Bergles, "Heat Transfer and Pressure Drop Correlations for the Rectangular Offset-Strip-Fin Compact Heat Exchanger," *Exp. Thermal and Fluid Sci.,* Vol. 10, pp. 171–180, 1995.

51. T. A. Cowell, M. R. Heikal, and A. Achaichia, "Flow and Heat Transfer in Compact Louvered Fin Surfaces," *Exp. Thermal and Fluid Sci.,* Vol. 10, pp. 192–199, 1995.

52. A. M. Jacobi and R. K. Shah, "Heat Transfer Surface Enhancement through the Use of Longitudinal Vortices: A Review of Recent Progress," *Exp. Thermal Fluid Sci.,* Vol. 11, pp. 295–309, 1995.

53. M. Fiebig, "Vortex Generators for Compact Heat Exchangers," *J. Enhanced Heat Trans.,* Vol. 2, pp. 43–61, 1995.

54. T. J. Rabas and J. Taborek, "Survey of Turbulent Forced-Convection Heat Transfer and Pressure Drop Characteristics of Low-Finned Tube Banks in Cross Flow," *Heat Transfer Eng.*, Vol. 8, No. 2, pp. 49–62, 1987.

55. A. Ganguli and S. B. Yilmaz, "New Heat Transfer and Pressure Drop Correlations for Crossflow over Low-Finned Tube Banks," *AIChE Symp. Ser. 257*, Vol. 83, pp. 9–14, 1987.

56. H. C. Chai, "A Simple Pressure Drop Correlation Equation for Low Finned Tube Crossflow Heat Exchangers," *Int. Commun. Heat Mass Transfer*, Vol. 15, pp. 95–101, 1988.

57. H. Nakamura, A. Matsuura, J. Kiwaki, N. Matsuda, S. Hiraoka, and I. Yamada, "The Effect of Variable Viscosity on Laminar Flow and Heat Transfer in Rectangular Ducts," *J. Chem. Eng. Jpn.*, Vol. 12, No. 1, pp. 14–18, 1979.

58. W. Aung, "Mixed Convection in Internal Flow," in *Handbook of Single-Phase Convective Heat Transfer*, S. Kakaç, R. K. Shah, and W. Aung (eds.), Chapter 15, John Wiley, New York, 1987.

59. A. E. Bergles, "Experimental Verification of Analyses and Correlation of the Effects of Temperature-Dependent Fluid Properties," in *Low Reynolds Number Flow Heat Exchangers*, S. Kakaç, R. K. Shah, and A. E. Bergles (eds.), Hemisphere/McGraw-Hill, Washington, DC, pp. 473–486, 1983.

60. G. F. Hewitt and D. N. Roberts, "Studies of Two-Phase Flow Patterns by Simultaneous X-Ray and Flash Photography," AERE-M 2159, Her Majesty's Stationery Office, London, 1969.

61. Y. Taitel, D. Bornea, and A. E. Dukler, "Modeling Flow Pattern Transitions for Steady Upward Gas-Liquid in Vertical Tubes," *AIChE J.*, Vol. 26, pp. 345–354, 1980.

62. J. Weisman and S. Y. Kang, "Flow Pattern Transitions in Vertical and Upwardly Inclined Tubes," *Int. J. Multiphase Flow*, Vol. 7, pp. 271–291, 1981.

63. Y. Taitel and A. E. Dukler, "A Model for Predicting Flow Regime Transitions in Horizontal and Near Horizontal Gas-Liquid Flow," *AIChE J.*, Vol. 22, pp. 47–55, 1976.

64. D. Barnea, "Transition from Annular Flow and from Dispersed Bubble Flow—Unified Models for the Whole Range of Pipe Inclinations," *Int. J. Multiphase Flow*, Vol. 12, pp. 733–744, 1986.

65. D. Barnea, "A Unified Model for Predicting Flow-Pattern Transitions for the Whole Range of Pipe Inclinations," *Int. J. Multiphase Flow*, Vol. 13, pp. 1–12, 1987.

66. D. Barnea and Y. Taitel, "Interfacial and Structural Stability of Separated Flow," in *Annual Reviews in Multiphase Flow 1994*, G. Hetsroni (ed.), Vol. 20, Suppl., pp. 387–414, 1994.

67. N. Kattan, J. R. Thome, and D. Favrat, "Flow Boiling in Horizontal Tubes: Part 1—Development of a Diabatic Two-Phase Flow Pattern Map," *ASME J. Heat Transfer*, Vol. 120, pp. 140–147, 1998.

68. M. K. Jensen, "Boiling on the Shell Side of Horizontal Tube Bundles," in *Two-Phase Flow Heat Exchangers: Thermal-Hydraulic Fundamentals and Design*, S. Kakaç, A. E. Bergles, and E. O. Fernandes (eds.), pp. 707–746, Kluwer Academic Publishers, Dordrecht, Netherlands, 1988.

69. D. Chrisholm, *Two Phase Flow in Pipelines and Heat Exchangers*, Godwin, London, 1983.

70. I. D. R. Grant and D. Chrisholm, "Two-Phase Flow on the Shell-Side of a Segmentally Baffled Shell-and-Tube Heat Exchanger with Horizontal Two-Phase Flow," *ASME J. Heat Transfer*, Vol. 101, pp. 38–42, 1979.

71. G. F. Hewitt, "Gas-Liquid Flow," in *Handbook of Heat Exchanger Design*, G. F. Hewitt (ed.), Ch. 2.3.2, pp. 1–33, Begell House, New York, 1992.

72. L. Friedel, "Improved Friction Pressure Drop Correlations for Horizontal and Vertical Two-Phase Pipe Flow," *European Two-Phase Flow Group Meeting*, Ispra, Italy, Paper E.2, 1979.

73. D. Chisholm, "Pressure Gradients due to Friction during the Flow of Evaporating Two-Phase Mixtures in Smooth Tubes and Channels," *Int. J. Heat Mass Transfer*, Vol. 16, pp. 347–358, 1973.

74. D. Chisholm, "A Theoretical Basis for the Lockhart-Martinelli Correlation for Two-Phase Flow," *Int. J. Heat Mass Transfer*, Vol. 10, pp. 1767–1778, 1967.

75. J. G. Collier and J. R. Thome, *Convective Boiling and Condensation*, 3d ed., McGraw-Hill, New York, 1994.

76. V. P. Carey, *Liquid-Vapor Phase-Change Phenomena*, Taylor and Francis, Bristol, PA, 1992.

77. K. Ishihara, J. W. Palen, and J. Taborek, "Critical Review of Correlations for Predicting Two-Phase Flow Pressure Drop across Tube Banks," *Heat Transfer Eng.*, Vol. 1, No. 2, pp. 23–32, 1980.

78. P. J. Marto, "Heat Transfer in Condensation," in *Boilers, Evaporators, and Condensers*, S. Kakaç (ed.), pp. 525–570, Wiley, New York, 1991.

79. I. D. R. Grant and D. Chisholm, "Horizontal Two-Phase Flow Across Tube Banks," *Int. J. Heat Fluid Flow*, Vol. 2, pp. 97–100, 1980.

80. D. S. Scharge, J. T. Hsu, and M. K. Jensen, "Void Fractions and Two-Phase Friction Multipliers in a Horizontal Tube Bundle," *AIChE Symp. Ser. 257*, Vol. 83, pp. 1–8, 1987.

81. D. Butterworth, "Film Condensation of Pure Vapor," in *Handbook of Heat Exchanger Design*, G. F. Hewitt (ed.), Ch. 2.6.2, pp. 1–17, Begell House, New York, 1992.

82. S. Kakaç (ed.), *Boilers, Evaporators & Condensers*, Wiley, New York, 1991.

83. J. Van der Walt and D. G. Kröger, "Heat Transfer During Film Condensation of Saturated and Superheated Freon-12," *Prog. Heat Mass Transfer*, Vol. 6, pp. 75–98, 1972.

84. D. Butterworth, "Filmwise Condensation," in *Two-Phase Flow and Heat Transfer*, D. Butterworth and G. F. Hewitt (eds.), pp. 426–462, Oxford University Press, London, 1977.

85. J. W. Rose, "Fundamentals of Condensation Heat Transfer: Laminar Film Condensation," *JSME Int. J.*, Vol. 31, pp. 357–375, 1988.

86. T. Fujii, H. Honda, and K. Oda, "Condensation of Steam on a Horizontal Tube—The Influence of Oncoming Velocity and Thermal Conduction at the Tube Wall," *18th Natl. Heat Transfer Conf.*, San Diego, ASME/AIChE, pp. 35–43, August 6–8, 1979.

87. J. C. Chato, "Laminar Condensation inside Horizontal and Inclined Tubes," *ASHRAE J.*, Vol. 4, No. 2, pp. 52–60, 1962.

88. M. M. Shah, "A General Correlation for Heat Transfer During Film Condensation inside Pipes," *Int. J. Heat Mass Transfer*, Vol. 22, pp. 547–556, 1979.

89. M. K. Dobson and J. C. Chato, "Condensation in Smooth Horizontal Tubes," *ASME J. Heat Transfer*, Vol. 120, pp. 193–213, 1998.

90. V. Srinivasan and R. K. Shah, "Condensation in Compact Heat Exchangers," *J. Enhanced Heat Transfer*, Vol. 4, 1997.

91. S. Q. Zhou, R. K. Shah, and K. A. Tagavi, "Advances in Film Condensation including Surface Tension Effect in Extended Surface Passages," in *Fundamentals of Bubble and Droplet Dynamics: Phase Change and Two-Phase Flow*, E. Ulucakli (ed.), ASME HTD-Vol. 342, pp. 173–185, 1997.

92. V. P. Carey, "Two-Phase Flow in Small Scale Ribbed and Finned Passages for Compact Evaporators and Condensers," *Nucl. Eng. Design*, Vol. 141, pp. 249–260, 1993.

93. M. W. Wambsganss, R. K. Shah, G. P. Celata, and G. Zummo, "Vaporization in Compact Heat Exchangers," *4th World Conference on Experimental Heat Transfer, Fluid Mechanics and Thermodynamics*, Brussels, Belgium, June 2–6, 1997.

94. J. R. Thome, *Enhanced Boiling Heat Transfer*, Hemisphere, New York, 1990.

95. J. G. Collier, "Boiling within Vertical Tubes, Convective Boiling inside Horizontal Tubes, and Boiling outside Tubes and Tube Bundles," in *Handbook of Heat Exchanger Design*, G. F. Hewitt (ed.), Chapters 2.7.3–2.7.5, Begell House, New York, 1992.

96. S. G. Kandlikar, "A General Correlation for Saturated Two-Phase Flow Boiling Heat Transfer Inside Horizontal and Vertical Tubes," *ASME J. Heat Transfer*, Vol. 112, pp. 219–228, 1990.

97. Y. Katto and H. Ohno, "An Improved Version of the Generalized Correlation of Critical Heat Flux for the Forced Convective Boiling in Uniformly Heated Vertical Tubes," *Int. J. Heat Mass Transfer*, Vol. 27, pp. 1641–1648, 1984.

98. J. W. Palen and W. M. Small, "A New Way to Design Kettle and Internal Reboilers," *Hydrocarbon Process*, Vol. 43, No. 7, pp. 199–208, 1964.

99. R. K. Shah, "Multidisciplinary Approach to Heat Exchanger Design, in Industrial Heat Exchangers," J-M. Buchlin (ed.), Lecture Series No. 1991-04, von Kármán Institute for Fluid Dynamics, Belgium, 1991.

100. R. K. Shah, "Compact Heat Exchangers," in *Heat Exchangers: Thermal-Hydraulic Fundamentals and Design*, S. Kakaç, A. E. Bergles, and F. Mayinger (eds.), pp. 111–151, Hemisphere Publishing Corp., Washington, DC, 1981.

101. R. K. Shah, "Plate-Fin and Tube-Fin Heat Exchanger Design Procedures," in *Heat Transfer Equipment Design*, R. K. Shah, E. C. Subbarao, and R. A. Mashelkar (eds.), pp. 255–266, Hemisphere Publishing Corp., Washington, DC, 1988.

102. R. K. Shah and A. D. Giovannelli, "Heat Pipe Heat Exchanger Design Theory," in *Heat Transfer Equipment Design*, R. K. Shah, E. C. Subbarao, and R. A. Mashelkar (eds.), pp. 609–653, Hemisphere Publishing Corp., Washington, DC, 1988.

103. R. K. Shah and A. S. Wanniarachchi, "Plate Heat Exchanger Design Theory," in *Industrial Heat Exchangers*, J. M. Buchlin (ed.), Lecture Series N. 1991-04, von Kármán Institute for Fluid Dynamics, Belgium, 1991.

104. D. P. Sekulić and R. K. Shah, "Thermal Design Theory of Three-Fluid Heat Exchangers," *Advances in Heat Transfer*, Vol. 26, pp. 219–328, Academic Press, New York, 1995.

105. K. J. Bell, "Delaware Method for Shell-Side Design," in *Heat Transfer Equipment Design*, R. K. Shah, E. C. Subbarao, and R. A. Mashelkar (eds.), pp. 145–166, Hemisphere, New York, 1988.

106. J. Taborek, "Shell-and-Tube Heat Exchangers: Single-Phase Flow," in *Handbook of Heat Exchanger Design*, G. F. Hewitt (ed.), pp. 3.3.3-1–3.3.11-5, Begell House, New York, 1992.

107. G. Breber, "Computer Programs for Design of Heat Exchangers," in *Heat Transfer Equipment Design*, R. K. Shah, E. C. Subbarao, R. A. Mashelkar (eds.), pp. 167–177, Hemisphere, New York, 1988.

108. D. Butterworth, "Developments in the Computer Design of Heat Exchangers," in *Heat Transfer 1994, Proc. 10th Int. Heat Transfer Conf.*, Vol. 1, pp. 433–444, Brighton, UK, 1994.

109. K. J. Bell, "Approximate Sizing of Shell-and-Tube Heat Exchangers," in *Handbook of Heat Exchanger Design*, G. F. Hewitt (ed.), pp. 3.1.4-1–3.1.4-9, Begell House, New York, 1992.

110. D. P. Sekulić, "Second Law Quality of Energy Transformation in a Heat Exchanger," *ASME J. Heat Transfer*, Vol. 112, pp. 295–300, 1990.

111. A. Bejan, G. Tsatsaronis, and M. Moran, *Thermal Design and Optimization*, Wiley, New York, 1996.

112. B. Linnhoff, D. W. Townsend, D. Boland et al. (eds.), *A User Guide on Process Integration for the Efficient Use of Energy*, Pergamon Press, Oxford, 1982.

113. D. Butterworth, "Steam Power Plant and Process Condensers," in *Boilers, Evaporators & Condensers*, S. Kakaç (ed.), Ch. 11, pp. 571–633, Wiley, New York, 1991.

114. A. C. Mueller, "Condensers," in *Handbook of Heat Exchanger Design*, G. F. Hewitt (ed.), pp. 3.4.1-1–3.4.9-5, Hemisphere, New York, 1990.

115. G. H. Hewitt, G. L. Shires, and T. R. Bott, *Process Heat Transfer*, CRC Press, Boca Raton, FL, 1994.

116. F. Kreith and R. F. Boehm, *Direct Contact Heat Transfer*, Hemisphere, New York, 1988.

117. M. Cumo, "Numerical Methods for the Analysis of Flow and Heat Transfer in a Shell-and-Tube Heat Exchanger with Shell-Side Condensation," in *Two-Phase Flow Heat Exchangers: Thermal-Hydraulic Fundamentals and Design*, S. Kakaç, A. E. Bergles, and E. O. Fernandes (eds.), pp. 829–847, Kluwer, Dordrecht, Netherlands, 1988.

118. H. R. Jacobs, "Direct-Contact Condensers," in *Handbook of Heat Exchanger Design*, G. F. Hewitt (ed.), pp. 1–16, Hemisphere, New York, 1990.

119. R. A. Smith, *Vaporisers, Selection, Design, and Operation*, Longman, New York, 1986.

120. J. G. Collier, "Evaporators," in *Two-Phase Flow Heat Exchangers: Thermal-Hydraulic Fundamentals and Design*, S. Kakaç, A. E. Bergles, and E. O. Fernandes (eds.), pp. 683–705, Kluwer, Dordrecht, Netherlands, 1988.

121. J. G. Collier, "Nuclear Steam Generators and Waste Heat Boilers," in *Boilers, Evaporators & Condensers*, S. Kakaç (ed.), pp. 471–519, Wiley, New York, 1991.

122. R. D. Blevins, *Flow-Induced Vibration*, 2d ed., Van Nostrand, New York, 1990.

123. P. R. Owen, "Buffeting Excitation of Boiler Tube Vibration," *J. Mech. Eng. Sci.*, Vol. 7, pp. 431–439, 1965.

124. H. J. Connors, "Fluidelastic Vibration of Tube Arrays Excited by Cross Flow," in *Flow-Induced Vibration in Heat Exchangers*, D. D. Reiff (ed.), Proc. of a WAM Symposium, ASME, New York, pp. 42–56, 1970.

125. M. J. Pettigrew, J. H. Tromp, C. E. Taylor et al., "Vibration of Tube Bundles in Two-Phase Cross Flow: Part 1 Hydrodynamic Mass and Damping," in *Symposium on Flow-Induced Vibration and Noise,* M. P. Paidoussis, S. S. Chen, and M. D. Berstein (eds.), Vol. 2, ASME, New York, pp. 79–104, 1988.

126. T. M. Mulcahu, H. Halle, and M. W. Wambsganss, "Prediction of Tube Bundle Instabilities: Case Studies," *Argonne National Laboratory Report ANL-86-49,* 1986.

127. R. D. Blevins, *Formulas for Natural Frequency and Mode Shape,* Van Nostrand, New York, 1979.

128. M. J. Pettigrew, H. G. D. Goyder, Z. L. Qiao et al., "Damping of Multi-Span Heat Exchanger Tubes," in *Flow-Induced Vibration—1986,* S. S. Chen, J. C. Simons, and Y. S. Shin (eds.), PVP-104, ASME, New York, 1986.

129. R. D. Blevins and M. M. Bressler, "Acoustic Resonance in Heat Exchanger Tube Bundles—Part I: Physical Nature of the Phenomena, Part II: Prediction and Suppression of Resonance," *ASME J. Pressure Vessel Technology,* Vol. 109, pp. 275–288, 1987.

130. J. M. Chenoweth, "Flow-Induced Vibration," in *Handbook of Heat Exchanger Design,* G. F. Hewitt (ed.), p. 4.6.6-1, Hemisphere, New York, 1990.

131. A. C. Mueller and J. P. Chiou, "Review of Various Types of Flow Maldistribution in Heat Exchangers," *Heat Transfer Eng.,* Vol. 9, No. 2, pp. 36–50, 1988.

132. M. T. Cichelli and D. F. Boucher, "Design of Heat Exchanger Heads for Low Holdup," *AIChE, Chem. Eng. Prog.,* Vol. 52, No. 5, pp. 213–218, 1956.

133. R. B. Fleming, "The Effect of Flow Distribution in Parallel Channels of Counterflow Heat Exchangers," *Advances in Cryogenic Engineering,* pp. 352–363, 1966.

134. K. Chowdhury and S. Sarangi, "The Effect of Flow Maldistribution on Multipassage Heat Exchanger Performance," *Heat Transfer Eng.,* Vol. 6, No. 4, pp. 45–54, 1985.

135. A. C. Mueller, "An Inquiry of Selected Topics on Heat Exchanger Design," *AIChE Symp. Ser. 164,* Vol. 73, pp. 273–287, 1977.

136. J. A. Kutchey and H. L. Julien, "The Measured Influence of Flow Distribution on Regenerator Performance," *SAE Trans.,* Vol. 83, SAE Paper No. 740164, 1974.

137. J. P. Chiou, "The Advancement of Compact Heat Exchanger Theory Considering the Effects of Longitudinal Heat Conduction and Flow Nonuniformity," in *Compact Heat Exchangers: History, Technological Advancement and Mechanical Design Problems,* Book No. G00183, HTD-Vol. 10, pp. 101–121, ASME, New York, 1980.

138. J. P. Chiou, "The Effect of Nonuniformities of Inlet Temperatures of Both Fluids on the Thermal Performance of Crossflow Heat Exchanger," *Heat Transfer 1982, Proc. 7th Int. Heat Transfer Conf.,* Vol. 6, pp. 179–184, 1982.

139. A. L. London, "Laminar Flow Gas Turbine Regenerators—The Influence of Manufacturing Tolerances," *ASME J. Eng. Power,* Vol. 92A, pp. 45–56, 1970.

140. R. K. Shah and A. L. London, "Effects of Nonuniform Passages on Compact Heat Exchanger Performance," *ASME J. Eng. Power,* Vol. 102A, pp. 653–659, 1980.

141. J. R. Mondt, "Effects of Nonuniform Passages on Deepfold Heat Exchanger Performance," *ASME J. Eng. Power,* Vol. 99A, pp. 657–663, 1977; Vol. 102A, pp. 510–511, 1980.

142. R. A. Bajura and E. H. Jones Jr., "Flow Distribution Manifolds," *ASME J. Fluid Eng.,* Vol. 98, pp. 654–666, 1976.

143. A. B. Datta and A. K. Majumdar, "Flow Distribution in Parallel and Reverse Flow Manifolds," *Int. J. Heat Fluid Flow,* Vol. 2, pp. 253–262, 1980.

144. A. C. Mueller, "Criteria for Maldistribution in Viscous Flow Coolers," *Heat Transfer 1974, Proc. 5th Int. Heat Transfer Conf.,* Vol. 5, pp. 170–174, 1974.

145. G. R. Putnam and W. M. Rohsenow, "Viscosity Induced Nonuniform Flow in Laminar Flow Heat Exchangers," *Int. J. Heat Mass Transfer,* Vol. 28, pp. 1031–1038, 1985.

146. Z. H. Ayub, "Effect of Flow Maldistribution on Partial Condenser Performance," *Chemical Processing,* No. 8, pp. 30–34, 37, 1990.

147. J. B. Kitto and J. M. Robertson, "Effects of Maldistribution of Flow on Heat Transfer Equipment Performance," *Heat Transfer Eng.,* Vol. 10, No. 1, pp. 18–25, 1989.

148. J. M. Chenoweth, "Final Report of the HTRI/TEMA Joint Committee to Review the Fouling Section of the TEMA Standards," *Heat Transfer Eng.,* Vol. 11, No. 1, pp. 73–107, 1990.

149. J. W. Palen, "On the Road to Understanding Heat Exchangers: A Few Steps Along the Way," *Heat Transfer Eng.,* Vol. 17, No. 2, pp. 41–53, 1996.

150. J. G. Knudsen, "Fouling in Heat Exchangers," in *Handbook of Heat Exchanger Design,* G. F. Hewit (ed.), pp. 3.17.1-1–3.17.7-9, Hemisphere, New York, 1990.

151. W. J. Marner, "Progress in Gas-Side Fouling of Heat-Transfer Surfaces," *App. Mech. Rev.,* Vol. 43, No. 3, pp. 35–66, 1990; Vol. 49, No. 10, Part 2, pp. S161–S166, 1996.

152. W. J. Marner and J. W. Suitor, "Fouling with Convective Heat Transfer," in *Handbook of Single-Phase Convective Heat Transfer,* S. Kakaç, R. K. Shah, and W. Aung (eds.), Chapter 21, John Wiley, New York, 1987.

153. M. G. Fontana and N. D. Greene, *Corrosion Engineering,* McGraw-Hill, New York, 1978.

154. K. P. Singh and A. I. Soler, *Mechanical Design of Heat Exchangers and Pressure Vessel Components,* Arcturus Publishers, Cherry Hill, NJ, 1984.

155. E. A. D. Saunders, *Heat Exchangers: Selection, Design and Construction,* John Wiley, New York, 1989.

156. M. A. Taylor, *Plate-Fin Heat Exchangers: Guide to Their Specification and Use,* HTFS, Harwell Laboratory, Oxon, UK, amendment to 1st ed., 1989.

157. J. P. Gupta, *Fundamentals of Heat Exchanger and Pressure Vessel Technology,* Hemisphere, Washington, DC, 1986.

158. R. K. Shah, "Brazing of Compact Heat Exchangers," in *Compact Heat Exchangers—A Festschrift for A. L. London,* R. K. Shah, A. D. Kraus, and D. E. Metzger (eds.), pp. 491–529, Hemisphere, Washington, DC, 1990.

159. M. S. Peters and K. D. Timmerhaus, *Plant Design and Economics for Chemical Engineers,* 4th ed., McGraw-Hill, New York, 1991.